Hosting Capacity Assessment of Distribution Systems

Mohammad Seidaliseifabad

Centre for Future Energy Networks
School of Electrical and Information Engineering
Faculty of Engineering and Information Technology
The University of Sydney

A thesis submitted in fulfilment of the requirements for the degree of
Doctor of Philosophy

March 2020

I would like to dedicate this thesis to my parents for making me be who I am and supporting me through this journey.

Declaration

I hereby declare that except where specific reference is made to the work of others, the contents of this dissertation are original and have not been submitted in whole or in part for consideration for any other degree or qualification in this, or any other university. This dissertation is my own work and contains nothing which is the outcome of work done in collaboration with others, except as specified in the text and Acknowledgements. This dissertation contains fewer than 61,500 words including appendices, bibliography, footnotes, tables and equations and has fewer than 69 figures.

Mohammad Seidaliseifabad
March 2020

Acknowledgements

I would like to express my deepest gratitude to my supervisor A/Prof. Jin Ma. He has been an exceptional mentor for me during the period of my candidature. His advice and encouragement in this thesis, as well as my professional career, have been crucial. I would not have been able to finish my dissertation without his guidance and support.

I would also like to sincerely thank Dr. Hesamoddin Marzooghi, Dr. Ahmad Shabir Ahmadyar, Dr. Mehdi Garmroodi, Sahar Ahmadyar and Yulia Cheplakova for their support.

I am particularly thankful to those who provided me financial support during my PhD program in the form of scholarship and prizes:

- The University of Sydney for the University of Sydney International Scholarship,
- The Commonwealth Scientific and Industrial Research Organisation for the postgraduate top-up scholarship,
- The University of Sydney for the Postgraduate Research Scholarship Scheme, and
- The School of Electrical and Information Engineering at The University of Sydney for the Norman I Price scholarship.

Last but not least, I would like to express my deepest appreciation to my family, especially my brother Mehdi, who has provided a tremendous amount of support throughout these years.

Abstract

The increasing penetration of distributed energy resources (DERs) in distribution systems may result in a number of technical problems such as over-voltage, overloading, maloperation of protection systems and power quality issues. One approach to address the above-mentioned issues is upgrading the distribution network, which is quite costly. The second approach is to limit the penetration of DERs to the hosting capacity (HC), which is defined as the maximum DER capacity that can be installed in a system without violating the operational constraints. Understanding this concept can assist utilities to ensure the reliable operation of the system. There have been different studies to identify the HC in a system. Nevertheless, the uncertainties associated with the DERs and loads have not been addressed properly in such studies. Besides, it is very difficult to quantify the findings of those studies and make general conclusions, as they were often based on specific networks, while their methods is time consuming in a big distribution network. Furthermore, the impact of voltage control schemes and emerging technologies, such as electric vehicles (EVs) and battery energy storage systems (BESSs) on the HC have not been studied, adequately. Thus, in this thesis, we propose a suitable HC assessment framework, as well as utilize some of the conventional and emerging resources to increase the HC.

Publications Included in this Thesis

Journal Articles

[JA1] M. Seydali Seyf Abad, J. Ma, D. Zhang, A.S. Ahmadyar, H. Marzooghi, "Probabilistic Assessment of Hosting Capacity in Radial Distribution Systems," *IEEE Transactions on Sustainable Energy*, vol. 9 no. 4, pp. 1935-1947, Oct. 2018.

[JA2] M. Seydali Seyf Abad, J. Ma, A.S. Ahmadyar, H. Marzooghi, "Distributionally Robust Distributed Generation Hosting Capacity Assessment in Distribution Systems," *Energies*, vol. 11 no. 11, pp. 1935-1947, Nov. 2018.

[JA3] M. Seydali Seyf Abad, J. Ma, "Photovoltaic Hosting Capacity Sensitivity to Active Distribution Network Management," Submitted to *IEEE Transactions on Power Systems*, Nov 2019.

[JA4] M. Seydali Seyf Abad, J. Ma, "Probabilistic Impact Assessment of Residential BESSs on the HC of LV Distribution Systems," Submitted to *IEEE Transactions on Smart Grid*, Nov 2019.

[JA5] D. Zhang, J. Ma, M. Seydali Seyf Abad, "A Chance-Constraints Based Islanding Strategy Considering Uncertainties," Submitted to *IEEE Transactions on Power Systems*, Aug. 2019.

Book Chapter

[BC1] M. Seydali Seyf Abad, J. Ma, X. Han, "Smart Power Distribution Systems, Control, Communication, and Optimization. Ch. Distribution systems hosting capacity assessment: Relaxation and linearization," *ScienceDirect-Academic Press*, Ch. 23, pp. 555 - 586, 2019.

[BC2] M. Seydali Seyf Abad, J. Ma, J. Qiu, "Hosting Capacity for Modern Power Grids. ch. A Scenario-based approach for storage capacity determination to improve the hosting capacity of distribution systems," *Springer*, Accepted, 2019.

Conference Papers

[CP1] M. Seydali Seyf Abad, G. Verbič, A. Chapman, J. Ma, "A linear method for determining the hosting capacity of radial distribution systems," in *2017 Australasian Universities Power Engineering Conference (AUPEC), Melbourne*, 19-22 Nov. 2017.

[CP2] Y. Ma, M. Seydali Seyf Abad, D. Azuatalam, G. Verbič, A. Chapman, "Impacts of community and distributed energy storage systems on unbalanced low voltage networks," in *2017 Australasian Universities Power Engineering Conference (AUPEC), Melbourne*, 19-22 Nov. 2017.

[CP3] M. Seydali Seyf Abad, J. Ma, D. Zhang, A.S. Ahmadyar, H. Marzooghi, "Sensitivity of Hosting Capacity to Data Resolution and Uncertainty Modeling," in *2017 Australasian Universities Power Engineering Conference (AUPEC), Auckland*, 27-30 Nov. 2018.

Table of contents

List of figures

List of tables

Symbols and Abbreviations

Parameters and Constraints

$\bar{\ell}_{ij}$ Define as $|\bar{I}_{ij}|^2$

η^{CES} The efficiency of the community BESS

η_i^{CES} The efficiency of the community BESS at bus (i)

ε A very small positive number

ε_i^{max} The maximum allowable stored energy level of the community BESS at bus (i)

ε_i^{min} The minimum allowable stored energy level of the community BESS at bus (i)

$E_{i,\acute{t}=0}^{\text{CES}}$ The initial stored energy in the community BESS at bus (i)

$E_i^{\text{CES},max}$ The maximum energy capacity of a given community BESS at bus (i)

$E_i^{\text{CES},min}$ The minimum energy capacity of a given community BESS at bus (i)

m_{br} Define as cardinality of set $\mathscr{B}$

$n+1$ Define as cardinality of set $\mathscr{N}$

p_i^{RURD} The charging/discharging rate of community BESS at bus (i)

$S_i^{\text{CES},max}$ The maximum power rating of a given community BESS at bus (i)

$S_i^{\text{CES},min}$ The minimum power rating of a given community BESS at bus (i)

y_{ij} Define as $\frac{1}{z_{ij}} =: g_{ij} - ib_{ij}$

y_i Define as $\frac{1}{z_i} =: g_i - ib_i$

$z_{ij} = r_{ij} + ix_{ij}$ The complex impedance of branch (i,j)

$z_i = r_i + ix_i$ The shunt impedance from bus i to ground

$1-\chi$ Minimum probability of finding an upper bound for the HC problem.

$[a,b]$ Interval from a to b

$[a_j,b_j]$ Interval from a_j to b_j

α A positive coefficient

$\alpha_{\mathrm{b}},\ \beta_{\mathrm{b}}$ Beta distribution shape parameters

α_{Pen} Acceptable error from the reference BESS penetration level,($BESS_{\mathrm{Pen}}$)

Δt time step

ΔTap_{ij} The turn ratio change per tap of the tap-changer of the transformer between bus (i) and (j)

$\eta^{\mathrm{bat}+}$ Charging efficiency of battery

$\eta^{\mathrm{bat}-}$ Discharging efficiency of battery

η_{i} The inverter efficiency

γ Risk level for the sample approximated HC problem, which is in the range of $[0,1)$

$\hat{\eta}^{\mathrm{g}}_{i,t}$ Predicted values of $\eta^{\mathrm{g}}_{i,t}$

$\hat{p}^{\mathrm{d}}_{i,t}$ Predicted values of $p^{\mathrm{d}}_{i,t}$

$\hat{p}^{\mathrm{EV}}_{i,t}$ Predicted values of $p^{\mathrm{EV}}_{i,t}$

$|V^0_{i,t}|$ Initial voltage magnitude at bus (j) and time (t)

$|V^{\mathrm{NDG}}_{i,t}|$ The voltage magnitude of bus (i) when DER at bus (i) is disconnected

$\boldsymbol{\rho_{\mathrm{apc}}}$ Maximum limitation on the feed-in active power

$\mathbf{LL_i}$ The lower limit of the constraint (i)

$\mathbf{M}$ Vector of positive large numbers

$\mathbf{PF_i}$ The vector of power factor at bus (i)

$\mathbf{UL}_{\max}$ Define as $\max(\mathbf{U_i})$

$\mathbf{v_{nom}}$ The nominal voltage in the system

$\mathbf{v_{band}}$ The acceptable error from the voltage reference

$\mathbf{v_{ref}}$ The voltage reference for the OLTC controller

$\mathbf{Z_{ij}} \in \mathbb{C}^{3\times 3}$ The impedance complex matrix of branch (i, j)

μ The mean for the Gaussian distribution

$\overline{\Delta V}$ The maximum acceptable voltage deviation in the system

$\overline{\mathbf{v}}$ The vector of upper voltage limit

$\overline{\upsilon}$ Square of the maximum acceptable voltage in the system

$\overline{I}_{ij}$ Maximum acceptable current for the line from bus (i) to bus (j)

$\overline{p^{\mathrm{g}}_{i,t}}$ The maximum acceptable DER at bus (i) based on the voltage deviation constraint

$\overline{p}^{\mathrm{bat}+}$ The maximum charging rate of battery

$\overline{p}^{\mathrm{bat}-}$ The maximum discharging rate of battery

$\overline{p}^{\mathrm{n}}$ The maximum power that can be exchanged with the network

$\overline{SoC}^{\mathrm{bat}}$ The maximum state of charge of battery

$\overline{S}_{ij}$ Maximum acceptable apparent power for the line from bus (i) to bus (j)

$\overline{V_{i,t}}$ The maximum voltage at bus (i) considering the voltage deviation constraint

$\phi_{i,t}$ Power factor angle of DER at bus (i) and time (t)

ψ Risk-aversion level

σ The standard deviation for the Gaussian distribution

σ_b Variance of Beta distribution

τ Risk level

$\tau^{'}$ Risk level for the joint chance constrained problem

θ The rotation angle for counterclockwise rotation matrix

$\underline{\upsilon}$ Square of the minimum acceptable voltage in the system

$\underline{SoC}^{\text{bat}}$ The minimum state of charge of battery

$\upsilon_{i,t}^{0}$ Square of initial voltage magnitude at bus (j) and time (t)

a_{scl} The dependency of SCL to the capacity of the DER at bus (j)

$B_{\text{Total}}^{\text{CES}}$ The total number of locations in which BESSs could be installed

$BESS_{\text{Pen}}$ The penetration level of BESS in the system

$Cycle_{\text{Day}}$ The number of charge/discharge cycles of the storage during a day

$Cycle_{\text{Total}}$ The number of charge/discharge cycles of the storage during its life cycle

F_{Factor} Future value of the battery replacement cost ($/kWh)

FOM Fixed unit cost ($/kW.year) of the maintenance and operation of BESS

H A positive integer number ($H \leq M$)

HC_{ref} The new minimum HC that can be reached by installing community battery storage

hzn Planning horizon

IR Annual interest rate

K_{ij} The total number of taps of the tap-changer of the transformer between bus (i) and (j)

L, U End points for bisection line search algorithm

M A positive integer number to represent the number of sets of samples

M_j A large positive number

N Number of samples in the SAA approach

$N^{i\%}$ The number of scenarios for the location penetration level of $i\%$

N_{BESS} The total number of expansion scenarios to identify the minimum required BESS

N_{pen} Number of location penetration levels

N_{scn} Number of expansion scenarios for each location penetration level

N_{Tech} The number of technology combination generated in the Monte Carlo simulation

N_{Total} The total number of expansion scenarios in the Monte Carlo simulation

N_{v} Number of variables

N_{year} The number of days in a year that storage system would operate

N_{BC} The number of pieces in the piecewise linear function

N_{ij} The length of binary representation of K_{ij}

NoC Number of constraints in a general optimization model

$P^0_{ij,t}$ Initial active power from bus (i) to bus (j) at time (t)

$Q^0_{ij,t}$ Initial reactive power from bus (i) to bus (j) at time (t)

SCL_{Rated} Rated SCL at substation

SCL_{sub} SCL at substation without DERs effects

T^{FIT} Feed-in-tariff

T^{grid}_t Network tariff at time (t)

$Tap^{\max}_{ij}$ The maximum turn ratio of the tap-changer of the transformer between bus (i) and (j)

$Tap^{\min}_{ij}$ The minimum turn ratio of the tap-changer of the transformer between bus (i) and (j)

TIC^{lpl}_i The total installed capacity for the (i^{th}) scenario of the LPL (lpl)

$UBOP$ Unit cost (\$/kWh) of the balance of plant

$UCPE$ Unit cost (\$/kW) of power electronic device which connects the BESS to the network

$UCSC$ The unit cost (\$/kWh) of storage device

UL_i Upper bound for the constraint (i)

Sets

$\mathscr{C}$ Set of inequality constraints in the HC model

$\mathscr{C}^{\mathrm{eq}}$ Set of equality constraints in the HC model

$\bar{\mathbb{Y}}(s)$ The solution set of the branch flow model after angle and cone relaxations

$\hat{\mathbb{Y}}(s)$ The solution set of the branch flow model after angle relaxation

$\mathbb{X}(s)$ The solution set of the original branch flow model

$\mathbb{Y}(s)$ The set of all points whose projections are the solutions of the branch flow model after angle relaxation

$\mathscr{B}$ Set of all branches

$\mathbb{C}$ Set of complex numbers

$\mathbb{R}$ Set of real numbers

$\mathbb{XX} \subset \mathbb{R}^n$ A deterministic feasible region

$\mathbb{X}_{\gamma}^{N}$ Feasible region for the sample average approximated HC problem

$\mathbb{X}_{\tau'_+}$ Feasible region for the joint chance constrained HC problem

$\mathscr{DG}$ Set of buses that have a DER

$\mathscr{D}_{\phi}$ Confidence set

$\mathscr{H}$ Set of all time steps

$\mathscr{LP}$ Set of all location penetration levels

$\mathscr{M}_+$ Set of all cumulative density functions (CDFs)

$\mathscr{N}$ Set of All buses

$\mathscr{N}^+$ Set of All buses except 0

$\mathscr{PV}$ The set of buses that have PVs

Ω A probability space

Φ Set of phases in the system

Variables

$\ell_{ij,t}$ Define as $|I_{ij,t}|^2$

ξ The vector of uncertain variables

$\mathbf{Cap}^{\mathrm{g}} \in \mathbb{R}^n$ A n-dimensional vector to represent the DER capacities on every bus of the system

$\upsilon_{i,t}$ Define as $|V_{i,t}|^2$

B_i^{CES} The binary variable to allocate community BESS at bus (i)

$DD_{1,i,t}$ Binary variable that identifies the discharging status of the community BESS at bus (i) and time (t)

$DD_{2,i,t}$ Binary variable that identifies the charging status of the community BESS at bus (i) and time (t)

E_i^{CES} The energy capacity of a given community BESS at bus (i)

$I_{ij,t}$ The complex current from bus (i) to bus (j) at time (t)

$Loss_{i,\acute{t}}^{\mathrm{CES}}$ The losses in the community BESS during the time step $(\acute{t})$

$p_{i,\acute{t}}^{\mathrm{CES}}$ Charging/Discharging power of the community BESS at bus (i) and time $(\acute{t})$

$s_{i,t} = p_{i,t} + iq_{i,t}$ The net complex power injection at bus (i) and time (t)

$s_{i,t}^{\mathrm{g}} = p_{i,t}^{\mathrm{g}} + iq_{i,t}^{\mathrm{g}}$ The generation complex power at bus (i) and time (t)

$S_{ij,t} = P_{ij,t} + Q_{ij,t}$ The sending-end complex power from bus (i) to bus (j) at time (t)

S_i^{CES} The power rating of a given community BESS at bus (i)

$V_{i,t}$ The complex voltage at bus (i) and time (t)

$XX_{i,t}$ Continuous variable, which helps to linearize the losses in the community BESS at bus (i) and time (t)

$YY_{i,t}$ Continuous variable, which helps to linearize the losses in the community BESS at bus (i) and time (t)

$\delta_{ij,t}$ Angle between V_i and V_j

$\eta_{i,t}^{\mathrm{g}}$ Capacity factor of DER at bus (i) and time (t)

λ A variable on interval $[0,1]$

$\lambda_{ij,\kappa}^{\mathrm{bin}}$ A binary variable

$\lambda_{v,j}$ A variable on interval $[0,1]$

λ_{v} A variable on interval $[0,1]$

$\eta^{\mathrm{g}}_{\mathbf{j,t}}$ The vector of capacity factor at bus (j) and time (t), which is defined as $[\eta^{\mathrm{a}}_{j,t}, \eta^{\mathrm{b}}_{j,t}, \eta^{\mathrm{c}}_{j,t}]^{\mathrm{T}}$

$\lambda_{\mathbf{i,t,l}}$ A vector of variables on interval $[0,1]$

$\omega_{\mathbf{ij},\kappa}$ A vector of continuous variable

$\xi \in \mathbb{R}^{K}$ A K-dimensional random vector defined on a probability space, Ω

$\mathbf{APC_{i,t}}$ The vector of active power curtailment at bus (i) and time (t)

$\mathbf{B^{ESS}_{j}}$ Define as $[B^{\mathrm{ESS}}_{j,a}, B^{\mathrm{ESS}}_{j,b}, B^{\mathrm{ESS}}_{j,c}]^{\mathrm{T}}$

$\mathbf{B^{g}_{j}}$ Define as $[B^{\mathrm{g}}_{j,a}, B^{\mathrm{g}}_{j,b}, B^{\mathrm{g}}_{j,c}]^{\mathrm{T}}$

$\mathbf{Cap^{g}_{j}}$ The vector of DERs installed capacity at bus (j) in different phases, which is defined as $[Cap^{\mathrm{g},a}_{i}, Cap^{\mathrm{g},b}_{i}, Cap^{\mathrm{g},c}_{i}]^{\mathrm{T}}$

$\mathbf{D_{i,t}}$ Define as $\left[D^{\mathrm{a}}_{i,t}, D^{\mathrm{b}}_{i,t}, D^{\mathrm{c}}_{i,t}\right]$, which is a vector of binary variables

$\mathbf{p^{ESS}_{j,t}}$ The vector of charging/discharging rate of BESSs at bus (j) at time (t)

$\mathbf{p^{ESS}_{j,t}}$ The vector of the charging/discharging rate of BESSs at bus (j) and time (t)

$\mathbf{s^{d}_{i,t}} = \mathbf{p^{d}_{i,t}} + i\mathbf{q^{d}_{i,t}}$ The complex vector of three phase load at bus (i) and time (t), where $\mathbf{p^{d}_{i,t}} = \left[p^{\mathrm{d},a}_{i,t}, p^{\mathrm{d},b}_{i,t}, p^{\mathrm{d},c}_{i,t}\right]^{\mathrm{T}}$ and $\mathbf{q^{d}_{i,t}} = \left[q^{\mathrm{d},a}_{i,t}, q^{\mathrm{d},b}_{i,t}, q^{\mathrm{d},c}_{i,t}\right]^{\mathrm{T}}$

$\mathbf{s^{g}_{i,t}} = \mathbf{p^{g}_{i,t}} + i\mathbf{q^{g}_{i,t}}$ The complex vector of three phase generated power at time (t), where, $\mathbf{p^{g}_{i,t}} = \left[p^{\mathrm{g},a}_{i,t}, p^{\mathrm{g},b}_{i,t}, p^{\mathrm{g},c}_{i,t}\right]^{\mathrm{T}}$ and $\mathbf{q^{g}_{i,t}} = \left[q^{\mathrm{g},a}_{i,t}, q^{\mathrm{g},b}_{i,t}, q^{\mathrm{g},c}_{i,t}\right]^{\mathrm{T}}$

$\mathbf{S_{ij,t}} = \mathbf{P_{ij,t}} + i\mathbf{Q_{ij,t}}$ The three phase complex power from bus (i) to bus (j) at time (t)

$\mathbf{v_{far,t}}$ The vector of three phase voltage of the farthest location from the transformer at time step (t)

$\mathbf{V_{i,t}}$ The complex vector of three phase voltage at bus (i) and time (t)

$\mathbf{w_{i,t,l}}$ A vector of binary variable

Υ Binary Variable

ϖ Binary Variable

$\Theta^{i\%}$ A vector to determine if a vector would cause over-voltage problem

$\xi^{\mathrm{d}}_{i,t}$ Prediction error of the Load at bus (i) at time (t)

$\xi^{\mathrm{EV}}_{i,t}$ Prediction error of the aggregated demand of EVs at bus (i) at time (t)

$\xi^{\mathrm{g}}_{i,t}$ Prediction error of the DER output at bus (i) at time (t)

ACC Total annual capital cost

$AOMC$ Total annual cost ($/year) of the maintenance and operation of BESS

$B^{\mathrm{ESS}}_{i,k}$ A binary variable to represent the status of BESS system at bus (i) and phase (k)

$B^{\mathrm{g}}_{i,k}$ A binary variable to represent the status of PV system at bus (i) and phase (k)

B^{spl}_{j} Binary variable

BEC Cost of storage device

BOP Total cost of the balance of plant

$Cap^{\mathrm{g}}_{i,t}$ Base capacity of DER at bus (i) and time (t)

Cap^{g}_{i} Variable to represent the capacity of DER on bus (i) over the study period

d^{n}_{t} Binary variable

$E^{\mathrm{CES}}_{\mathrm{Total}}$ The energy capacity of the designed storage device (kWh) to increase the HC

$Loc^{i\%}_{\mathrm{pen}}$ Location penetration level of $i\%$

$N^{\mathrm{g}}_{i,t}$ Number of DERs with the size of base capacity at bus (i) and time (t)

$p^{\mathrm{EV}}_{i,t}$ Aggregated EV active demand at bus (i) at time (t)

$p^{\mathrm{bat}+}_{t}$ Charging power of residential battery

$p^{\mathrm{bat}-}_{t}$ Discharging power of residential battery

P^{ESS}_{t} The power that battery exchange with the network

$p^{\mathrm{n}+}_{t}$ Power flow from network

$p_t^{\mathrm{n}-}$ Power flow to network

PEC Total cost of power electronic device which connects the BESS to the network

$Pr_{N^{i\%}}$ The non-compliance probability of each location penetration level $i\%$

$q_{i,t}^{\mathrm{EV}}$ Aggregated EV reactive demand at bus (i) at time (t)

$S_{\mathrm{Total}}^{\mathrm{CES}}$ Rated power of the designed BESS in (kW)

$s_{i,t}^{\mathrm{EV}}$ Aggregated EV complex demand at bus (i) at time (t)

$S_{ij,t}^{r}$ Defined as $S_{ij,t} - z_{ij}|I_{ij,t}|^2$

s_t^{bat} Operation status of residential battery

SoC_t^{bat} State of charge of residential battery

TAC Total annual cost of the BESS

TCC Total capital cost

$w_{v,j}$ A binary variable

$zz,\ zz_0$ Dual variables for reformulating the distributionally robust optimization model as a joint chance constrained

$s_{i,t}^{\mathrm{d}} = p_{i,t}^{\mathrm{d}} + iq_{i,t}^{\mathrm{d}}$ The load consumption at bus (i) and time (t)

Other Symbols

G_k An inequality constraint in the HC optimization model

G_k^{eq} An equality constraint in the HC optimization model

$(k,l) \in \mathbb{T}_j$ Refer to line (k,l) in subtree $\mathbb{T}_j$

(i,j) Branch from bus (i) to bus (j) in set $\mathscr{B}$

$\acute{x}$ The variables for forward orientation of the relaxed power flow model. x could be $S,\ \ell$ and υ

$\acute{x}^{\mathrm{lin}}$ The variables for the forward orientation of the relaxed linear power flow model. x could be $S,\ \ell$ and υ

$\hat{h}(\cdot)$ the projection of $(S,I,V,s_0) \in \mathbb{C}^{2m+n+1}$ to $(P,Q,\ell,\upsilon,p_0,q_0) \in R^{3m+n+2}$

$\hat{x}$ The variables for backward orientation of the relaxed power flow model. x could be S, ℓ and υ

$\hat{x}^{\text{lin}}$ The variables for the backward orientation of the relaxed linear power flow model. x could be S, ℓ and υ

$\left(P_{\gamma}^{N}\right)$ Sample average approximated HC problem

$\mathbb{P}_j$ The set of lines on the path from substation to bus (j)

$\mathbb{T}_j$ The subtree rooted at bus (j) (including j)

$\tilde{x}$ The optimal solution for the HC model after angle and cone relaxations. x could be S, ℓ, υ, s^{g}, s^{d}, s_0^{g} and s_0^{d}

$i \longrightarrow j$ Branch from bus (i) to bus (j) in set $\mathscr{B}$

$i \sim j$ A connection between (i) and (j)

$k \in \mathbb{T}_j$ Refer to bus (k) in subtree $\mathbb{T}_j$

x^* The optimal solution for the HC model after angle relaxation. x could be S, ℓ, υ, s^{g}, s^{d}, s_0^{g} and s_0^{d}

$\ominus$ Element-wise division

$\hat{f}(\cdot)$ Piecewise linear approximation of $f(\cdot)$

$\hat{f}_i(\cdot)$ Piecewise linear approximation of $f_i(\cdot)$

$\hat{g}''_{i,j}(\cdot)$ Piecewise linear approximation of $g''_{i,j}(\cdot)$

$\hat{z}^N_{\gamma,[H]}$ Solution of the approximated HC problem with the sample set H such that $\hat{z}^N_{\gamma,[1]} \leq \cdots \leq \hat{z}^N_{\gamma,[M]}$

$\hat{z}^N_{\gamma}$ Solution of the sample average approximated HC problem

$\Lambda_i^{lpl}(t)$ Total active power curtailment for the (i^{th}) scenario of the LPL (lpl) at time (t)

$\left(P_{\tau'_+}\right)$ Original joint chance constrained HC problem

$\mathbb{I}(\cdot)$ Indicator function, which takes value one when the argument is true and zero otherwise

$\mathbb{PR}_0(\cdot)$ Probability distribution defined by estimated PDF, $f_{\text{df},0}$

$\xi^1, \xi^2, \cdots, \xi^N$ N independent Monte Carlo samples of the uncertainty vector ξ

$\Pr[\cdot]$ Probability distribution induced by ξ

$\odot$ Element-wise multiplication

$\overline{m}(\phi^*)$ Is defined as $\inf\{m \in \mathbb{R} : \phi^*(m) = +\infty\}$

$\phi : \mathbb{R} \longrightarrow \mathbb{R}$ A convex function on $\mathbb{R}^+$

$\phi_{\mathrm{VD}}(x)$ Variation distance function

τ'_+ Define as $\max\left\{\tau', 0\right\}$

$\Theta_{\mathrm{BESS}}(j)$ Indicator to identify the DER expansion scenarios that would result in active power curtailment

$\underline{m}(\phi^*)$ Is defined as $\sup\{m \in \mathbb{R} : \phi^* \text{is a finite constant on } (-\infty, m]\}$

$APCI_i^{lpl}(t)$ Active power curtailment indicator for the (i^{th}) scenario of the LPL (lpl) at time (t)

$f(\cdot)$ A Continuous function

$f_{\mathrm{df},0}$ Empirical density function

f_{df} A density function in the confidence set, $\mathscr{D}_\phi$

f_{HC} Probability density function of HC

$f_{ij}(\cdot)$ A nonlinear function

$f_i(\cdot)$ A single variable function

$g''_{i,j}(\cdot)$ A single variable function

$G(\mathbf{Cap}^{\mathrm{g}}, \xi)$ Is defined as $\max\ \{T(\mathbf{Cap}^{\mathrm{g}}, \xi)\}$

$L_{ij}(\cdot)$ Linear approximation of the function $f_{ij}(\cdot)$

$Leb\{\cdot\}$ Lebesgue measure on $\mathbb{R}^k$

$Prob_{\mathrm{CV}}$ Probability of constraint violations for the new minimum HC, i.e, (HC_{ref})

$T(\mathbf{Cap}^{\mathrm{g}}, \xi)$ Is defined as $\begin{cases} G_k^{\mathrm{eq}}(\mathbf{Cap}^{\mathrm{g}}, \xi) = 0 & \forall k \in \mathscr{C}^{\mathrm{eq}} \\ G_k(\mathbf{Cap}^{\mathrm{g}}, \xi) \leq 0 & \forall k \in \mathscr{C} \end{cases}$

$z^{*\prime}_{\tau_+}$ Solution of the original joint chance constrained HC problem.

Acronyms / Abbreviations

AEMO Australian Energy Market Operation

ANM Active Network Management

APC Active Power Curtailment

APCI Active Power Curtailment Indicator

BESS Battery Energy Storage System

CDF Cumulative Density Function

CPF Comprehensive Power Flow

CPFM Constant Power Factor Mode

CVR Conservation Voltage Reduction

DERs Distributed Energy Resources

DGs Distributed Generations

DRO Distributionally Robust Optimization

DSOs Distribution System Operators

EVs Electric Vehicles

FIT Feed-in-tariff

HC Hosting Capacity

ILP Integer Linear Program

JCC Joint Chance Constraint

LA Lead Acid

LAPFM Limitation of Active Power Feed-in Mode

LP Linear Programming

LPL	Location Penetration Level
LV	Low Voltage
MILP	Mixed Integer Linear Program
MPVHC	Minimum Photovoltaic Hosting Capacity
MV	Medium Voltage
NaS	Sodium Sulfur
NHTS	National Household Travel Survey
OLTC	On-Load Tap Changer
OPF	Optimal Power Flow
PDF	Probability Density Function
PV	Photovoltaic
PVHC	Photovoltaic Hosting Capacity
RESs	Renewable Energy Resources
RO	Robust Optimization
SAA	Sample Average Approximation
SCL	Short Circuit Level
SCM	Self Consumption Maximization
SDP	Semidefinite Programming
SO	Stochastic Optimization
SoC	State of Charge
SOCP	Second Order Cone Program
SOS2	Special Order Set of type 2
TIC	Total Installed Capacity
ToU	Time-of-Use

VRB	Vanadium Redox
VRLA	Valve Regulated Lead Acid
VUF	Voltage Unbalanced Factor
VVOM	Volt-Var Operation Mode
VVWOM	Volt-Var-Watt Operation Mode
VWOM	Volt-Watt Operation Mode
ZnBr	Zinc/Bromine

Chapter 1

Introduction

1.1 Motivation

Due to environmental concerns, economic constraints of new transmission and distribution lines, fuel cost uncertainties and liberalization of electricity markets, deployment and utilization of distributed energy resources (DERs) have been increasing in recent years. The increasing penetration of DERs at distribution level does not come without technical challenges. In fact, DER integration into distribution networks may cause a number of technical issues such as over-voltage, overloading [2], maloperation of protection systems and power quality issues [3, 4], among which the steady state over-voltage is considered as the most important one [5]. There are two approaches to address the above-mentioned issues; *i*) upgrading the distribution network to which DERs are connected [6],[7], which is quite costly. Additionally, this creates another question that is who should pay for network augmentation [8]. *ii*) the hosting capacity (HC) concept, which is defined as the maximum DER capacity that can be connected to a system without any violation in operational constraints [9]. Understanding this concept can assist utilities to make decisions regarding interconnection requests to ensure the reliable operation of the system.

Traditionally, distribution systems' planners had to deal with fewer interconnection requests and had the ability to analyze each one of them as they came in. However, the increasing penetration of DERs can make the traditional method impractical due to the limited personnel, extensive required input data and the fact that the small DERs have a negligible effect on some systems (this may be the case for the first few small DER applicants, but the cumulative capacity of them at some point affects the system). To address this issue, conservative simplified methodologies and practical rules of thumbs are often used to assess/control the interconnection of DERs to the main grid. Every power system has its own configuration and standards. Currently, one of the most widely accepted criterion by

distribution system operators (DSOs) in the US for assessing the HC of a feeder is taking a percentage of the peak load of the feeder [10]. However, the Electric Power Research Institute (EPRI) studies have shown that there is a very low correlation between the peak load and the HC of a feeder [11]. EPRI studies revealed that the HC of a feeder varies from less than 10 % of its peak load in some cases to more than 100 % in others [12]. In Australia, the assessment process of photovolatic (PV) installation varies from one DSO to another. Some DSOs allow PV integration only up to a certain limit [13], [14], while others use the transformer capacity as the determining factor [15]. For example, Ausgrid, a DSO in the state of New South Wales (NSW), which is experiencing a high PV penetration, examines all PV installations to determine their contribution to voltage rise and check if the network augmentation is required [16]. Ergon Energy, another DSO in Australia, undertakes a complete assessment if the size of PV is greater than 3.5 kW [17, 14]. Setting a hard limit on the total capacity that can be installed in the system or not assessing PV systems under a certain size can either result in an underutilization of the HC or in over-voltage problem. Therefore, industry needs a more accurate HC method that has the ability to distinguish among the aspects of feeder characteristics, as well as technology, size and location of DERs.

Further, as it has been mentioned, over-voltage is considered as one of the main restriction for higher integration of DERs [18]. This implies that DSOs can increase HC by addressing such an issue. Besides classical grid augmentation measures, DER-based local control actions, smart control of on-load tap changer (OLTC), and exploiting the potentials of battery energy storage systems (BESSs), which are also referred to as active distribution network management (ANM) schemes, can be used to alleviate the over-voltage problem [7]. Although all these methods can be used for resolving the issue, their effectiveness in increasing the HC should be assessed and quantified. Thus, the underlying question is how distribution systems should accommodate more DERs without unacceptable adverse impacts on prosumers and network performance, and without unacceptable increases in costs. The need to answer this question is the second motive for the work described in this thesis.

In the following, we will review literature related to HC assessment of distribution systems. Furthermore, we will review studies related to the existing methods for increasing the HC using potentials of DERs and BESSs.

1.2 Literature Review

The bound on the DER penetration level is set by the technical issues incurred by DERs. In order to identify the HC, we need to know those issues and properly model them in our HC assessment.

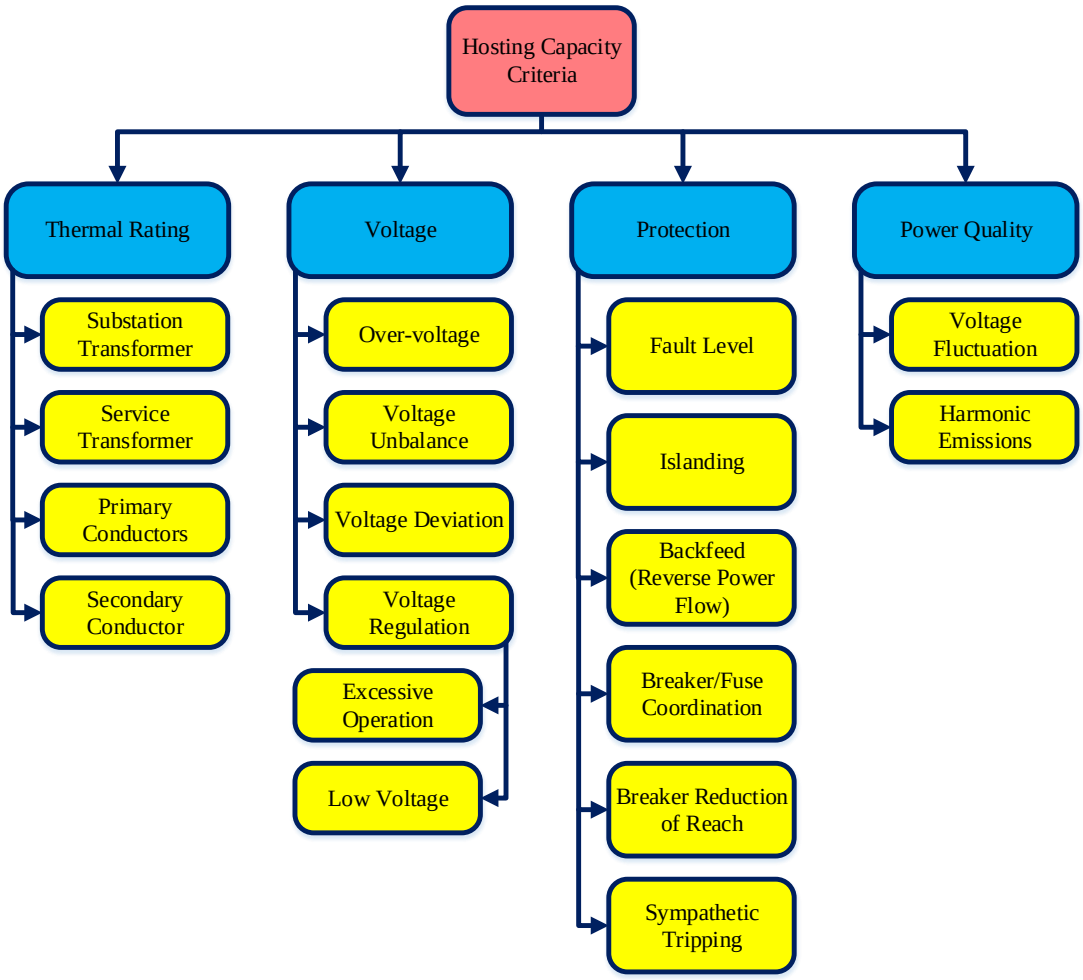

Fig. 1.1 HC criteria classification.

1.2.1 Technical Criteria That Could Limit HC

Figure 1.1 demonstrates a comprehensive list of the technical criteria, based on which, DSOs have established evaluation methodologies for DERs integration. These technical criteria are briefly described as follows [19]:

- **Thermal rating criteria:** every distribution infrastructure element such as lines, cables and transformers is characterized by a current-carrying capacity, which is referred to as thermal rating. If this limit is exceeded for a sufficient time, the element physical and/or electrical characteristics may be permanently damaged. Connecting DERs to a distribution network would change the current flows in the network. High DER penetration, especially in case of maximum generation and minimum load, could cause the current level to be higher than the thermal ratings in some parts of the system.

In this case, the developer may opt to reinforce or upgrade some elements. However, if the cost of this reinforcement is very high, an alternative connection arrangement, possibly to a higher voltage level might be worth considering.

- **Voltage criteria**
  - **Over-voltage:** this criterion is the primary concern of DSOs. Traditionally, radial distribution systems have been operated based on this assumption that there is a voltage drop across the distribution transformer and the feeder's conductors. However, DERs can counter this voltage drop and if the DER penetration is high, under high generation and low demand conditions, customers may experience voltages higher than normal service voltage.
  - **Voltage unbalance:** this is due to unbalance consumption and generation in distribution systems. In general, unbalance distribution of the single phase DERs among the grids' phases leads to an unbalance flow of power, hence unbalanced voltage.
  - **Voltage deviation (rapid voltage change):** this may happen due to the fast variation in generation output and tripping or switching of DERs. The output power of PV systems usually varies more rapidly than the typical voltage regulation controls utilized in the system. Hence, the voltage controllers are not able to properly regulate the voltage of the system. Moreover, the rapid change of the output of rooftop PV systems can increase the operation of equipment such as tap changer and switching capacitors.
  - **Voltage regulations:** distribution networks' voltage regulation is usually achieved by on-load tap changers controlled by automatic voltage control schemes. DERs could interfere in voltage regulation process and causes technical problems as follows [20]:
    - **Excessive operations:** uncertainty in the output of renewable energy resources (RESs) can disrupt the normal operation of voltage regulating devices and contribute to excessive tap changes of on load tap changer or switching of capacitors.
    - **Low voltage:** voltage regulators are often equipped with line drop compensation to control the voltage at a downstream point by raising the regulator output voltage to compensate for line voltage drop between the regulator and the load center. A DER may interfere with proper operation of regulator if the DER is located immediately downstream of a voltage regulator and its

generation is a significant fraction of the heavy load seen by the regulator. In other words, the feeder's voltage still drop from the DER to the load center, but the regulator output voltage is not increased due to the low loading seen by the regulator. Consequently, low voltage may occur at the load center.

- **Protection criteria**
  - **Fault level:** fault level at a point in a distribution system is a measure of maximum fault current expected at that point. Fault currents need to be quickly detected and interrupted due to their extensive damage to cables, overhead lines, transformers and other equipment. The circuit breakers' rating limits the fault level in the feeder. This limit is referred to as the design fault level [21]. Design fault levels in distribution networks can sometimes be a limiting factor to the DERs. New DER connection can increase the fault level. The DER fault level contribution depends on several factors such as the DER type, the distance of the DER from the fault location, the configuration of the network between the DER and the fault, and method of coupling the DER to the network. It should be mentioned that DER with directly connected electrical generators would contribute significantly higher fault current than DER connected via power electronics interfaces such as PVs. Therefore, fault level is much more important for directly connected DERs in comparison to the DERs connected via power electronics interfaces.
  - **Islanding:** this problem happens when some DERs continue to supply the load in a part of the network that is disconnected from the upstream grid. Using safety measures called anti-islanding such as IEEE 1547-2008 or making sure that the DER does not exceed the local load are common ways to prevent this problem.
  - **Back-feed (reverse power flows):** traditional distribution networks have been designed based on this assumption that power flows from a higher voltage network to a lower voltage network. However, increasing DER penetration can change the power direction when the total generation of DERs exceeds the network load. There are two main factors that limit the back-feed in a network. The first one is the reverse power rating of some elements, such as transformers, and the second one is the network's automatic control systems' ability to correctly respond under reverse power flow condition. For instance, reverse power flow in transformers can present a problem with the operation of the transformer's automatically controlled tap changer. Readjustment of control setting of control systems such as voltage regulators and replacement of circuit breaker protection relays can resolve the back-feed limit on the HC.

  - **Breaker/fuse coordination:** Fuses, re-closers and over-current relays are the most common used protection devices in distribution systems. DER interconnection can change the fault current that protection devices sense. Fuse mis-coordination issues usually happen due to an increase in fuse fault current relative to the breaker or recloser. In the cases that the fault current is the same for both fuse and breaker/recloser, mis-coordination happens if the fault current is higher than the maximum coordination current.
  - **Breaker reduction of reach:** voltage support from DERs and their influence on the system Thevenin equivalent leads to a decrease in the fault current at the start of the feeder. The higher the distributed generation capacity is, the lower the current would be at the start of the feeder. When the fault current passed though the breaker installed at the start of the feeder drops below the over-current setting, breaker may fail to operate.
  - **Sympathetic tripping:** this can happen due to circulating the zero-sequence current from DERs to a fault above the feeder circuit breaker. The increase in this current can lead to the breaker trip when it exceeds the setting of the ground current relay.

- **Power quality criteria:** a high DER penetration may raise power quality issues such as voltage fluctuations and harmonics. In case of rooftop PV systems, power quality issues could be caused by voltage and power fluctuations due to irradiance uncertainty. The voltage fluctuation can cause excessive feeder's voltage regulator operation. Harmonic emissions may be another issue for the DERs connected via power electronic converters to the grid. Although advanced pulse width modulation techniques and harmonic filters are usually used in converters, voltage distortion limits can be exceeded in high penetration levels. It should be mentioned that the evaluation of harmonic problems is somewhat complicated and is not in the routine investigations performed by the DSOs.

The importance and frequency of occurrence of the aforementioned issues are not the same. Further, some of the reviewed issues are very specific and highly depends on the network structure or DER technology. However, some technical issues such as over-voltage and overloading are more general and their frequency of occurrence is higher than other constraints. That is why most of HC studies have focused on over-voltage and overloading constraints.

The value of the HC depends on the feeder physical characteristics, DERs' size, location and technology. Therefore, feeder's HC determination is not a straightforward process and

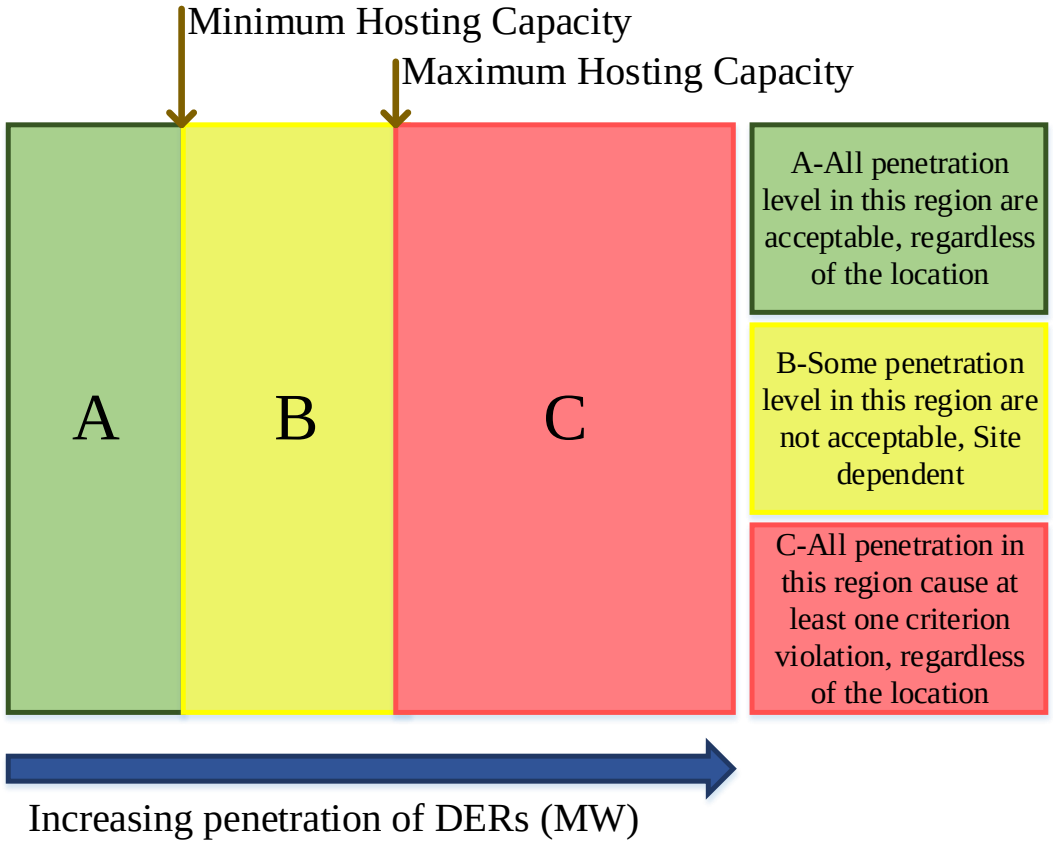

Fig. 1.2 Different regions of the HC in a system.

HC is not a single value for any given feeder. Generally, three regions as shown in Fig. 1.2, can be defined for the HC of a feeder. Region (A) includes all the penetration levels that do not cause any constraint violation, regardless of DERs' location. Region (B) demonstrates the penetration levels that are acceptable in specific sites along the feeder. Region (C) includes all DER deployments that are not acceptable, regardless of DERs' location [11]. The border between (A) and (B) is defined as the minimum HC and the border between (B) and (C) is defined as the maximum HC. Generally, all the existing HC estimation methods can be divided int two categories; *i*) min-HC category including methods that estimate the minimum HC *ii*) region-B category including the methods that converge to the maximum HC or a value in region (B). DSOs are usually interested in the minimum HC as it is independent of DERs' location. However, estimation of minimum HC is often very difficult as all the uncertainties associated with DERs and loads should be modelled. We will further discuss this in Section 1.2.2.

1.2.2 Hosting Capacity Estimation Methods

In terms of HC assessment, studies in [22–26, 14, 27–36, 18, 37–40] can be categorized as region-B approach. The HC in region-B methods is usually modelled as the objective of

an optimization problem [25, 27, 28, 30–32, 35, 36, 18, 37–40]. However, there are some other approaches such as analytical [14, 22, 24, 26, 29, 33], and Monte Carlo-based [23, 34] methods that are belong to region-B category. In analytical methods, an equation is driven based on technical constraints such as over-voltage [22, 29], overloading [24, 26] and harmonic distortion [33] to estimate the maximum DER that could be connected to a certain location of the system. However, the Monte Carlo-based methods in region-B category are often based on traditional power flow calculation. In this approach, numerous power flow calculation is performed to identify the HC of a certain location [23] or an area [34] of a distribution network. Further, this approach could be revised to identify the minimum HC if the number and location of DERs are considered as a variable in the Monte Carlo simulator.

Some of the factors that has to be considered for the HC assessment include network characteristics, load variation and DER uncertainties. The region-B methods, however, neglect at least one of the aforementioned factors. For instance, analytical methods such as [14, 22, 24, 26, 29, 33], are deterministic methods. This indicates that the uncertainties associated with the loads and DERs have been neglected in those methods. The study in [22] presented a HC model based on over-voltage constraint. That study, nevertheless, represents the network by its thevenin equivalent circuit. Besides, it can only estimate the HC for a certain location in the system. In a similar approach, in [24], an analytical equation is proposed based on thermal capacity constraint to estimate the HC. Similarly, thevenin equivalent is used to model the network. Furthermore, all loads and DERs are aggregated at one location. Although the approaches in [22] and [24] can provide an estimation of lacational HC, the network model and considered assumptions are too simplistic. A real distribution system can have a complex structure and some voltage regulating devices such as OLTC. Therefore, the work in [29] derived an equation for the HC based on a linear model of the network. Though that method used a more accurate model of network than [22] and [24], it still aggregated all DERs at a location.

The optimization-based methods in region-B category such as [25, 27, 28, 30–32, 35, 36, 18, 37–40], are generally more accurate than analytical methods. If the location of DERs are modelled as a variable in the optimization problem [31], the HC model would converge to the maximum HC, which is not the interest of this thesis. Besides, modelling the location of DERs in the optimization problem would make the model difficult to solve. Therefore, most of the optimization-based methods in region-B category such as [25, 27, 28, 30, 32, 35, 36, 18, 37, 38], limit the number of potential locations for DERs. One of the advantages of the optimization-based methods is that the network is modelled accurately. Though an accurate network model improves the accuracy of the solution, it makes it difficult to model the uncertainties associated with loads and output power of DERs in the HC problem. Hence,

studies such as [25, 27, 28, 30, 32] assumed that there is no change in the loads and output power of DERs. However, there are some studies such as [18, 37, 38], that used different optimization techniques to model the uncertainties.

Although Monte Carlo approach [23, 34] can always be used to model the uncertainties, it has not been a popular approach in the HC methods that belong to region-B category. Two dominant approaches that have been used to model the uncertainties in region-B category methods are (*i*) the robust optimization (RO) [18, 37] and (*ii*) the stochastic optimization (SO) [38, 41, 40]. In RO approach, the probability distribution functions (PDFs) of uncertainties are not required, and the only necessary data are the boundaries of the uncertain variables. Furthermore, the decisions are made based on the worst-case scenarios in the predefined uncertainty intervals, which result in a conservative solution. In SO-based approach, the uncertainties are considered as random variables with given PDFs. Nevertheless, as obtaining the exact PDFs of uncertain variables is impossible, the robustness of the obtained solution cannot be guaranteed. Both RO and SO approaches are based on historical data. In practice, historical data can present more information than the boundaries of uncertain variables. Nevertheless, historical data can only be used to obtain an empirical PDF, not the exact PDF for the uncertain variable. To cope with such cases, distributionally robust optimization (DRO) has been recently developed. In DRO, it is assumed that the exact PDFs of uncertain variables are not available. However, it is supposed that the PDFs of uncertainties are in a confidence set. The confidence set can be constructed using the distributional information of uncertain variables, which is derived from the historical data. For instance, the confidence set can be consist of all the PDFs with common mean and covariance matrix [42]. In recent years, DRO have been applied to some power system optimization problems including unit commitment [43], and reserve scheduling [44]. However, those studies often consider the first- and second-order moments of historical data to build the confidence set. Further, all those studies neglected the empirical distribution of uncertainties. Thus, to properly model the uncertainty associated with loads and output power of DERs, we will propose a DRO-HC model in Chapter 4.

The aim in the second category of the HC methods, i.e. min-HC, is to estimate the minimum HC. Studies in [7, 9, 45–49] belong to this category. These methods are generally based on Monte Carlo simulation, where a high number of DER expansion scenarios is generated. Then, traditional power flow calculation is performed for all generated scenarios over the study period. Next, the minimum HC is defined based on the scenarios that may cause a voltage or thermal capacity violation. Although, general idea of studies such as [7, 9, 45–48] is the same, the implementation details of the Monte Carlo process including generating scenarios, analyzing scenarios over the study period and defining the minimum

HC are different. For example, studies [7, 9, 45] assumed that the size of DERs is a fix number. Nevertheless, studies [46, 47] used different sizes for DERs. Similarly, the study period and time series impact analysis, which addresses the uncertainties associated with the loads and output power of DERs, could be different. For instance, in [7, 9, 45], it is assumed that the study period could be limited to the worst condition, i.e. maximum DER generation and minimum load consumption. Nevertheless, study [47] randomly allocated the daily load and DER profiles and performed the power flow calculation. The advantage of min-HC methods is that they could easily be improved to include all DER technical criteria. However, this approach has some drawbacks. First of all, the computation burden in this approach could be really high as it is based on running power flow for a high number of DER expansion scenarios. Besides, this approach can only estimate the minimum HC and there is no guarantee in the estimated value. Increasing the number of generated scenarios or the iteration of Monte Carlo simulation can increase the accuracy of the estimated minimum HC. However, this would entail a higher computation burden. A comprehensive HC method could be a combination of optimization and Monte Carlo approaches. By doing so, we can exploit the advantages of both approaches. such an approach will be presented in Chapter 3 in details.

Studies [22–26, 14, 27–36, 18, 37–40, 7, 9, 45, 46, 48, 49] presented different methods to identify the HC. However, none of them have modelled emerging technologies such as EVs and BESSs. Authors in [47] attempted to estimate the maximum allowable penetration level of EVs. However, that study did not assess the impacts of EVs on the maximum allowable penetration level of DERs, i.e. HC. These new technologies would affect the load profiles of the customers. Though there is not a linear relationship between the HC and loads, assessing the HC results in the aforementioned studies suggests that there is a positive correlation between HC and loads. There are quite a few studies on the impacts of emerging technologies on different aspects of distribution systems including load and voltage profiles, but their impact on the minimum HC has not been quantified. We will further discuss the HC assessment in presence of BESS in Section 1.2.4. Another part of the literature related to the HC are the studies that are focused on increasing the HC. Though researchers proposed quite a few methods to increase the HC of a system, the effectiveness of such methods has not been quantified. We will further discuss this in Section 1.2.3.

1.2.3 Increasing the HC

Over-voltage is considered as one of the main restriction for higher integration of DERs [18]. This implies that DSOs can increase HC by addressing such an issue. Different approaches including classical grid augmentation measures, DER-based control schemes, and control

of OLTC can be used to resolve the over-voltage problem [7]. Therefore, it is important for DSOs to understand and quantify the impact of these control schemes on HC.

Several methods for alleviating the voltage rise issue in presence of DERs have been proposed. One simple method is decreasing the substation voltage using OLTC [45]. The effectiveness of this method highly depends on the control strategy and the location of the OLTC's control bus. Controlling the reactive power [50, 51], or curtailing the active power [5, 52] of DERs by using local control actions are also utilized to address over-voltage issues. These methods can be used for alleviating the voltage rise in distribution systems, but their effectiveness in increasing the HC should be assessed and quantified.

Reactive Power Control

In transmission systems in which the X/R ratio is relatively high, the voltage control is mainly accomplished by reactive power control. Since this ratio is lower in distribution networks, reactive power control is not as effective as in transmission grids. It, however, is still an effective solution in certain grids. Reactive power management is designed to enable DERs to absorb reactive power and ensure that DERs' real power injection do not cause an over-voltage problem. The reactive power control is usually applied to the inverter controllers by controlling either the reactive power as a function of voltage at the DER connection point (Q(V)) or the power factor (PF) as a function of injected active power (PF(P)) [45]. In the Q(V) method, the DER inverter absorbs reactive power when the terminal voltage is higher than a specific value [53, 54]. In the PF(P) method, the reactive power is a function of the generated active power, so during low DER generation hours, no reactive power is absorbed by DERs' inverter [45]. There are quite a few studies that proposed absorbing reactive power to alleviate the voltage rise problem. However, we will not review those studies as the focus of this thesis is to study the impacts of the conventional reactive power schemes described in IEEE 1547 standard [55]. It should be mentioned that the reactive power absorption by DERs increases the power loss and congestion of distribution lines, which are the main drawbacks of this approach. This solution may also reduce the power factor at the substation, depending on the reactive power absorbed by DERs.

Active Power Control

This can be performed using three main approaches: active power curtailment (APC), demand side management (DSM), and application of BESSs. In APC approach, the output power of DER is curtailed to decrease the injected power to the system. Due to the high R/X ratio in distribution networks, the APC is more effective in comparison with the reactive power

control. However, the APC technique adversely affects the DER owner revenue and may lead to the reduced use of the DER generation capacity [7]. DSM is another approach proposed to increase the HC of low voltage distribution grids [56]. The voltage rise problem can also be resolved by transferring some load from peak periods to the high DER generation periods. As DSM depends to a great extent on customers' behavior, it cannot be considered as a reliable solution for increasing the HC. In recent years, BESS has been proposed as a potential solution to mitigate the over-voltage problem [57, 6, 58, 56]. To this aim, the DER output power is limited to a certain amount by storing the excess energy. The stored energy can be used when load consumption or the electricity price is high. Although BESSs can increase HC if they are controlled for such an objective, residential BESSs are controlled for the sole benefit of owners. Hence, there is no guarantee that BESSs would charge when DSOs need them the most. We will further discuss the APC schemes that are considered in this thesis in Chapter 5. BESSs will also be discussed in more detail in Section 1.2.4.

Voltage Control Using OLTC

OLTC is one of the most practical tools for controlling the voltage along a feeder. When the voltage in a feeder is low, OLTC can bring it up by increasing the substation voltage. Similarly, if the voltage is high along the feeder, OLTC can bring it down by decreasing the substation voltage. Studies in [59–62] aimed to increase HC by controlling OLTC. The study in [60] presented a framework to assess the performance of different OLTC-based control schemes based on BS EN50160[1] standard. That study proposed three control strategies for OLTC and assessed their effectiveness in increasing the HC. Authors in [61] used a power flow platform to compare the performance of three strategies including controlling OLTC, reactive power control (RPC) and hybrid control (OLTC and RPC) in increasing the HC. Their study demonstrated that OLTC could be a more robust option than RPC. Similarly, authors in [62] tried to increase the HC by coordinating OLTC and RPC. That study showed that coordinating RPC and OLTC can increase the HC while decreasing the number of OLTC switching. Although different methods have been proposed to increase the HC by controlling OLTC, their effectiveness under different distribution system characteristics is not clear. Further, there is still a need for a HC estimation methodology, which can considers the voltage control schemes. Such a methodology should be used to perform a comprehensive study on quite a few number of distribution systems to quantify the impacts of voltage control schemes on the minimum HC. This will be discussed further in Chapter 5.

[1] EUROPEAN STANDARD: Voltage characteristics of electricity supplied by public distribution systems

1.2.4 Battery Energy Storage Systems

Normally, it is assumed that BESSs are charged from DERs' surpluses. Thus, DERs' feed-in power could be significantly reduced. From DSOs' perspective, this may alleviate the technical impacts incurring from high DER penetration. Therefore, many studies have attempted to mitigate the technical challenges using BESSs, hence increase the HC. BESSs in distribution systems could be divided in residential and community categories. BESSs can increase the HC if they are controlled for such an objective. Therefore, assuming that the residential BESSs would increase the HC is not a valid assumption as they are controlled to benefit their owners.

Residential BESSs

The application of residential BESS in supporting distribution networks has been an active research subject in recent years. Researchers proposed different methods to coordinate the residential BESSs with other available resources to increase the HC by resolving over-voltage problem [56, 63–65]. In those studies, it is supposed that the capacity and the location of the BESSs are known and the aim is to control the BESSs. In a different attempt in [66], a scenario-based method was presented to identify the minimum BESSs required to increase the HC. Nevertheless, the focus in the aforementioned studies have been maximizing DSOs' benefit at the cost of prosumers. Therefore, those methods are not practical from prosumers' point of view.

Uncertainty associated with the location of BESSs and their scheduling could considerably affect the impact of residential BESSs on the HC. Several strategies have been proposed to charge/discharge residential BESSs [67–72]. The aim in scheduling the residential BESSs is most often minimizing the electricity cost [67, 71, 72]. However, self consumption maximization (SCM) is also a popular scheduling scheme [70]. In SCM approach, the battery is charged when DER generation is higher than the load consumption and discharged when the load is higher than DER output. According to [71], SCM is the default strategy utilized by battery suppliers and retailers. Most of the studies that assessed the impacts of charging/discharging strategies of BESSs carried out their assessment from an economical perspective. However, there are some studies that focused on the technical impacts of residential BESSs [73–75]. Authors in [73] presented a techno-economical analysis of BESSs assuming that consumers use their BESSs to maximize their self-consumption. Nonetheless, that study overlooked the impact of BESSs on the voltage, as well as the uncertainty associated with the location of BESSs. Unlike [73], studies presented in [74, 75] proposed Monte Carlo-based frameworks to assess the impact of residential BESS on HC. The assessment

in study [74] showed that residential BESSs in some cases could even decrease the HC. Similarly, the study in [75] concluded that, generally, residential BESSs increase the HC. However, a very high penetration of BESSs, i.e. approximately 100%, could result in a decrease in the HC. Unfortunately, the observed results in both [74, 75] are case specific and cannot be generalized. Considering the uncertainties associated with residential BESSs including their locations and charging/discharging schemes, it is still not clear to what extent they can improve the HC. What is currently missing is a comprehensive approach to study impacts of residential BESSs on the HC. Furthermore, such an approach should be applied to distribution systems with different characteristics to better quantify the impacts of residential BESSs on HC. This will be further discussed in Chapter 6.

Community BESSs

Studies that focused on the application of community BESSs in resolving the technical issues associated with high penetration of DERs can be divided into two categories: *i*) those that resolved the technical issues by controlling the BESSs [76, 77]; *ii*) and those that resolved the technical issues by optimally allocating the BESSs [78–80, 38, 41]. In the first category, the size and location of DERs and BESSs are provided, and the unknown variables are the active and reactive power of the BESSs. For instance, study in [76] proposed a method to identify the set points for managing BESSs using a voltage sensitivity analysis. In a different approach, [77] developed a multi-timescale model predictive control strategy to optimally dispatch a BESS in order to keep the voltage in operation range. Researchers in [81] proposed a method to reshape the PVs injected power by controlling the BESSs to reduce the peak-to-average ratio and curtailed energy. However, if BESSs are to be utilized for increasing the HC of a system, their sizes and locations are unknown. Therefore, the approach of the first category is not recommended for increasing the HC. Furthermore, the second category, which is based on the optimal allocation of BESSs could have a better performance as the optimal size, location and control action can all be identified, simultaneously.

Studies related to the allocation of BESSs have mainly focused on following aspects: in [78], a methodology for allocating BESSs in a distribution network is developed to minimize the wind energy curtailment as well as the annual supply cost of the electricity. Authors in [82], defined a multi-objective optimization to allocate the BESS by identifying a trade-off between the technical and economic goals by minimizing the voltage deviation, network losses, feeder congestions and costs of supplying loads. In a similar attempt, [80] presented a methodology to assess BESSs in congested distributed systems from both technical and economical perspective. That study, however, did not address the uncertainty associated with the location of BESSs. In [79], a method for optimal placement, sizing, and control

of a community BESS to increase the HC of rooftop PVs in low voltage (LV) networks is proposed. Authors in [38, 41], developed a new stochastic multi-stage model to maximize the integration of DERs by determining the optimal size and location of BESSs, reactive power sources and DERs. Likewise, authors in [83] developed a stochastic optimization-based method for BESS allocation and operation to ensure a desired voltage stability margin in wind-intensive distribution systems. In [84], a convex optimization approach has been used for BESSs planning and operation in systems with high PV penetration level. In that study, the minimum BESS required for mitigating the technical impacts of high uptake of PVs has been estimated using OpenDSS simulation tool. Then, an optimization model has been used to identify the location of BESSs. The study in [85] proposed a heuristic strategy based on voltage sensitivity in combination with an optimal power flow (OPF) framework to identify the optimal number, size, and location of BESSs that prevent over-voltage and under-voltage in an LV distribution network. The advantage of the second category, i.e. optimal allocation of BESSs, is that it can consider both technical and economical aspects of the problem. Nevertheless, the problem with the methods that aimed to optimally allocate BESSs is that they most often did not consider the uncertainty associated with the location of DERs. This implies that those methods optimally allocated BESSs considering certain location for DERs. To address this issue, researchers in [66] proposed a scenario-based method to identify the minimum required BESSs that prevents over-voltage in distribution system with high PV penetration level. That study, however, did not discuss the economic feasibility of the required BESS. Therefore, there is still a need for a techno-economic model to allocate community BESS in order to increase the HC. We will discuss this further in Chapter 7.

1.3 Research Questions

Considering the uncertainties associated with the DERs and loads in HC assessment of distribution systems is a challenging task. Although there are some HC studies addressing uncertainties using iterative power flow, it is very difficult to quantify their findings and make general conclusions, because most of them are based on specific networks and computationally cumbersome. Furthermore, the impact of voltage control strategies, as well as emerging technologies, such as EVs and BESSs on HC, have been overlooked. Considering these, some of the fundamental issues that need to be addressed are as follows:

- HC depends on different constraints and uncertain factors. However, the HC model should be simple and lead to an accurate estimation of the HC. How should the HC problem be modelled?

- There are different uncertainties associated with DERs and loads. Further, distribution systems have different characteristics. How should these factors be modelled in the HC problem. What effects do uncertainties and network characteristics have on HC?
- There are emerging technologies such as EVs and residential BESSs that are becoming popular among customers. How should these technologies be modelled in the HC problem. What effect do these emerging technologies have on the HC of a system?
- There are quite a few voltage control strategies based on controlling the active and/or reactive power of DERs as well as tap of the transformer. However, there is no comprehensive study regarding the effectiveness of those strategies in increasing the HC. What voltage control strategy is the suitable option (economically and technically) to increase the HC from DSOs' point of view and how does it impact the prosumers?
- Community BESSs can be used to increase the HC of a system. How much community BESS is required to increase the HC to a certain level. Is installing community BESS an economically feasible option?

1.4 Research Contributions

The answers to the above questions lead us to the aims of this research thesis, as summarised in the following.

In Chapter 2, we present HC as a deterministic optimization problem. We prove that angular and conic relaxations of the HC model, that have been used to solve other power system optimization problems is not exact, which means that non-convex HC model can not be substituted with a convex conic program. As solving the original nonlinear HC model especially in presence of uncertainties is difficult, we replace it with a linear HC model. Thus, we identify the conditions under which the linearized HC model is valid. We demonstrate that linearizing the HC model is valid if the linear approximation of the branch losses is less than the actual quadratic term. Furthermore, we linearize the HC problem based on the identified criteria.

In Chapter 3, we propose a probabilistic framework based on the linear HC model presented in Chapter 2 to address the uncertainties associated with the type, size and location of DERs. The developed framework has three modules. The first module of the framework addresses the uncertainties associated with type, number, and location of DERs by using the Monte Carlo simulation. A time series impact analysis is conducted in the second module to consider the impacts of load variation and uncertainty in DERs output. Then, in the third

module, a probabilistic estimation of the HC is defined based on the time series analysis. The proposed methodology is also used to assess the effects of voltage deviation constraint, load growth, network structure, and the DER type on the HC.

In Chapter 3, we use a time series impact analysis to model the uncertainties associated with the loads and the output power of DERs. Thus, we have to solve the HC model numerous times to estimate the HC of a network. However, in Chapter 4, we propose a distributionally robust HC model to treat those uncertainties as optimization variables. Thus, we only need to solve the proposed distributionally robust HC model once to estimate the HC of the network. Then, the distributionally robust HC model is used to assess the impacts of EVs and their charging stations of the HC.

In Chapter 5, we investigate the effects of autonomous voltage control strategies on the photovoltaic HC (PVHC) in low voltage (LV) distribution feeders. The investigated strategies are based on the active and reactive power control capabilities of photovoltaic (PV) systems as well as the OLTC of transformers. We propose an optimization-based framework to determine the PVHC considering the voltage control capabilities. To do so, we model the voltage control strategies as equality and inequality constraints in the HC problem. The efficacy of the proposed methodology is examined using 128 LV UK feeders as a test-bed. The results show that active power curtailment based on local voltage measurement is still the most effective control scheme to increase the PVHC. Further, our simulations demonstrate that unlike the general believe, OLTC could decrease the PVHC.

In Chapter 6, we quantify the impacts of residential BESSs on the HC. To do so, we model the scheduling of BESSs in an optimization-based HC framework. We consider a rule-based as well as a mixed integer linear programming (MILP)-based home energy management schemes to schedule the BESSs. To the best of author's knowledge, all the studies focused on the minimum HC including the Monte Carlo- and optimization-based methods could only provide an estimation of the minimum HC. However, the proposed HC model in this chapter would converge to the actual minimum HC. We show that the proposed method is more accurate than all existing Monte Carlo-based HC methods. Further, our simulations show that the effectiveness of residential BESSs in increasing the minimum PVHC (MPVHC) depends on the penetration of BESSs in the system and the scheduling scheme of BESSs. Further, we demonstrate that the cost minimization scheme is more effective than SCM in increasing the MPVHC. In addition, we quantify the impacts of flat and Time-of-Use tariffs on the MPHVC.

In Chapter 7, we propose a probabilistic method to determine the required community BESS to increase the HC of a system to a certain level. The proposed method is based on an optimization problem aiming to maximize the injected power while minimizing APC.

The optimization model is used in a probabilistic framework to address the uncertainties associated with the loads as well as the location and output power of DERs. Further, we also carry out an economic analysis to assess the feasibility of the required community BESS. We demonstrate that the BESS technology highly affects the economic feasibility of BESSs for HC improvement. Further, our simulations show that none of the considered BESS technologies is currently economically feasible for increasing the HC. However, with the decreasing trend in the BESS price, using community storage to increase the HC becomes an economically feasible solution.

Finally, Chapter 8 concludes this thesis and provides some directions for potential future works.

Chapter 2

Distribution systems hosting capacity assessment: relaxation and linearization

2.1 Introduction

As explained in Chapter 1, hosting capacity (HC) can be modelled as an optimization problem. Different nonlinear and linear models have been used for identifying the HC [25, 27, 28, 30–32, 35, 36, 18, 37–40]. However, the validity of those models have not mostly been assessed. As using an improper model could yield in an inaccurate solution, it is of great importance to develop an accurate, yet simple model for the HC assessment. Therefore, in this chapter, HC is modelled as a nonlinear optimization problem. Generally, solving a convex optimization is easier than non-convex problems. So, even if the model is not convex by itself, we would like to make it convex by using some techniques such as relaxing some constraints and/or convex approximation. We prove that the nonlinear HC model is not convex. Moreover, we show that the conic relaxation of power flow, which has been extensively used in distribution systems' optimization, is not exact for the HC problem. Therefore, we linearize the HC problem to approximate it by a simple convex model. To do so, we identify the required condition under which linear HC model is valid to approximate the original nonlinear HC problem. Finally, we proposed a linear HC model based on the proven condition. The outcome of this chapter is published as a book chapter[1] and a conference paper[2].

The remainder of this chapter is organized as follows: in Section 2.2, we develop the mathematical model of the HC and assess its convexity. In Section 2.3, we identify the

[1] Smart Power Distribution Systems, Control, Communication, and Optimization. Academic Press, 2019, ch. Distribution systems hosting capacity assessment: Relaxation and linearization [86].

[2] "A linear method for determining the hosting capacity of radial distribution systems," in 2017 Australasian Universities Power Engineering Conference (AUPEC), Nov 2017, pp. 1–6 [25].

required condition to develop a valid linear HC model. Further, we propose a linear HC model based on the proven condition. In Section 2.4, we examine the performance of our proposed linear model in comparison to traditional HC linear models. Finally, Section 2.5 summarizes the chapter.

2.2 Hosting Capacity Mathematical Modeling

The aim of HC assessment is to find the maximum distributed energy resources (DERs) capacity that can be installed in a system without violating the technical criteria. If one can model the technical criteria mathematically, the HC assessment becomes a constraint optimization. Power flow equations, thermal rating criteria and over-voltage constraint are the technical criteria that can be considered within mathematical models. So, the HC could be defined as the maximization of DERs capacity considering mathematical model of such criteria as the constraints. In this section, the convexity of the HC will be assessed. To do so, branch flow model, which was used for convexifying the optimal power flow (OPF) problem, will be firstly discussed. The HC problem has the same constraints as OPF. In [87], it was proven that conic relaxation of branch flow model is exact, which means that solving the convex conic model gives the same solution as the original OPF problem. We prove here that the conic relaxation of branch flow model is not exact for the HC problem. Therefore, the only way to convexify the problem is a linear approximation, which is discussed in section 2.3.

2.2.1 Branch Flow Model

Branch flow model is first proposed by Baran and Wu in [88] and [89] for the optimal allocation of capacitors in distribution systems. A distribution system is a graph of buses and lines connecting these buses in a radial (tree) topology. Let $\mathscr{N} = \{0,\dots,n\}$ denote the set of buses and define $\mathscr{N}^+ := \mathscr{N} \setminus \{0\}$. Let $\mathscr{B}$ denote the set of all branches with cardinality $|\mathscr{B}| := m_{\text{br}}$ and (i,j) or $i \longrightarrow j$ a branch from bus (i) to bus (j) in set $\mathscr{B}$. We use $i \sim j$ for a connection between (i) and (j), i.e., either $(i,j) \in \mathscr{B}$ or $(j,i) \in \mathscr{B}$ (but not both). For every bus $i \in \mathscr{N}$, let $V_{i,t}$ denote the complex voltage at time (t) and define $v_{i,t} = |V_{i,t}|^2$. Let $s_{i,t} = p_{i,t} + iq_{i,t}$ denote the net complex power injection on bus (i), $s^{\text{g}}_{i,t} = p^{\text{g}}_{i,t} + iq^{\text{g}}_{i,t}$ the generation complex power on bus (i) and $s^{\text{d}}_{i,t} = p^{\text{d}}_{i,t} + iq^{\text{d}}_{i,t}$ the load consumption on bus (i) at time (t). Let $z_i = r_i + ix_i$ denote the shunt impedance from bus (i) to ground and $y_i := \frac{1}{z_i} =: g_i - ib_i$. For every branch $(i,j) \in \mathscr{B}$, let $z_{ij} = r_{ij} + ix_{ij}$ denote the complex impedance of the line, and $y_{ij} := \frac{1}{z_{ij}} =: g_{ij} - ib_{ij}$ the corresponding admittance. Let

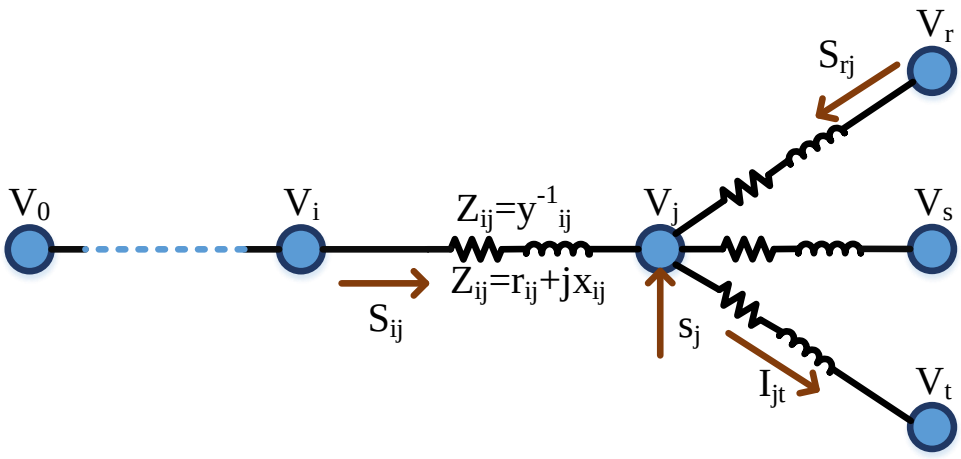

Fig. 2.1 Summary of the notations for branch flow model.

$S_{ij,t} = P_{ij,t} + Q_{ij,t}$ denote the sending-end complex power from bus (i) to bus (j), and $I_{ij,t}$ the complex current from bus (i) to bus (j). It is also assumed that substation voltage $V_{0,t}$ is given. Fig. 2.1 demonstrates a summary of the notations. Given $(z_{ij}, (i,j) \in \mathscr{B})$, $V_{0,t}$ and $(s_{i,t}, i \in \mathscr{N}^+)$, the following equation can be written based on the Ohm's law [25]:

$$V_{i,t} - V_{j,t} = z_{ij} I_{ij,t} \quad \forall (i,j) \in \mathscr{B}, \tag{2.1}$$

Based on the complex power definition, the branch power flow is as follows:

$$S_{ij,t} = V_{i,t} I^*_{ij,t} \quad \forall (i,j) \in \mathscr{B}, \tag{2.2}$$

and power balance at each bus $j \in \mathscr{N}$ is as follows:

$$s_{j,t} = \sum_{k:j \longrightarrow k} S_{jk,t} - \sum_{i:i \longrightarrow j} (S_{ij,t} - z_{ij} |I_{ij,t}|^2) + y^*_j |V_{j,t}|^2 \quad \forall j \in \mathscr{N}, \tag{2.3}$$

Equations (2.1) to (2.3) are referred as branch flow model. This model consists of $2m_{\text{br}} + n + 1$ nonlinear equations in $2m_{\text{br}} + n + 1$ complex variables $\{(S_{ij,t} \quad (i,j) \in \mathscr{B}), (I_{ij,t} \quad (i,j) \in \mathscr{B}), (V_i \quad i \in \mathscr{N}^+), (s_{0,t})\}$.

2.2.2 Original Model of the Hosting Capacity

The mathematical structure of the constraints for the HC assessment is similar to the more familiar OPF problem. The main difference lies in the objective, which is the total generation

capacity in the network as follows:

$$\text{maximize} \sum_{i \in \mathscr{N}^+} p^{\mathrm{g}}_{i,t}, \tag{2.4}$$

Regarding constraints, in addition to branch flow equations, the voltage and thermal capacity constraints should be considered. In other words, the voltage magnitude of buses must be maintained in the operational range and the current of branches should be less than their maximum currents. These constraints can be modelled as follows:

$$\underline{\upsilon} \leq |V_{i,t}|^2 \leq \overline{\upsilon} \quad \forall i \in \mathscr{N}, \tag{2.5}$$

$$|I_{ij,t}| \leq \bar{I}_{ij} \quad \forall (i,j) \in \mathscr{B}, \tag{2.6}$$

therefore, the HC problem is given as:

HC:

$$\begin{aligned} &\text{maximize} \quad \sum_{i \in \mathscr{N}^+} p^{\mathrm{g}}_{i,t}, \\ &\text{subject to } (1)-(3),(5),(6). \end{aligned} \tag{2.7}$$

The presented HC model in (2.7) is a nonlinear optimization, which implies that solving the HC problem could be difficult. Considering that there is a convex formulation for branch flow model, which is the source of non-convexity in constraints of the HC problem, the main question is whether using this convex branch flow model in the HC problem makes the HC convex or not. Based on the proposed method in [87], the main steps for convexification of the branch flow model are two relaxations, which are explained in the next subsection.

2.2.3 Relaxed Branch Flow Model

In the first step of relaxation, the voltage and current angles will be eliminated from the branch flow equations. To do so, equation (2.2) is substituted in (2.1), which results in (2.8):

$$V_{j,t} = V_{i,t} - z_{ij} \frac{S^*_{ij,t}}{V^*_{i,t}}, \tag{2.8}$$

taking the magnitude squared from (2.8) results in:

$$\upsilon_{j,t} = \upsilon_{i,t} + |z_{ij}|^2 \ell_{ij,t} - (z_{ij} S^*_{ij,t} + z^*_{ij} S_{ij,t}) \quad \forall (i,j) \in \mathscr{B}, \tag{2.9}$$

where,

$$\ell_{ij,t} = \frac{P_{ij,t}^2 + Q_{ij,t}^2}{\upsilon_{i,t}} \quad \forall (i,j) \in \mathscr{B}. \tag{2.10}$$

writing (2.3) and (2.9) in terms of real variables leads to following equations:

$$p_{j,t} = \sum_{k:j\longrightarrow k} P_{jk,t} - \sum_{i:i\longrightarrow j} (P_{ij,t} - r_{ij}\ell_{ij,t}) + g_j \upsilon_{j,t} \quad \forall j \in \mathscr{N}, \tag{2.11}$$

$$q_{j,t} = \sum_{k:j\longrightarrow k} Q_{jk,t} - \sum_{i:i\longrightarrow j} (Q_{ij,t} - x_{ij}\ell_{ij,t}) + b_j \upsilon_{j,t} \quad \forall j \in \mathscr{N}, \tag{2.12}$$

$$\upsilon_{j,t} = \upsilon_{i,t} - 2(r_{ij}P_{ij,t} + x_{ij}Q_{ij,t}) + (r_{ij}^2 + x_{ij}^2)\ell_{ij,t} \quad \forall (i,j) \in \mathscr{B}. \tag{2.13}$$

Authors in [87] referred to (2.10)-(2.13) as the relaxed branch flow equations. In contrast to the original model, i.e. equations (2.1) - (2.3), the relaxed model (2.10)-(2.13) consists of $2(m_{\text{br}}+n+1)$ equations in $3m_{\text{br}}+n+2$ real variables $\{(P_{ij,t}, Q_{ij,t}, \ell_{ij,t} \ \ (i,j) \in \mathscr{B}), (\upsilon_{i,t} \ \ \forall i \in \mathscr{N}^+), p_{0,t}, q_{0,t}\}$. Structure of distribution systems are usually radial, which implies that $m_{\text{br}} = |\mathscr{B}| = |\mathscr{N}| - 1 = n$. Hence, the relaxed branch flow model in radial distribution systems consists of $4n+2$ equations in $4n+2$ real variables. Nevertheless, the relaxed branch flow model is still non-convex due to the quadratic equality constraint in (2.10). Moreover, the solution of (2.10)-(2.13) might be infeasible for the original branch flow equations. To explain this in more detail, suppose that there is a point in the complex plane. As it can be seen in Fig. 2.2, relaxing the angle of this point is similar to projecting this point to a circle with a radius equal to the distance of the point from the origin. However, a point on the circle may result in an angle different from the origin point.

To have a better understanding of the relation between relaxed branch flow equations and the original model, suppose that $s := (s_{i,t} \ \ \forall i \in \mathscr{N}^+)$ is fixed. To simplify the notation, let define $s_0 := s_{0,t}$, $S := (S_{ij,t} \ \ \forall (i,j) \in \mathscr{B}), P := (P_{ij,t} \ \ \forall (i,j) \in \mathscr{B}), Q := (Q_{ij,t} \ \ \forall (i,j) \in \mathscr{B}), I := (I_{ij,t} \ \ \forall (i,j) \in \mathscr{B})$ $\ell := (\ell_{ij,t} \ \ \forall (i,j) \in \mathscr{B}), V := (V_{i,t} \ \ \forall i \in \mathscr{N}^+)$ *and* $\upsilon := (\upsilon_{i,t} \ \ \forall i \in \mathscr{N}^+)$. For a given s, let $\mathbb{X}(s)$ denote the solution set of the original branch flow equations given in (2.1)-(2.3) and $\hat{\mathbb{Y}}(s)$ the solution set of the relaxed model stated in (2.10)-(2.13). So, $\mathbb{X}(s) \subseteq \mathbb{C}^{2m_{\text{br}}+n+1}$ and $\hat{\mathbb{Y}}(s) \subseteq \mathbb{R}^{3m_{\text{br}}+n+2}$ can be defined as follows:

$$\mathbb{X}(s) := \{x := (S, I, V, s_0) | x \text{ solves } (1)-(3)\}, \tag{2.14}$$

$$\hat{\mathbb{Y}}(s) := \{\hat{y} := (P, Q, \ell, \upsilon, p_0, q_0) | \hat{y} \text{ solves } (10)-(13)\}, \tag{2.15}$$

Let $\hat{h}$ define the mapping of $(S, I, V, s_0) \in \mathbb{C}^{2m_{\text{br}}+n+1}$ to $(P, Q, \ell, \upsilon, p_0, q_0) \in \mathbb{R}^{3m_{\text{br}}+n+2}$ where:

$$P_{ij,t} = \text{Re}\{S_{ij,t}\}, \ Q_{ij,t} = \text{Im}\{S_{ij,t}\}, \ \ell_{ij,t} = |I_{ij,t}|^2 \quad \forall (i,j) \in \mathscr{B}, \tag{2.16}$$

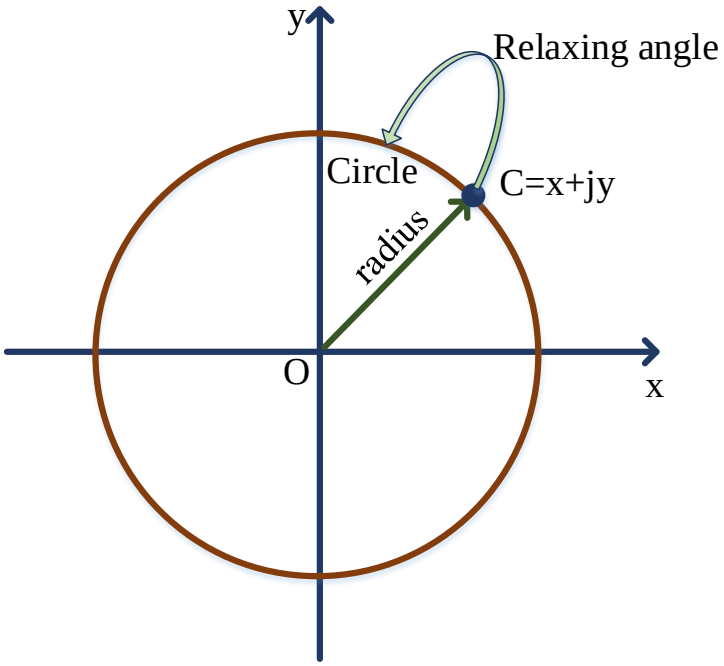

Fig. 2.2 Angle relaxation of a complex point.

$$p_{i,t} = \mathrm{Re}\{s_{i,t}\},\ q_{i,t} = \mathrm{Im}\{s_{i,t}\},\ \upsilon_{i,t} = |V_{i,t}|^2 \quad \forall i \in \mathscr{N}, \tag{2.17}$$

Assume $\mathbb{Y}(s)$ denotes the set of all points whose projections are the solutions of the relaxed branch flow equations. So, $\mathbb{Y}(s) \subseteq \mathbb{C}^{2m_{\mathrm{br}}+n+1}$ can be represented as follows:

$$\mathbb{Y}(s) := \{\acute{y} := (S, I, V, s_0) | \hat{h}(\acute{y}) \text{ solves } (10)-(13)\}, \tag{2.18}$$

Based on what was shown in Fig. 2.2, one can say that $\mathbb{X}$ is a subset of $\mathbb{Y}$ and $\hat{h}(\mathbb{X})$ is a subset of $\hat{\mathbb{Y}}$. This relation is illustrated in Fig. 2.3. It was proven in [87] that for radial networks, $\hat{h}(\mathbb{X}) = \hat{\mathbb{Y}}$, which means angle relaxation is exact. In other words, there is always a unique inverse projection that maps any relaxed solution $\hat{y}$ to a solution of the original branch flow model in $\mathbb{X}$. Relaxing the voltage and current angles in the constraints of the HC problem result in the relaxed problem as follows:

HC-ar

$$\begin{aligned} &\text{maximize} \quad \sum_{i \in \mathscr{N}^+} p^{\mathrm{g}}_{i,t}, \\ &\text{subject to} \ \ (5), (6), (10)-(13). \end{aligned} \tag{2.19}$$

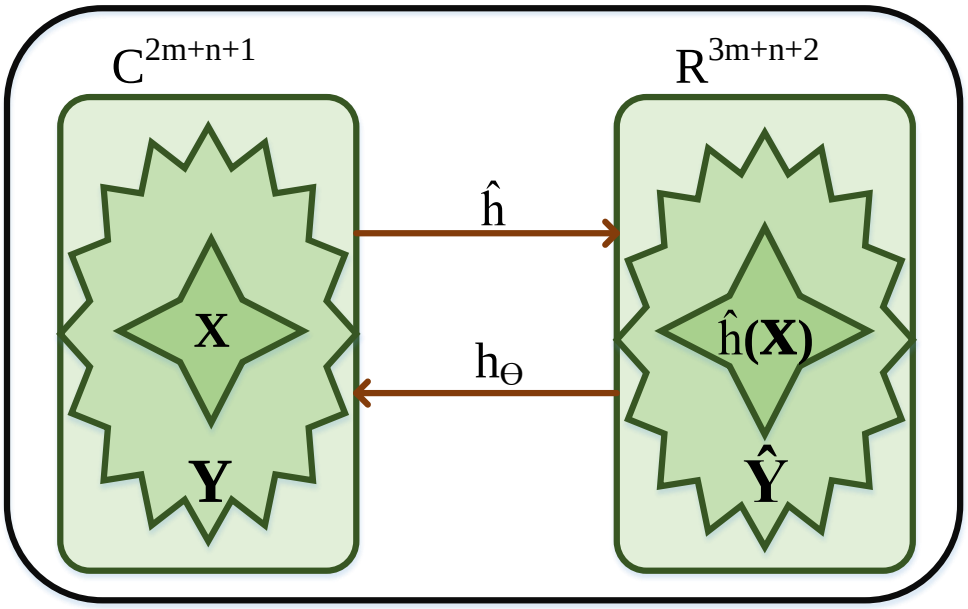

Fig. 2.3 Relation of the projection of the branch flow and relaxed model solutions.

Since $\mathbb{X} \subseteq \mathbb{Y}$, the HC-ar provides a higher bound on the HC. The problem is that HC-ar is still non-convex. The source of non-convexity is the quadratic equation (2.10). Equation (2.10) can be rewritten as:

$$P_{ij,t}^2 + Q_{ij,t}^2 = v_{i,t}\ell_{ij,t} \quad \forall (i,j) \in \mathscr{B}, \tag{2.20}$$

Equation (2.20) is similar to a rotating second order cone. Relaxing (2.20) to an inequality leads to:

$$P_{ij,t}^2 + Q_{ij,t}^2 \leq v_{i,t}\ell_{ij,t} \quad \forall (i,j) \in \mathscr{B}, \tag{2.21}$$

since $v_{i,t}$ and $\ell_{ij,t}$ are non-negative, (2.21) is a rotating second order cone. Therefore, the conic relaxation of HC can be given as follows:

HC-cr

$$\begin{aligned} &\text{maximize} \quad \sum_{i \in \mathscr{N}^+} p_{i,t}^{\mathrm{g}}, \\ &\text{subject to} \quad (5),(6),(11)-(13),(21). \end{aligned} \tag{2.22}$$

Let $\bar{\mathbb{Y}}$ denotes the solution set of equation (2.11)-(2.13) and (2.21). So, $\bar{\mathbb{Y}}(s) \subseteq R^{3m_{\mathrm{br}}+n+2}$ can be represented as follows:

$$\bar{\mathbb{Y}}(s) := \{\hat{y} := (P,Q,\ell,v,p_0,q_0) | \hat{y} \text{ solves } (11)-(13),(21)\}, \tag{2.23}$$

Note that (2.10) is a specific case of (2.21), and $\hat{\mathbb{Y}}$ is a subset of $\bar{\mathbb{Y}}(\hat{\mathbb{Y}} \subseteq \bar{\mathbb{Y}})$, which means HC-cr provides an upper bound to HC-ar. Nonetheless, the more important point is whether solving the HC-cr can lead to the exact solution of the original HC problem or not. In order to assess this, the objective function of HC problem is reformulated as a minimization problem as follows:

HC-cr

$$\begin{aligned} &\text{minimize} \quad \sum_{i\in\mathscr{N}^+} -p^{\mathrm{g}}_{i,t}, \\ &\text{subject to} \;\; (5),(6),(11)-(13),(21). \end{aligned} \tag{2.24}$$

To evaluate the exactness of the HC-cr, it is needed to check if any optimal solution of (2.24) attains equality in (2.21). Hence, assume that $(\hat{y}^*, s^*) := (S^*, \ell^*, \upsilon^*, s^{*\mathrm{g}}, s^{*\mathrm{d}}, s_0^{*\mathrm{g}}, s_0^{*\mathrm{d}})$ is the optimal solution for HC-cr that attains equality in (2.21), i.e., ${P^*_{ij,t}}^2 + {Q^*_{ij,t}}^2 = \upsilon^*_{i,t}\ell^*_{ij,t}\ \forall (i,j) \in \mathscr{B}$ and inequality in (2.6), i.e., $\ell^*_{ij,t} < \bar{\ell}_{ij}\ \forall (i,j) \in \mathscr{B}$. For some $\varepsilon > 0$, consider another point $(\tilde{y}, \tilde{s}) := (\tilde{S}, \tilde{\ell}, \tilde{\upsilon}, \tilde{s}^{\mathrm{g}}, \tilde{s}^{\mathrm{d}}, \tilde{s}^{\mathrm{g}}_0, \tilde{s}^{\mathrm{d}}_0)$ defined by:

$$\tilde{\upsilon} = \upsilon^*, \quad \tilde{s}^{\mathrm{d}} = s^{*\mathrm{d}}, \tag{2.25a}$$

$$\tilde{\ell}_{ij,t} = \ell^*_{ij,t} + \varepsilon, \quad \tilde{\ell}_{-ij,t} = \ell^*_{-ij,t}, \tag{2.25b}$$

$$\tilde{S}_{ij,t} = S^*_{ij,t} + z_{ij}\frac{\varepsilon}{2}, \quad \tilde{S}_{-ij,t} = S^*_{-ij,t}, \tag{2.25c}$$

$$\tilde{s}^{\mathrm{g}}_{i,t} = s^{*\mathrm{g}}_{i,t} + z_{ij}\frac{\varepsilon}{2}, \quad \tilde{s}^{\mathrm{g}}_{j,t} = s^{*\mathrm{g}}_{j,t} + z_{ij}\frac{\varepsilon}{2}, \tag{2.25d}$$

$$\tilde{s}^{\mathrm{g}}_{-i,-j,t} = s^{*\mathrm{g},}_{-i,-j,t} \tag{2.25e}$$

where, a negative index means excluding the indexed elements from a set. Thus, incremental change in generation at buses (i) and (j) are set to counter the variation in $(\ell^*_{ij,t})$ and $(S^*_{ij,t})$. As $\tilde{s}^{\mathrm{g}}_{i,t} = s^{*\mathrm{g}}_{i,t} + z_{ij}\frac{\varepsilon}{2}$, $\tilde{s}^{\mathrm{g}}_{j,t} = s^{*\mathrm{g}}_{j,t} + z_{ij}\frac{\varepsilon}{2}$, $(\tilde{y}, \tilde{s})$ has a strictly smaller objective value than $(\hat{y}^*, s^*)$. If $(\tilde{y}, \tilde{s})$ is feasible, then the optimal solution of conic relaxation is different from HC-ar. To prove this, it suffices to demonstrate that there is an $\varepsilon > 0$ such that $(\tilde{y}, \tilde{s})$ holds for (2.5), (2.6), (2.11)-(2.13), and (2.21). Since $(\hat{y}^*, s^*)$ is a feasible point, (2.5) holds for $(\tilde{y}, \tilde{s})$; and since $(\hat{y}^*, s^*)$ attains inequality in (2.6), there is an $\varepsilon > 0$ that (2.6) holds for $(\tilde{y}, \tilde{s})$. Due to condition (2.25), $(\tilde{y}, \tilde{s})$ satisfies (2.11)-(2.12) for all buses except (i) and (j); In a similar manner, $(\tilde{y}, \tilde{s})$ satisfies (2.13) and (2.21) for all lines except $(i \longrightarrow j)$. To prove the feasibility of $(\tilde{y}, \tilde{s})$, we only need to demonstrate that $(\tilde{y}, \tilde{s})$ satisfies (2.11)-(2.12) at buses (i), (j), and (2.13) and (2.21) over line $(i \longrightarrow j)$. To do so, we reformulated (2.11)-

(2.12) at bus (i) as follows:

$$\begin{aligned}\tilde{s}_{i,t} = \tilde{s}^{\mathrm{g}}_{i,t} - \tilde{s}^{\mathrm{d}}_{i,t} = s^{*\mathrm{g}}_{i,t} + z_{ij}\frac{\varepsilon}{2} - s^{*\mathrm{d}}_{i,t} = \sum_{i\longrightarrow \acute{j}} S^{*}_{i\acute{j},t} - \sum_{k\longrightarrow i}(S^{*}_{ki,t} - z_{ki}\ell^{*}_{ki,t}) + y^{*}_{i}\upsilon^{*}_{i,t} + z_{ij}\frac{\varepsilon}{2}\\ = \sum_{\substack{i\longrightarrow \acute{j},\\ \acute{j}\neq j}} \tilde{S}_{i\acute{j},t} - \sum_{k\longrightarrow i}(\tilde{S}_{ki,t} - z_{ki}\tilde{\ell}_{ki,t}) + y^{*}_{i}\tilde{\upsilon}_{i,t} + S^{*}_{ij,t} + z_{ij}\frac{\varepsilon}{2}\\ = \sum_{i\longrightarrow \acute{j}} \tilde{S}_{i\acute{j},t} - \sum_{k\longrightarrow i}(\tilde{S}_{ki,t} - z_{ki}\tilde{\ell}_{ki,t}) + y^{*}_{i}\tilde{\upsilon}_{i,t}. \qquad (2.26)\end{aligned}$$

Similarly, reformulated (2.11)-(2.12) at bus (j) can be given as:

$$\begin{aligned}\tilde{s}_{j,t} = \tilde{s}^{\mathrm{g}}_{j,t} - \tilde{s}^{\mathrm{d}}_{j,t} = s^{*\mathrm{g}}_{j,t} + z_{ij}\frac{\varepsilon}{2} - s^{*\mathrm{d}}_{j,t} = \sum_{j\longrightarrow k} S^{*}_{jk,t} - \sum_{\acute{i}\longrightarrow j}(S^{*}_{\acute{i}j,t} - z_{\acute{i}j}\ell^{*}_{\acute{i}j,t}) + y^{*}_{j}\upsilon^{*}_{j,t} + z_{ij}\frac{\varepsilon}{2}\\ = \sum_{j\longrightarrow k} \tilde{S}_{jk,t} - \sum_{\substack{\acute{i}\longrightarrow j,\\ \acute{i}\neq i}}(\tilde{S}_{\acute{i}j,t} - z_{\acute{i}j}\tilde{\ell}_{\acute{i}j,t}) - S^{*}_{ij,t} + z_{ij}\ell^{*}_{ij,t} + y^{*}_{j}\tilde{\upsilon}_{j,t} + z_{ij}\frac{\varepsilon}{2}\\ = \sum_{j\longrightarrow k} \tilde{S}_{jk,t} - \sum_{\substack{\acute{i}\longrightarrow j,\\ \acute{i}\neq i}}(\tilde{S}_{\acute{i}j,t} - z_{\acute{i}j}\tilde{\ell}_{\acute{i}j,t}) - (\tilde{S}_{ij,t} - z_{ij}\frac{\varepsilon}{2}) + z_{ij}(\tilde{\ell}_{ij,t} - \varepsilon) + y^{*}_{j}\tilde{\upsilon}_{j,t} + z_{ij}\frac{\varepsilon}{2}\\ = \sum_{j\longrightarrow k} \tilde{S}_{jk,t} - \sum_{\acute{i}\longrightarrow j}(\tilde{S}_{\acute{i}j,t} - z_{\acute{i}j}\tilde{\ell}_{\acute{i}j,t}) + y^{*}_{j}\tilde{\upsilon}_{j,t}. \qquad (2.27)\end{aligned}$$

This implies that (2.11) and (2.12) hold at buses (i) and (j). To check if (2.13) holds over line $(i \longrightarrow j)$, we need to substitute $(\upsilon^{*}_{j,t}, \upsilon^{*}_{i,t}, P^{*}_{ij,t}, Q^{*}_{ij,t}, \ell^{*}_{ij,t})$ in (2.13) with their equivalent value from (2.25) as follows:

$$\begin{aligned}&\upsilon^{*}_{j,t} = \upsilon^{*}_{i,t} - 2(r_{ij}P^{*}_{ij,t} + x_{ij}Q^{*}_{ij,t}) + (r^{2}_{ij} + x^{2}_{ij})\ell^{*}_{ij,t} \Rightarrow\\ &\tilde{\upsilon}_{j,t} = \tilde{\upsilon}_{i,t} - 2(r_{ij}(\tilde{P}_{ij,t} - r_{ij}\frac{\varepsilon}{2}) + x_{ij}(\tilde{Q}_{ij,t} - x_{ij}\frac{\varepsilon}{2})) + (r^{2}_{ij} + x^{2}_{ij})(\tilde{\ell}_{ij,t} - \varepsilon)\\ &= \tilde{\upsilon}_{i,t} - 2(r_{ij}\tilde{P}_{ij,t} + x_{ij}\tilde{Q}_{ij,t}) + (r^{2}_{ij} + x^{2}_{ij})\tilde{\ell}_{ij,t}. \qquad (2.28)\end{aligned}$$

Hence, (2.13) holds for line $(i \longrightarrow j)$. Regarding (2.21) over line $(i \longrightarrow j)$, we need to substitute $\tilde{\upsilon}_{i,t}, \tilde{P}_{ij,t}, \tilde{Q}_{ij,t}$ and $\tilde{\ell}_{ij,t}$ in (2.21) by their equivalent from (2.25) as follows:

$$\begin{aligned}&\tilde{\upsilon}_{i,t}\tilde{\ell}_{ij,t} - \tilde{P}^{2}_{ij,t} - \tilde{Q}^{2}_{ij,t} = \upsilon^{*}_{i,t}(\ell^{*}_{ij,t} + \varepsilon) - (P^{*}_{ij,t} + r_{ij}\frac{\varepsilon}{2})^{2} - (Q^{*}_{ij,t} + x_{ij}\frac{\varepsilon}{2})^{2}\\ &= (\upsilon^{*}_{i,t}\ell^{*}_{ij,t} - {P^{*}_{ij,t}}^{2} - {Q^{*}_{ij,t}}^{2}) + \varepsilon(\upsilon^{*}_{i,t} - r_{ij}P^{*}_{ij,t} - x_{ij}Q^{*}_{ij,t} - \varepsilon(\frac{r^{2}_{ij} + x^{2}_{ij}}{4}))\\ &= \varepsilon(\upsilon^{*}_{i,t} - r_{ij}P^{*}_{ij,t} - x_{ij}Q^{*}_{ij,t} - \varepsilon(\frac{r^{2}_{ij} + x^{2}_{ij}}{4})) \qquad (2.29)\end{aligned}$$

If it is shown that under some conditions, equation (2.29) is always positive, then $\tilde{\upsilon}_{i,t}\tilde{\ell}_{ij,t} > \tilde{P}^2_{ij,t} + \tilde{Q}^2_{ij,t}$. It is clear that with a negative $P^*_{ij,t}$ and $Q^*_{ij,t}$, there would exist a ε that (2.29) becomes positive. Even, if both $P^*_{ij,t}$ and $Q^*_{ij,t}$ are positive values, it is easy to show that (2.29) is positive (Considering the phasor diagram of the voltage drop over line $(i \longrightarrow j)$ as well as the low X/R ratio in distribution systems). Since there is an $\varepsilon > 0$ that $\upsilon^*_{i,t} - r_{ij}P^*_{ij,t} - x_{ij}Q^*_{ij,t} - \varepsilon(\frac{r^2_{ij}+x^2_{ij}}{4}) > 0$, hence $\tilde{\upsilon}_{i,t}\tilde{\ell}_{ij,t} > \tilde{P}^2_{ij,t} + \tilde{Q}^2_{ij,t}$. Thus, we proved that there is a feasible solution for HC-cr with a lower objective value that attains inequality in (2.21), i.e., $\tilde{\upsilon}_{i,t}\tilde{\ell}_{ij,t} > \tilde{P}^2_{ij,t} + \tilde{Q}^2_{ij,t}$. In other words, the solution of convex conic relaxed HC model, i.e. HC-cr, is not the same as that of the original HC problem.

2.3 Linear Model of Hosting Capacity

In the previous section, it was proven that conic relaxation is not exact for the HC problem. It means that linear approximation is the only way to convexify the HC problem which will allow us to develop a simple HC model. The need for this simple model comes from modelling the uncertainty that exists in the output power of renewable energy resources (RESs). Generally, robust and stochastic optimization are two approaches to deal with uncertain parameters in constraints. However, if the deterministic model is nonlinear and non-convex, both approaches lead to computationally intractable counterparts. Further, robust counterpart of linear programming (LP) is a second order cone program (SOCP), and robust counterpart of a SOCP requires a semidefinite programming (SDP), and robust SDP becomes NP-hard. Linear approximation of HC problem leads to a LP model, which means that the robust counterpart is SOCP. Therefore, linear approximation reduces the complexity of robust counterpart. In this section, a proper linear model of the HC is presented. To do so, the equations with nonlinear terms are linearized as explained below in detail.

2.3.1 Linearizing the Relaxed Power Flow Model

Commonly, the linearization of the relaxed branch flow model is based on approximating the quadratic term in (2.10), which is the main source of nonlinearity and non-convexity. A distribution system is a graph in which lines have no orientation. So, the relaxed branch flow equations (2.11)-(2.13) holds for any graph orientation. Given an undirected graph $GR(\mathscr{N}, \mathscr{B})$, there are $2^{|\mathscr{B}|}$ orientations. In this section, we discuss two orientations: 1) every bus points toward the substation (backward orientation); and 2) every bus points away the substation (forward orientation). Fig. 2.4 shows some notations for these two orientations.

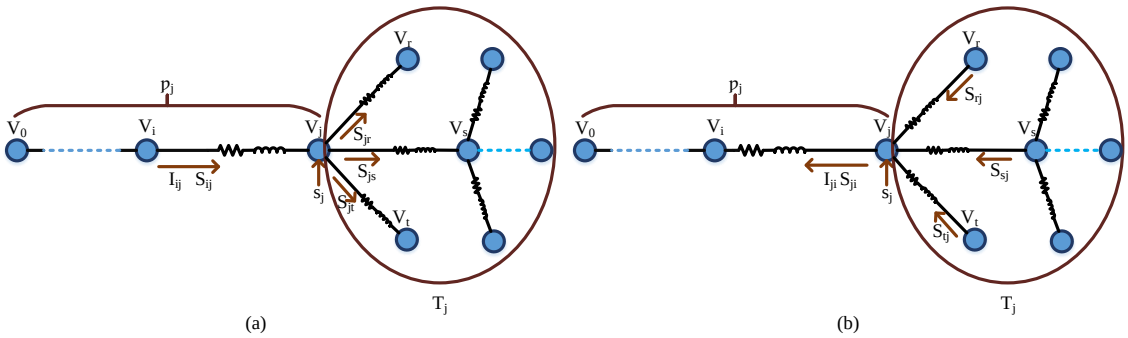

Fig. 2.4 Notation summary of the forward (a) and backward (b) orientations.

Backward orientation

In this section, without loss of generality, it is supposed that $y_i = 0 \; \forall i \in \mathscr{N}$. Considering this assumption, the relaxed power flow model reduces to (2.30)-(2.33) in backward orientation.

$$\hat{\ell}_{ji,t} = \frac{\hat{P}^2_{ji,t} + \hat{Q}^2_{ji,t}}{\hat{v}_{j,t}} \quad \forall (i,j) \in \mathscr{B}, \tag{2.30}$$

$$\hat{P}_{ji,t} = \sum_{k:k\longrightarrow j} (\hat{P}_{kj,t} - r_{kj}\hat{\ell}_{kj,t}) + p_{j,t} \quad \forall j \in \mathscr{N}, \tag{2.31}$$

$$\hat{Q}_{ji,t} = \sum_{k:k\longrightarrow j} (\hat{Q}_{kj,t} - x_{kj}\hat{\ell}_{kj,t}) + q_{j,t} \quad \forall j \in \mathscr{N}, \tag{2.32}$$

$$\hat{v}_{j,t} = \hat{v}_{i,t} + 2(r_{ji}\hat{P}_{ji,t} + x_{ji}\hat{Q}_{ji,t}) - (r^2_{ji} + x^2_{ji})\hat{\ell}_{ji,t} \quad \forall (i,j) \in \mathscr{B}, \tag{2.33}$$

if $j = 0$ then $\hat{P}_{ji,t} := 0$ and $\hat{Q}_{ji,t} := 0$. In addition, if j is a node that is connected to just one line, then all $\hat{P}_{kj,t} := 0$, $\hat{Q}_{kj,t} := 0$ and $\hat{\ell}_{kj,t} := 0$. As it was mentioned above, the key solution to convexify the problem lies in linearizing the relaxed model given in (2.30)-(2.33) via approximating the quadratic equation $\hat{\ell}_{ji,t}$, in (2.30). There are different methods to linearly approximate $\hat{\ell}_{ji,t}$. Let $\hat{\ell}^{\text{lin}}_{ji,t}$ denotes the linear approximation of $\hat{\ell}_{ji,t}$. Then, the general linear model of backward orientation is as follows:

$$\hat{P}^{\text{lin}}_{ji,t} = \sum_{k:k\longrightarrow j} (\hat{P}^{\text{lin}}_{kj,t} - r_{kj}\hat{\ell}^{\text{lin}}_{kj,t}) + p_{j,t} \quad \forall j \in \mathscr{N}, \tag{2.34}$$

$$\hat{Q}^{\text{lin}}_{ji,t} = \sum_{k:k\longrightarrow j} (\hat{Q}^{\text{lin}}_{kj,t} - x_{kj}\hat{\ell}^{\text{lin}}_{kj,t}) + q_{j,t} \quad \forall j \in \mathscr{N}, \tag{2.35}$$

$$\hat{v}^{\text{lin}}_{j,t} = \hat{v}^{\text{lin}}_{i,t} + 2(r_{ji}\hat{P}^{\text{lin}}_{ji,t} + x_{ji}\hat{Q}^{\text{lin}}_{ji,t}) - (r^2_{ji} + x^2_{ji})\hat{\ell}^{\text{lin}}_{ji,t} \quad \forall (i,j) \in \mathscr{B}. \tag{2.36}$$

The important question is whether this approximation is valid for the HC problem. Linear HC model is valid as long as the constraints of original problem would not be violated with the solution of the linear model. Linearizing the relaxed model directly affect the voltages of the system. If we make sure that the voltage of buses in linear model is higher than that of the original relaxed model, we can guarantee that the solution of linear model would not cause any voltage violation in the original model. To find the condition that $\hat{\upsilon}_{j,t} \leq \hat{\upsilon}^{\text{lin}}_{j,t} \ \forall j \in \mathscr{N}$, let $\mathbb{T}_j$ denotes the subtree rooted at bus (j) (including j). We use $k \in \mathbb{T}_j$ to refer to bus (k) in subtree $\mathbb{T}_j$ and $(k,l) \in \mathbb{T}_j$ to refer to line (k,l) in subtree $\mathbb{T}_j$. Let $\mathbb{P}_j$ denotes the set of lines on the path from substation to bus (j). For a given $\upsilon_{0,t}$ and $s_{i,t}$ $\forall i \in \mathscr{N}$, let $(\hat{P}^{\text{lin}}, \hat{Q}^{\text{lin}}, \hat{\ell}^{\text{lin}}, \hat{\upsilon}^{\text{lin}})$ and $(\hat{P}, \hat{Q}, \hat{\ell}, \hat{\upsilon})$ be solutions of the linear model (2.34)-(2.36) and the backward relaxed model (2.30)-(2.33) respectively. Then

$$\hat{P}^{\text{lin}}_{ji,t} = \sum_{k \in \mathbb{T}_j} (p_{k,t}) - \sum_{(k,l) \in \mathbb{T}_j} (r_{kl} \hat{\ell}^{\text{lin}}_{kl,t}) \quad \forall (i,j) \in \mathscr{B}, \tag{2.37}$$

$$\hat{Q}^{\text{lin}}_{ji,t} = \sum_{k \in \mathbb{T}_j} (q_{k,t}) - \sum_{(k,l) \in \mathbb{T}_j} (x_{kl} \hat{\ell}^{\text{lin}}_{kl,t}) \quad \forall (i,j) \in \mathscr{B}, \tag{2.38}$$

$$\hat{P}_{ji,t} = \sum_{k \in \mathbb{T}_j} (p_{k,t}) - \sum_{(k,l) \in \mathbb{T}_j} (r_{kl} \hat{\ell}_{kl,t}) \quad \forall (i,j) \in \mathscr{B}, \tag{2.39}$$

$$\hat{Q}_{ji,t} = \sum_{k \in \mathbb{T}_j} (q_{k,t}) - \sum_{(k,l) \in \mathbb{T}_j} (x_{kl} \hat{\ell}_{kl,t}) \quad \forall (i,j) \in \mathscr{B}. \tag{2.40}$$

Considering the unique path from each bus to substation in radial distribution systems and the equations (2.36) and (2.33), voltage of each bus can be calculated by:

$$\hat{\upsilon}^{\text{lin}}_{j,t} = \upsilon_{0,t} + \sum_{(k,l) \in \mathbb{P}_j} 2(r_{kl} \hat{P}^{\text{lin}}_{kl,t} + x_{kl} \hat{Q}^{\text{lin}}_{kl,t}) - \sum_{(k,l) \in \mathbb{P}_j} (r^2_{kl} + x^2_{kl}) \hat{\ell}^{\text{lin}}_{kl,t} \quad \forall j \in \mathscr{N}, \tag{2.41}$$

$$\hat{\upsilon}_{j,t} = \upsilon_{0,t} + \sum_{(k,l) \in \mathbb{P}_j} 2(r_{kl} \hat{P}_{kl,t} + x_{kl} \hat{Q}_{kl,t}) - \sum_{(k,l) \in \mathbb{P}_j} (r^2_{kl} + x^2_{kl}) \hat{\ell}_{kl,t} \quad \forall j \in \mathscr{N}. \tag{2.42}$$

The linear approximation of $\hat{\ell}_{kl,t}$ is either larger or smaller than $\hat{\ell}_{kl,t}$. If $\hat{\ell}^{\text{lin}}_{kl,t} \leq \hat{\ell}_{kl,t}$, then

$$\hat{P}^{\text{lin}}_{kl,t} \geq \hat{P}_{kl,t}, \hat{Q}^{\text{lin}}_{kl,t} \geq \hat{Q}_{kl,t} \quad \forall (i,j) \in \mathscr{B}, \tag{2.43}$$

$$2(r_{kl} \hat{P}^{\text{lin}}_{kl,t} + x_{kl} \hat{Q}^{\text{lin}}_{kl,t}) \geq 2(r_{kl} \hat{P}_{kl,t} + x_{kl} \hat{Q}_{kl,t}) \quad \forall (i,j) \in \mathscr{B}. \tag{2.44}$$

It means that following equations holds:

$$\upsilon_{0,t} + \sum_{(k,l) \in \mathbb{P}_j} 2(r_{kl} \hat{P}^{\text{lin}}_{kl,t} + x_{kl} \hat{Q}^{\text{lin}}_{kl,t}) \geq \upsilon_{0,t} + \sum_{(k,l) \in \mathbb{P}_j} 2(r_{kl} \hat{P}_{kl,t} + x_{kl} \hat{Q}_{kl,t}) \quad \forall j \in \mathscr{N}, \Rightarrow \tag{2.45}$$

$$\upsilon_{0,t} + \sum_{(k,l)\in\mathbb{P}_j} 2(r_{kl}\hat{P}^{\text{lin}}_{kl,t} + x_{kl}\hat{Q}^{\text{lin}}_{kl,t}) - \sum_{(k,l)\in\mathbb{P}_j} (r^2_{kl} + x^2_{kl})\hat{\ell}^{\text{lin}}_{kl,t}$$
$$\geq \upsilon_{0,t} + \sum_{(k,l)\in\mathbb{P}_j} 2(r_{kl}\hat{P}_{kl,t} + x_{kl}\hat{Q}_{kl,t}) - \sum_{(k,l)\in\mathbb{P}_j} (r^2_{kl} + x^2_{kl})\hat{\ell}^{\text{lin}}_{kl,t} \quad \forall j \in \mathscr{N}, \Rightarrow \tag{2.46}$$

$$\hat{\upsilon}^{\text{lin}}_{j,t} \geq \upsilon_{0,t} + \sum_{(k,l)\in\mathbb{P}_j} 2(r_{kl}\hat{P}_{kl,t} + x_{kl}\hat{Q}_{kl,t}) - \sum_{(k,l)\in\mathbb{P}_j} (r^2_{kl} + x^2_{kl})\hat{\ell}^{\text{lin}}_{kl,t} \quad \forall j \in \mathscr{N}, \tag{2.47}$$

since we assumed that $\hat{\ell}^{\text{lin}}_{kl,t} \leq \hat{\ell}_{kl,t}$

$$\upsilon_{0,t} + \sum_{(k,l)\in\mathbb{P}_j} 2(r_{kl}\hat{P}_{kl,t} + x_{kl}\hat{Q}_{kl,t}) - \sum_{(k,l)\in\mathbb{P}_j} (r^2_{kl} + x^2_{kl})\hat{\ell}^{\text{lin}}_{kl,t}$$
$$\geq [\upsilon_{0,t} + \sum_{(k,l)\in\mathbb{P}_j} 2(r_{kl}\hat{P}_{kl,t} + x_{kl}\hat{Q}_{kl,t}) - \sum_{(k,l)\in\mathbb{P}_j} (r^2_{kl} + x^2_{kl})\hat{\ell}_{kl,t}] = \hat{\upsilon}_{j,t} \quad \forall j \in \mathscr{N}, \tag{2.48}$$

therefore,

$$\hat{\upsilon}^{\text{lin}}_{j,t} \geq \hat{\upsilon}_{j,t} \quad \forall j \in \mathscr{N}. \tag{2.49}$$

Following the same procedure, if $\hat{\ell}^{\text{lin}}_{kl,t} \geq \hat{\ell}_{kl,t}$, then

$$\hat{P}^{\text{lin}}_{kl,t} \leq \hat{P}_{kl,t}, \hat{Q}^{\text{lin}}_{kl,t} \leq \hat{Q}_{kl,t} \quad \forall (i,j) \in \mathscr{B}, \tag{2.50}$$

$$2(r_{kl}\hat{P}^{\text{lin}}_{kl,t} + x_{kl}\hat{Q}^{\text{lin}}_{kl,t}) \leq 2(r_{kl}\hat{P}_{kl,t} + x_{kl}\hat{Q}_{kl,t}) \quad \forall (i,j) \in \mathscr{B}. \tag{2.51}$$

It means that following equations holds:

$$\upsilon_{0,t} + \sum_{(k,l)\in\mathbb{P}_j} 2(r_{kl}\hat{P}^{\text{lin}}_{kl,t} + x_{kl}\hat{Q}^{\text{lin}}_{kl,t}) \leq \upsilon_{0,t} + \sum_{(k,l)\in\mathbb{P}_j} 2(r_{kl}\hat{P}_{kl,t} + x_{kl}\hat{Q}_{kl,t}) \quad \forall j \in \mathscr{N}, \Rightarrow \tag{2.52}$$

$$\upsilon_{0,t} + \sum_{(k,l)\in\mathbb{P}_j} 2(r_{kl}\hat{P}^{\text{lin}}_{kl,t} + x_{kl}\hat{Q}^{\text{lin}}_{kl,t}) - \sum_{(k,l)\in\mathbb{P}_j} (r^2_{kl} + x^2_{kl})\hat{\ell}^{\text{lin}}_{kl,t}$$
$$\leq \upsilon_{0,t} + \sum_{(k,l)\in\mathbb{P}_j} 2(r_{kl}\hat{P}_{kl,t} + x_{kl}\hat{Q}_{kl,t}) - \sum_{(k,l)\in\mathbb{P}_j} (r^2_{kl} + x^2_{kl})\hat{\ell}^{\text{lin}}_{kl,t} \quad \forall j \in \mathscr{N}, \Rightarrow \tag{2.53}$$

$$\hat{\upsilon}^{\text{lin}}_{j,t} \leq \upsilon_{0,t} + \sum_{(k,l)\in\mathbb{P}_j} 2(r_{kl}\hat{P}_{kl,t} + x_{kl}\hat{Q}_{kl,t}) - \sum_{(k,l)\in\mathbb{P}_j} (r^2_{kl} + x^2_{kl})\hat{\ell}^{\text{lin}}_{kl,t} \quad \forall j \in \mathscr{N}, \tag{2.54}$$

since we assumed that $\hat{\ell}^{\text{lin}}_{kl,t} \geq \hat{\ell}_{kl,t}$

$$\upsilon_{0,t} + \sum_{(k,l)\in\mathbb{P}_j} 2(r_{kl}\hat{P}_{kl,t} + x_{kl}\hat{Q}_{kl,t}) - \sum_{(k,l)\in\mathbb{P}_j} (r^2_{kl} + x^2_{kl})\hat{\ell}^{\text{lin}}_{kl,t}$$

$$\leq [\upsilon_{0,t} + \sum_{(k,l)\in\mathbb{P}_j} 2(r_{kl}\hat{P}_{kl,t} + x_{kl}\hat{Q}_{kl,t}) - \sum_{(k,l)\in\mathbb{P}_j} (r_{kl}^2 + x_{kl}^2)\hat{\ell}_{kl,t}] = \hat{\upsilon}_{j,t} \quad \forall j \in \mathscr{N}, \tag{2.55}$$

therefore,

$$\hat{\upsilon}_{j,t}^{\text{lin}} \leq \hat{\upsilon}_{j,t} \quad \forall j \in \mathscr{N}. \tag{2.56}$$

In the linear model, the over-voltage constraint would limit the voltage magnitude. Thus, if the original voltage is always below the linear voltage, the estimated HC by using the linear model would not cause an over-voltage in the original model. Thus, linearization is valid as long as the linear approximation of the quadratic term (2.10), is smaller than the original quadratic term.

Forward orientation

In this orientation, the relaxed power flow model reduces to (2.57)-(2.60).

$$\acute{\ell}_{ij,t} = \frac{\acute{P}_{ij,t}^2 + \acute{Q}_{ij,t}^2}{\acute{\upsilon}_{i,t}} \quad \forall (i,j) \in \mathscr{B}, \tag{2.57}$$

$$\acute{P}_{ij,t} - r_{ij}\acute{\ell}_{ij,t} = \sum_{k:j\longrightarrow k} (\acute{P}_{jk,t}) - p_{j,t} \quad \forall j \in \mathscr{N}, \tag{2.58}$$

$$\acute{Q}_{ij,t} - x_{jk}\acute{\ell}_{jk,t} = \sum_{k:j\longrightarrow k} (\acute{Q}_{jk,t}) - q_{j,t} \quad \forall j \in \mathscr{N}, \tag{2.59}$$

$$\acute{\upsilon}_{j,t} = \acute{\upsilon}_{i,t} - 2(r_{ij}\acute{P}_{ij,t} + x_{ij}\acute{Q}_{ij,t}) + (r_{ij}^2 + x_{ij}^2)\acute{\ell}_{ij,t} \quad \forall (i,j) \in \mathscr{B}. \tag{2.60}$$

One should notice that if $j = 0$ then $\acute{P}_{ij,t} := 0$, $\acute{Q}_{ij,t} := 0$ and $\acute{\ell}_{ij,t} := 0$. In addition, if j is a node that is connected to just one line, then all $\acute{P}_{jk,t} := 0$ and $\acute{Q}_{jk,t} := 0$. Let $\acute{\ell}_{ij,t}^{\text{lin}}$ denotes the linear approximation of $\acute{\ell}_{ij,t}$. Then, the linear approximation of the forward orientation is as follows:

$$\acute{P}_{ij,t}^{\text{lin}} - r_{ij}\acute{\ell}_{ij,t}^{\text{lin}} = \sum_{k:j\longrightarrow k} (\acute{P}_{jk,t}^{\text{lin}}) - p_{j,t} \quad \forall j \in \mathscr{N}, \tag{2.61}$$

$$\acute{Q}_{ij,t}^{\text{lin}} - x_{jk}\acute{\ell}_{jk,t}^{\text{lin}} = \sum_{k:j\longrightarrow k} (\acute{Q}_{jk,t}^{\text{lin}}) - q_{j,t} \quad \forall j \in \mathscr{N}, \tag{2.62}$$

$$\acute{\upsilon}_{j,t}^{\text{lin}} = \acute{\upsilon}_{i,t}^{\text{lin}} - 2(r_{ij}\acute{P}_{ij,t}^{\text{lin}} + x_{ij}\acute{Q}_{ij,t}^{\text{lin}}) + (r_{ij}^2 + x_{ij}^2)\acute{\ell}_{ij,t}^{\text{lin}} \quad \forall (i,j) \in \mathscr{B}. \tag{2.63}$$

For a given $\upsilon_{0,t}$ and $s_{i,t}$ $\forall i \in \mathscr{N}$, let $(\acute{P}^{\text{lin}}, \acute{Q}^{\text{lin}}, \acute{\ell}^{\text{lin}}, \acute{\upsilon}^{\text{lin}})$ and $(\acute{P}, \acute{Q}, \acute{\ell}, \acute{\upsilon})$ be solutions of the linear model represented in (2.61)-(2.63) and the forward relaxed model given in (2.57)-

(2.60), respectively. Then

$$\acute{P}^{\text{lin}}_{ij,t} = -\sum_{k\in\mathbb{T}_j}(p_{k,t}) + r_{ij}\hat{\ell}^{\text{lin}}_{ij,t} + \sum_{(k,l)\in\mathbb{T}_j}(r_{kl}\hat{\ell}^{\text{lin}}_{kl,t}) \quad \forall (i,j)\in\mathscr{B}, \tag{2.64}$$

$$\acute{Q}^{\text{lin}}_{ij,t} = -\sum_{k\in\mathbb{T}_j}(q_{k,t}) + x_{ij}\hat{\ell}^{\text{lin}}_{ij,t} + \sum_{(k,l)\in\mathbb{T}_j}(x_{kl}\hat{\ell}^{\text{lin}}_{kl,t}) \quad \forall (i,j)\in\mathscr{B}, \tag{2.65}$$

$$\acute{P}_{ij,t} = -\sum_{k\in\mathbb{T}_j}(p_{k,t}) + r_{ij}\acute{\ell}_{ij,t} + \sum_{(k,l)\in\mathbb{T}_j}(r_{kl}\acute{\ell}_{kl,t}) \quad \forall (i,j)\in\mathscr{B}, \tag{2.66}$$

$$\acute{Q}_{ij,t} = -\sum_{k\in\mathbb{T}_j}(q_{k,t}) + x_{ij}\acute{\ell}_{ij,t} + \sum_{(k,l)\in\mathbb{T}_j}(x_{kl}\acute{\ell}_{kl,t}) \quad \forall (i,j)\in\mathscr{B}. \tag{2.67}$$

Considering the unique path from substation to each bus in radial systems and the equations (2.63) and (2.60), the voltage of each bus can be calculated by:

$$\acute{v}^{\text{lin}}_{j,t} = v_{0,t} - \sum_{(k,l)\in\mathbb{P}_j} 2(r_{kl}\acute{P}^{\text{lin}}_{kl,t} + x_{kl}\acute{Q}^{\text{lin}}_{kl,t}) + \sum_{(k,l)\in\mathbb{P}_j}(r^2_{kl}+x^2_{kl})\hat{\ell}^{\text{lin}}_{kl,t} \quad \forall j\in\mathscr{N}, \tag{2.68}$$

$$\acute{v}_{j,t} = v_{0,t} - \sum_{(k,l)\in\mathbb{P}_j} 2(r_{kl}\acute{P}_{kl,t} + x_{kl}\acute{Q}_{kl,t}) + \sum_{(k,l)\in\mathbb{P}_j}(r^2_{kl}+x^2_{kl})\acute{\ell}_{kl,t} \quad \forall j\in\mathscr{N}. \tag{2.69}$$

Similar to backward orientation, by substituting (2.64)-(2.67) in (2.68) and (2.69) it can be proved for the forward orientation that linear approximation is valid if $\hat{\ell}^{\text{lin}}_{kl,t} \le \acute{\ell}_{kl,t}$. One of the most used linearization method is setting $\hat{\ell}^{\text{lin}}_{kl,t} = 0$ ($\hat{\ell}^{\text{lin}}_{kl,t} = 0$ for backward orientation). Based on what we proved in this section, if the linear approximation is always smaller than the original quadratic term, the voltage obtained by linear model is always higher than the voltage obtained by the original relaxed model.

In the following, we discuss how to define a linear model by approximating the original quadratic equation in the original HC problem. Let consider a continuous function $f(tt)$ of the variable $tt \in [a,b]$ aiming to approximate it with the piecewise linear function $\hat{f}(tt)$. First, the interval $[a,b]$ is divided into smaller intervals via the points $a = tt_0 < tt_1 < tt_2 < \cdots < tt_k = b$ as shown in Fig. 2.5. Let $\lambda \in [0,1]$ to define $tt \in [tt_v, tt_{v+1}]$ as a convex combination of tt_v and tt_{v+1} as follows:

$$tt = \lambda tt_v + (1-\lambda)tt_{v+1}, \tag{2.70}$$

Then, function $f(tt)$ can be linearly approximated in interval $tt \in [tt_v, tt_{v+1}]$ as follows:

$$\hat{f}(tt) - \hat{f}(tt_v) = \frac{\hat{f}(tt_{v+1}) - \hat{f}(tt_v)}{tt_{v+1} - tt_v}(tt - tt_v), \tag{2.71}$$

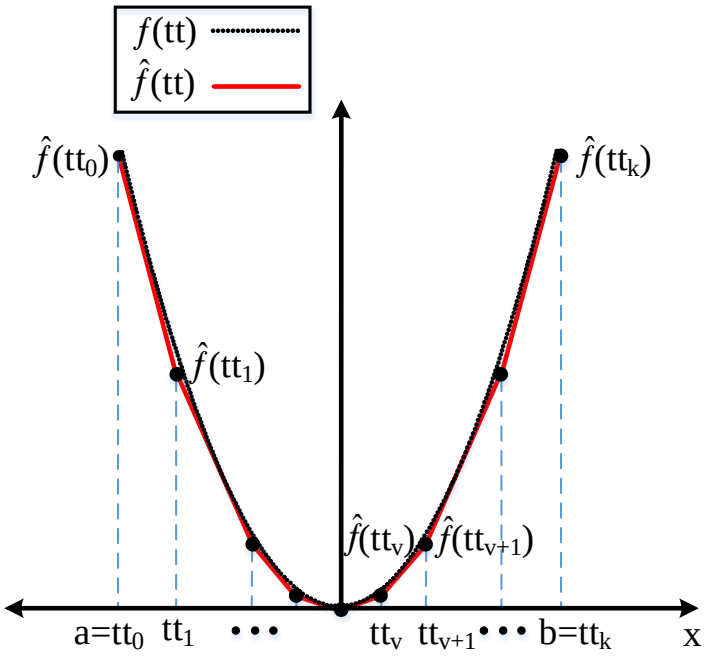

Fig. 2.5 Piecewise linear approximation of a function.

Substituting (2.70) in (2.71) results in:

$$\hat{f}(tt) = \lambda \hat{f}(tt_v) + (1-\lambda)\hat{f}(tt_{v+1}). \tag{2.72}$$

More generally, function $f(tt)$ can be approximated over interval $[a,b]$ by $\hat{f}(tt)$ via points $a = tt_0 < tt_1 < tt_2 < ... < tt_k = b$ as follows [90]:

$$tt = \sum_{v=0}^{k} \lambda_v tt_v, \quad \sum_{v=0}^{k} \lambda_v = 1, \quad \lambda_v \geq 0 \ \ \forall v \in \{0,1,2,\ldots,k\}, \tag{2.73}$$

$$\hat{f}(tt) = \sum_{v=0}^{k} \lambda_v (tt_v). \tag{2.74}$$

where, λ_v are special order set of type 2 (SOS2) variables, which means only two of them are non-zero, and they must be adjacent. It is worth mentioning that increasing the number of points increases the approximation accuracy. The above piecewise linear approximation is valid for single variable functions. In the HC problem, the nonlinear equation (2.10) is a function of (P,Q,υ), which means that we still cannot use the suggested piecewise approximation. If it is supposed that the υ is fixed, then (2.10) becomes separable. Generally, a function $f(Var_1, Var_2, ..., Var_{N_v})$ is said to be separable if it can be expressed as the sum

of N_{v} single variable functions $f_1(Var_1), f_2(Var_2), ..., f_{N_{\mathrm{v}}}(Var_{N_{\mathrm{v}}})$. Therefore, each single variable function in (2.10) can be replaced by a piecewise linear approximation. For the sake of generality, let suppose that both objective and constraints are separable functions as follows:

$$\begin{aligned} &\text{SP : minimize} \quad \sum_{j=1}^{N_{\mathrm{v}}} f_j(Var_j), \\ &\textit{subject to} \\ &\sum_{j=1}^{N_{\mathrm{v}}} g''_{i,j}(Var_j) \leq UL_i \ \ \forall i \in \{0,1,2,\ldots,NoC\}. \end{aligned} \tag{2.75}$$

Let define set $\mathscr{L}$ as follows:

$$\mathscr{L} = \{j : f_j \ \&\& g''_{i,j} \text{ are linear } \forall i \in \{1,2,\ldots,NoC\}\}. \tag{2.76}$$

Considering the interval $[a_j, b_j]$ for each $j \notin \mathscr{L}$, the grid points of jth variable, Var_j, are defined as follows:

$$a_j = Var_{0,j} < Var_{1,j} < Var_{2,j} < \cdots < Var_{k_j,j} = b_j, \tag{2.77}$$

thus, the (SP) can be approximated as follows:

$$\begin{aligned} &\text{LASP : minimize} \quad \sum_{j\in\mathscr{L}} f_j(Var_j) + \sum_{j\notin\mathscr{L}} \hat{f}_j(Var_j), \\ &\textit{subject to} \\ &\sum_{j\in\mathscr{L}} g''_{i,j}(Var_j) + \sum_{j\notin\mathscr{L}} \hat{g}''_{i,j}(Var_j) \leq UL_i \ \ \forall i \in \{0,1,2,\ldots,NoC\}, \end{aligned} \tag{2.78}$$

where

$$\hat{f}_j(Var_j) = \sum_{v=0}^{k_j} \lambda_{v,j} \hat{f}_j(Var_{v,j}) \quad \forall j \notin \mathscr{L}, \tag{2.79a}$$

$$\hat{g}''_{i,j}(Var_j) = \sum_{v=0}^{k_j} \lambda_{v,j} \hat{g}''_{i,j}(Var_{v,j}), \ \ \forall i \in \{1,2,\ldots,NoC\}, \ \ \forall j \notin \mathscr{L}, \tag{2.79b}$$

$$\sum_{v=0}^{k_j} \lambda_{v,j} = 1, \ \ \lambda_{v,j} \geq 0 \quad \forall j \notin \mathscr{L}, \tag{2.79c}$$

$$Var_j = \sum_{v=0}^{k_j} \lambda_{v,j} Var_{v,j} \quad \forall j \notin \mathscr{L}, \tag{2.79d}$$

and two adjacent $\lambda_{v,j}$ are non-zero for $j \notin \mathscr{L}$, due to which, the LASP is not a linear program anymore. This restriction can be removed by using binary variables. In other words, considering this restriction result in a mixed integer program as follows:

$$\text{LASP : minimize} \quad \sum_{j\in\mathscr{L}} f_j(Var_j) + \sum_{j\notin\mathscr{L}} \sum_{v=0}^{k_j} \lambda_{v,j} \hat{f}_j(Var_{v,j}), \tag{2.80a}$$

subject to

$$\sum_{j\in\mathscr{L}} g''_{i,j}(Var_j) + \sum_{j\notin\mathscr{L}} \sum_{v=0}^{k_j} \lambda_{v,j} \hat{g}''_{i,j}(Var_{v,j}) \leq UL_i \quad \forall i \in \{0,1,2,\ldots,NoC\}, \tag{2.80b}$$

$$0 \leq \lambda_{0,j} \leq w_{0,j} \quad j \notin \mathscr{L}, \tag{2.80c}$$

$$0 \leq \lambda_{v,j} \leq w_{v-1,j} + w_{v,j}, \quad \forall v \in \{1,2,\ldots,k_j-1\}; \ \forall j \notin \mathscr{L}, \tag{2.80d}$$

$$0 \leq \lambda_{k_j,j} \leq w_{k_j-1,j} \quad \forall j \notin \mathscr{L}, \tag{2.80e}$$

$$\sum_{v=0}^{k_j-1} w_{v,j} = 1 \quad \forall j \notin \mathscr{L}, \tag{2.80f}$$

$$\sum_{v=0}^{k_j} \lambda_{v,j} = 1 \quad \forall j \notin \mathscr{L}, \tag{2.80g}$$

$$Var_j = \sum_{v=0}^{k_j} \lambda_{v,j} Var_{v,j} \quad \forall j \notin \mathscr{L}, \tag{2.80h}$$

$$w_{v,j} = 0 \text{ or } 1, \quad \forall v \in \{0,1,2,\ldots,k_j-1\}; \ \forall j \notin \mathscr{L}. \tag{2.80i}$$

It is worth mentioning that increasing the number of break points to improve the accuracy of the approximation, increases the number of constraints and integer variables significantly. So, there is a compromise between the accuracy of the approximation and the number of break points. The minimum number of points that are needed for approximating a nonlinear function is equal to two. It means that the approximation function is a linear function passing from those two points. In such situation, the approximation results in a LP. Fig. 2.6 demonstrates two linear approximations (by using two points) that can be used in linearizing (2.10). Since in both approximations $\hat{\ell}^{\text{lin}}_{kl,t} \leq \hat{\ell}_{kl,t}$ ($\hat{\ell}^{\text{lin}}_{kl,t} \leq \acute{\ell}_{kl,t}$ in forward orientation), the linear models are valid.

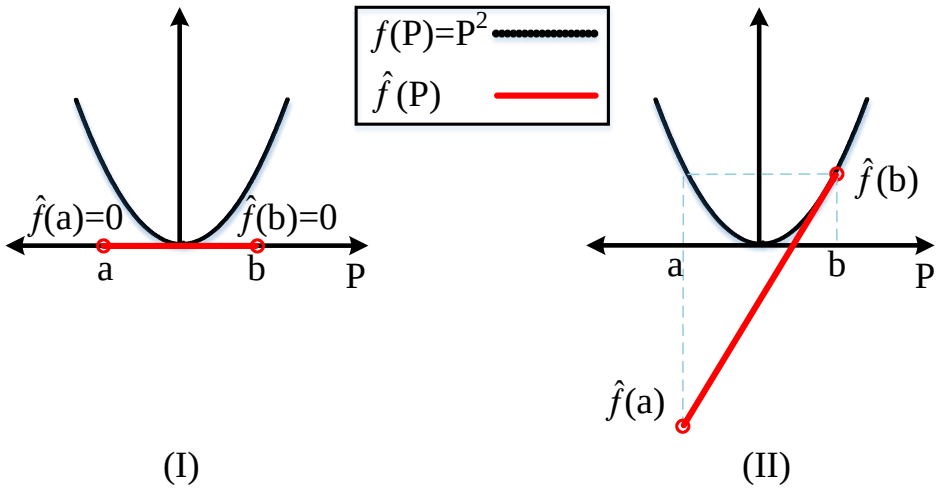

Fig. 2.6 Two linear approximation of the loss quadratic function (by using two points).

2.3.2 Linearizing the Thermal Capacity Constraint

It is important to consider the thermal capacity as one of the constraints in the HC problem. Equation (2.6) represents this constraint in the original HC problem. Multiplying (2.6) with nominal voltage leads to:

$$|S_{ij,t}| \leq \bar{S}_{ij} \quad \forall (i,j) \in \mathscr{B}, \tag{2.81}$$

$$\sqrt{P_{ij,t}^2 + Q_{ij,t}^2} \leq \bar{S}_{ij} \quad \forall (i,j) \in \mathscr{B}. \tag{2.82}$$

Equation (2.82) is a circle in (P,Q) coordination. In order to linearize this circle, we use a rotating line. The following line is tangent to the circle (2.82).

$$Q_{ij,t} + P_{ij,t} \leq \sqrt{2}\bar{S}_{ij} \quad \forall (i,j) \in \mathscr{B}, \tag{2.83}$$

in two dimensions, we can rotate the point $(P_{ij,t}, Q_{ij,t})$ by using the counterclockwise rotation matrix as follow:

$$\begin{bmatrix} P''_{ij,t} \\ Q''_{ij,t} \end{bmatrix} = \begin{bmatrix} \cos(\theta) & -\sin(\theta) \\ \sin(\theta) & \cos(\theta) \end{bmatrix} \times \begin{bmatrix} P_{ij,t} \\ Q_{ij,t} \end{bmatrix}, \tag{2.84}$$

Rotating the line (2.83) using the rotation matrix (2.84) leads to:

$$(\cos(\theta) + sin(\theta))Q''_{ij,t} + (\cos(\theta) - sin(\theta))P''_{ij,t} \leq \sqrt{2}\bar{S}_{ij} \quad \forall (i,j) \in \mathscr{B}. \tag{2.85}$$

This equation implies that for each θ, there is a line. So, a set of lines can replace the circle. The smaller the step in θ is, the higher the number of the lines and the higher the accuracy of

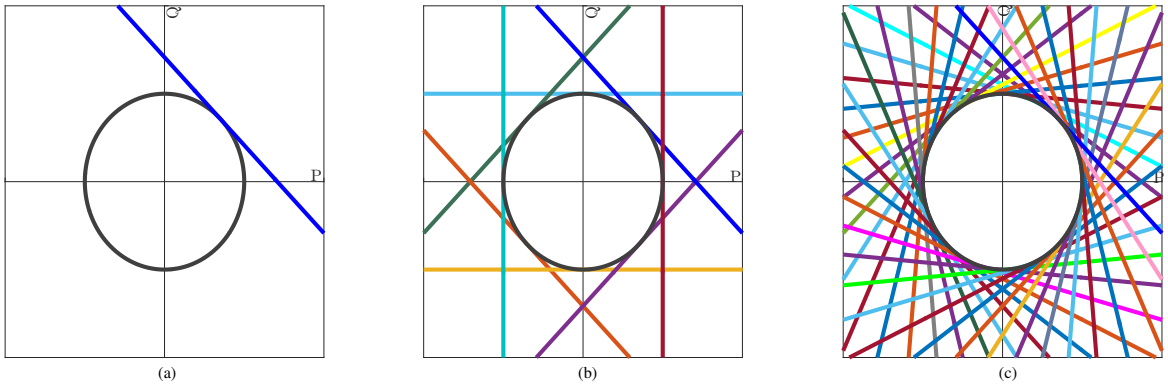

Fig. 2.7 Circular thermal capacity constraint linearization method for step sizes (B) $\theta = 45^\circ$ and (C) $\theta = 10^\circ$.

the linearization would be. Fig. 2.7 Shows the linear approximation of the thermal constraint with the proposed rotating line for step sizes $\theta = 45^\circ$ and $\theta = 10^\circ$.

After linearizing the thermal capacity constraint, the HC problem can be formulated by a LP, which is proper to be used as the base model in stochastic or robust optimization. In the next section, results of different linear models are compared.

2.4 Simulations

In this section, the performance of different linear methods is compared. The test network is the IEEE 33 buses distribution system. This network is a radial system as shown in Fig. 2.8, with a total load of 3.715 MW and 2.300 MVAr [91]. It is supposed that rating current of all lines in the test system is 500 A. The HC nonlinear and linear models are implemented in AMPL [92] environment, and solved by KNITRO and CPLEX solvers, respectively.

First the performance of the proposed piecewise linear model is assessed. Fig. 2.9 shows the voltage profile of the test grid for different number of points in (2.73) when the maximum DER capacity is installed at bus (6). As it can be seen, increasing the number of break points improves the accuracy of the proposed method. Moreover, as it was proven in section 2.3.1, the voltage profile obtained by the proposed method is always higher than that of the original model. Additionally, neglecting the loss quadratic term, which is a specific case of the proposed method, results in a higher voltage bound to the proposed model, so neglecting the loss term and the original model are two boundaries of the proposed method.

It appeared to us that neglecting the loss term (zero approximation) could have enough accuracy to approximate the voltage profile. So, what is the advantage of the proposed method? Fig. 2.10 demonstrates the advantage of our model compared to the zero approximation. As

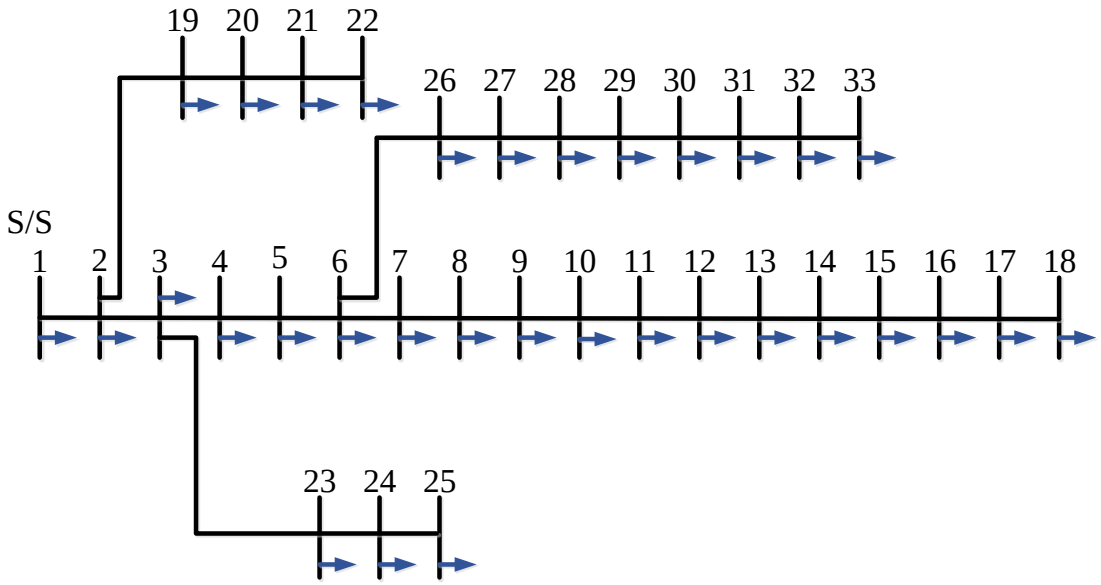

Fig. 2.8 IEEE 33-bus distribution system.

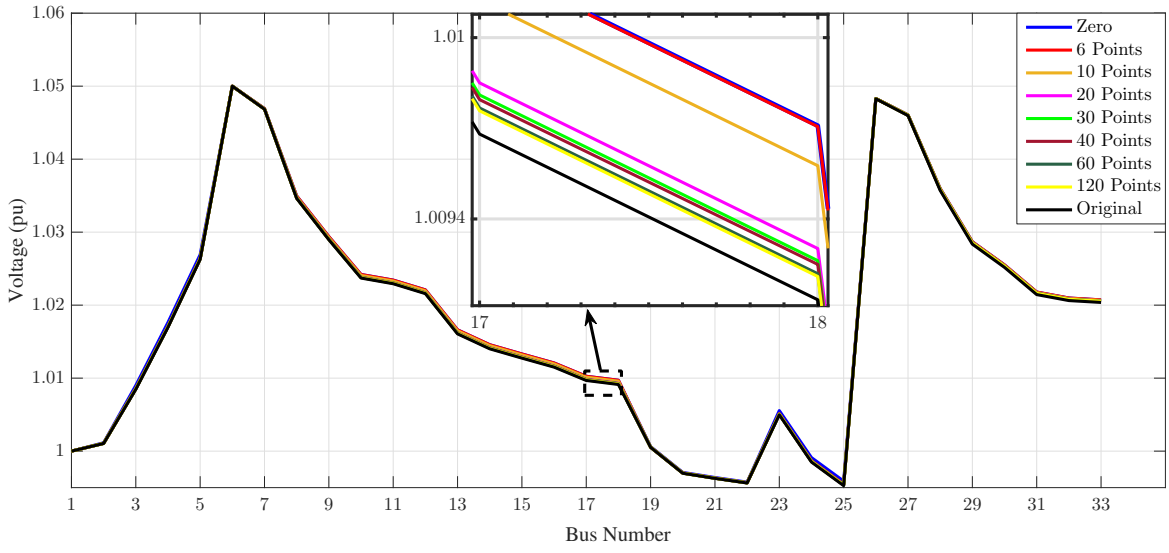

Fig. 2.9 Voltage profile of the test grid for different accuracy of the proposed piecewise linear method when the maximum distributed generation is installed at bus (6).

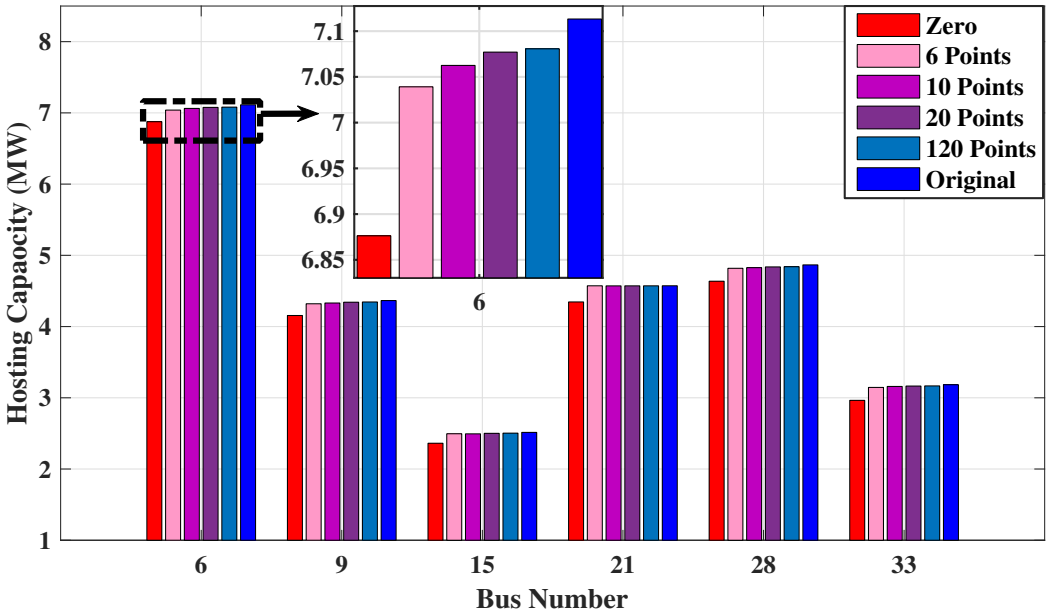

Fig. 2.10 Locational HC obtained by the proposed method for different accuracy.

it can be seen, both the proposed method and the neglection of loss term result in the lower bounds to the locational HC. Nonetheless, the lower bound obtained by the proposed method is more accurate than the obtained bound by the zero approximation of the loss term. This is because the sensitivity of the HC is very high to the voltage and a small change in the voltage could result in a tangible change in the objective function, which is HC.

HC of a system depends on quite a few technical constraints. As it was mentioned in section 1.2, three range for HC can be defined based on each technical issue. The first range determines the capacities that would not cause any violation, regardless of the location of DERs. The second range determines the capacities that are acceptable if DERs are installed at specific locations, and third range determines the capacities that would result in the violation, regardless of the location of DER. Note that these three ranges for HC of a feeder can be found by considering the technical constraints altogether or by combining the stacked bar charts of all constraints. Fig. 2.11 shows the barchart diagram of the HC of the test grid for over-voltage and thermal capacity constraints. As it can be seen in this figure, the proposed linear models for branch flow equations and thermal capacity constraints approximates the HC bar charts with high accuracy. Moreover, the combination of stacked bar charts of over-voltage and thermal capacity constraints give the same result as applying both of them at the same time. This means that it is not necessary to build a complicated HC model considering all the technical constraints. Sometimes, it is easier to identify the HC based on different technical constraint, separately. Then, the HC considering all the technical constraints can be

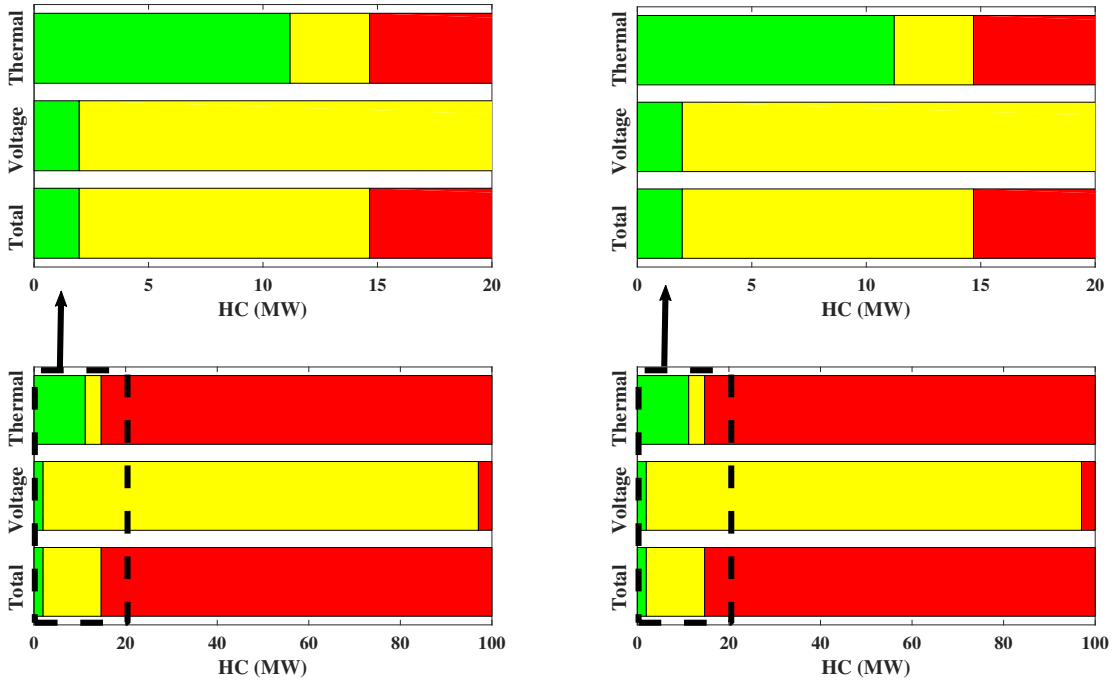

Fig. 2.11 HC bar charts obtained by the original nonlinear model and the proposed linear method.

estimated by combining the results for every constraint. This idea could be really effective to include any technical constraint in HC assessment.

Another important point that should be discussed is the importance of the constraints in the HC assessment. Fig. 2.12 demonstrates the HC obtained by the proposed method based on three constraints, namely, over-voltage, thermal, and back-feed constraints. As it can be seen, back-feed put a lower limit on the HC in comparison to the over-voltage and thermal constraints. Another observation is that the thermal constraint is more important than over-voltage constraint at the beginning of the feeder. Performing this analysis can help DSOs to understand the available options to increase the HC effectively. For instance, Fig. 2.13 demonstrates the HC stacked bar charts with relaxation of the back-feed constraint. As it can be seen, this relaxation increases the second range of the HC. Therefore, one available option to effectively increase the HC could be modifying the network to allow bidirectional power flow. In this regard, DSOs may need to readjust the control setting of the voltage regulators or replace the protection relay of circuit breaker.

In the second part of the simulation results, we compare the performance of different linearization methods. The linear methods to be compared are as follows:

A : Linearizing the relaxed power flow with $\hat{\ell}^{\text{lin}}_{ij,t} = 0 \;\; \forall (i,j) \in \mathscr{B}$ [93, 37].

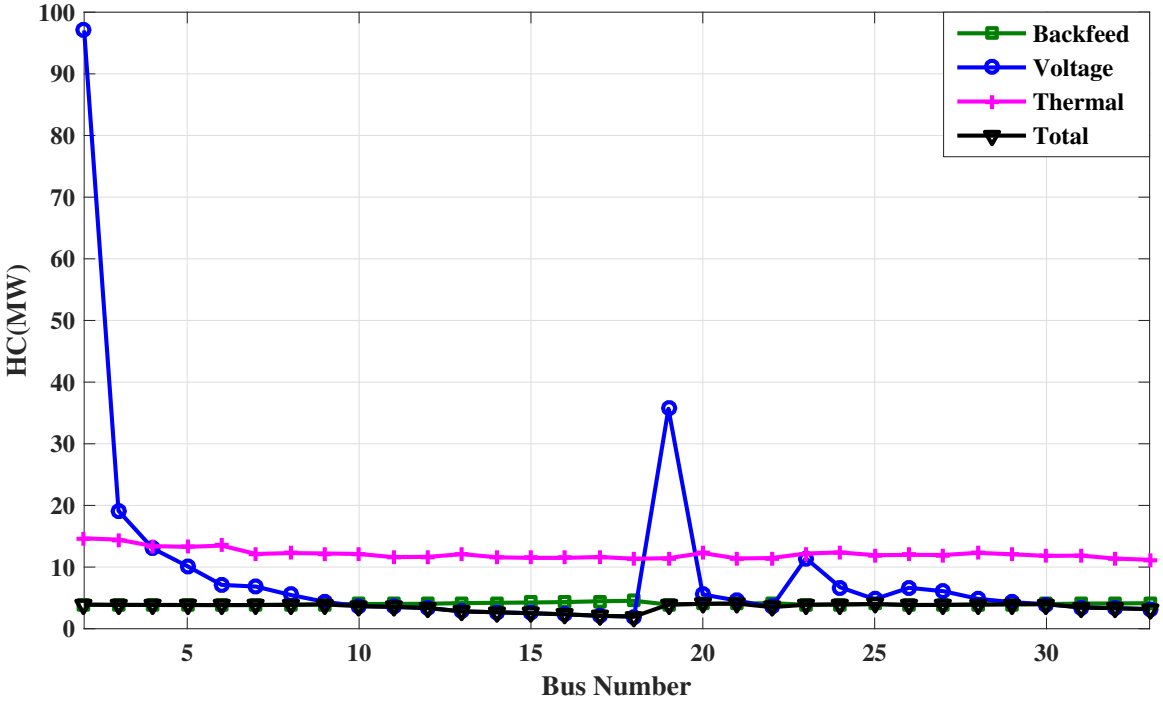

Fig. 2.12 Locational HC based on over-voltage, back-feed, and thermal capacity constraints obtained by the proposed linear method.

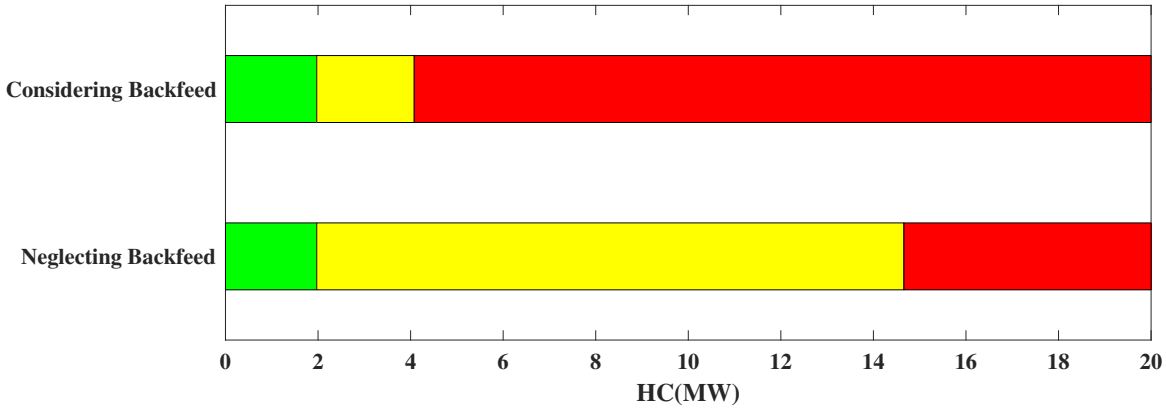

Fig. 2.13 Effect of the back-feed constraint relaxation on the HC.

B : Linear relaxed power flow proposed in [94]: in this model, the $\acute{\ell}_{ij,t} \approx \hat{\ell}^{\text{lin}}_{ij,t} := \frac{1}{\upsilon_{0,t}}(2P^0_{ij,t}P_{ij,t} + 2Q^0_{ij,t}Q_{ij,t} - {P^0_{ij,t}}^2 - {Q^0_{ij,t}}^2)$, in which, $P^0_{ij,t}$ and $Q^0_{ij,t}$ are the line $(i \longrightarrow j)$ initial active and reactive power flows.

C : Linearizing the relaxed power flow with $\acute{\ell}_{ij,t} \approx \hat{\ell}^{\text{lin}}_{ij,t} := \frac{1}{\upsilon^0_{j,t}}(2P^0_{ij,t}P_{ij,t} + 2Q^0_{ij,t}Q_{ij,t} - {P^0_{ij,t}}^2 - {Q^0_{ij,t}}^2)$, in which, $P^0_{ij,t}$ and $Q^0_{ij,t}$ are the line $(i \longrightarrow j)$ initial active and reactive power flows and $\upsilon^0_{j,t}$ is the square of the initial voltage magnitude at bus (j).

D Neglecting the $\acute{\ell}_{ij,t}$ in (2.11)-(2.12), and using the linear approximation $\acute{\ell}_{ij,t} \approx \hat{\ell}^{\text{lin}}_{ij,t} := \frac{1}{\upsilon_{0,t}}(2P^0_{ij,t}P_{ij,t} + 2Q^0_{ij,t}Q_{ij,t} - {P^0_{ij,t}}^2 - {Q^0_{ij,t}}^2)$ in (2.13).

E : Linearizing the relaxed power flow with $\acute{\ell}_{ij,t} \approx \hat{\ell}^{\text{lin}}_{ij,t} := \frac{1}{\upsilon_{0,t}}(P^0_{ij,t}P_{ij,t} + Q^0_{ij,t}Q_{ij,t})$, in which, $P^0_{ij,t}$ and $Q^0_{ij,t}$ are the initial distribution line power flows.

F : The traditional linear power flow model: in this model, $\Delta V_{ij,t} \simeq \frac{r_{ij}P^r_{ij,t} + x_{ij}Q^r_{ij,t}}{|V_{0,t}|}$, in which $\Delta V_{ij,t}$ represents the voltage change from bus (i) to bus (j). Further, $S^r_{ij,t} := S_{ij,t} - z_{ij}|I_{ij,t}|^2$ denotes the receiving complex power at bus (j) from bus (i).

G : The traditional linear model proposed in [25]: in this model, $\Delta V_{ij,t} \simeq \frac{r_{ij}P^r_{ij,t} + x_{ij}Q^r_{ij,t}}{|V^0_{j,t}|}$, in which $|V^0_{j,t}|$ is the initial voltage magnitude of bus (j).

H : The proposed piecewise linear function with four points.

In the following, the performance of these methods in approximating the voltage of the system is assessed. Fig. 2.14 demonstrates the voltage profile of the test grid by using the above mentioned linear power flow approximations. As it can be seen, the voltage profile obtained by the proposed piecewise linear method (H) and linear approximation (A) is always higher than the original profile. Additionally, it can be observed that all these linear methods have good performance in approximating the voltage. So, we need another index to compare the performance of these methods.

Fig. 2.15 shows the HC of the test grid obtained by different linear power flow model. As it can be seen, these linearization methods result in a lower approximation of the HC and the proposed piecewise linear method is more accurate than other models. It is also observed that the performance of other linear models (A, B, C, D, E, F, G) depends on the characteristics of the system and each of them could have the highest performance at some locations. Further, Fig. 2.16 shows the box plot of error in estimating the HC for different linear methods. On each box, the red and purple central marks are the mean and median, the horizontal edges are the 25th and 75th percentiles, the whiskers extend to the most extreme

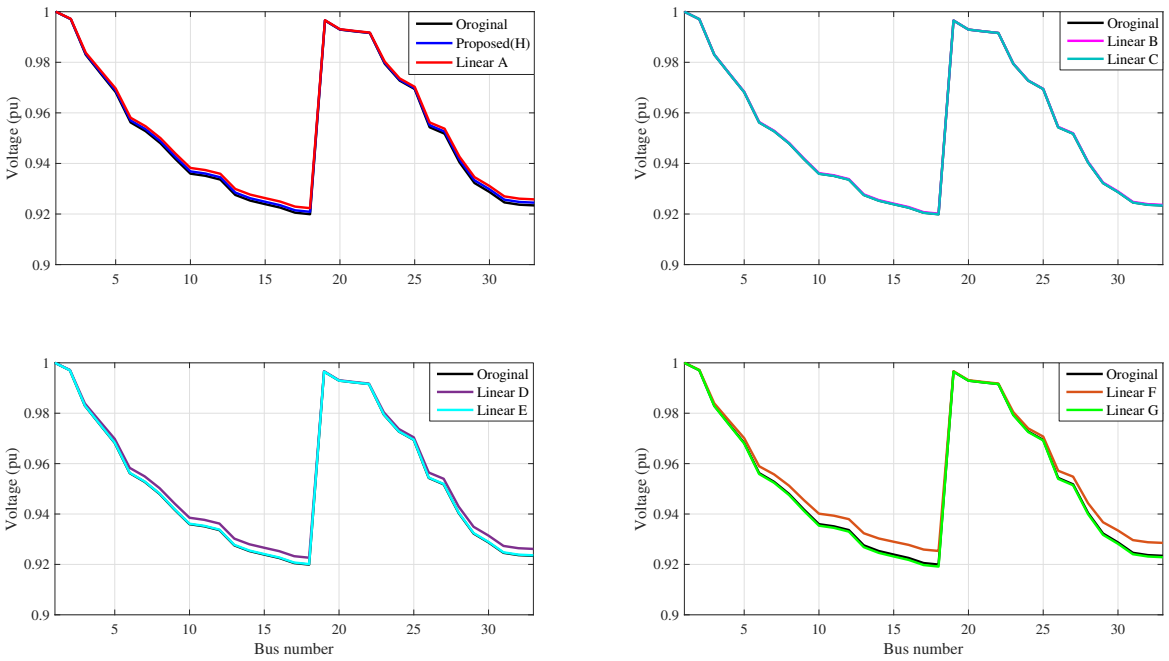

Fig. 2.14 Voltage profile of the test grid obtained by different linear models (A, B, C, D, E, F, G, H).

values not considered outliers, and outliers, i.e. yellow dots, are plotted individually. As it can be seen, the proposed method has the lowest error with an average error of 0.378%. Moreover, after the proposed methods, linear models D and A with an average error of 4.38% and 4.86% have the highest performance.Furthermore, models B and C with an average error of 6.56% and 6.74% have the worst performance in estimating the HC of the test system. This implies that a linearization method might have an acceptable performance in approximating the voltage in absence of DERs. However, it might have a poor performance in modeling the HC.

2.5 Summary

In this chapter, the HC modeling of radial distribution systems is presented. First, it is proved that conic relaxation for the HC problem is not exact. In other words, one cannot solve a convex conic program instead of the original non-convex model. Then, the conditions under which the linearization of the relaxed branch flow model is valid for the HC problem, is identified. It is demonstrated that linearization of the relaxed power flow model is valid if the linear approximation of the branch losses is less than the actual quadratic term. Further, a linear model for the thermal capacity constraint is proposed. Finally, different linear HC

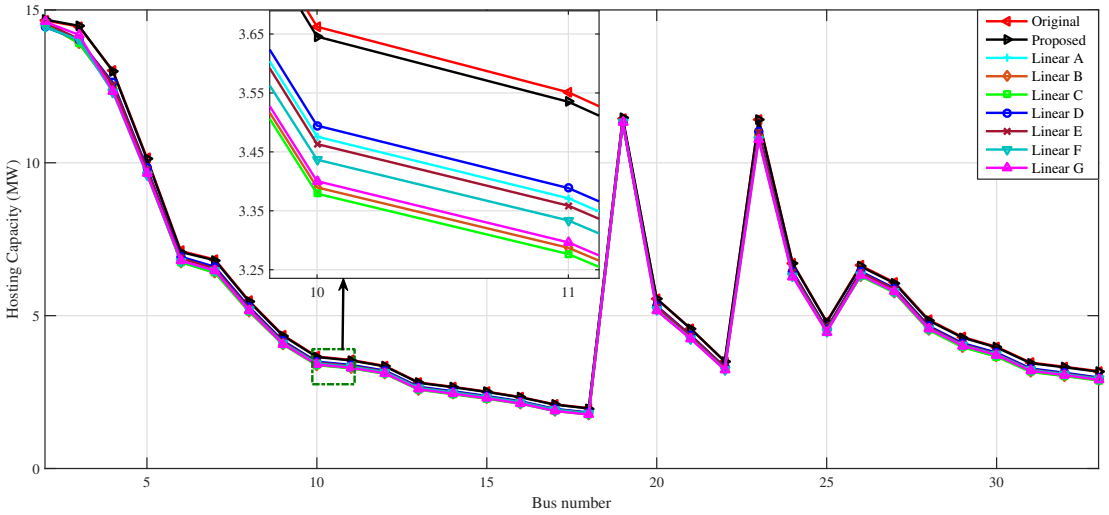

Fig. 2.15 Locational HC of the test grid obtained by different linear models (A, B, C, D, E, F, G, H).

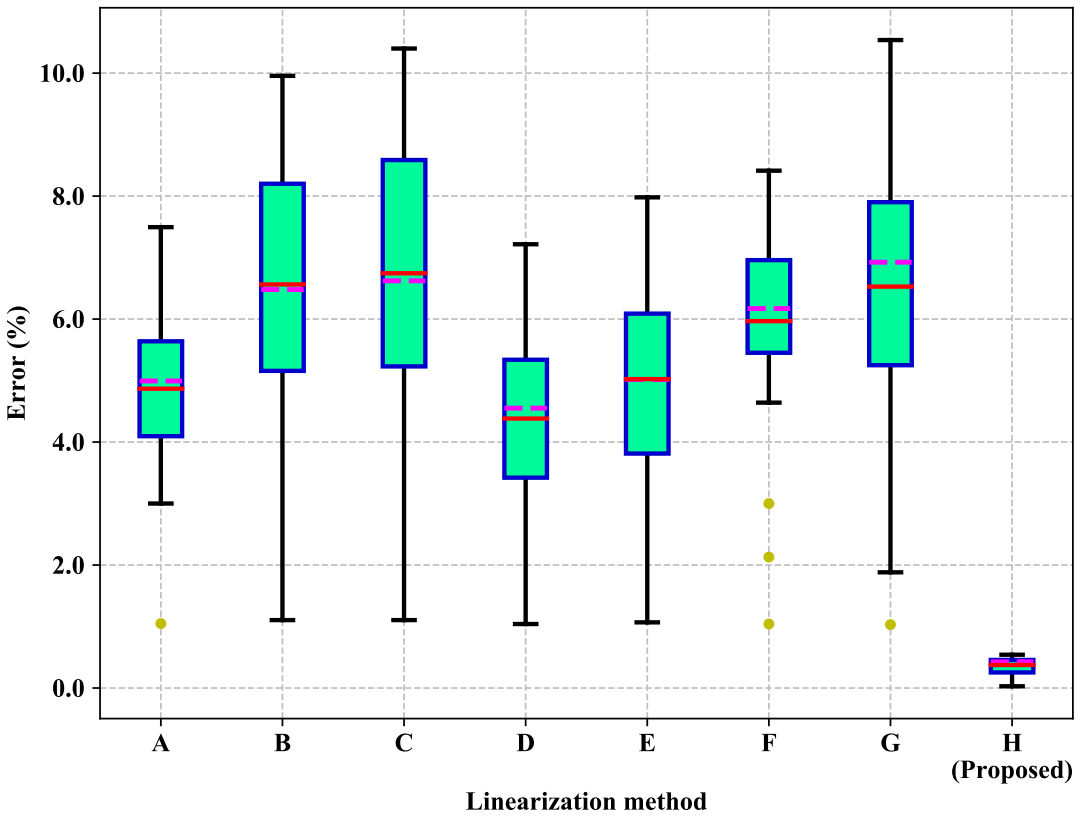

Fig. 2.16 Error in the estimated HC of the test grid obtained by different linear models (A, B, C, D, E, F, G, H).

model were examined on the IEEE 33-bus system to compare the effectiveness and suitability of each one of them. Based on the simulation results, the following conclusions can be made in order:

- It was observed that if the conductor type is the same for all branches, the thermal capacity constraint is the main limiting factor of the HC for the location which are closer to the substation. However, for the locations that are far from the substation, the main limiting factor is voltage constraint. In other words, increasing the distance from substation decreases the importance of the thermal capacity constraint and increases the importance of the voltage constraint.
- The investigated linear models in section (1.4) results in lower bounds to the HC of the feeder, which is close to actual HC. Moreover, proposed piecewise linear method and the proposed method (D) have the highest performance in the HC calculation.

Chapter 3

Probabilistic Assessment of Hosting Capacity in Radial Distribution Systems

3.1 Introduction

As mentioned in Chapter 1, uncertainties associated with the loads and distributed energy resources (DERs) are important factors that could affect the hosting capacity (HC) of a distribution system. Generally, there are two approaches to consider the uncertainties. The first approach is based on Monte Carlo simulation, in which a high number of scenarios are generated. Then, power flow calculation is performed for all the scenarios. The drawback of this approach is its computational burden. The second approach is based on optimization. In this approach, stochastic and robust techniques have been used to address the uncertainties associated with the loads and output power of DERs. However, modelling the uncertainty associated with the location and size of DERs is challenging in this approach. Our aim in this chapter is exploiting the advantages of both approaches by combining them.

In Chapter 2, we assessed the performance of HC deterministic model. In this chapter, we propose a probabilistic framework that considers the uncertainties of loads and DERs in the HC estimation of radial distribution systems. The framework includes formulation of the HC, which is represented by an optimization problem considering the over-voltage and voltage deviation constraints. Note that for considering the voltage deviation constraint at a location, we need to compare the voltage of that location with and without a DER. Therefore, considering the voltage deviation constraint in the HC model results in an unsolvable optimization problem. In order to solve the formulated HC problem, a two-step algorithm is proposed to linearize the HC model and to derive a solvable and accurate equivalent model. The modified HC optimization problem is integrated in our framework and validated using a balanced

system (i.e., an agricultural distribution network in Australia) and an unbalanced system (i.e., the IEEE 123-bus network). The outcome of this chapter is published as a conference[1] and a journal paper[2].

The remainder of this chapter is organized as follows: Section 3.2 formulates the problem. Section 3.3 presents the proposed methodology. First, a two-step linearization method is described to linearize the HC model. Then, a probabilistic framework is developed to assess DER uncertainties and load variation. Section 3.4 presents the test feeder, numerical results and discussion. Finally, the major conclusions are summarized in Section 3.5.

3.2 Problem Formulation

We already defined most of the variables for modelling distribution systems. However, in order to make the thesis easy to follow, we reintroduce them here. Consider the radial network. Let $\mathscr{N} = \{0, \ldots, n\}$ denotes the set of buses, and $\mathscr{DG} = \{\mathrm{B}_1^{\mathrm{dg}}, \ldots, \mathrm{B}_n^{\mathrm{dg}}\}$ represents the set of buses that have a DER ($\mathscr{DG} \subset \mathscr{N}$). Let $\mathscr{B}$ denotes the set of all branches, and (i, j) or $i \longrightarrow j$ represents a branch from bus (i) to bus (j) in set $\mathscr{B}$. Let $\mathscr{H}$ denote the set of all time steps. For every bus $i \in \mathscr{N}$ and for every $t \in \mathscr{H}$, let $V_{i,t}$ denote the complex voltage, and define $\upsilon_{i,t} = |V_{i,t}|^2$; Let $S_{i,t}^{\mathrm{d}} = p_{i,t}^{\mathrm{d}} + iq_{i,t}^{\mathrm{d}}$ represents the load at bus (i). For every line $(i, j) \in \mathscr{B}$ and for every $t \in \mathscr{H}$, let $z_{ij} = r_{ij} + ix_{ij}$ denote the impedance, $S_{ij,t} = P_{ij,t} + iQ_{ij,t}$ the sending-end complex power from bus (i) to bus (j), and $I_{ij,t}$ the sending-end complex current from bus (i) to bus (j) . For every bus $i \in \mathscr{DG}$ and for every $t \in \mathscr{H}$, let $s_{i,t}^{\mathrm{g}} = p_{i,t}^{\mathrm{g}} + iq_{i,t}^{\mathrm{g}}$ denote the generation complex power. Let $\mathbb{T}_j$ denote the subtree rooted at bus (j) (including (j)). We use $k \in \mathbb{T}_j$ to refer to bus (k) in subtree $\mathbb{T}_j$ and $(k, l) \in \mathbb{T}_j$ to refer to line (k, l) in subtree $\mathbb{T}_j$. Let $\mathbb{P}_j$ denote the set of lines on the path from substation to bus (j). As shown in Chapter 2, the following equation can be written based on the Ohm's law:

$$\upsilon_{j,t} = \upsilon_{i,t} - 2(r_{ij}P_{ij,t} + x_{ij}Q_{ij,t}) + |z_{ij}|^2 \frac{P_{ij,t}^2 + Q_{ij,t}^2}{\upsilon_{i,t}}, \forall (i, j) \in \mathscr{B}, \tag{3.1}$$

and according to the nodal power balance equations, we have:

$$P_{ij,t} = \sum_{k:j \longrightarrow k} P_{jk,t} + p_{j,t}^{\mathrm{d}} - p_{j,t}^{\mathrm{g}} + r_{ij} \frac{P_{ij,t}^2 + Q_{ij,t}^2}{\upsilon_{i,t}}, \ \forall j \in \mathscr{DG}, \tag{3.2}$$

$$P_{ij,t} = \sum_{k:j \longrightarrow k} P_{jk,t} + p_{j,t}^{\mathrm{d}} + r_{ij} \frac{P_{ij,t}^2 + Q_{ij,t}^2}{\upsilon_{i,t}}, \ \forall j \in \{\mathscr{N} \setminus \mathscr{DG}\}, \tag{3.3}$$

[1] "Sensitivity of hosting capacity to data resolution and uncertainty modeling," in 2018 Australasian Universities Power Engineering Conference (AUPEC), Nov 2018, pp. 1–6 [95].

[2] "Probabilistic assessment of hosting capacity in radial distribution systems," IEEE Transactions on Sustainable Energy, 2018 [96].

$$Q_{ij,t} = \sum_{k:j\longrightarrow k} Q_{jk,t} + q^{\mathrm{d}}_{j,t} - q^{\mathrm{g}}_{j,t} + x_{ij}\frac{P^2_{ij,t}+Q^2_{ij,t}}{\upsilon_{i,t}},\ \forall j \in \mathscr{DG}, \tag{3.4}$$

$$Q_{ij,t} = \sum_{k:j\longrightarrow k} Q_{jk,t} + q^{\mathrm{d}}_{j,t} + x_{ij}\frac{P^2_{ij,t}+Q^2_{ij,t}}{\upsilon_{i,t}},\ \forall j \in \{\mathscr{N}\setminus\mathscr{DG}\}. \tag{3.5}$$

considering the unique path from the substation to each bus, the voltage at bus (j) can be calculated as follows:

$$\upsilon_{j,t} = \upsilon_{0,t} - \sum_{(l,k)\in\mathbb{P}_j} 2(r_{ij}P_{ij,t} + x_{ij}Q_{ij,t}) + \sum_{(l,k)\in\mathbb{P}_j} |z_{ij}|^2\frac{P^2_{ij,t}+Q^2_{ij,t}}{\upsilon_{i,t}},\quad \forall (i,j)\in\mathscr{B}. \tag{3.6}$$

The focus of this chapter is to identify the HC of a distribution system based on the voltage quality impacts of DERs, so in addition to the power flow equations, the over-voltage and voltage deviation constraints must be satisfied, as follows:

$$\underline{\upsilon} \le \upsilon_{i,t} \le \overline{\upsilon}, \qquad \forall i \in \mathscr{N}, \tag{3.7}$$

$$|V_{i,t}| - |V^{\mathrm{NDG}}_{i,t}| \le \overline{\Delta V}, \quad \forall i \in \mathscr{DG}, \tag{3.8}$$

where, $\underline{\upsilon}$, $\overline{\upsilon}$, $\overline{\Delta V}$ and $|V^{\mathrm{NDG}}_i|$, are the square of minimum acceptable voltage, the square of maximum acceptable voltage, the maximum voltage deviation, and the voltage of bus (i) when the DER at bus (i) is disconnected, respectively. The voltage deviation is defined as the difference between the bus voltage with and without a DER. Thus, the deterministic HC problem is formulated as follows:

$$\begin{aligned} &\underset{p^{\mathrm{g}}_{i,t}}{\text{maximize}} \quad \sum_{i\in\mathscr{DG}} p^{\mathrm{g}}_{i,t}, \\ &\text{s.t.}\ \ (2)-(8). \end{aligned} \tag{3.9}$$

This is a deterministic model of the HC, i.e., the location of DERs and other uncertain parameters must be given. The solution of this optimization problem is the HC of the system for the given condition. However, in practice, it is difficult to quantify the number, location, and the output of DERs. Further, all studies that model the HC as an optimization problem used a set of predefined locations for DERs. Additionally, they usually used robust optimization techniques to model uncertainties of load and DERs' output power, which can result in a conservative approximation of the HC of a system. Thus, the proposed methodology should be able to deal with uncertain number and location of DERs. Additionally, the proposed method should not result in a conservative HC.

3.3 Methodology

A probabilistic framework is proposed in this section to deal with the uncertainty in load, the set $\mathscr{DG}$ (i.e., the number and location of DERs), and the output power of DERs. This framework is based on the linearized HC model (3.9) and is presented in section 3.3.2. The HC formulation (3.9) is a nonlinear optimization problem, hence solving it for big distribution systems is difficult if possible (due to constraint (3.8)). To deal with this issue, we propose a two-step method in section 3.3.1 to derive a solvable equivalent model for (3.9).

3.3.1 Linearization of the Original Model

The source of nonlinearity in equations (3.2)-(3.6) is the following term:

$$f_{ij}(P_{ij,t}, Q_{ij,t}, \upsilon_{i,t}) = \frac{P_{ij,t}^2 + Q_{ij,t}^2}{\upsilon_{i,t}}, \quad \forall (i,j) \in \mathscr{B}. \tag{3.10}$$

Therefore, any linearizion method has to deal with this term in (3.2)-(3.6). Given an operating point $(P_{ij,t}^0, Q_{ij,t}^0, \upsilon_{i,t}^0)$, the first order Taylor approximation of f_{ij} for all $(i,j) \in \mathscr{B}$ is as follows:

$$\begin{aligned} f_{ij}(P_{ij,t}, Q_{ij,t}, \upsilon_{i,t}) \approx & \frac{1}{\upsilon_{i,t}^0}(2P_{ij,t}^0 P_{ij,t} + 2Q_{ij,t}^0 Q_{ij,t}) \\ & - \frac{1}{\upsilon_{i,t}^0}((P_{ij,t}^0)^2 + (Q_{ij,t}^0)^2) - \frac{(P_{ij,t}^0)^2 + (Q_{ij,t}^0)^2}{(\upsilon_{i,t}^0)^2}(\upsilon_{i,t} - \upsilon_{i,t}^0), \end{aligned} \tag{3.11}$$

the third right hand side term in (3.11) is smaller than other terms because of having $(\upsilon_{i,t}^0)^2$ in the denominator, so we can neglect it and approximate (3.11) as follows:

$$\begin{aligned} f_{ij}(P_{ij,t}, Q_{ij,t}, \upsilon_{i,t}) \approx L_{ij}(P_{ij,t}, Q_{ij,t}) = & \frac{1}{\upsilon_{i,t}^0}(2P_{ij,t}^0 P_{ij,t} + 2Q_{ij,t}^0 Q_{ij,t}) \\ & - \frac{1}{\upsilon_{i,t}^0}((P_{ij,t}^0)^2 + (Q_{ij,t}^0)^2), \ \forall (i,j) \in \mathscr{B}, \end{aligned} \tag{3.12}$$

where, L_{ij} is the linear approximation of nonlinear term f_{ij}. Next issue is related to constraint (3.8), which compares the voltage of a node with and without a DER. However, we either have a DER at a node or we do not. To deal with this situation, we focus on this constraint from the power injection point of view. The whole point of this constraint is limiting the maximum DER capacity that can be installed at a location. Therefore, the constraint (3.8) can be replaced by the following equation:

$$p_{i,t}^{\mathrm{g}} \leq \overline{p_{i,t}^{\mathrm{g}}}, \qquad \forall i \in \mathscr{DG}, \tag{3.13}$$

where, $\overline{p^{\mathrm{g}}_{i,t}}$ is the maximum acceptable DER at bus (i) based on the voltage deviation constraint. The higher the $\overline{\Delta V}$, the higher the $\overline{p^{\mathrm{g}}_{i,t}}$. To find $\overline{p^{\mathrm{g}}_{i,t}}$, we use (3.12) to linearize constraints (3.2)-(3.6). Using this set of linear equations, the voltage of all buses before DER installation is obtained. Then, the maximum voltage at each bus is obtained as follows:

$$\overline{V_{i,t}} = |V^{\mathrm{NDG}}_{i,t}| + \overline{\Delta V}, \quad \forall i \in \mathscr{DG}, \tag{3.14}$$

where, $\overline{V_{i,t}}$ is the maximum voltage at bus (i) considering the voltage deviation constraint. For every bus $i \in \mathscr{DG}$, $\overline{p^{\mathrm{g}}_{i,t}}$ is obtained by solving the following model:

$$\begin{aligned}
&\underset{p^{\mathrm{g}}_{i,t}}{\text{maximize}} \quad p^{\mathrm{g}}_{i,t},\\
&\text{s.t.}\\
&(7) \text{ and the linearized } (2)-(6) \text{ using } (12),\\
&\upsilon_{i,t} \le \overline{V_{i,t}}^2.
\end{aligned} \tag{3.15}$$

Thus, for a given operating point, the HC model is as follows:

$$\underset{p^{\mathrm{g}}_{i,t}}{\text{maximize}} \quad \sum_{i \in \mathscr{DG}} p^{\mathrm{g}}_{i,t}, \tag{3.16a}$$

s.t.

$$P_{ij,t} = \sum_{k:j \longrightarrow k} P_{jk,t} + p^{\mathrm{d}}_{j,t} - p^{\mathrm{g}}_{j,t} + r_{ij}L_{ij}(P_{ij,t}, Q_{ij,t}),\ \forall j \in \mathscr{DG}, \tag{3.16b}$$

$$P_{ij,t} = \sum_{k:j \longrightarrow k} P_{jk,t} + p^{\mathrm{d}}_{j,t} + r_{ij}L_{ij}(P_{ij,t}, Q_{ij,t}),\ \forall j \in \{\mathscr{N} \setminus \mathscr{DG}\}, \tag{3.16c}$$

$$Q_{ij,t} = \sum_{k:j \longrightarrow k} Q_{jk,t} + q^{\mathrm{d}}_{j,t} - q^{\mathrm{g}}_{j,t} + x_{ij}L_{ij}(P_{ij,t}, Q_{ij,t}),\ \forall j \in \mathscr{DG}, \tag{3.16d}$$

$$Q_{ij,t} = \sum_{k:j \longrightarrow k} Q_{jk,t} + q^{\mathrm{d}}_{j,t} + x_{ij}L_{ij}(P_{ij,t}, Q_{ij,t}),\ \forall j \in \{\mathscr{N} \setminus \mathscr{DG}\}, \tag{3.16e}$$

$$\begin{aligned}
\upsilon_{j,t} = \upsilon_{0,t} &- \sum_{(l,k) \in \mathbb{P}_{j,t}} 2(r_{ij}P_{ij,t} + x_{ij}Q_{ij,t})\\
&+ \sum_{(l,k) \in \mathbb{P}_{j}} |z_{ij}|^2 L_{ij}(P_{ij,t}, Q_{ij,t}), \quad \forall (i,j) \in \mathscr{B},
\end{aligned} \tag{3.16f}$$

$$\upsilon_{i,t} \le \overline{\upsilon}, \qquad \forall i \in \mathscr{N}, \tag{3.16g}$$

$$p^{\mathrm{g}}_{i,t} \le \overline{p^{\mathrm{g}}_{i,t}}, \qquad \forall i \in \mathscr{DG}. \tag{3.16h}$$

Occasionally, the base capacity of DERs are given and the aim of HC problem is to determine the number of DERs at each bus. To address this situation, we need to replace the model of

DERs in (3.16) as follows:

$$p^{\mathrm{g}}_{i,t} = Cap^{\mathrm{g}}_{i,t} N^{\mathrm{g}}_{i,t} \eta^{\mathrm{g}}_{i,t},\ \forall i \in \mathscr{DG}, \tag{3.17}$$

where, $Cap^{\mathrm{g}}_{i,t}$ and $N^{\mathrm{g}}_{i,t}$ are the base capacity and number of units at bus (i), respectively. This new model is an integer linear program (ILP) and the results of solving this model is the number of units that can be installed at each location. To assure that there is at least one DER unit at each location, we consider the following constraint.

$$N^{\mathrm{g}}_{i,t} \geq 1, \quad \forall i \in \mathscr{DG}. \tag{3.18}$$

The prerequisite of using the HC linear model (3.16) is knowing the operating point. Note that the accuracy of the operating point approximation directly affects the results of (3.16). The difficulty in finding the operating point is that it is the final solution of the model (3.9), which is the main reason of the linearization. Approximation of the operating point starts with simplification of the HC model (3.16). Since the nonlinear terms in (3.2)-(3.6) are much smaller than the other terms, they can be neglected for such studies [97] without compromising the results. We will come to this point when discussing the results in section 3.4.2. Considering this, the HC model (3.16) can be simplified into the following linear optimization problem, which is independent of the operating point.

$$\underset{p^{\mathrm{g}}_{i,t}}{\text{maximize}} \quad \sum_{i \in \mathscr{DG}} p^{\mathrm{g}}_{i,t}, \tag{3.19a}$$

s.t.

$$P_{ij,t} = \sum_{k:\, j \longrightarrow k} P_{jk,t} + p^{\mathrm{d}}_{j,t} - p^{\mathrm{g}}_{j,t},\ \forall j \in \mathscr{DG}, \tag{3.19b}$$

$$P_{ij,t} = \sum_{k:\, j \longrightarrow k} P_{jk,t} + p^{\mathrm{d}}_{j,t},\ \forall j \in \{\mathscr{N} \setminus \mathscr{DG}\}, \tag{3.19c}$$

$$Q_{ij,t} = \sum_{k:\, j \longrightarrow k} Q_{jk,t} + q^{\mathrm{d}}_{j,t} - q^{\mathrm{g}}_{j,t},\ \forall j \in \mathscr{DG}, \tag{3.19d}$$

$$Q_{ij,t} = \sum_{k:\, j \longrightarrow k} Q_{jk,t} + q^{\mathrm{d}}_{j,t},\ \forall j \in \{\mathscr{N} \setminus \mathscr{DG}\}, \tag{3.19e}$$

$$\upsilon_{j,t} = \upsilon_{0,t} - \sum_{(l,k) \in \mathbb{P}_j} 2(r_{ij} P_{ij,t} + x_{ij} Q_{ij,t}), \quad \forall (i,j) \in \mathscr{B}, \tag{3.19f}$$

$$\upsilon_{i,t} \leq \overline{\upsilon}, \qquad \forall i \in \mathscr{N}, \tag{3.19g}$$

$$p^{\mathrm{g}}_{i,t} \leq \overline{p^{\mathrm{g}}_{i,t}}, \qquad \forall i \in \mathscr{DG}, \tag{3.19h}$$

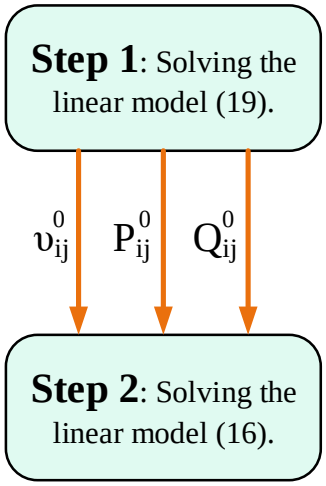

Fig. 3.1 The flowchart of two-step optimization algorithm.

the linear power flow equation (3.19b)-(3.19f) are called linear DistFlow equations. The solution of the linear model (3.19) is an approximation of the operating point. In summary, we solve the HC model (3.9) by using a two-step method explained above, as shown in Fig. 3.1. It is worth mentioning that the proposed two-step method is applicable for both balanced and unbalanced systems. However, equations (3.2)-(3.6) present the branch model of power flow in balance systems. The extension of equations (3.2)-(3.6) for unbalanced systems could be find in [94].

3.3.2 Stochastic Analysis Framework

In order to consider the impacts of load variability and DERs uncertainties, we develop a probabilistic framework to estimate the HC. The developed framework has three modules, as shown in Fig. 3.2. The first module of the framework addresses the uncertainties associated with type, number, and location of DERs by simulating potential DER expansion scenarios, which are characterized by using the Monte Carlo simulation. Next, a time series impact analysis is conducted in Module 2 to consider the impacts of load variation and uncertainty in DERs generation. Finally, in Module 3, based on the time series analysis, the over-voltage and HC probability functions are obtained. In the following, the modules of the proposed framework are explained in detail.

1) *DER Expansion Scenarios (Module 1):* In this module, multiple DER expansion scenarios are generated. The number of locations in which DERs could be installed, the type of DERs, and the location of DERs are three uncertain variables that are needed for generating the expansion scenarios. The steps for generating scenarios are as follows:

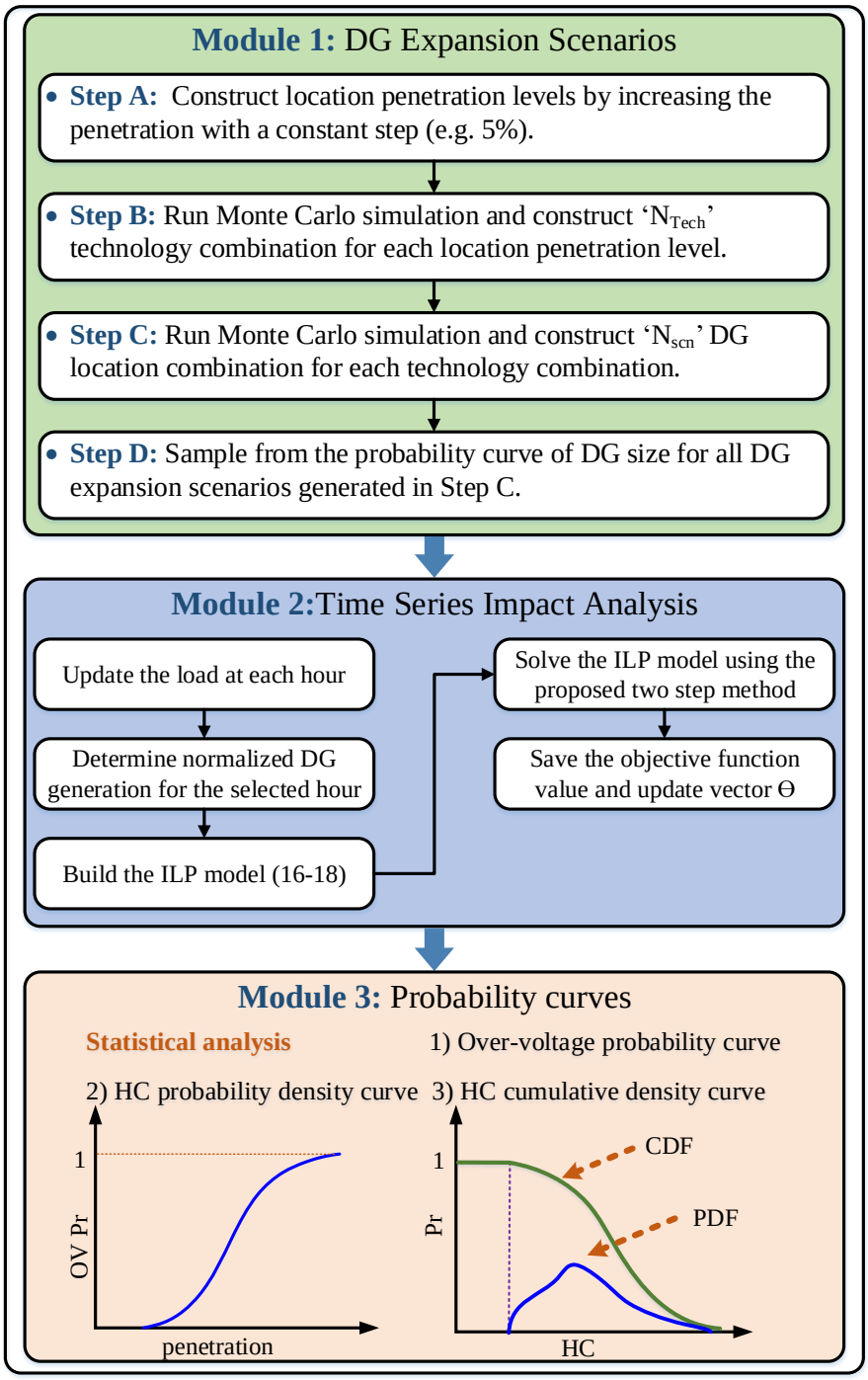

Fig. 3.2 The proposed HC analysis framework.

- **Step A:** This step addresses the uncertainty associated with the number of locations in which DERs could be installed. The minimum number of potential locations for DER installation is zero and the maximum number is equal to the total number of buses (i.e., customers in low voltage (LV) feeders). The ratio of the number of potential DER location to the number of all potential location is called the location penetration level. In order to cover a variety of cases, the location penetration is increased by a fixed step from 0% to 100%. Let $Loc_{\text{pen}}^{i\%}$ denote the location penetration of $i\%$.

- **Step B:** The uncertainty associated with the type of DERs is addressed in this step. To do so, a Monte Carlo approach is used for each location penetration to determine the share of each technology. As an example, suppose that the location penetration is 40% and technologies that we want to consider are photovoltaic (PV) and wind. Our objective in this step is to determine the share of PV and wind technologies. For instance, it could be [30% PV, 10% wind], [20% PV, 20% wind], or any combination with the summation of 40%. Since assessing all combinations is not possible, a Monte Carlo approach is used to generate N_{Tech} combinations.

- **Step C:** This step deals with uncertainty associated with the location of DERs. For doing so, a Monte Carlo approach is used to simulate N_{scn} combinations of locations for each one of N_{Tech} technology combinations generated in Step B. Each combination of locations is selected randomly using a uniform distribution from the pool of potential DER locations.

- **Step D:** In this step, a base DER capacity is determined for each combination of DER locations generated in Step C. The DER base size for each location is determined based on the load type (commercial or residential) and the corresponding distribution for the DER size [46].

The location penetration level is increased and the Monte Carlo process is repeated until it reaches 100% ($Loc_{\text{pen}}^{100\%}$).

2) *Time Series Impact Analysis (Module 2):* This module assesses DER impacts in an hourly interval to include the impacts of DER output uncertainty and load variation. To do so, the optimization model presented in (3.16)-(3.18) is solved for each DER expansion scenario generated in Module 1. By solving the proposed ILP model for all $h \in \mathscr{H}$, a vector Π of length $|\mathscr{H}|$ is obtained for each expansion scenario. The elements of this vector include two values as follows:

- 1**:** for indicating that the ILP model does not have a solution, which means that the scenario at that hour leads to the over-voltage problem.

- 0**:** for indicating that the ILP model has a feasible solution.

Vector Π is used to determine the scenarios with over-voltage problem. A scenario causes over-voltage problem if the vector Π has at least one none-zero element. Vector $\Theta^{i\%}$ is defined as follow to show if a scenario would cause over-voltage.

$$\Theta^{i\%}(j) = \begin{cases} 1 & \sum_{i=1}^{|\mathscr{H}|} \Pi(i) \geq 1 \\ 0 & Otherwise \end{cases} \quad j \in \{1...N^{i\%}\}, \tag{3.20}$$

where, $N^{i\%} = N_{\text{Tech}} \times N_{\text{scn}}$.

3) *Drawing Probability Curves (Module* 3*):* We can illustrate the over-voltage and HC probability curves based on the time series impact analysis. The probability of over-voltage at each location penetration level is required to draw the over-voltage probability curve. Therefore, the statistical data (3.21) is obtained, representing in what percentage of the scenarios of each location penetration level, the voltage constraint is violated.

$$Pr_{N^{i\%}} = \frac{\sum_{j=1}^{N^{i\%}} \Theta^{i\%}(j)}{N^{i\%}} \times 100\%, \tag{3.21}$$

where, $Pr_{N^{i\%}}$ is the non-compliance probability of each location penetration level $i\%$. Increasing $N^{i\%}$ (i.e., the number of expansion scenarios for each location penetration level $i\%$) leads to a more accurate probability. If this procedure is conducted for different location penetration levels, a curve that provides the probability density of over-voltage with respect to the location penetration level can be obtained.

The HC probability function for each location penetration level at each hour can be drawn by using time series impact analysis. The higher the $N^{i\%}$, the more accurate the probability function. In this chapter, two curves for the HC are drawn.

- **Probability density curve:** Solving the ILP model for all location penetration levels results into at most $N_{\text{Total}} = 100 \times N^{i\%}$ total DER capacity at each hour (it is supposed that the resolution of the location penetration level is 1%, hence 100 step). The probability density function can be obtained by using the total DER capacity ranges as the horizontal axes and the number of cases that have a total DER capacity in a specific range as the vertical axes.
- **Cumulative density curve:** This curve is based on the probability density curve. It has a descending trend and shows the probability of having a HC higher than an specific value.

The proposed method can be used for both LV and medium voltage (MV) feeders. The only difference is that instead of location penetration level, customer penetration is defined. customer penetration is the percentage of customers with a DER.

3.4 Numerical Results

In this section, simulations are carried out to assess the performance of the proposed methodology. Initially, the effectiveness of the proposed two-step method for solving the HC optimization model is demonstrated. Then, the efficacy of the proposed framework in evaluation of both balanced and unbalanced test networks is shown. Finally, the effect of different technologies on the HC of distribution system is assessed using the proposed framework.

3.4.1 Test Systems

The performance of the proposed methodology is evaluated on a balanced and an unbalanced distribution networks. The balanced system is a 33 kV feeder in Australia, as shown in Fig. 3.3. This feeder is the representative of agricultural feeders in Australia, which supplies agricultural loads such as irrigation pumps or dairies [98]. The unbalanced network is the IEEE 123-bus test system, as shown in Fig. 3.4. This feeder operates at a nominal voltage of 4.16kV with a maximum load of 3.378MW [99]. The Australian demand profile is used to model the load variation in both systems. The load profile is derived from the data made available by the Australian Energy Market Operator (AEMO) [100]. Normalized PV and wind generation profiles are derived from [101] and [102], respectively. The distribution for PV size is shown in Fig. 3.5 [1] and the distribution of small and medium wind generation is presented in Table 3.1 [103].

Table 3.1 Probability distribution of small and medium size wind turbines

Capacity	0-1.5kW	1.5-15kW	15-100kW	100-500kW
Probability	0.723	0.223	0.041	0.013

3.4.2 The Two-step Algorithm Validation

The performance of the proposed two-step algorithm to solve the optimization model of the HC is examined on the test system presented in Fig. 3.3. Tables 3.2 and 3.3 present the maximum DER capacity obtained by two-step algorithm for one and two DER, respectively. As shown, the obtained HCs by the first step of the proposed algorithm have some differences with results of the original nonlinear model. This is due to linearizing the nonlinear terms in equations (3.2)-(3.6). Moreover, using the results of the first step as the operating points for linearizing the nonlinear terms in the second step (Fig. 3.1) leads to the convergence to the results of the original model.

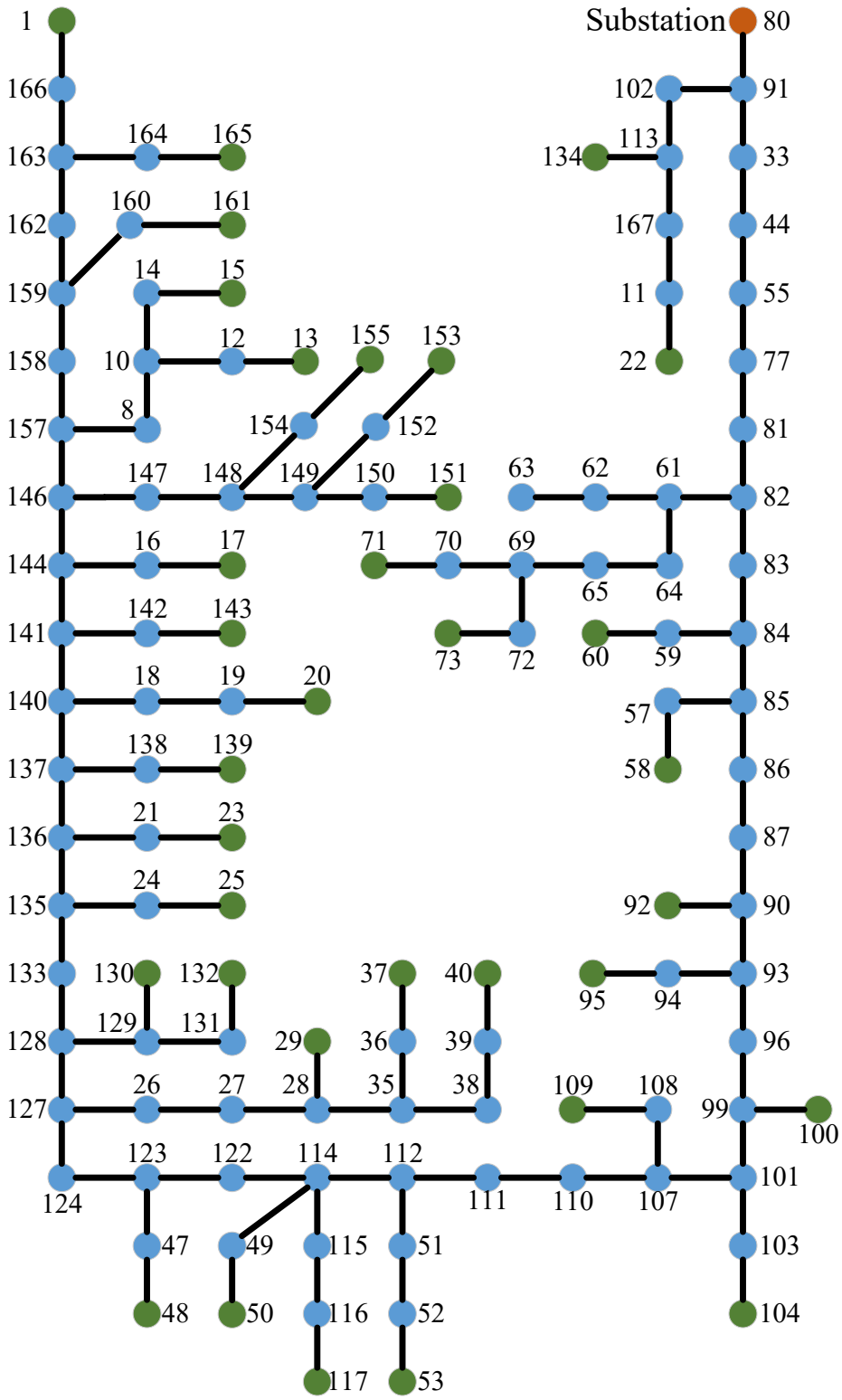

Fig. 3.3 Topology of an agricultural feeder in Australia.

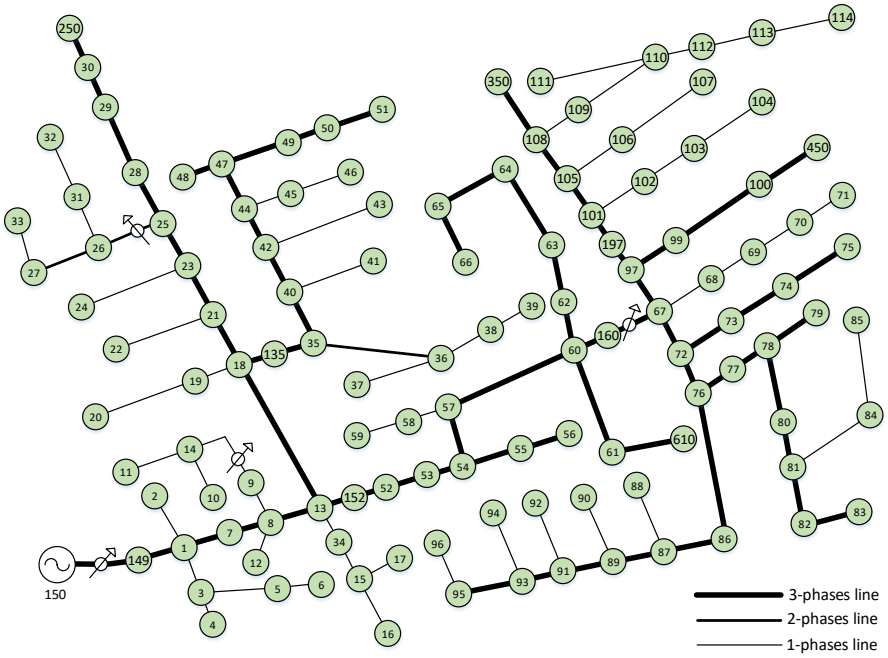

Fig. 3.4 The IEEE 123-bus radial distribution feeder.

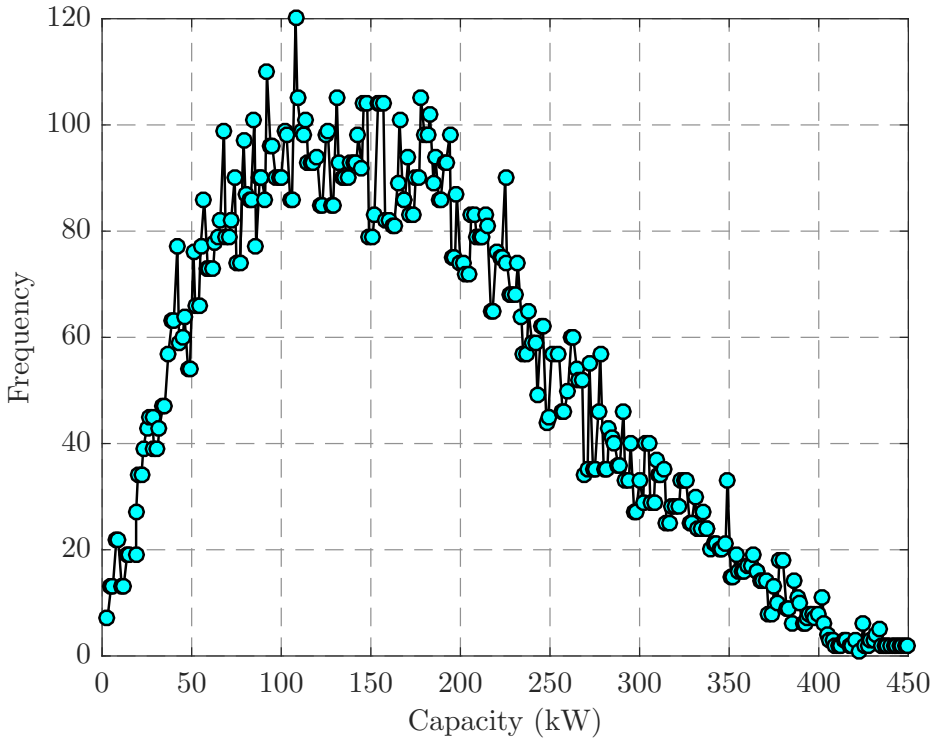

Fig. 3.5 Probability curve of PV array sizes.

Table 3.2 Locational HC calculated the proposed method at different buses in the agricultural feeder.

Bus	Substation voltage (pu)	Original (MW)	Step 1 (MW)	Step 2 (MW)
82	1.03	35.86	32.77	35.80
	1.04	21.33	20.08	21.33
	1.05	7.75	7.01	7.75
96	1.03	20.05	18.12	20.03
	1.04	13.32	12.38	13.32
	1.05	7.04	6.59	7.04
101	1.03	17.83	16.06	17.81
	1.04	12.13	11.25	12.13
	1.05	6.83	6.39	6.83
110	1.03	9.02	8.62	9.02
	1.04	6.69	6.42	6.69
	1.05	4.40	4.19	4.40
114	1.03	8.89	8.48	8.89
	1.04	6.63	6.36	6.63
	1.05	4.41	4.19	4.40
123	1.03	8.51	8.11	8.51
	1.04	6.41	6.13	6.41
	1.05	4.34	4.14	4.34
127	1.03	6.74	6.47	6.74
	1.04	5.22	5.02	5.22
	1.05	3.72	3.56	3.72
135	1.03	4.78	4.61	4.78
	1.04	3.85	3.71	3.85
	1.05	2.92	2.81	2.92
158	1.03	2.41	2.33	2.41
	1.04	2.07	2.01	2.07
	1.05	1.73	1.68	1.73

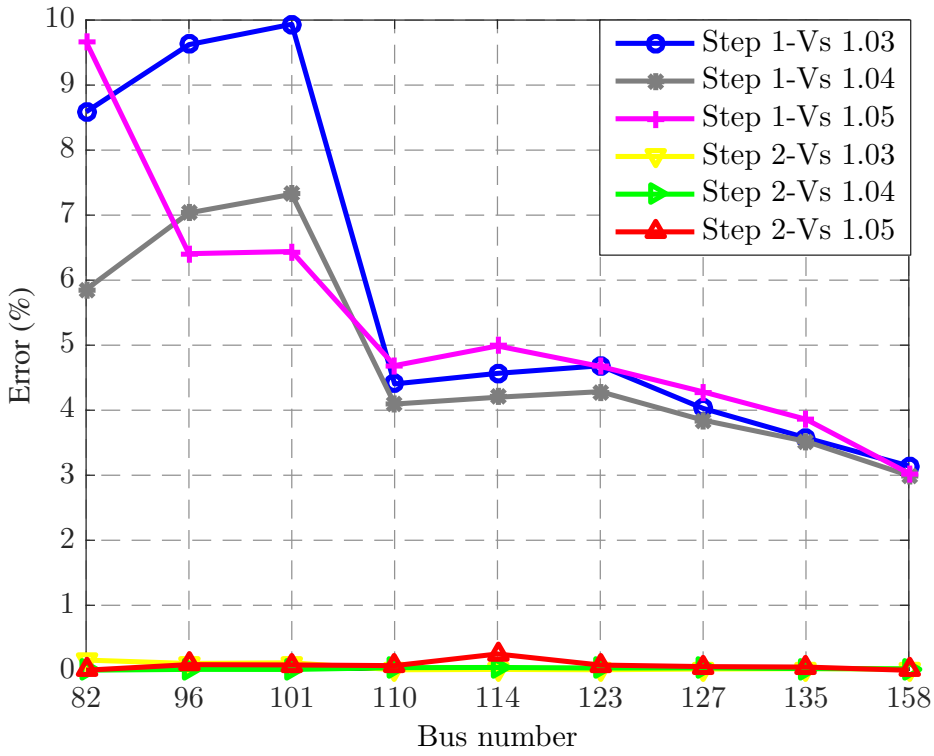

Fig. 3.6 Error of Step 1 and Step 2 in finding the locational HC in the agricultural feeder.

Table 3.3 Maximum DER capacity at buses 114 and 133 of the agricultural feeder.

Substation voltage (pu)		Original (MW)	Step 1 (MW)	error (%)	Step 2 (MW)	error (%)
1.03	p^{g}_{114}	8.887	8.48	4.57	8.888	0.013
	p^{g}_{133}	0	0	0	0	0
	total	8.887	8.48	4.57	8.888	0.013
1.04	p^{g}_{114}	6.63	6.35	4.20	6.634	0.04
	p^{g}_{133}	0	0	0	0	0
	total	6.63	6.35	4.2	6.634	0.04
1.05	p^{g}_{114}	4.41	4.19	4.99	4.4	0.25
	p^{g}_{133}	0	0	0	0	0
	total	4.41	4.19	4.99	4.4	0.25

Fig. 3.6 demonstrates the error of the obtained locational HC by the proposed algorithm. Observe that the error of the first step is highly dependent on the location of DER and it could be as high as 10 %. Besides, the accuracy of the HC model in the first step increases by moving away from the substation, i.e., the first step model is more accurate at locations that are electrically far from the substation. Moreover, it can be seen that the error of the first step is usually less than 5%, which means that it has enough accuracy unless the resistances of the lines is low. Note that the error of the second step of the proposed method is negligible and it is independent from the location of DER. Thus, using the proposed two steps algorithm significantly improves the accuracy of the model compared to the situation where the nonlinear terms in (3.2)-(3.6) are ignored.

We also address the sensitivity of the HC models (Step 1 and Step 2) to their parameters. One of the most important parameters in the HC assessment is the voltage of substation. As can be seen in Tables 3.2 and 3.3, decreasing the substation voltage can effectively increase the HC considering the over-voltage issue. Thus, operation strategies such as conservation voltage reduction (CVR) can have a positive effect on the HC. It is worth mentioning that substation voltage reduction strategies such as CVR leads to an increase in the HC, where voltage rise is the limiting factor for HC. However, this strategy is not effective when the limiting factors are other technical constraints (e.g. power quality and protection issues).

Finally, in this subsection, we assess the effect of network structure and the number of DERs on the results of HC model. Observe in Table 3.3, that if the goal is to maximize the DER penetration, it is better to install all the capacity at the closest potential location (electrically) to the substation. To a large extent, this is because the impedance between substation and this location (i.e., bus 114 in Table 3.3) is smaller than the impedances between substation and other potential locations of DERs, which means that it can tolerate more reverse power flow compared to other potential locations before reaching to the maximum voltage boundary. However, this is not a general rule for all the situations. Also, it can be observed that the locational HC at Bus 114 is equal to the total allowable DER capacity of buses 114 and 133 (Table 3.3). Generally, in normal distribution feeders, the total penetration of multiple DER units is almost equal to the maximum penetration level of the nearest location to the substation. In other words, in a feeder where the main limiting constraint of HC is over-voltage, increasing the number of DER units does not increase the maximum penetration level. This is because if the total capacity of DERs in the feeder is greater than the maximum penetration level of the nearest DER location to the substation, that bus certainly experiences over-voltage.

3.4.3 Probabilistic HC Assessment of PVs in the Balanced Test System

The performance of the proposed framework is examined on the Australian feeder shown in Fig. 3.3. We limit the DER technology to PV in this subsection and we assume that DERs are operated with unity power factor. Multiple PV expansion scenarios are generated using the first module of the proposed framework. To do so, the location penetration level is varied from 1% to 100% with 1% increment step. For each location penetration, 100 PV expansion scenarios are generated. The PV base size for each one of 100 scenarios is determined using the distribution curve shown in Fig. 3.5. The generated expansion scenarios are given to the second module as the input. For each scenario expansion, the HC optimization model is solved using the proposed two-step algorithm for a year. The required data is provided in Subsection 3.4.1. In order to verify the importance of the second module (times series impact analysis) for the HC assessment, this module is performed at two other specific conditions. Thus, three cases as follows are assessed:

A: Time series assessment of all scenarios for a year: it means that the proposed framework is performed thoroughly.

B: Assessing all scenarios at maximum generation and minimum load (traditional conservative planning): in this case, all DER expansion scenarios are assessed only at one point, which is the minimum load and maximum generation. This case is a condition that distribution system operators (DSOs) consider at the planning stage when a DER aims to be connected to the distribution system [104]. we called this as the traditional conservative planning.

C: Assessing all scenarios at maximum generation and minimum load scenario at each hour: in this case, all DER expansion scenarios are assessed at the minimum load and maximum PV generation of each hour (from 6 am to 6 pm). In other words, all DER expansion scenarios are examined at 13 point.

Fig. 3.7 shows the over-voltage probability curve for cases A, B and C obtained by using the developed framework and the comprehensive power flow (CPF) method. CPF is a Monte Carlo based method for assessing the integration of DERs in distribution systems. The basic idea of CPF is generating quite a few DER expansion scenarios and running the power flow calculation to check if the operation limits of the system are violated. Based on the results of the power flow for all scenarios, the violation probability curve is obtained. As shown in Fig. 3.7, the proposed method leads to a similar over-voltage probability curve as the CPF method. If a DSO does not want to accept any potential problem, the HC will be considered as the location penetration level that over-voltage probability becomes

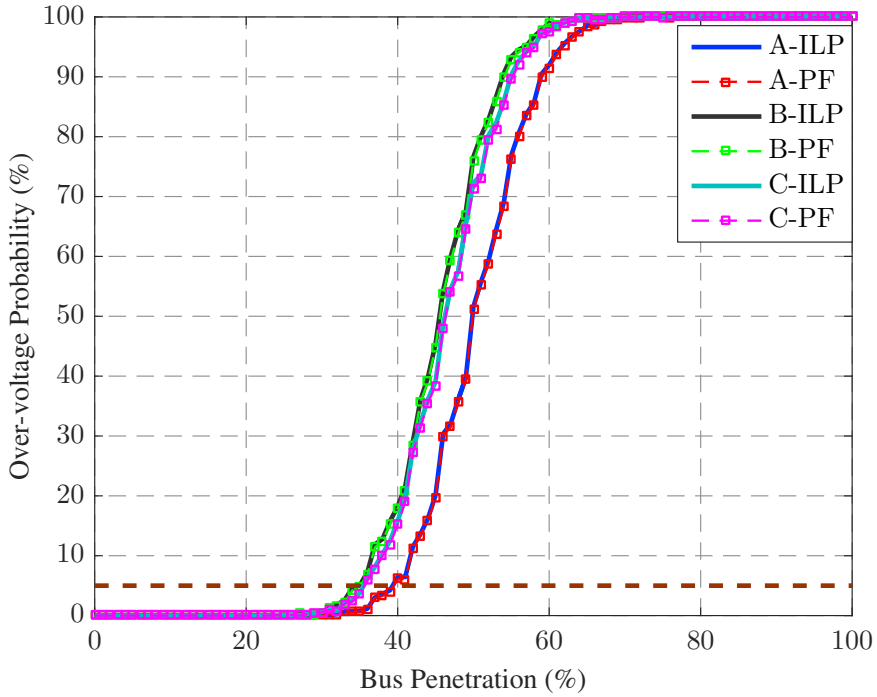

Fig. 3.7 Over-voltage probability curve for cases A, B and C by using the developed and CPF methods in the agricultural feeder.

higher than zero. In contrast, if the DSO is able to accept some level of potential issues, the over-voltage probability threshold can be set to a higher value. If DSO does not accept any risk, the maximum location penetration level for cases A, B and C are 29%, 25% and 24%, respectively. However, accepting 5% risk increases the maximum location penetration level for cases A, B and C to 39%, 35% and 35%, respectively. Observe that using cases B and C for the HC assessment results in underestimating the maximum location penetration level. Moreover, cases B and C result in a similar probability curve, which indicates that case C is not a good replacement for case B (traditional conservative planning).

The advantage of the proposed method over CPF is that it can calculate the HC for each expansion scenario and at each hour. Given a large number of possible DER expansion scenarios corresponding to the Monte Carlo simulation of different penetration level, different HC is likely to be observed. The HC calculated based on the proposed framework resulted in at most N_{Total} values. The HC distribution is shown in Fig. 3.8. This curve can be approximated by using the Gaussian-shape distribution as (3.22) with $\alpha = 0.56$, $\mu = 19.97$MW and $\sigma = 6.42$MW. It is worth mentioning that the HC of the test system is 3.198MW with 100% certainty, which is 71.39% of the maximum total load (4.48MW). Fig. 3.8 also presented the HC in terms of the percentage of load demand provided by the PVs. As it can be seen, up to

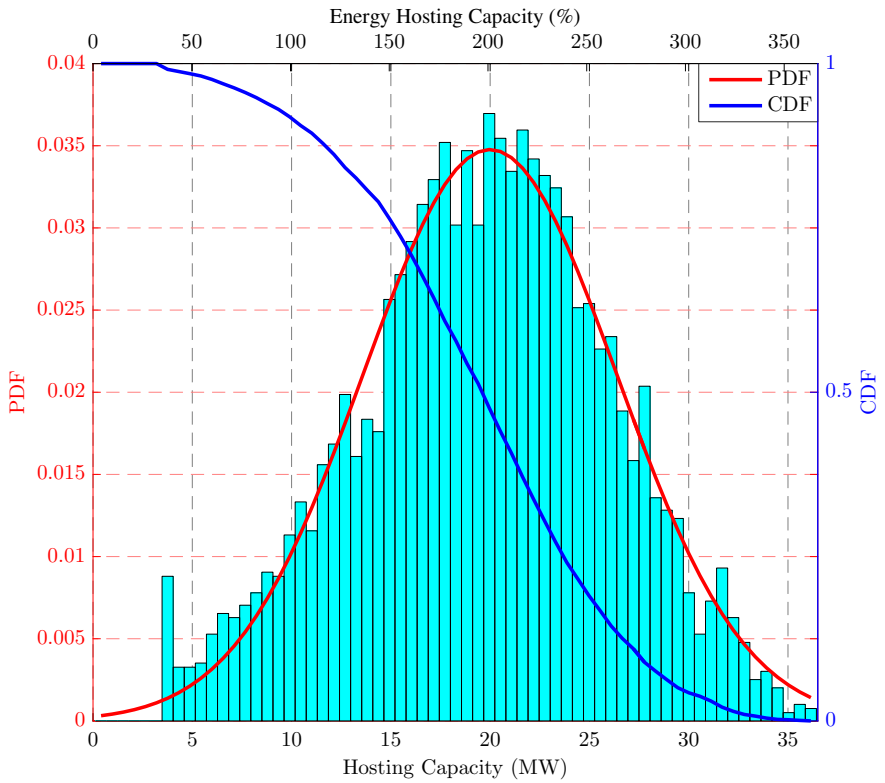

Fig. 3.8 Probability curves of the HC for the agricultural feeder obtained using the developed framework.

32.47% of the required energy can be provided by PVs with 100% certainty.

$$HC \sim \alpha \times N(\mu, \sigma^2) = \frac{\alpha}{\sqrt{2\pi\sigma^2}} e^{-\frac{(x-\mu)^2}{2\sigma^2}}. \tag{3.22}$$

Fig. 3.9 demonstrates the effect of voltage deviation constraint on the probability density function (PDF) of the HC. As shown, the PDF of HC with and without the voltage deviation constraint is almost the same. Notice that this similarity does not imply that the voltage deviation constraint is ineffective on the HC. It rather reflects the fact that distributing the DERs over the system decreases the importance of the voltage deviation constraint.

Finally, it is worth to mention that there is no relationship between the network characteristics such as minimum and maximum total load and the required parameters for determining the HC Gaussian distribution. However, as mentioned, the higher the load, the greater the HC. This means that annual load growth of 2% should cause an increase in the HC of the system. Fig. 3.10 demonstrates the Gaussian-shape curve of the HC after 3 and 5 years. Observe how the load growth shifts the HC curve toward right. This implies that if the main limiting constraint of the HC is over-voltage, the obtained HC becomes more conservative over time.

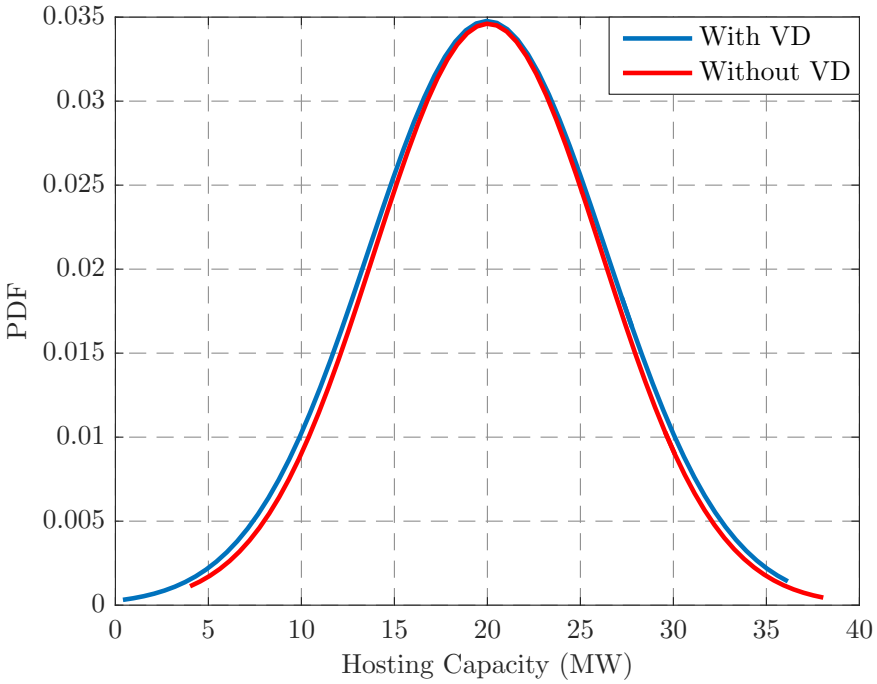

Fig. 3.9 Effect of voltage deviation constraint on the PDF of the HC in the agricultural feeder.

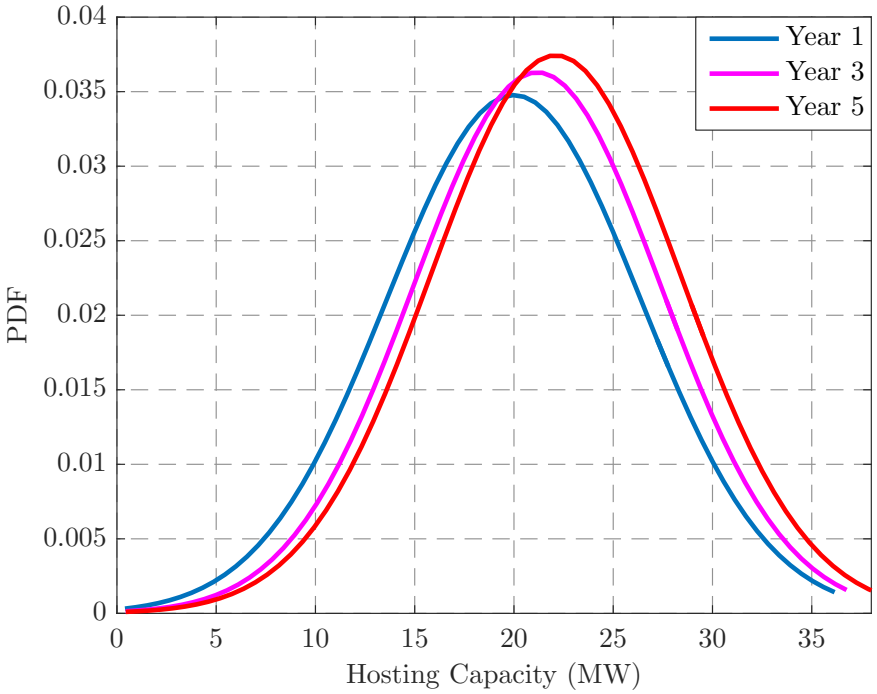

Fig. 3.10 Effect of load growth on the HC in the agricultural feeder.

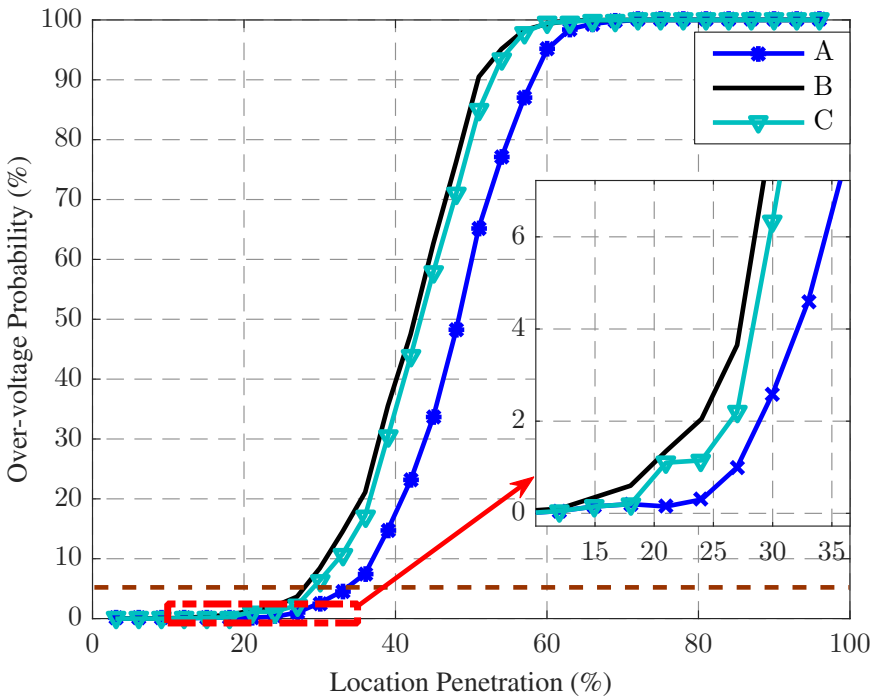

Fig. 3.11 Over-voltage probability curve for cases A, B and C using the developed method in the IEEE 123-bus test system.

3.4.4 Probabilistic HC Assessment of PVs in the Unbalanced Test System

The proposed framework is also examined on the IEEE 123-bus test system. Fig. 3.11 shows the over-voltage probability curve. Similar to the balanced system, the cases B and C yielded conservative results. As it can be seen, in case A, the voltage problem started from the location penetration of 15%, which is lower than that of the balanced system. In other words, the voltage-rise issue in the unbalanced system occurs earlier than that of the balanced system. Another important output of the framework is the HC distribution, which is shown in Fig. 3.12. Similar to the balanced system, we can approximate this curve using a Gaussian-shape distribution given in (3.22) with $\alpha = 0.22$, $\mu = 6.71$MW (i.e., 1.99 times of the peak load) and $\sigma = 1.11$MW (i.e., 0.33 times of the peak load). Fig. 3.12 also presented the energy HC of the system. As shown, 17.75% of the required energy can be provided by PVs with 100% certainty, which is 14.72% less than the balanced system.

Another important index that assessed in the IEEE 123-bus is voltage unbalanced factor (VUF), which is defined as the ratio of the negative sequence voltage to the positive sequence voltage. According to the ANSI C84.1 standard, VUF should be less than 3% [105]. Fig. 3.13 shows the box plot of VUF for different location penetration. On each box, the red central mark is the median, the horizontal edges are the 25^{th} and 75^{th} percentiles, the whiskers

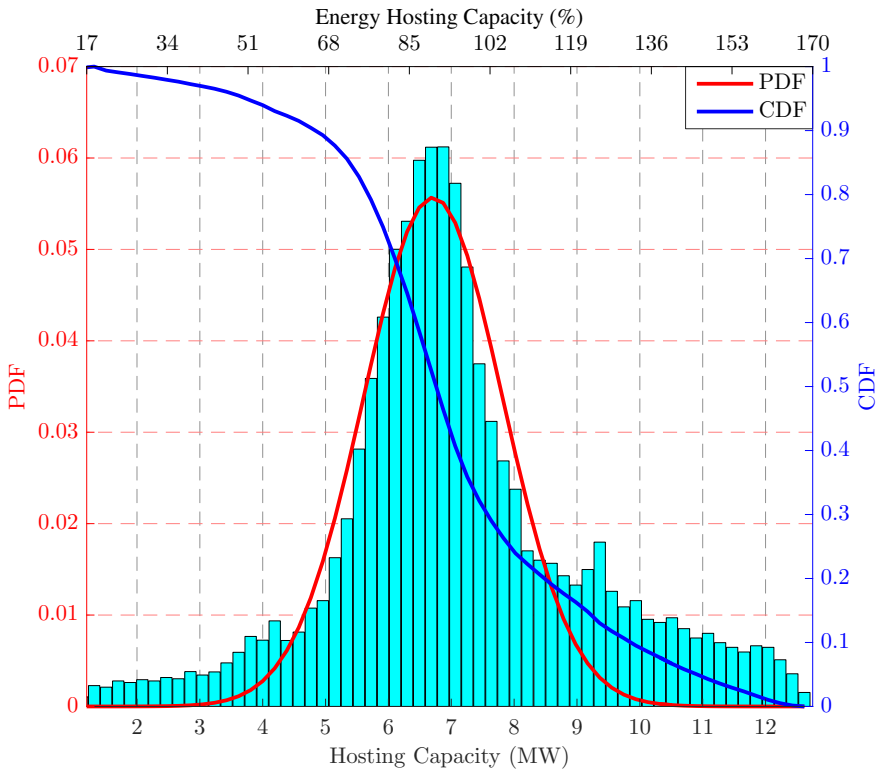

Fig. 3.12 Probability curves of the HC for the IEEE 123-bus obtained by the developed framework for PV technology.

extend to the most extreme VUF not considered outliers, and outliers are plotted individually. As shown in Fig. 3.13, VUF often is in the standard range. In other words, although a high DER penetration can increase the VUF of the test system, the VUF is not a limiting constraint for the HC. It can also be seen that unlike the over-voltage issue, increasing the location penetration decreases the VUF range.

3.4.5 Effect of DER Technology

In order to examine the effect of DER technology on the HC and to show the generality of the proposed method, we evaluated the HC of the IEEE 123-bus test system for PV and wind technologies. For doing so, the location penetration is increased from 5% to 100% with 5% increment step. For each location penetration, 20 PV and wind combination are generated (e.g., 30% PV and 70% wind). For each technology combination, 100 expansion scenarios are generated. The PV and wind base sizes for each one of 100 scenarios are determined using the distribution curve shown in Fig. 3.5 and Table 3.1. Fig. 3.14 shows the HC probability curve for PV and wind technologies. Observe that the HC curve can be approximated using a Gaussian-shape distribution as (3.22) with $\alpha = 0.31$, $\mu = 9.65$MW (i.e., 2.86 times of the peak load) and $\sigma = 2.88$MW (i.e., 0.85 times of the peak load). As shown,

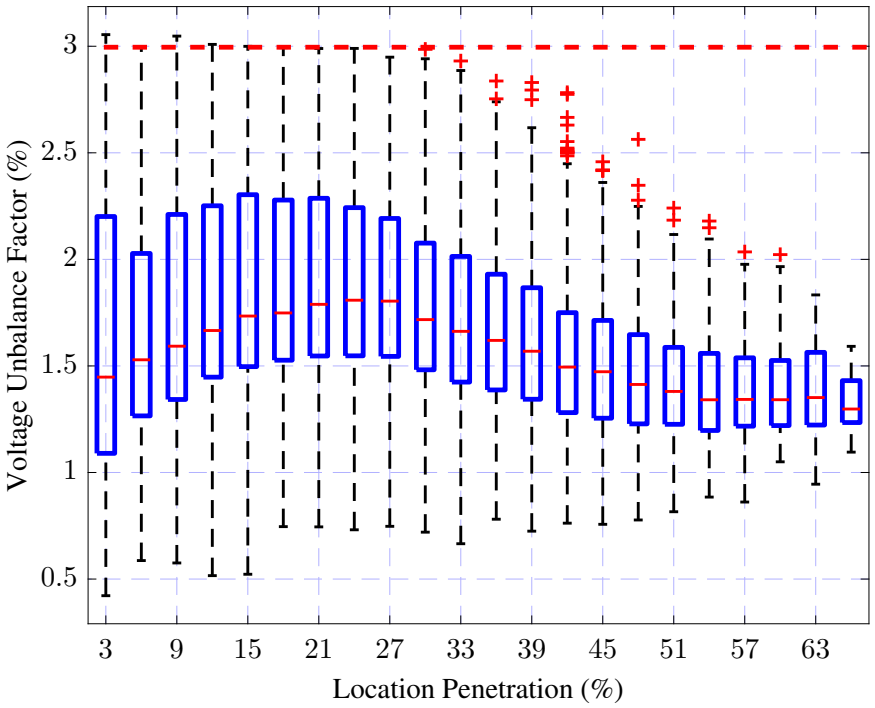

Fig. 3.13 VUF in the IEEE 123-bus at different location penetration.

if both technologies are considered, the HC of the test system with 100 certainty is 1.33MW, which is 39.37% of the peak load. Note that if the prospective technology is only PV, the HC of the system with 100 certainty is 39.02% of the peak load. So, if both wind and PV are the prospective technologies, the minimum HC of the test system is almost equal to that of the case in which only PV is the prospective technology. Finally, Fig. 3.15 shows the HC probability curve of the test system for wind technology. As before, the HC curve can be approximated using a Gaussian-shape distribution given in (3.22) with $\alpha = 0.018$, $\mu = 12.07$MW (i.e., 3.57 times of the peak load) and $\sigma = 0.077$MW (i.e., 0.021 times of the peak load). It is also shown in Fig. 3.15 that 15.37% of required energy can be provided by wind generation with 100% certainty. It is interesting to observe that changing technology from PV to wind can decrease the allowable energy penetration from 17.75% to 15.37%. Thus, the HC that is calculated for an specific type of DER can not be used to show the HC for other technologies. Fig. 3.16 demonstrates the HC curves of different combinations of PV and wind technologies. Observe that the HC curve obtained for both PV and wind technologies is between the HC curve of wind technology and the HC curve of PV technology. Further, note that how increasing the penetration of wind in the test system shifts the HC curve toward right.

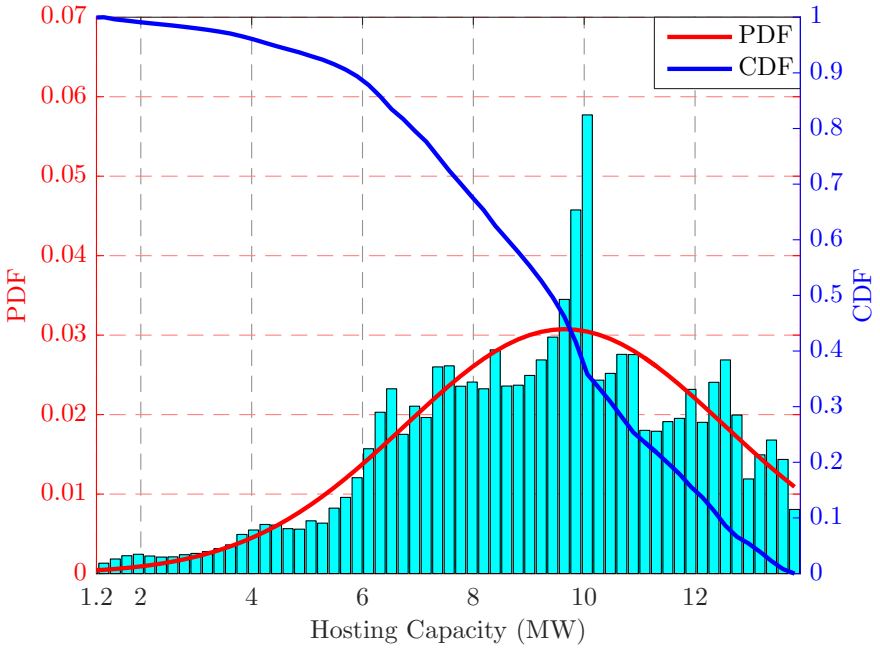

Fig. 3.14 Probability curves of for the IEEE 123-bus obtained by the developed framework for PV and wind technologies together.

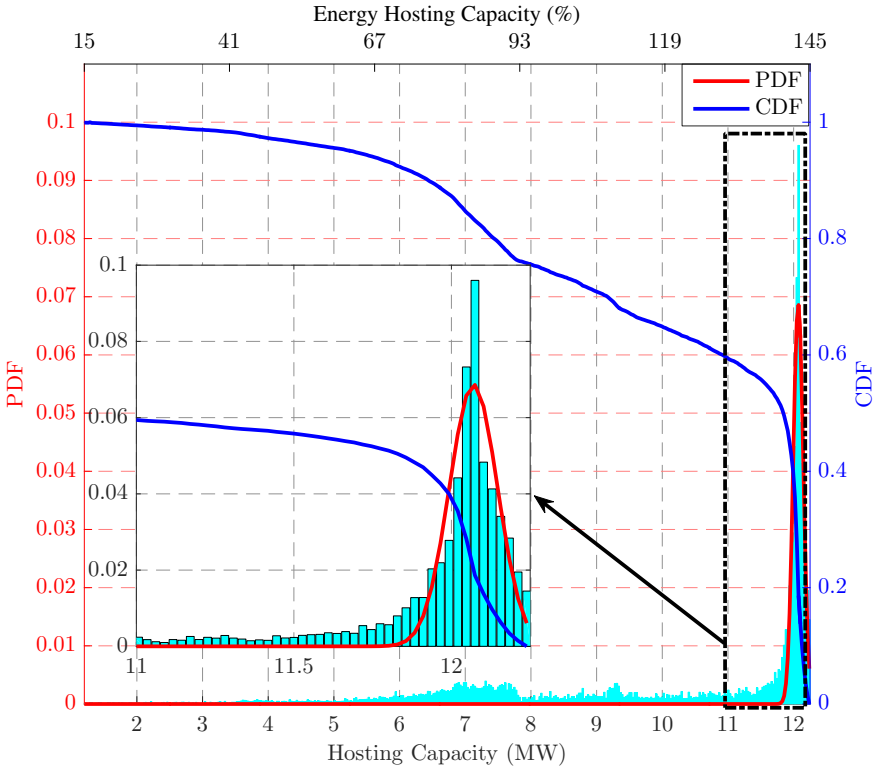

Fig. 3.15 Probability curves of for the IEEE 123-bus obtained by the developed framework for wind technology.

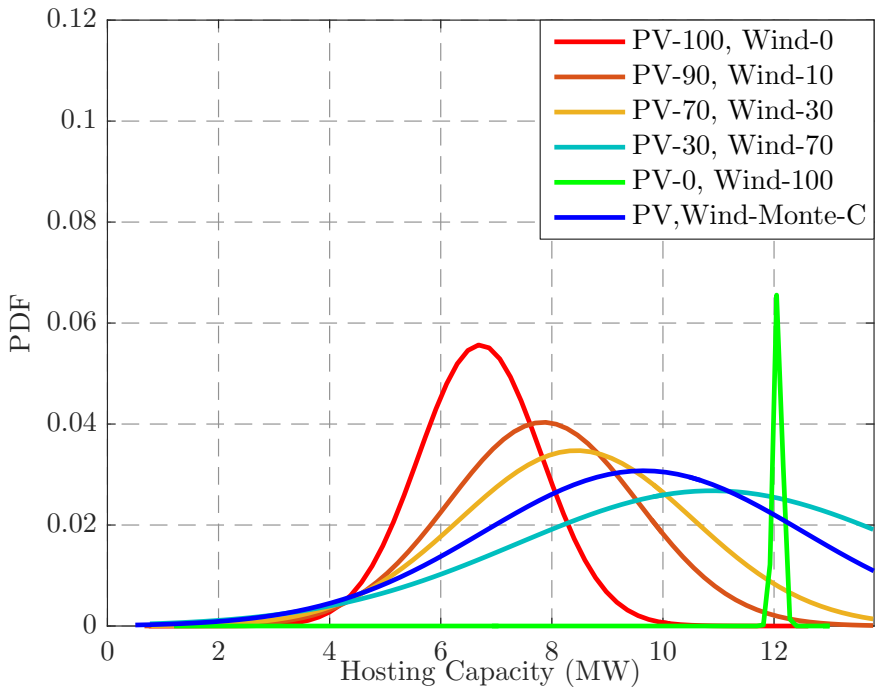

Fig. 3.16 HC probability curves of the IEEE 123-bus for different combination of PV and wind technologies.

3.5 Summary

Due to uncertainties of loads, output power and locations of DERs, the HC of a system cannot be considered as a fix value as it varies over time and location of DERs, i.e., even if we fix the location of DERs, the HC of the system changes over time due to the variations in loads and output of DERs. Thus, designing a framework to throughly assess the HC of a system is inevitable. This chapter presented a probabilistic framework based on an accurate HC model considering the over-voltage and voltage deviation constraints. As for the HC model, it was shown that using linear DistFlow equations to solve the HC problem can cause up to 10% error in the results. So, we proposed a two-step algorithm to linearize the HC model. The derived model has near to zero error, which implies that it converges to almost the same solution as the nonlinear model. The efficacy of our framework is demonstrated using an agricultural feeder in Australia and the IEEE 123-bus test system. The results obtained by the proposed framework are compared with those of the CPF and traditional conservative methods. It was also shown that the HC can be approximated by a Gaussian-shape distribution.

The proposed method is also used to assess the effects of voltage deviation constraint, load growth, network structure, and the DER type on the HC. Following are the conclusions derived from the simulation results:

- Although linear DistFlow equations do not have the accuracy of our proposed linear model, they still can provide a lower bound for the HC. Depending on the characteristics of the network, the provided lower bound could be close to the actual value of the HC.
- Voltage deviation constraint does not affect the HC probability curve significantly, which implies that distributing DERs over the system decreases the importance of the voltage deviation constraint. In other words, the voltage deviation constraint often limits the locational HC but not the HC.
- The annual load growth of 2% shifts the HC probability curve toward right. So, the HC calculated now might be a conservative approximation of the HC in the future.
- The minimum energy HC for PVs in the balanced test system is 32.47%, which is 14.72% higher than that of the unbalanced system. It is also observed that VUF, which is an important index for unbalanced systems does not constrain the HC of the test system.
- DER type has a great effect on the probability curve of the HC. Changing the technology from PV to wind shifted the mean of the HC probability curve from 1.99 times of the peak load to 3.57 times of the peak load. Note that although the HC probability curve for wind technology is higher than that of PV, the minimum energy HC of PV is 2.48% higher than that of wind technology. This is probably because the PV capacity factor is higher than wind capacity factor in the test system.

Chapter 4

Distributionally Robust Hosting Capacity Assessment in Distribution Systems

4.1 Introduction

In Chapter 3, we presented a modular probabilistic framework to assess the hosting capacity (HC). In the proposed framework, we used a time series analysis, i.e. the second module, to address the uncertainty associated with the loads and output power of distributed energy resources (DERs). However, to properly model the uncertainties using the time series analysis, we need to perform it over a long study period, which could be a time consuming process. In this chapter, we propose a more efficient model to address the uncertainties associated with loads and output power of DERs. This new model can replace the time series impact analysis, i.e. the second module, of the HC framework presented in Chapter 3. Further, the proposed model considers the uncertainties as variables in the optimization problem.

As mentioned in Chapter 1, considering the available historical data, the right approach to address the uncertainties is a combination of robust and stochastic optimization, i.e. distributionally robust optimization (DRO). In DRO, we assume that the exact PDFs of uncertain variables are not available. However, we assume that the PDFs of uncertainties are in a confidence set. The confidence set can be derived from the historical data. For instance, the confidence set can be a set of PDFs with common mean and covariance matrix [42]. In this chapter, we propose a DRO-based method to model the uncertainties associated with loads and output power of DERs in the HC problem. Further, the DRO HC model is used to assess whether electric vehicles (EVs) and their charging stations increase the HC. To do so,

the proposed DRO model is applied to a modified IEEE 33-bus system and the sensitivity of the HC to the DER technology, the EVs aggregate load, the load of EVs charging station and historical data has been assessed. The outcome of this chapter is published as a journal paper[1].

The remainder of this chapter is organized as follows: Section 4.2 formulates the problem. Section 4.3 presents the uncertainty modelling. In Section 4.4, the solution methodology is described. First, the DRO model is transformed into a joint chance constraint (JCC) problem. Then, a solution for the corresponding JCC is introduced. Section 4.5 presents the numerical results and discussion. Finally, the major conclusions are summarized in Section 4.6.

4.2 Mathematical Modelling

The HC is defined as the maximum DER capacity that can be installed in a system without violating its technical constraints irrespective of DERs' locations. This implies that DERs' locations should not be defined as independent variables in the optimization model. This, however, raises a question on how to address the uncertainty associated with DERs' locations in the HC problem. This can be tackled using the HC calculation framework shown in Fig. 4.1. As it can be seen, it is required to generate a large number of location combinations for DERs. Then, the maximum DER capacity for different location scenarios can be identified using the mathematical model. Finally, the minimum of the identified DER capacities for all location scenarios is defined as the actual HC. The chapter develops a mathematical model to identify the maximum DER capacity for any sets of DER locations considering EVs. The objective function of this model is presented as follows:

$$\underset{Cap_j^{\mathrm{g}}}{\text{minimize}} \quad \sum_{j \in \mathscr{DG}} -Cap_j^{\mathrm{g}}, \tag{4.1}$$

where, $\mathscr{DG}$ is the set of buses that have DERs, and Cap_j^{g} denotes the installed DER capacity at bus (j). The system operation constraints are presented in Sections 4.2.1 and 4.2.2.

[1] "Distributionally Robust Distributed Generation Hosting Capacity Assessment in Distribution Systems," Energies, 2018 [106].

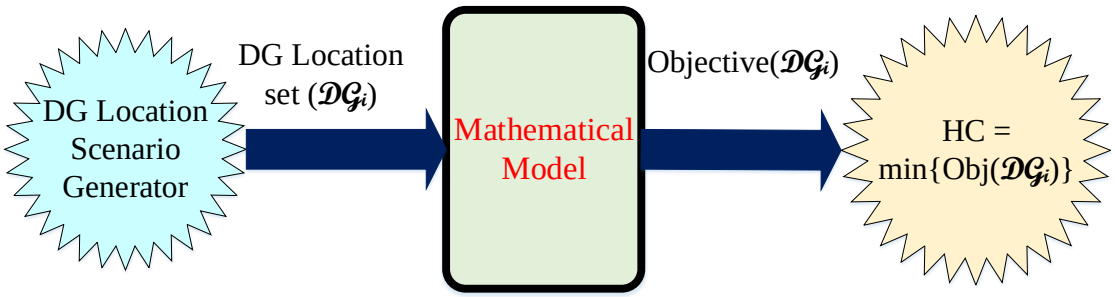

Fig. 4.1 The HC calculation framework.

4.2.1 Distribution System Model

We already defined most of the variables for modeling distribution systems. However, in order to make the thesis easy to follow, we reintroduce them here. Consider a radial network, where $\mathcal{N} = \{0, \ldots, n\}$ denotes the set of buses and $\mathcal{DG}$ represents the set of buses that have a DER ($\mathcal{DG} \subset \mathcal{N}$). Let $\mathcal{B}$ represents the set of all branches and (i, j) or $i \longrightarrow j$ as a branch from bus (i) to bus (j) in the set $\mathcal{B}$. Let $\mathcal{H}$ denotes the set of time periods. For every bus $i \in \mathcal{N}$ and for all $t \in \mathcal{H}$, let $V_{i,t}$ denotes the complex voltage, where $\upsilon_{i,t} = |V_{i,t}|^2$. Let $s^{\mathrm{d}}_{i,t} = p^{\mathrm{d}}_{i,t} + iq^{\mathrm{d}}_{i,t}$ represents the load at bus (i) at time (t). For every line $(i, j) \in \mathcal{B}$ and for all $t \in \mathcal{H}$, $z_{ij} = r_{ij} + ix_{ij}$ denotes the complex impedance, $S_{ij,t} = P_{ij,t} + iQ_{ij,t}$ denotes the sending-end complex power from bus (i) to bus (j), and $I_{ij,t}$ defines the sending-end complex current from bus (i) to bus (j). Let $s^{\mathrm{g}}_{i,t} = p^{\mathrm{g}}_{i,t} + iq^{\mathrm{g}}_{i,t}$ denotes the generation complex power at bus (i) at time (t), and $s^{\mathrm{EV}}_{i,t} = p^{\mathrm{EV}}_{i,t} + iq^{\mathrm{EV}}_{i,t}$ represents the EV aggregated complex demand at bus (i) at time (t). For every bus $i \in \mathcal{DG}$, $\eta^{\mathrm{g}}_{i,t}$ represents the capacity factor at time period (t). Let $\mathbb{P}_j$ defines the set of lines on the path from substation to bus (j). The linear power flow equation for branch (i, j) is formulated as follows [42, 86]:

$$P_{ij,t} = \sum_{k:j \longrightarrow k} P_{jk,t} + p^{\mathrm{d}}_{j,t} - p^{\mathrm{g}}_{j,t} + p^{\mathrm{EV}}_{j,t}, \ \forall j \in \mathcal{N}, \ \ \forall t \in \mathcal{H}, \tag{4.2}$$

$$Q_{ij,t} = \sum_{k:j \longrightarrow k} Q_{jk,t} + q^{\mathrm{d}}_{j,t} - q^{\mathrm{g}}_{j,t} + q^{\mathrm{EV}}_{j,t}, \ \forall j \in \mathcal{N}, \ \ \forall t \in \mathcal{H}, \tag{4.3}$$

$$\upsilon_{j,t} = \upsilon_{0,t} - \sum_{(l,k) \in \mathbb{P}_j} 2(r_{lk}P_{lk,t} + x_{lk}Q_{lk,t}), \ \ \forall j \in \mathcal{N}, \ \forall t \in \mathcal{H}, \tag{4.4}$$

$$\begin{cases} p^{\mathrm{g}}_{i,t} = \eta^{\mathrm{g}}_{i,t} Cap^{\mathrm{g}}_{i}, \\ q^{\mathrm{g}}_{i,t} = \tan(\phi_{i,t}) p^{\mathrm{g}}_{i,t}, \end{cases} \quad \forall i \in \mathcal{DG}, \ \forall t \in \mathcal{H}, \tag{4.5}$$

where, $\phi_{i,t}$ is the power factor angle at bus (i) at time period (t).

4.2.2 Technical Constraints

The following technical constraints are considered for determining the HC:

1- Steady State Voltage Constraint

$$\underline{\upsilon} \leq \upsilon_{i,t} \leq \overline{\upsilon}, \qquad \forall i \in \mathscr{N}, \ \forall t \in \mathscr{H}, \tag{4.6}$$

where, $\underline{\upsilon}$ and $\overline{\upsilon}$ are the square of minimum and maximum voltage limits, respectively.

2- Thermal Capacity Constraints

The apparent power flow of lines and substation transformer is limited by a higher bound as follows:

$$P_{ij,t}^2 + Q_{ij,t}^2 \leq \overline{S}_{ij}{}^2, \ \forall (i,j) \in \mathscr{B}, \forall t \in \mathscr{H}, \tag{4.7}$$

where, $\overline{S}_{ij}$ is the maximum apparent power of line (i,j). As it has been proposed in Section 2.3.2, the nonlinear constraint (4.7) can be substituted by a set of linear constraints as follows:

$$[\cos(\theta)+\sin(\theta)]P_{ij,t} + [\cos(\theta)-\sin(\theta)]Q_{ij,t} \leq \sqrt{2}\,\overline{S}_{ij}, \ \forall (i,j) \in \mathscr{B}, \forall t \in \mathscr{H}, \tag{4.8}$$

where, θ is the rotation angle in the rotation matrix.

3- Short Circuit Level (SCL) Constraint

One of the important characteristics of distribution systems is SCL, which is defined as the maximum acceptable fault level. A basic requirement for connecting DERs to the networks is that the SCL in presence of DERs should remain below the designed SCL [107]. It is shown in [108] that the SCL can be modelled as follows:

$$\sum_{j \in \mathscr{D}\mathscr{G}} a_{\text{scl}} Cap_j^{\text{g}} + SCL_{\text{sub}} \leq SCL_{\text{Rated}}, \tag{4.9}$$

where, a_{scl} is the dependency of SCL to the capacity of the DER at bus (j), SCL_{sub} is the SCL at substation without DERs, and SCL_{Rated} is the rated SCL at substation. It is worth mentioning that a_{scl} depends on the structure of the system and the DER type; e.g., a_{scl} is very small for photovoltaic systems (PVs) [109].

4.2.3 Deterministic Problem Formulation Summary

The deterministic HC problem is formulated as follows:

$$\begin{aligned} &\underset{Cap_j^{\mathrm{g}}}{\text{minimize}} \quad \sum_{j\in\mathscr{DG}} -Cap_j^{\mathrm{g}}, \\ &\text{s.t.} \quad (4.2)-(4.6),(4.8),(4.9) \end{aligned} \tag{4.10}$$

In practice, the output power of DERs and the loads are uncertain variables and modelling them as deterministic variables is not realistic. Therefore, the HC optimization model should include such uncertainties, as explained in the next subsection.

4.2.4 Distributionally Robust Optimization (DRO) HC Model

The uncertainties of the DER output ($p_{i,t}^{\mathrm{g}}$), load ($p_{i,t}^{\mathrm{d}}$), and EVs aggregated demand ($p_{i,t}^{\mathrm{EV}}$) at bus (i) are modelled as follows:

$$\begin{cases} \eta_{i,t}^{\mathrm{g}} = \hat{\eta}_{i,t}^{\mathrm{g}} + \xi_{i,t}^{\mathrm{g}} \\ p_{i,t}^{\mathrm{d}} = \hat{p}_{i,t}^{\mathrm{d}} + \xi_{i,t}^{\mathrm{d}} \\ p_{i,t}^{\mathrm{EV}} = \hat{p}_{i,t}^{\mathrm{EV}} + \xi_{i,t}^{\mathrm{EV}} \end{cases}, \tag{4.11}$$

where, $\xi_{i,t}^{\mathrm{g}}$, $\xi_{i,t}^{\mathrm{d}}$, and $\xi_{i,t}^{\mathrm{EV}}$ model the prediction error of the DER output, load and aggregated demand of EVs, respectively; $\hat{\eta}_{i,t}^{\mathrm{g}}$, $\hat{p}_{i,t}^{\mathrm{d}}$ and $\hat{p}_{i,t}^{\mathrm{EV}}$ are the predicted values of $\eta_{i,t}^{\mathrm{g}}$, $p_{i,t}^{\mathrm{d}}$ and $p_{i,t}^{\mathrm{EV}}$, respectively. Considering the definition of subtree $\mathbb{T}_j$, substituting (4.11) in (4.2)–(4.5), and denoting $\xi = \{\xi_{i,t}^{\mathrm{g}}, \xi_{i,t}^{\mathrm{d}}, \xi_{i,t}^{\mathrm{EV}}\}$ to the vector of uncertain variables, the power flow state variables ($P_{ij,t}, Q_{ij,t}, \upsilon_{j,t}$) can be written as functions of $\mathbf{Cap}^{\mathrm{g}}$ and ξ. Thus, all constraints can be expressed as follows:

$$G_k^{\mathrm{eq}}(\mathbf{Cap}^{\mathrm{g}}, \xi) = 0, \quad \forall k \in \mathscr{C}^{\mathrm{eq}}, \tag{4.12}$$

$$G_k(\mathbf{Cap}^{\mathrm{g}}, \xi) \leq 0, \quad \forall k \in \mathscr{C}, \tag{4.13}$$

where, $\mathscr{C}^{\mathrm{eq}}$ and $\mathscr{C}$ are the sets of equality and inequality constraints for the HC problem; $\mathbf{Cap}^{\mathrm{g}} \in \mathbb{R}^n$ is the vector of DER capacities in distribution system. Hence, the uncertain HC model is presented as follows:

$$\begin{aligned} &\underset{Cap_j^{\mathrm{g}}}{\text{minimize}} \quad \sum_{j\in\mathscr{DG}} -Cap_j^{\mathrm{g}}, \\ &\text{s.t.} \end{aligned} \tag{4.14}$$

$$G_k^{\mathrm{eq}}(\mathbf{Cap}^{\mathrm{g}}, \xi) = 0, \quad \forall k \in \mathscr{C}^{\mathrm{eq}},$$
$$G_k(\mathbf{Cap}^{\mathrm{g}}, \xi) \leq 0, \quad \forall k \in \mathscr{C}.$$

To immunize the HC model (4.14) against the uncertainty vector, ξ, we adapt a distributionally robust approach. In this approach, a risk level is defined to adjust the conservatism of the solution. From a modelling prospective, the distributionally robust HC problem is defined as follows:

$$\begin{aligned} &\underset{Cap_j^{\mathrm{g}}}{\text{minimize}} \quad \sum_{j \in \mathscr{D}\mathscr{G}} -Cap_j^{\mathrm{g}}, \\ &\text{s.t.} \\ &\inf_{f_{\mathrm{df}} \in \mathscr{D}_\phi} \left\{ \Pr_{\xi \sim f_{\mathrm{df}}} \left[T(\mathbf{Cap}^{\mathrm{g}}, \xi) \right] \right\} \geq 1 - \tau, \end{aligned} \tag{4.15}$$

where, $T(\mathbf{Cap}^{\mathrm{g}}, \xi) = \begin{cases} G_k^{\mathrm{eq}}(\mathbf{Cap}^{\mathrm{g}}, \xi) = 0 & \forall k \in \mathscr{C}^{\mathrm{eq}} \\ G_k(\mathbf{Cap}^{\mathrm{g}}, \xi) \leq 0 & \forall k \in \mathscr{C} \end{cases}$, τ is the risk level, and $\mathscr{D}_\phi$ is the confidence set; $\Pr[.]$ represents the probability distribution induced by ξ . The next step is modelling the uncertainty vector, ξ, and the confidence set, $\mathscr{D}_\phi$, which is detailed in the next section.

4.3 Uncertainty Modelling

In this section, the uncertainties associated with the outputs of DERs, loads and aggregated demands of EVs as well as the confidence set are modelled based on the historical data. Herein, the generation technologies are PV, wind, and biomass.

Uncertainty Modelling of PV Generation

The stochastic variations of PVs from their predicted output values follow a Beta distribution [110]. This distribution, defined by two shape parameters, α_{b} and β_{b}, enables us to represent the prediction error of a predicted output power, $\hat{p}_{i,t}^{\mathrm{g}}$, with the normalized predicted output power and a standard deviation, which varies with $\hat{\eta}_{i,t}^{\mathrm{g}}$. The Beta function for modelling the occurrence of an output power, x, if a prediction value, $\hat{p}_{i,t}^{\mathrm{g}}$, has been forecast, is as follows:

$$f_{\hat{\eta}_{i,t}^{\mathrm{g}}}(x) = x^{\alpha_{\mathrm{b}}-1}(1-x)^{\beta_{\mathrm{b}}-1}. \tag{4.16}$$

The shape parameters α_b and β_b are related to the normalized predicted output power and variance as follows:

$$\hat{\eta}^{g}_{i,t} = \frac{\hat{p}^{g}_{i,t}}{Cap^{g}_{i}} = \frac{\alpha_b}{\alpha_b + \beta_b}, \tag{4.17}$$

$$\sigma_b^2 = \frac{\alpha_b.\beta_b}{(\alpha_b + \beta_b)^2.(\alpha_b + \beta_b + 1)}. \tag{4.18}$$

The historical data can provide $\hat{\eta}^{g}_{i,t}$ and σ_b^2. Thus, α_b and β_b can be calculated by using (4.17) and (4.18).

Uncertainty Modelling of Wind Generation

A Beta function is justified to model the prediction error of the wind power [111]. The relation between the parameters of Beta distribution (i.e., α_b and β_b) and the normalized predicted output power and variance are presented in (4.17) and (4.18).

Uncertainty Modelling of Biomass Generation

The biomass DERs are considered as firm generation. Thus, the output powers of such DERs are considered constant at their rated capacities [112].

Uncertainty Modelling of Load

Load uncertainty is usually modelled by a normal distribution, in which, the mean value is the forecast load and the standard deviation is set to be 2% of the mean value [113].

Uncertainty Modelling of EV Demand

The demand of EVs depends on the number of EVs, their state of charge (SoC), charging start time and its duration. These variables are uncertain, so the overall charging demand of EVs is uncertain as well. Considering the charging behavior of EVs, the overall demand can be categorized as follows:

–Overall Charging Demand of EVs in a Local Residential Community

It was shown in [114, 115] that the aggregated demand of EVs in a residential community follows a normal distribution at each hour, and the average and standard deviation of the distribution depend on the number of EVs and the transportation data of the area.

–Overall Charging Demand of an EV Charging Station

The demand of a charging station depends on the number of EVs that arrive in different time intervals, the duration of a charging process and the charging power profile [114, 116]. It was shown in [114] that the demand uncertainty of a charging station can be modelled by using a Weibull distribution.

4.3.1 Modelling the Confidence Set

A challenging difficulty of handling the uncertainties in HC optimization is the accessibility to the exact PDFs. Since the historical data is limited or there might be not much trust in it, assuming the perfect knowledge about the PDFs of uncertainties is unrealistic. To address this, an ambiguity set of distributions can be used. A common method to create an ambiguity set exploiting the empirical distributions is $\phi-$divergence, which is defined as follows:

$$D_{\phi}(f_{\mathrm{df}} \| f_{\mathrm{df},0}) = \int_{\Omega} \phi\left(\frac{f_{\mathrm{df}}(\xi)}{f_{\mathrm{df},0}(\xi)}\right) f_{\mathrm{df},0}(\xi) d\xi, \tag{4.19}$$

where, f_{df} and $f_{\mathrm{df},0}$ are the actual and empirical density functions, respectively; $\xi \in \mathbb{R}^K$ represents a K-dimensional random vector defined on a probability space, Ω, and $\phi : \mathbb{R} \longrightarrow \mathbb{R}$ is a convex function on $\mathbb{R}^+$. We refer the readers to [117] for more details on characteristics of $\phi-$divergences. One of the most common used members of the $\phi-$divergence families is Variation Distance, which is defined as:

$$\phi_{\mathrm{VD}}(x) = |x-1| \quad for\, x \geq 0, \tag{4.20}$$

Based on the $\phi-$divergences, a confidence set can be built as follows:

$$\mathscr{D}_{\phi} = \left\{ \mathbb{CD} \in \mathscr{M}_{+} : D_{\phi}(f_{\mathrm{df}} \| f_{\mathrm{df},0}) \leq \psi, \quad f_{\mathrm{df}} = d\mathbb{CD}/d\xi \right\}, \tag{4.21}$$

where, $\mathscr{M}_{+}$ represents the set of all cumulative density functions (CDFs), and ψ denotes the risk-aversion level. The higher the risk-aversion level (ψ) is, the bigger the ambiguity set and the more conservative the result of the optimization model would be. However, as compared to uncertainty sets in the RO or the moment-based ambiguity sets, the confidence set, $\mathscr{D}_{\phi}$, can more accurately depict the profile of PDFs, and so provides a less conservative result.

4.4 Solution Methodology

To solve the HC problem (4.15), we convert it to an equivalent JCC optimization by employing a theory presented in [117]. Then, the sample average approximation is used to solve the equivalent JCC [118, 119]. Before presenting the equivalent JCC problem, we need to review the definition of conjugate duality. For a given function $g:\mathbb{R}\longrightarrow\mathbb{R}$, the conjugate g^*:$\mathbb{R}\longrightarrow\mathbb{R}\cup\{+\infty\}$ is defined as follows:

$$g^*(t)=\sup_{x\in\mathbb{R}}\{tx-g(x)\}, \tag{4.22}$$

Based on the properties of the conjugate of $\phi-$divergence functions, we can have the following definition [117]:
Definition 1: For a convex function $\phi:\mathbb{R}\longrightarrow\mathbb{R}$ that $\phi(1)=0$ and $\phi(x)=+\infty\ \forall x<0$, define:

1 : $\underline{m}(\phi^*):=\sup\{m\in\mathbb{R}:\phi^*\text{is a finite constant on }(-\infty,m]\}$

2 : $\overline{m}(\phi^*):=\inf\{m\in\mathbb{R}:\phi^*(m)=+\infty\}$

4.4.1 Equivalent JCC

Let $\mathbb{PR}_0\left(T\left(\mathbf{Cap}^{\mathrm{g}},\xi\right)\right)$ be the probability distribution defined by empirical PDF $f_{\mathrm{df},0}$. Then, the distributionally robust chance constraint, $\inf\limits_{f\in\mathscr{D}_\phi}\left\{\Pr\limits_{\xi\sim f}\left[T\left(\mathbf{Cap}^{\mathrm{g}},\xi\right)\right]\right\}\geq 1-\tau$, can be reformulated equivalently as a JCC [117] given in (4.23):

$$\mathbb{PR}_0\left(T\left(\mathbf{Cap}^{\mathrm{g}},\xi\right)\right)\geq 1-\tau^{'}_{+}, \tag{4.23}$$

where,

$$\tau^{'}=1-\inf_{\substack{zz>0,\ \pi\times zz\leq\ell_\phi\\ \underline{m}(\phi^*)\leq zz_0+zz\leq\overline{m}(\phi^*)}}\left\{\frac{\phi^*(zz_0+zz)-zz_0-\tau\times zz+\psi}{\phi^*(zz_0+zz)-\phi^*(zz_0)}\right\},$$

Table 4.1 Value of ℓ_ϕ, $\underline{\mathrm{m}}\ (\phi^*)$ and $\overline{m}\ (\phi^*)$ for variation distance ϕ-divergence.

Divergences	ℓ_ϕ	$\underline{m}(\phi^*)$	$\overline{m}(\phi^*)$
Variation distance	1	-1	1

where, $zz_0 \in \mathbb{R}$, $\tau_+^{'} = \max\left\{\tau^{'}, 0\right\}$ for $\tau^{'} \in \mathbb{R}$, $\ell_\phi = \lim\limits_{x \longrightarrow +\infty}\left(\frac{\phi(x)}{x}\right)$, and

$$\pi = \begin{cases} -\infty & Leb\{[f_{\mathrm{df},0} = 0]\} = 0, \\ 0 & Leb\{[f_{\mathrm{df},0} = 0]\} > 0 \text{ and} \\ & Leb\left\{[f_{\mathrm{df},0} = 0] \backslash T\left(\mathbf{Cap}^{\mathrm{g}}, \xi\right)\right\} = 0, \\ 1 & o.w, \end{cases}$$

where, $Leb\{\cdot\}$ is the Lebesgue measure on $\mathbb{R}^k$ and $[f_{\mathrm{df},0} = 0] := \{\xi \in \Omega :\ f_{\mathrm{df},0}(\xi) = 0\}$; Lebesgue measure is an extension of the classical notions of length, area and volume to sets of k-dimensional Euclidean space. For the reformulated distributionally robust HC presented in (4.23), the value of ℓ_ϕ, $\underline{m}(\phi^*)$, and $\overline{m}(\phi^*)$ for variation distance $\phi-$divergence is presented in Table 4.1.

Therefore, if we have a function $\tau(\tau_+^{'}, \phi, \psi)$ that maps the $\tau_+^{'}$ to the original risk level, τ, for the given tolerance, ψ, and $\phi-$divergence, it can be stated that if (4.23) is satisfied by some $\mathbf{Cap}^{\mathrm{g}}$, then $\inf\limits_{f \in \mathscr{D}_\phi}\left\{\Pr\limits_{\xi \sim f}\left[T\left(\mathbf{Cap}^{\mathrm{g}}, \xi\right)\right]\right\} \geq 1 - \tau(\tau_+^{'}, \phi, \psi)$ is held for ϕ and ψ. However, we still need to know how to obtain the $\tau_+^{'}$ and the mapping function. It was shown that the worst-case probability bound of $\inf\limits_{f \in \mathscr{D}_\phi}\left\{\Pr\limits_{\xi \sim f}\left[T\left(\mathbf{Cap}^{\mathrm{g}}, \xi\right)\right]\right\}$ is equal to the optimal value of the following optimization problem:

$$\begin{aligned} &\underset{r,s,tt>0}{\text{minimize}} \quad \varpi \times r + \mathbb{PR}_0 \times s, \\ &\text{s.t.} \\ &\Upsilon \times \ell_\phi \times r + \mathbb{PR}_0 \times \phi(s) + (1 - \mathbb{PR}_0) \times \phi(tt) \leq \psi, \\ &\Upsilon \times r + \mathbb{PR}_0 \times s + (1 - \mathbb{PR}_0) \times tt = 1, \end{aligned} \tag{4.24}$$

where, we let $\mathbb{PR}_0 = \mathbb{PR}_0\left(T\left(\mathbf{Cap}^{\mathrm{g}}, \xi\right)\right)$ for notation brevity, and

$$(\varpi, \Upsilon) = \begin{cases} (0,0) & Leb\{[f_{\mathrm{df},0} = 0]\} = 0 \text{ or } \ell_\phi = +\infty, \\ (1,1) & \ell_\phi \leq +\infty,\ Leb\{[f_{\mathrm{df},0} = 0]\} > 0 \text{ and} \\ & Leb\left\{[f_{\mathrm{df},0} = 0] \backslash T\left(\mathbf{Cap}^{\mathrm{g}}, \xi\right)\right\} = 0, \\ (0,1) & \ell_\phi \leq +\infty, \text{ and} \\ & Leb\left\{[f_{\mathrm{df},0} = 0] \backslash T\left(\mathbf{Cap}^{\mathrm{g}}, \xi\right)\right\} > 0, \end{cases}$$

this follows that the mapping function $\tau(\tau_+^{'}, \phi, \psi)$ can be defined as the optimal objective value of (4.24) with setting $\mathbb{PR}_0$ to be $1 - \tau_+^{'}$. As we already know the upper and lower limits of the new risk level, $\tau_+^{'}$, it can be evaluated using a bisection line search algorithm, as given in **Algorithm 1**.

Algorithm 1: Bisection line search algorithm for $\tau_+^{'}$

Input: ε, τ
Output: $\tau_+^{'}$
Step1: Set $L \longleftarrow 1 - \tau$, $U \longleftarrow 1$, and $\varepsilon \longleftarrow 10^{-6}$;
Step2: **if** $U - L \geq \varepsilon$ **then**
    go to **step3**;
else
    $\tau_+^{'} \longleftarrow 1 - U$;
    stop;
Step3: (I) solve (4.24) with $\mathbb{PR}_0 \longleftarrow (U + L)/2$
  (II) record the optimal solution $(\hat{r}, \hat{s})$;
Step4: **if** $\varpi \hat{r} + (U + L)\hat{s}/2 \geq 1 - \tau$ **then**
    update $U \longleftarrow (U + L)/2$;
else
    update $L \longleftarrow (U + L)/2$;
    go to **Step2**;

In this section, we converted the distributionally robust HC model into a JCC optimization, which is much simpler than the original HC problem. However, we still need to solve the equivalent JCC problem presented in (4.23). In the next section, we exploit sample average approximation (SAA) technique to solve the JCC problem.

4.4.2 Sample Average Approximation

Due to the intractability of JCC programs, we use the sample approximation in which the distribution of the random vector ξ is replaced with the empirical distribution obtained from the historical data. In the SAA method, an approximation problem, which is based on an independent Monte Carlo samples of the uncertainty vector, is solved. To simplify the presentation, we replace the constraints set $T(\mathbf{Cap}^{\mathrm{g}}, \xi)$ with a real-valued function G as follows:

$$G(\mathbf{Cap}^{\mathrm{g}}, \xi) := \max \{T(\mathbf{Cap}^{\mathrm{g}}, \xi)\}. \tag{4.25}$$

Thus, the JCC HC problem can be represented as:

$$\left(P_{\tau_+^{'}}\right) \qquad z^*_{\tau_+^{'}} = \min\left\{Obj(\mathbf{Cap}^{\mathrm{g}}) : \mathbf{Cap}^{\mathrm{g}} \in \mathbb{X}_{\tau_+^{'}}\right\}, \tag{4.26}$$

where,

$$\mathbb{X}_{\tau_+^{'}} = \left\{\mathbf{Cap}^{\mathrm{g}} \in \mathbb{XX} : \Pr\{G(\mathbf{Cap}^{\mathrm{g}}, \xi) \leq 0\} \geq 1 - \tau_+^{'}\right\}, \tag{4.27}$$

where, $\mathbb{XX} \subset \mathbb{R}^n$ represents a deterministic feasible region. Let $\xi^1, \xi^2, \cdots, \xi^N$ be N independent Monte Carlo samples of the uncertainty vector ξ. Then, for $\gamma \in [0,1)$, the sample approximation problem is defined as follows:

$$\left(P^N_\gamma\right) \qquad \hat{z}^N_\gamma = \min\left\{Obj(\mathbf{Cap}^{\mathrm{g}}) : \mathbf{Cap}^{\mathrm{g}} \in \mathbb{X}^N_\gamma\right\}, \tag{4.28}$$

where,

$$\mathbb{X}^N_\gamma = \left\{\mathbf{Cap}^{\mathrm{g}} \in \mathbb{XX} : \frac{1}{N}\sum_{i=1}^{N} \mathbb{I}(G(\mathbf{Cap}^{\mathrm{g}}, \xi) \leq 0) \geq 1 - \gamma\right\}, \tag{4.29}$$

where, $\mathbb{I}(\cdot)$ is the indicator function, which takes value one when the argument is true and zero otherwise; $\left(P_{\tau_+^{'}}\right)$, and $\left(P^N_\gamma\right)$ are referred as the true and SAA problems, respectively. It can be proved that if $\left(P_{\tau_+^{'}}\right)$ has an optimal solution, then:

$$\Pr\left\{\hat{z}^N_\gamma \leq z^*_{\tau_+^{'}}\right\} \geq \rho\left(\gamma, \tau_+^{'}, N\right), \tag{4.30}$$

where,

$$\rho\left(\gamma, \tau_+^{'}, N\right) = \sum_{i=0}^{\lfloor \gamma N \rfloor} \binom{N}{i} \left(\tau_+^{'}\right)^i \left(1 - \tau_+^{'}\right)^{N-i}, \tag{4.31}$$

If $\gamma > \tau_+^{'}$, then:

$$\Pr\left\{\hat{z}^N_\gamma \leq z^*_{\tau_+^{'}}\right\} \geq 1 - \exp\left\{-2N\left(\gamma - \tau_+^{'}\right)^2\right\}. \tag{4.32}$$

This means that if $\gamma > \tau_+^{'}$, the solution of SAA problem, i.e. $\left(P_\gamma^N\right)$, is a lower bound to the solution of the actual JCC problem, i.e. $\left(P_{\tau_+^{'}}\right)$. However, the required sample size, i.e. N, could be really high. A good approach to avoid a very high sample size is using M sets of N independent samples. Using M set of N independent samples of ξ, the lower bound that is valid with confidence $1-\chi$ can be obtained using Theorem 1.

Theorem 1: If $\chi \in (0,1)$, $\gamma \in [0,1)$, N, H, and M be positive integer variables such that $H \leq M$ and,

$$\sum_{i=0}^{H-1} \left(\begin{array}{c} M \\ i \end{array} \right) \left(\rho\left(\gamma, \tau_+^{'}, N\right)\right)^i \left(1-\rho\left(\gamma, \tau_+^{'}, N\right)\right)^{N-i} \leq \chi, \tag{4.33}$$

then,

$$\Pr\left\{\hat{z}_{\gamma,[H]}^N \leq z_{\tau_+^{'}}^*\right\} \geq 1-\chi, \tag{4.34}$$

where, $\hat{z}_{\gamma,[H]}^N$ is the optimal value of the set H such that $\hat{z}_{\gamma,[1]}^N \leq \cdots \leq \hat{z}_{\gamma,[H]}^N \leq \cdots \leq \hat{z}_{\gamma,[M]}^N$ [118]. Other than identify a lower bound, SAA problem, i.e. $\left(P_\gamma^N\right)$, could also converge to the optimal solution of the actual JCC problem, i.e. $\left(P_{\tau_+^{'}}\right)$. It is proven that if $\gamma < \tau_+^{'}$, the feasible region of the $\left(P_\gamma^N\right)$ will be a subset of the feasible region of the $\left(P_{\tau_+^{'}}\right)$. It is also proven that if 1) $\gamma = \tau_+^{'}$, 2) the set $\mathbb{XX}$ is compact, 3) the function $f(\mathbf{Cap}^{\mathrm{g}})$ is continuous, 4) $G(\mathbf{Cap}^{\mathrm{g}}, \xi)$ is a Caratheodory function, and 5) there is an optimal solution $\overline{\mathbf{Cap}^{\mathrm{g}}}$ of the true problem such that for all $\varepsilon > 0$ there is $\mathbf{Cap}^{\mathrm{g}} \in \mathbb{XX}$ in $\|\mathbf{Cap}^{\mathrm{g}} - \overline{\mathbf{Cap}^{\mathrm{g}}}\| \leq \varepsilon$ and $\Pr\{G(\mathbf{Cap}^{\mathrm{g}}, \xi) \leq 0\} \geq 1-\tau_+^{'}$, then, $\hat{z}_\gamma^N \longrightarrow z_{\tau_+^{'}}^*$ [119]. Thus, under aforementioned condition, the solution of SAA problem would converge to the solution of the actual JCC problem. The sample approximation problem (4.28) is reformulated as a mix-integer problem as follows:

$$\begin{aligned}
&\underset{Cap_j^{\mathrm{g}}}{\text{minimize}} \quad \sum_{j \in \mathscr{DG}} -Cap_j^{\mathrm{g}}, \\
&\text{s.t.} \\
&G\left(\mathbf{Cap}^{\mathrm{g}}, \boldsymbol{\xi}^{\mathbf{j}}\right) \leq M_j B_j^{\mathrm{spl}} \quad \forall j \in \{1,2,\cdots,N\}, \\
&\sum_{j=1}^{N} B_j^{\mathrm{spl}} \leq \gamma N, \\
&B_j^{\mathrm{spl}} \in \{0,1\} \forall j \in \{1,2,\cdots,N\},
\end{aligned} \tag{4.35}$$

where, B_j^{spl} is a binary variable and M_j is a large positive number.

4.5 Numerical Results

In this section, simulations are carried out to assess the performance of the proposed methodology. Firstly, the modified IEEE 33-bus network is presented in Subsection 4.5.1. Then, the efficacy of the proposed method is evaluated in Subsection 4.5.2.

4.5.1 Test System

The performance of the proposed method is evaluated on the modified IEEE 33-bus system, shown in Fig. 4.2. The bus 1 is connected to the 33kV grid using a Dy transformer with 8.5% reactance. The SCL and the rated SCL at the 33kV side are 200MVA and 250MVA, respectively. The system nominal voltage is 12.66kV.

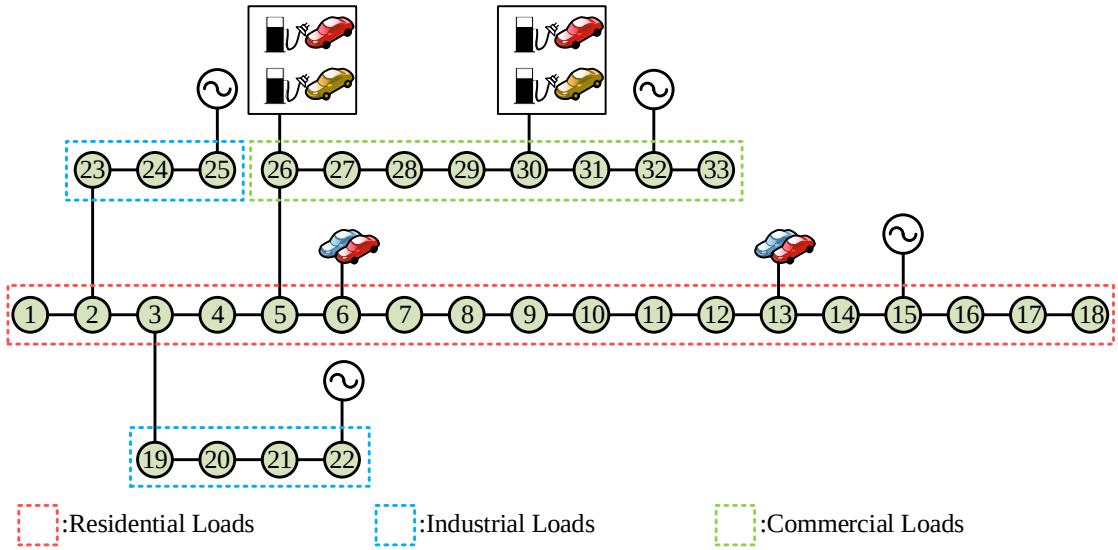

Fig. 4.2 The modified IEEE 33-bus distribution system.

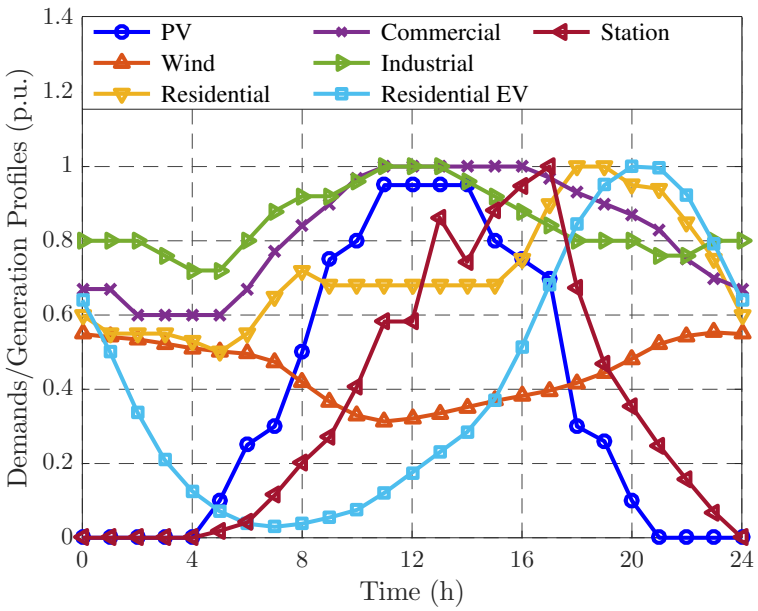

Fig. 4.3 The daily PV, wind, aggregated EVs, charging stations and load normalized profiles.

There are four candidate sites for DERs, i.e., $\mathscr{DG} = \{15, 22, 25, 32\}$. There are two charging stations at buses 26 and 30. Additionally, the charging demand of EVs in the residential area is aggregated at buses 6 and 13. The detail description of the test system is presented in [91]. To have a real situation, three load models (i.e., industrial, commercial, and residential) are considered, as shown in Fig. 4.2. The PV and wind generation profiles, the aggregated EVs charging demand in residential area, the EV charging station demand curve and the load profiles are provided in Fig. 4.3. The PV output profile and the residential, commercial, and industrial load profiles are general profiles that are derived from [18]. The aggregated EVs demand profile is derived from [120, 121], which are based on the National Household Travel Survey (NHTS). As for the demand of charging stations, the obtained profile using the NHTS data provided in [116] is used. Since the NHTS data presents the driving behavior of American public, the wind generation profile is derived from the data provided for the continental United States in [122]. The presented curves in Fig. 4.3 are normalized multipliers. Please note that basic values of DERs and loads are the capacity of DERs and the nominal loads, respectively. The basic value for charging stations' demand is 224kW and for aggregated demand of residential EV is 285kW.

4.5.2 Simulation Results and Discussions

The proposed DRO-based method is examined on the IEEE 33-bus system for the four cases as follows:

- **PV-HC:** All DERs are PV systems.

- **Wind-HC:** All DERs are wind generators.
- **Biomass-HC:** All DERs are biomass generators.
- **Combined-HC:** The DERs at buses 15 and 32 are PV units, and the DERs at buses 22 and 25 are wind and biomass generators, respectively.

Fig. 4.4 shows the estimated HC of different generation technologies for different risk levels. Observe that the HC grows by increasing the risk level, which indicates that looser security requirement leads to a higher HC. Furthermore, as can be seen in Fig. 4.4, the HC curve slope depends on the DER technology. For instance, accepting 20% security risk, increases the HC by 2.48%, 20.3% and 1.17% for PV, wind, and biomass technologies, respectively. This implies that accepting a higher risk to increase the HC of the system is not a good idea if the DERs technologies are PV and biomass.

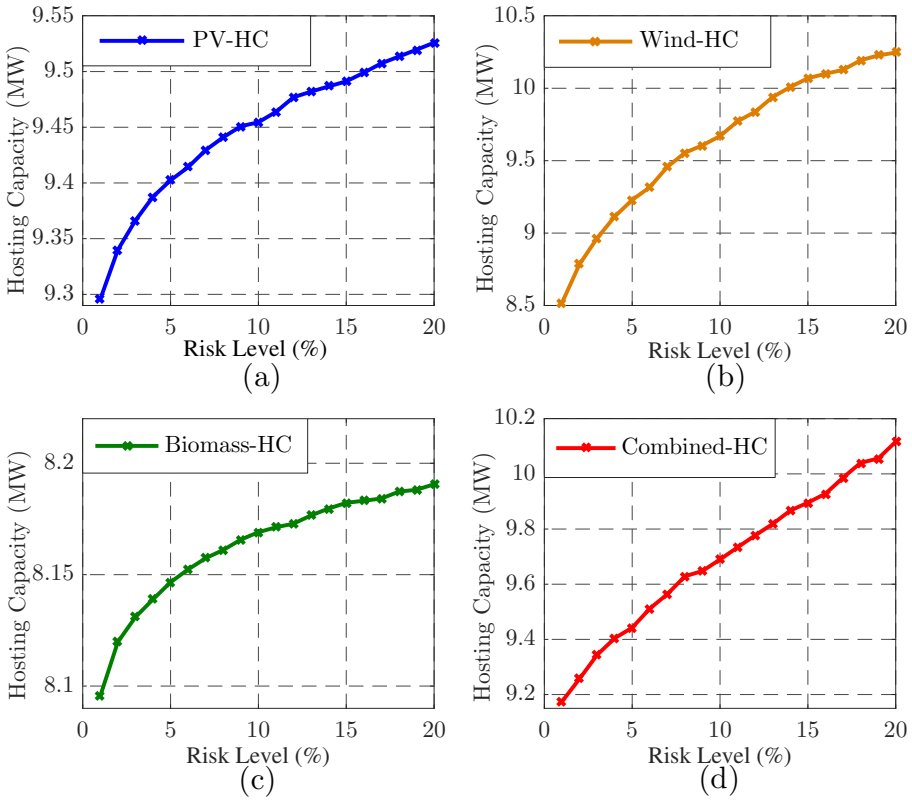

Fig. 4.4 The HC obtained via the proposed DRO-HC method with different risk levels for different technologies including: (a) PV; (b) wind; (c) biomass; and (d) combination of PV, wind and biomass.

An important factor that affects the estimated HC of the system is the existence of the historical data. Intuitively, as the sample size of historical data increases, the empirical

distribution becomes closer to the actual distribution. Thus, the conservativeness of the HC estimation decreases. In DRO-based method, ψ is the parameter to present the value of data. The higher the number of samples, the more accurate the empirical distribution, the smaller the risk-aversion level, ψ, and the smaller the confidence set, $\mathscr{D}_\phi$. Fig. 4.5 demonstrates the effect of risk-aversion level (hence historical data) on the HC for different technologies. As it can be seen in Fig. 4.5, the shortage of historical data increases the conservativeness of the HC estimation. For instance, the shortage of data decreases the estimated HC for PV, wind, and biomass technologies by 3.09%, 14.52% and 2.06%, respectively. Observe that the value of data in the test system for wind technology is much higher than that of PV or biomass technologies. Furthermore, as the slope of HC curves for small values of risk-aversion level (i.e., $\psi \in [0\%, 5\%]$) is small, increasing the size of historical data to get a more accurate empirical distribution does not have a tangible effect on the estimated HC. As shown in Fig. 4.5, 5% error in empirical distributions only decreases the HC by 0.21%, 1.41%, and 0.11% for PV, wind, and biomass technologies, respectively.

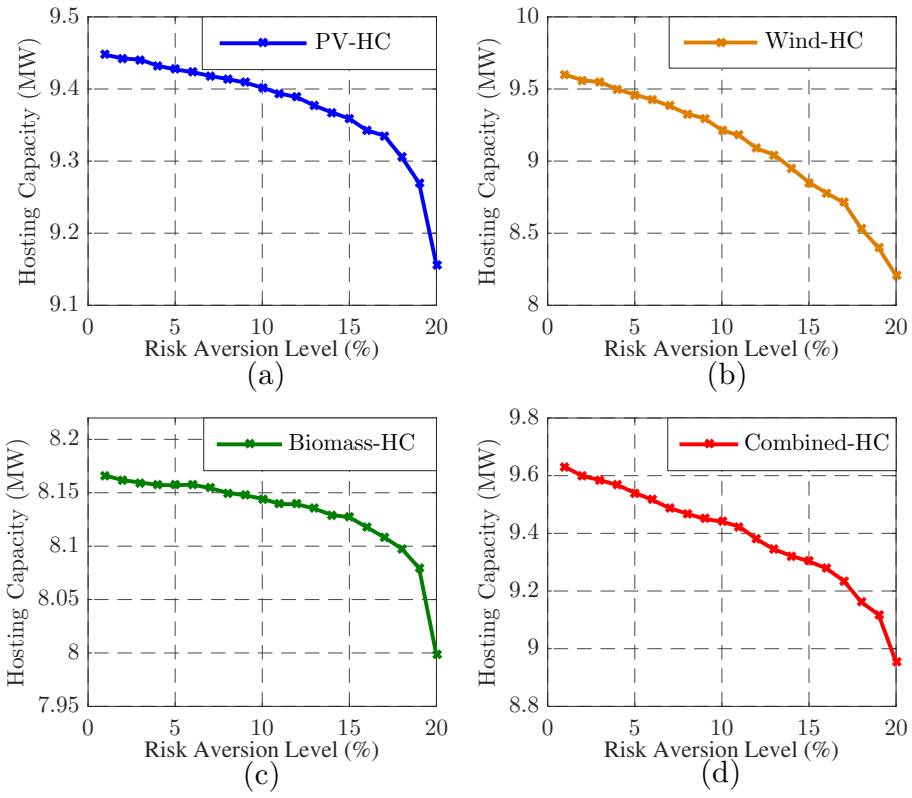

Fig. 4.5 The value of data for the HC obtained via the proposed DRO-HC method with $\tau = 10\%$ for different technologies including: (a) PV; (b) wind; (c) biomass; and (d) combination of PV, wind and biomass.

A prospective technology that may affect the HC of a system is EVs. Fig. 4.6 indicates the effect of EVs' aggregated demand on the HC. Observe that increasing the peak value of EVs' aggregated demand to 640kW can only increase the HC of the system by 0.29%, 0.25%, and 0.13% for PV, wind and biomass technologies, respectively. Thus, the aggregated impact of EV loads on the HC of the system is not tangible. This is because the HC reaches its maximum value during time period $t = 11$ for PV, $t = 5$ for wind, $t = 5$ for biomass and $t = 9$ for combined generation. We will call these periods as the critical time periods. During critical time periods, the normalized aggregated demand of residential EVs is below 10%, which means that increasing the EVs cannot effectively increase the load. To demonstrate that the concluded result does not depend on the aggregation points of EVs, the sensitivity of the HC to the location of aggregated EVs demand is also presented using error bars in Fig. 4.6.

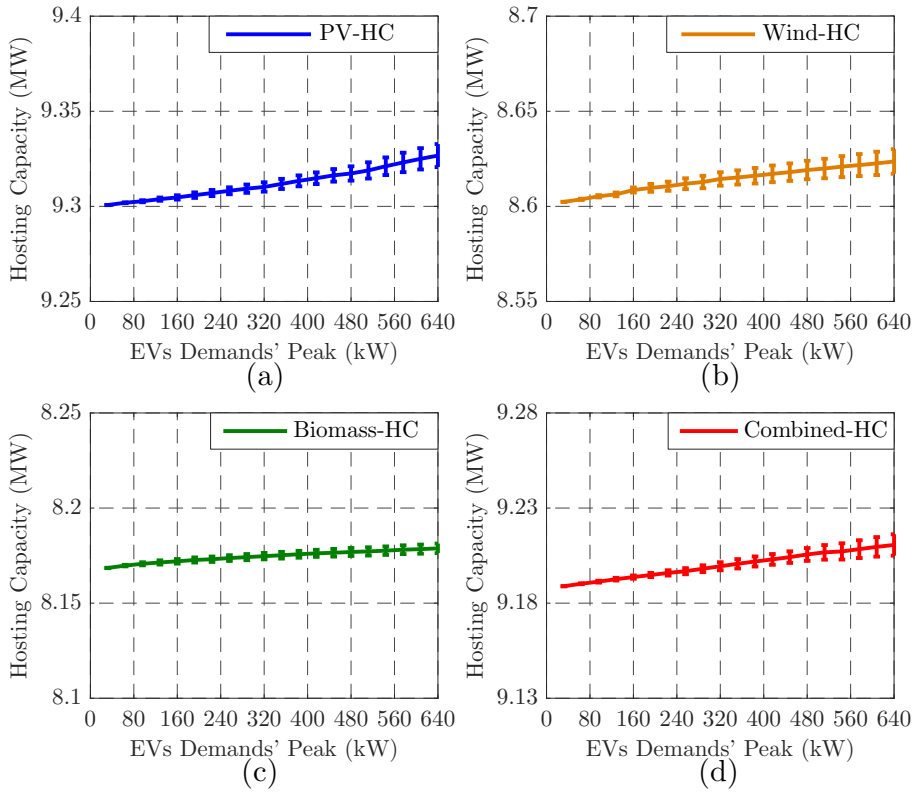

Fig. 4.6 The effect of aggregate demand of residential EVs on the HC obtained via the proposed DRO-HC method with $\tau = 1\%$ for different technologies including: (a) PV; (b) wind; (c) biomass; and (d) combination of PV, wind and biomass.

Observe that changing the location of aggregated demand of residential EVs deviates the obtained HC by 0.068%, 0.072%, and 0.032% for PV, wind, and biomass technologies, respectively. In other words, irrespective of locations that demands of residential EVs are

aggregated, increasing the peak value of aggregated EVs demand does not increase the HC, effectively.

Finally, the effect of charging stations' demands on the HC is assessed. To do so, the peak value of charging stations' demands is varied from 0kW to 480kW, as shown in Fig. 4.7. Observe that increasing the demand of charging stations can linearly increase the HC of the system. However, the rate of increase in the HC depends on the generation technology. Increasing the peak value of charging stations' demands from 0 to 480kW grows the HC by 1.81%, 0.15%, and 0.1% for PV, wind, and biomass technologies, respectively. This is because the critical time period depends on the DERs technologies. The charging station demand profile at critical time period for PV, wind, biomass, and combined generations are 58.26%, 1.83%, 1.83%, and 27.06%, respectively. Since the demand profile of charging stations during the critical time period of PV generation is higher than that of other technologies, the charging stations' demands have a higher effect on the HC of the system for PV generation.

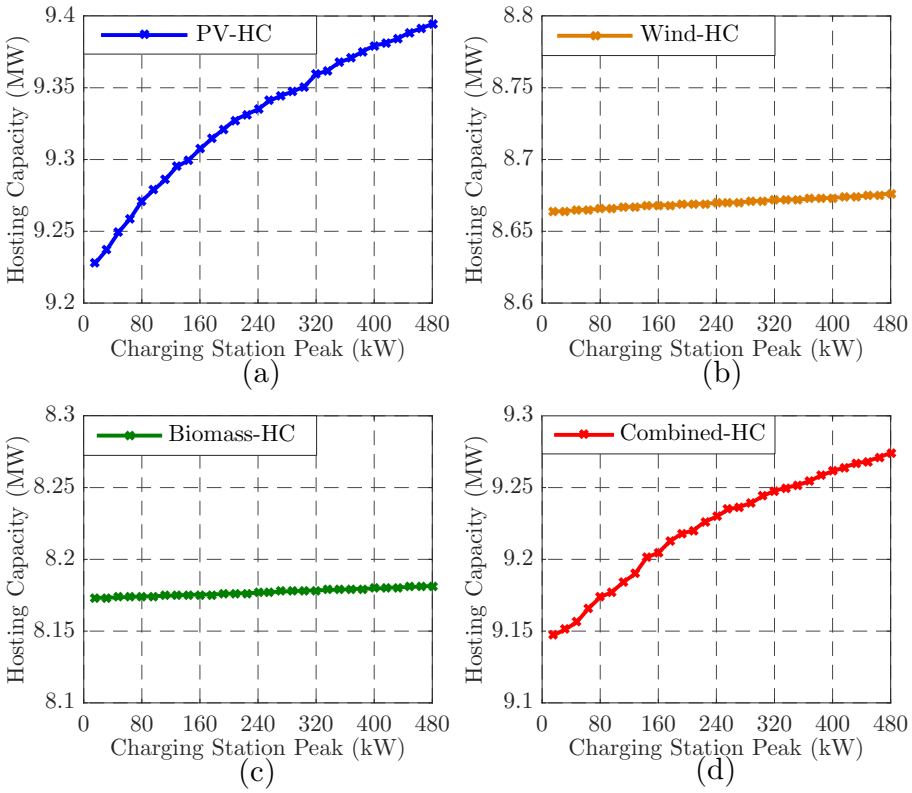

Fig. 4.7 The effect of charging stations' demands on the HC obtained via the proposed DRO-HC method with $\tau = 1\%$ for different technologies including: (a) PV; (b) wind; (c) biomass; and (d) combination of PV, wind and biomass.

4.6 Summary

In this chapter, a DRO-based method is proposed to assess the HC of distribution networks. In the proposed method, the empirical distributions of uncertain variables are used to define a confidence set. The more accurate the empirical distribution is, the smaller the confidence set and the less conservative the obtained result would be. The effectiveness of the proposed method was examined on the modified IEEE 33-bus system and the effects of risk level and size of historical data on the HC of the system were assessed. It was demonstrated that the proposed method yields in a less conservative solution by increasing the risk level. However, the increase in the HC by accepting a higher risk level depends on the DER type. For instance, accepting 20% risk level can increase the HC of the system by 2.48%, 20.3% and 1.17% for PV, wind and biomass technologies, respectively. Thus, accepting a higher risk level to increase the HC of the test system may not be a good idea if the DERs technologies are PV and biomass. As for the historical data, it was observed that shortage of data can exponentially increase the conservativeness of the estimated HC. For instance, the shortage of historical data decreased the estimated HC for wind technology up to 14.52%.

The proposed method is also used to assess the effects of the aggregated residential EVs and charging stations' demand on the HC for different DER technologies. Following are the conclusions derived from the simulation results:

- Although aggregated demand of residential EVs increases the peak load of the distribution system, it does not affect the HC significantly. This is because the HC of the system reaches its maximum value during the time periods that the aggregated demand of EVs is below 10% of its peak value. This may vary depending on EVs behavior in the future.
- The effect of charging stations' demand on the HC depends on the DER technology. If DERs are PV units, increasing the charging stations' demand to its maximum increases the HC up to 1.81%. Nevertheless, it cannot effectively increase the HC of the system if DERs are wind and biomass based.

Chapter 5

Photovoltaic Hosting Capacity Sensitivity to Active Distribution Network Management

5.1 Introduction

As discussed in Chapter 1, one approach to improve the hosting capacity (HC) in distribution systems is controlling the active and reactive power of distributed energy resources (DERs). Different local control strategies have been proposed to alleviate the over-voltage issue by curtailing the output power of DERs and/or absorbing reactive power [45, 50, 51, 5, 52]. However, a considerable part of the existing literature has focused on identifying the HC without considering the impacts of control schemes. Further, most of the studies that focused on increasing the HC using control schemes are hard to generalize as their finding are specific to the case studies, albeit having real results. There are a few studies that attempted to assess the effectiveness of the control schemes in increasing the HC in multiple distribution systems [7, 9]. However, they either modelled distribution systems as balanced systems or focused on medium voltage (MV) distribution systems. Besides, the number of test systems assessed in those studies is limited, which implies there is a need for more comprehensive studies.

Voltage control schemes in general and in particular local Volt-Var control schemes, are accompanied with several challenges including voltage oscillations [123, 124]. Therefore, integrating local Volt-Var controllers in power flow equations might result in an oscillatory behavior in the system. Convergence to the equilibrium point would be time-consuming as it requires running many power flow iterations. For instance, Fig. 5.1 shows a simple radial

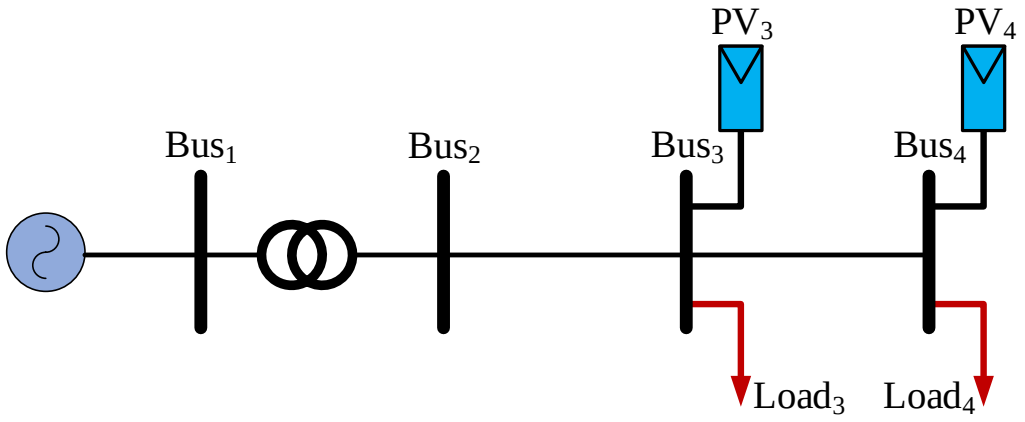

Fig. 5.1 Test system to illustrate the oscillation of local Volt-Var controllers.

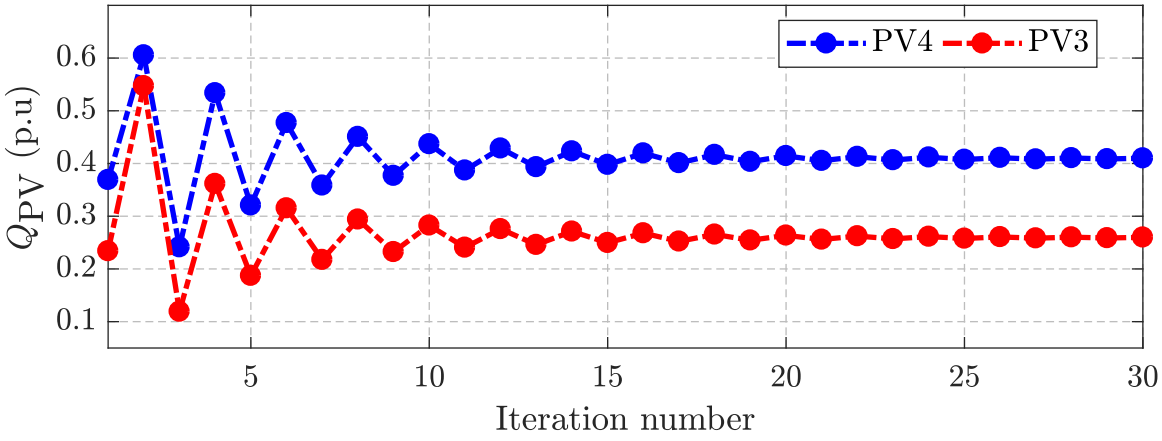

Fig. 5.2 The convergence of reactive power with Volt-Var controllers.

distribution system, where phtovoltaic (PV) systems utilize the conventional Volt-Var droop control recommended by the IEEE 1547 standard [55]. As shown in Fig. 5.2, the reactive power of PV systems (Q_{PV}) oscillates and reaches an equilibrium point after 30 power flow iterations. To the best of the authors' knowledge, all existing studies that assessed the impacts of control schemes on the HC of a set of distribution systems integrated control schemes in power flow equations. Therefore, they would require numerous power flow iteration to identify the HC. Hence, they are computationally cumbersome. Thus, there is a need to develop a methodology to assess the effectiveness of control schemes in increasing the HC of distribution systems. Further, to address the diversity of the characteristics of LV networks, a high number of LV systems should be assessed.

In Chapters 2, 3 and 4, the HC has been assessed without considering active network management (ANM) schemes. In this chapter, we develop an optimization-based framework to assess the impact of ANM schemes on increasing the photovoltaic HC (PVHC). To do so, the ANM schemes are modelled as linear equality and inequality constraints in the optimization model. Further, unlike most studies, the network is modelled as an unbalanced system in the optimization problem. Moreover, a mathematical definition of minimum PVHC is laid out based on the solution of the developed optimization model. The main advantage of this method over the existing power flow method is that it converges to the solution without requiring more than one iteration. To cover the diversity in the characteristics of distribution systems, the proposed method is used to examine the effects of ANM schemes on increasing the PVHC on 128 LV UK feeders. Further, the total annual energy losses is defined as an index to assess the PV-based ANM schemes from an economic perspective. Finally, the sensitivity of the results to the R/X ratio of the feeders is assessed. The outcome of this chapter is presented as a journal paper, which is currently under reviewed[1].

The remainder of this chapter is organized as follows: Section 5.2 describes the optimization-based framework to determine the PVHC. The problem formulation is presented in Section 5.3. Section 5.4 presents characteristics of the test feeders, as well as the numerical results and discussion. Finally, Section 5.5 summarizes the chapter.

5.2 Probabilistic Framework

In practice, quantifying the number, location, and capacity of PV systems is difficult. To properly model these uncertain variables, a stochastic framework as shown in Fig. 5.3 is developed. The framework includes three modules. The first module addresses the uncertainties associated with the number and location of PV systems by defining expansion scenarios. The second module addresses the uncertainties associated with the loads and output power of PV systems by solving the developed optimization model (5.48) in a time series simulation. Then, the minimum PV hosting capacity (MPVHC) is identified based on the objective function values and active power curtailments (APCs) calculated in the second module. In the following, these three modules are explained in details.

Module 1) PV Expansion Scenarios: The number, location and size of PVs are three uncertain variables that depend on the costumers' decision. If these variables are considered as the decision variables, the PVHC optimization model converges to a set of decision variables that would result in the maximum PVHC. However, based on the definition,

[1] "Photovoltaic Hosting Capacity Sensitivity to Active Distribution Network Management," IEEE Transactions on Power Systems, 2019 [125].

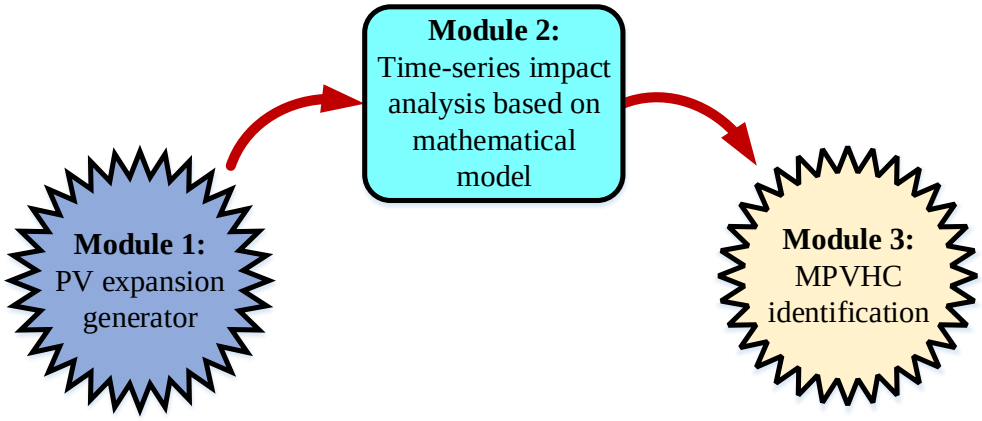

Fig. 5.3 The proposed PVHC analysis framework.

identifying the MPVHC in a distribution system is more desirable. Thus, an acceptable method to deal with this situation is assessing the PVHC by generating a high number of scenarios. The steps for generating the scenarios are as follows:

- **Step A:** This step addresses the uncertainty associated with the number of PV systems that could be installed. The minimum number of PV installation is zero and the maximum number is equal to the total number of customers. To cover a wide range of scenarios, the location penetration level (LPL), i.e. the ratio of the number of potential PV location to the total number of customers, is increased by a fixed step from 1% to 100%.

- **Step B:** To address the uncertainty associated with the location of PV systems, a Monte Carlo approach is used to generate N_{scn} combinations of locations for each one of LPLs defined in Step A. Each combination is generated by random selection from the pool of all customers.

- **Step C:** The base capacity of each of the combinations defined in Step B can be determined by using the distribution function for the size of PV systems [96].

- **Step D:** Considering the base capacity determined in Step C, the total installed capacity (TIC) for each scenario is calculated.

Module 2) Time Series Impact Analysis: This module addresses the uncertainties associated with the loads and output power of PV systems. The module is designed to assess whether the generated scenarios in Module 1 violates the operational constraints of the system over the study period or not. The core of this module is an optimization model, in which the

operation criteria are modelled as equality and inequality constraints. Thus, the solution of this optimization model is used to identify the scenarios that violate the system constraints. The details of the optimization model are provided in Section 5.3. The model is developed in a way that it converges in any condition. The total amount of APC is the indicator to detect the violation of the constraints over the study period. If the total amount of the APC is higher than the APC indicator (APCI), it implies that the scenario violates the operational constraints. The APCI for different control strategies is as follows:

$$APCI_i^{lpl}(t) = \begin{cases} 0 & No\ Control, \\ 0 & OLTC, \\ 0 & CPFM, \\ \sum_{j\in\mathscr{N}} \left| \left(\eta^{\mathbf{g}}_{\mathbf{j,t}} - \rho_{\mathbf{apc}}\right) \odot \mathbf{Cap}^{\mathbf{g}}_{\mathbf{j}} \right|_1 & LAPFM, \\ 0 & VVOM, \\ \sum_{j\in\mathscr{N}} |\eta^{\mathbf{g}}_{\mathbf{j,t}} \odot \mathbf{Cap}^{\mathbf{g}}_{\mathbf{j}}|_1 & VWOM, \\ \sum_{j\in\mathscr{N}} |\eta^{\mathbf{g}}_{\mathbf{j,t}} \odot \mathbf{Cap}^{\mathbf{g}}_{\mathbf{j}}|_1 & VVWOM, \end{cases} \tag{5.1}$$

where, $\odot$ denotes the element-wise multiplication; $APCI_i^{lpl}(t)$ is the APC indicator for the (i^{th}) scenario of the LPL (lpl) at time (t); OLTC, CPFM, LAPFM, VVOM, VWOM and VVWOM are different voltage control schemes that will be discussed in Section 5.3; $\mathbf{Cap}^{\mathbf{g}}_{\mathbf{j}} = [Cap_j^{\mathrm{g,a}}, Cap_j^{\mathrm{g,b}}, Cap_j^{\mathrm{g,c}}]^{\mathrm{T}}$ represents the vector of DERs installed capacity; $\eta^{\mathbf{g}}_{\mathbf{j,t}} = [\eta^{\mathrm{a}}_{j,t}, \eta^{\mathrm{b}}_{j,t}, \eta^{\mathrm{c}}_{j,t}]^{\mathrm{T}}$ denotes the vector of capacity factors at bus (j) and at time (t); and $\rho_{\mathbf{apc}}$ is the maximum limitation on the feed-in active power. By solving the developed optimization model (5.48) for the study period, i.e. all $t \in \mathscr{H}$, a vector Λ of length $|\mathscr{H}|$ is obtained for each expansion scenario. This vector contains the total APC for all $t \in \mathscr{H}$. A scenario violates the operational constraints if there is a time step in which the APC is higher than APCI. To mathematically represent this condition, for all $lpl \in \mathscr{LP}$, the vector Γ^{lpl} is defined as follow:

$$\Gamma^{lpl}(j) = \begin{cases} 1 & \left(\sum_{t=1}^{|\mathscr{H}|} \Phi_j^{lpl}(t)\right) \geq 1 \\ 0 & Otherwise \end{cases} \quad j \in \{1...N_{scn}\}, \tag{5.2}$$

where, $\mathscr{LP}$ is the set of all LPL and

$$\Phi_j^{lpl}(t) = \begin{cases} 1 & \Lambda(t)_j^{lpl} > APCI_j^{lpl}(t) \\ 0 & Otherwise \end{cases} \quad t \in \mathscr{H}. \tag{5.3}$$

Module 3) MPVHC Identification: Th MPVHC is defined as the lowest total PV capacity that yields a violation in the distribution system operational constraints. Based on this definition, the MPVHC can be mathematically formulated as follows:

$$MPVHC = \min_{lpl \in \mathscr{LP}} \min_{1 \le i \le N_{scn}} \left\{ TIC_i^{lpl} | \Gamma^{lpl}(i) = 1 \right\}, \tag{5.4}$$

where, TIC_i^{lpl} represents the TIC for the (i^{th}) scenario of the LPL (lpl).

5.3 Problem Formulation

The PVHC is the minimum PV capacity that results in a violation of technical constraints in the system. The PVHC problem for a set of locations at time (t) can be formulated as an optimization problem as follows:

$$\text{minimize} \quad \sum_{i \in \mathscr{PV}} \sum_{k \in \Phi} -p_{i,t}^{\text{g},k} + APC_{i,t}^{k}, \tag{5.5}$$

where, $\mathscr{PV}$ is the set of buses that have PVs; Φ denotes the set of phases; $p_{i,t}^{\text{g},k}$ denotes the active power that can be injected at bus (i), phase (k) and time (t); and $APC_{i,t}^{k}$ represents the curtailed active power at bus (i), phase (k) and time (t). The operation constraints are presented in Subsections 5.3.1 and 5.3.2.

5.3.1 Distribution System Model

In Chapters 2 and 3, the formulation was presented for a balanced system. In this chapter, we present the formulation for an unbalanced network. Consider a radial distribution network. Let $\mathscr{N} = \{o, \ldots, n\}$ represents the set of all buses. Let $\mathscr{B}$ denotes the set of all branches, and (i, j) or $i \to j$ represents a branch between bus (i) and (j) in set $\mathscr{B}$. For every bus $i \in \mathscr{N}$, let $\mathbf{V_{i,t}} = [V_{i,t}^a, V_{i,t}^b, V_{i,t}^c]^{\text{T}}$ denotes the complex vector of three phase voltage at time (t), and $\mathbf{s_{i,t}^d} = \mathbf{p_{i,t}^d} + i\mathbf{q_{i,t}^d}$ represents the complex vector of three phase load at time (t), where, $\mathbf{p_{i,t}^d} = \left[p_{i,t}^{\text{d},a}, p_{i,t}^{\text{d},b}, p_{i,t}^{\text{d},c}\right]^{\text{T}}$ and $\mathbf{q_{i,t}^d} = \left[q_{i,t}^{\text{d},a}, q_{i,t}^{\text{d},b}, q_{i,t}^{\text{d},c}\right]^{\text{T}}$. For every line $(i, j) \in \mathscr{B}$, $\mathbf{Z_{ij}} \in \mathbb{C}^{3\times 3}$ denotes the impedance complex matrix, and $\mathbf{S_{ij,t}} = \mathbf{P_{ij,t}} + i\mathbf{Q_{ij,t}}$ represents the three phase complex power from bus (i) to bus (j) at time (t). For every bus $i \in \mathscr{N}$, $\mathbf{APC_{i,t}} = [APC_{i,t}^a, APC_{i,t}^b, APC_{i,t}^c]^{\text{T}}$ represents the vector of active power curtailment at time (t), and $\mathbf{s_{i,t}^g} = \mathbf{p_{i,t}^g} + i\mathbf{q_{i,t}^g}$ denotes the complex vector of three phase generated power at time (t), where, $\mathbf{p_{i,t}^g} = \left[p_{i,t}^{\text{g},a}, p_{i,t}^{\text{g},b}, p_{i,t}^{\text{g},c}\right]^{\text{T}}$ and $\mathbf{q_{i,t}^g} = \left[q_{i,t}^{\text{g},a}, q_{i,t}^{\text{g},b}, q_{i,t}^{\text{g},c}\right]^{\text{T}}$. Thus, the branch flow model

can be summarized as follow:

$$\mathbf{v}^{\mathbf{2}}_{\mathbf{j},\mathbf{t}} = \mathbf{v}^{\mathbf{2}}_{\mathbf{i},\mathbf{t}} - 2\left(\widetilde{\mathbf{r}}_{\mathbf{ij}}\mathbf{P}_{\mathbf{ij},\mathbf{t}} + \widetilde{\mathbf{x}}_{\mathbf{ij}}\mathbf{Q}_{\mathbf{ij},\mathbf{t}}\right) + \mathrm{W}^{\mathrm{v}}_{ij}\left(\mathbf{P}_{\mathbf{ij},\mathbf{t}}, \mathbf{Q}_{\mathbf{ij},\mathbf{t}}\right), \tag{5.6}$$

where, $\mathbf{v}_{\mathbf{i},\mathbf{t}} = |\mathbf{V}_{\mathbf{i},\mathbf{t}}| = \left[|V^a_{i,t}|, |V^b_{i,t}|, |V^c_{i,t}|\right]^{\mathrm{T}}$ and $\mathbf{v}^{\mathbf{2}}_{\mathbf{i},\mathbf{t}} = \left[|V^a_{i,t}|^2, |V^b_{i,t}|^2, |V^c_{i,t}|^2\right]^{\mathrm{T}}$.

$$\widetilde{\mathbf{r}}_{\mathbf{ij}} = Re\left\{\mathbf{a}_i\mathbf{a}_i^H\right\} \odot Re\left\{\mathbf{Z}_{\mathbf{ij}}\right\} + Im\left\{\mathbf{a}_i\mathbf{a}_i^H\right\} \odot Im\left\{\mathbf{Z}_{\mathbf{ij}}\right\}, \tag{5.7}$$

$$\widetilde{\mathbf{x}}_{\mathbf{ij}} = Re\left\{\mathbf{a}_i\mathbf{a}_i^H\right\} \odot Im\left\{\mathbf{Z}_{\mathbf{ij}}\right\} - Im\left\{\mathbf{a}_i\mathbf{a}_i^H\right\} \odot Re\left\{\mathbf{Z}_{\mathbf{ij}}\right\}, \tag{5.8}$$

$$\mathbf{a}_i = \left[1 \;\; e^{-j2\pi/3} \;\; e^{j2\pi/3}\right]^{\mathrm{T}}, \tag{5.9}$$

$$\mathrm{W}^{\mathrm{v}}_{ij}\left(\mathbf{P}_{\mathbf{ij}}, \mathbf{Q}_{\mathbf{ij}}\right) = \left[\mathbf{Z}_{\mathbf{ij}}\left(\mathbf{S}_{\mathbf{ij}} \ominus \mathbf{V}_{\mathbf{i}}\right)^*\right] \odot \left[\mathbf{Z}_{\mathbf{ij}}{}^*\left(\mathbf{S}_{\mathbf{ij}} \ominus \mathbf{V}_{\mathbf{i}}\right)\right]. \tag{5.10}$$

where, $\odot$ and $\ominus$ denote the element-wise multiplication and division, respectively. For every branch $(i, j) \in \mathscr{B}$, power balance equations are as follows:

$$\mathbf{P}_{\mathbf{ij},\mathbf{t}} = \sum_{k:\, j \longrightarrow k} \mathbf{P}_{\mathbf{jk},\mathbf{t}} + \mathbf{p}^{\mathbf{d}}_{\mathbf{j},\mathbf{t}} - \mathbf{p}^{\mathbf{g}}_{\mathbf{j},\mathbf{t}} + \mathbf{APC}_{\mathbf{j},\mathbf{t}} + \mathrm{W}^{\mathrm{p}}_{ij}\left(\mathbf{P}_{\mathbf{ij},\mathbf{t}}, \mathbf{Q}_{\mathbf{ij},\mathbf{t}}\right), \tag{5.11}$$

$$\mathbf{Q}_{\mathbf{ij},\mathbf{t}} = \sum_{k:\, j \longrightarrow k} \mathbf{Q}_{\mathbf{jk},\mathbf{t}} + \mathbf{q}^{\mathbf{d}}_{\mathbf{j},\mathbf{t}} - \mathbf{q}^{\mathbf{g}}_{\mathbf{j},\mathbf{t}} + \mathrm{W}^{\mathrm{q}}_{ij}\left(\mathbf{P}_{\mathbf{ij},\mathbf{t}}, \mathbf{Q}_{\mathbf{ij},\mathbf{t}}\right), \tag{5.12}$$

$$\mathbf{p}^{\mathbf{g}}_{\mathbf{j},\mathbf{t}} \leq \eta^{\mathbf{g}}_{\mathbf{j},\mathbf{t}} \odot \mathbf{Cap}^{\mathbf{g}}_{\mathbf{j}}, \tag{5.13}$$

where, $\eta^{\mathbf{g}}_{\mathbf{j},\mathbf{t}}$ represents the vector of capacity factors at time (t) and

$$\mathrm{W}^{\mathrm{p}}_{ij}\left(\mathbf{P}_{\mathbf{ij},\mathbf{t}}, \mathbf{Q}_{\mathbf{ij},\mathbf{t}}\right) = \mathbf{P}_{\mathbf{ij},\mathbf{t}} \odot \left[\widetilde{\mathbf{r}}_{\mathbf{ij}}\mathbf{P}_{\mathbf{ij},\mathbf{t}} + \widetilde{\mathbf{x}}_{\mathbf{ij}}\mathbf{Q}_{\mathbf{ij},\mathbf{t}}\right] + \mathbf{Q}_{\mathbf{ij},\mathbf{t}} \odot \left[\widetilde{\mathbf{r}}_{\mathbf{ij}}\mathbf{Q}_{\mathbf{ij},\mathbf{t}} - \widetilde{\mathbf{x}}_{\mathbf{ij}}\mathbf{P}_{\mathbf{ij},\mathbf{t}}\right], \tag{5.14}$$

$$\mathrm{W}^{\mathrm{q}}_{ij}\left(\mathbf{P}_{\mathbf{ij},\mathbf{t}}, \mathbf{Q}_{\mathbf{ij},\mathbf{t}}\right) = \mathbf{P}_{\mathbf{ij},\mathbf{t}} \odot \left[\widetilde{\mathbf{x}}_{\mathbf{ij}}\mathbf{P}_{\mathbf{ij},\mathbf{t}} - \widetilde{\mathbf{r}}_{\mathbf{ij}}\mathbf{Q}_{\mathbf{ij},\mathbf{t}}\right] + \mathbf{Q}_{\mathbf{ij},\mathbf{t}} \odot \left[\widetilde{\mathbf{r}}_{\mathbf{ij}}\mathbf{P}_{\mathbf{ij},\mathbf{t}} + \widetilde{\mathbf{x}}_{\mathbf{ij}}\mathbf{Q}_{\mathbf{ij},\mathbf{t}}\right]. \tag{5.15}$$

The terms $\mathrm{W}^{\mathrm{v}}_{ij}\left(\mathbf{P}_{\mathbf{ij},\mathbf{t}}, \mathbf{Q}_{\mathbf{ij},\mathbf{t}}\right)$, $\mathrm{W}^{\mathrm{p}}_{ij}\left(\mathbf{P}_{\mathbf{ij},\mathbf{t}}, \mathbf{Q}_{\mathbf{ij},\mathbf{t}}\right)$ and $\mathrm{W}^{\mathrm{q}}_{ij}\left(\mathbf{P}_{\mathbf{ij},\mathbf{t}}, \mathbf{Q}_{\mathbf{ij},\mathbf{t}}\right)$ make equations (5.6), (5.11) and (5.12) nonlinear. To simplify the model, authors in [96] presented a method to linearize $\mathrm{W}^{\mathrm{v}}_{ij}\left(\mathbf{P}_{\mathbf{ij},\mathbf{t}}, \mathbf{Q}_{\mathbf{ij},\mathbf{t}}\right)$, $\mathrm{W}^{\mathrm{p}}_{ij}\left(\mathbf{P}_{\mathbf{ij},\mathbf{t}}, \mathbf{Q}_{\mathbf{ij},\mathbf{t}}\right)$, and $\mathrm{W}^{\mathrm{q}}_{ij}\left(\mathbf{P}_{\mathbf{ij},\mathbf{t}}, \mathbf{Q}_{\mathbf{ij},\mathbf{t}}\right)$. We refer the readers to [96] and [94] for more details. Further, under normal operation of distribution networks, the following approximation is valid:

$$\mathbf{v}^{\mathbf{2}}_{\mathbf{i},\mathbf{t}} - \mathbf{v}^{\mathbf{2}}_{\mathbf{j},\mathbf{t}} \approx 2\left(\mathbf{v}_{\mathbf{i},\mathbf{t}} - \mathbf{v}_{\mathbf{j},\mathbf{t}}\right) \odot \mathbf{v}_{\mathrm{nom}}, \tag{5.16}$$

where, $\mathbf{v}_{\mathrm{nom}}$ is the nominal voltage in the system. This approximation causes at most 0.25 % - 1 % error when there is 5 % - 10 % deviation in voltage magnitudes [126]. Thus, the

linearized distribution system model can be established as follows:

$$\mathbf{v_{j,t}} = \mathbf{v_{i,t}} - \left(\widetilde{\mathbf{r}}_{\mathbf{ij}}\mathbf{P_{ij,t}} + \widetilde{\mathbf{x}}_{\mathbf{ij}}\mathbf{Q_{ij,t}}\right) \ominus \mathbf{v}_{\text{nom}} + \text{Wlin}_{ij}^{\text{v}}\left(\mathbf{P_{ij,t}}, \mathbf{Q_{ij,t}}\right) \ominus (2\mathbf{v}_{\text{nom}}), \tag{5.17}$$

$$\mathbf{P_{ij,t}} = \sum_{k:j\longrightarrow k} \mathbf{P_{jk,t}} + \mathbf{p}_{\mathbf{j,t}}^{\mathbf{d}} - \mathbf{p}_{\mathbf{j,t}}^{\mathbf{g}} + \mathbf{APC_{j,t}} + \text{Wlin}_{ij}^{\text{p}}\left(\mathbf{P_{ij,t}}, \mathbf{Q_{ij,t}}\right), \tag{5.18}$$

$$\mathbf{Q_{ij,t}} = \sum_{k:j\longrightarrow k} \mathbf{Q_{jk,t}} + \mathbf{q}_{\mathbf{j,t}}^{\mathbf{d}} - \mathbf{q}_{\mathbf{j,t}}^{\mathbf{g}} + \text{Wlin}_{ij}^{\text{q}}\left(\mathbf{P_{ij,t}}, \mathbf{Q_{ij,t}}\right), \tag{5.19}$$

where, $\text{Wlin}_{ij}^{\text{v}}\left(\mathbf{P_{ij,t}}, \mathbf{Q_{ij,t}}\right)$, $\text{Wlin}_{ij}^{\text{p}}\left(\mathbf{P_{ij,t}}, \mathbf{Q_{ij,t}}\right)$, and $\text{Wlin}_{ij}^{\text{q}}\left(\mathbf{P_{ij,t}}, \mathbf{Q_{ij,t}}\right)$ are the linear approximation of $\text{W}_{ij}^{\text{v}}\left(\mathbf{P_{ij,t}}, \mathbf{Q_{ij,t}}\right)$, $\text{W}_{ij}^{\text{p}}\left(\mathbf{P_{ij,t}}, \mathbf{Q_{ij,t}}\right)$, and $\text{W}_{ij}^{\text{q}}\left(\mathbf{P_{ij,t}}, \mathbf{Q_{ij,t}}\right)$, respectively.

5.3.2 Modelling Active Distribution Network Management Schemes

There are different ANM schemes that can affect the PVHC of distribution systems, e.g., voltage control using OLTC, reactive power control and active power curtailment. Hence, it is important to model them in the PVHC problem formulation. In the following, we presented the OLTC-based and PV-based ANM schemes as new constraints for the PVHC problem.

OLTC Modelling

Fig. 5.4 shows the model of a transformer that is installed between bus (i) and (j). As it can be seen, the transformer is divided into two branches; branch (i,m), which models the impedance of the transformer; and branch (m,j), representing the tap-changer. The power equations for the transformer are as follows:

$$\mathbf{P_{ij,t}} = \sum_{k:j\longrightarrow k} \mathbf{P_{jk,t}} + \mathbf{p}_{\mathbf{j,t}}^{\mathbf{d}} - \mathbf{p}_{\mathbf{j,t}}^{\mathbf{g}} + \mathbf{APC_{j,t}} + \text{Wlin}_{ij}^{\text{p}}\left(\mathbf{P_{ij,t}}, \mathbf{Q_{ij,t}}\right). \tag{5.20}$$

$$\mathbf{Q_{ij,t}} = \sum_{k:j\longrightarrow k} \mathbf{Q_{jk,t}} + \mathbf{q}_{\mathbf{j,t}}^{\mathbf{d}} - \mathbf{q}_{\mathbf{j,t}}^{\mathbf{g}} + \text{Wlin}_{ij}^{\text{q}}\left(\mathbf{P_{ij,t}}, \mathbf{Q_{ij,t}}\right). \tag{5.21}$$

$$\mathbf{v_{m,t}} = \mathbf{v_{i,t}} - \left(\widetilde{\mathbf{r}}_{\mathbf{ij}}\mathbf{P_{ij,t}} + \widetilde{\mathbf{x}}_{\mathbf{ij}}\mathbf{Q_{ij,t}}\right) + \text{Wlin}_{ij}^{\text{v}}\left(\mathbf{P_{ij,t}}, \mathbf{Q_{ij,t}}\right). \tag{5.22}$$

$$\mathbf{v_{m,t}} = Tap_{ij}\mathbf{v_{j,t}}, \tag{5.23}$$

where, Tap_{ij} denotes the transformer tap, and

$$Tap_{ij} = Tap_{ij}^{\min} + T_{ij}\Delta Tap_{ij}, \;\; 0 \leq T_{ij} \leq K_{ij}, \tag{5.24}$$

$$\Delta Tap_{ij} = \left(Tap_{ij}^{\max} - Tap_{ij}^{\min}\right)/K_{ij}, \tag{5.25}$$

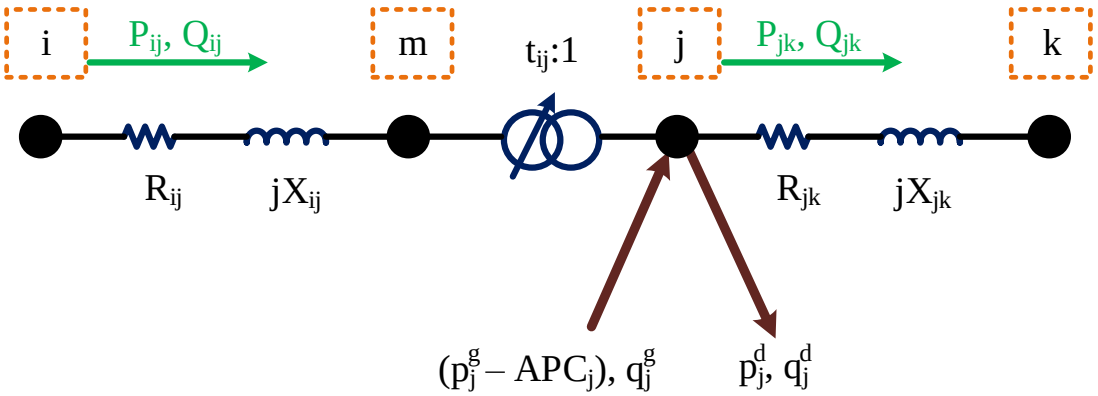

Fig. 5.4 The model of a transformer with on-load tap-changer (OLTC).

where, $Tap_{ij}^{\min}$, $Tap_{ij}^{\max}$ and K_{ij} represent the minimum turn ratio, the maximum turn ratio and the total taps of the tap-changer, respectively; ΔTap_{ij} denotes the turn ratio change per tap. Equation (5.23) has a nonlinear term. In order to represent it by linear equations, Tap_{ij} can be expressed by the binary expansion technique as follows [127]:

$$Tap_{ij} = Tap_{ij}^{\min} + \Delta Tap_{ij} \sum_{\kappa=0}^{N_{ij}} 2^{\kappa} \lambda_{ij,\kappa}^{\text{bin}}, \tag{5.26}$$

$$\sum_{\kappa=0}^{N_{ij}} 2^{\kappa} \lambda_{ij,\kappa}^{\text{bin}} \leq K_{ij}, \tag{5.27}$$

where, $\lambda_{ij,\kappa}^{\text{bin}}$ is a binary variable; and N_{ij} is the length of binary representation of the total taps, i.e. K_{ij}. Multiplying both sides of equation (5.26) by $\mathbf{v_{j,t}}$ yields to:

$$\mathbf{v_{m,t}} = Tap_{ij}^{\min} \mathbf{v_{j,t}} + \Delta Tap_{ij} \sum_{\kappa=0}^{N_{ij}} 2^{\kappa} \boldsymbol{\omega}_{\mathbf{ij},\kappa}, \tag{5.28}$$

where, the variable $\boldsymbol{\omega}_{\mathbf{ij},\kappa} = \lambda_{ij,\kappa}^{\text{bin}} \mathbf{v_{j,t}}$ can be replaced by the following equations:

$$\mathbf{0} \leq \mathbf{v_{j,t}} - \boldsymbol{\omega}_{\mathbf{ij},\kappa} \leq \left(1 - \lambda_{ij,\kappa}^{\text{bin}}\right) \mathbf{M}, \tag{5.29}$$

$$\mathbf{0} \leq \boldsymbol{\omega}_{\mathbf{ij},\kappa} \leq \lambda_{ij,\kappa}^{\text{bin}} \mathbf{M}, \tag{5.30}$$

where, $\mathbf{M}$ is a vector of positive large numbers. Thus, instead of OLTC constraints (5.23)-(5.25), the mixed integer linear constraints (5.27)-(5.30) can be used. Finally, it should be noted that the OLTC can be controlled based on different schemes. The control schemes considered in this study are as follows:

- **OLTC-1:** OLTC controls the voltage of the secondary side of the transformer. This control schemes can be modelled as follows:

$$\mathbf{v_{ref}} - \frac{\mathbf{v_{band}}}{2} \leq \mathbf{v_{j,t}} \leq \mathbf{v_{ref}} + \frac{\mathbf{v_{band}}}{2}, \tag{5.31}$$

  where, $\mathbf{v_{ref}}$ is the voltage reference for the OLTC controller; and $\mathbf{v_{band}}$ is the acceptable error from the voltage reference.

- **OLTC-2:** OLTC controls the voltage of the farthest location from the transformer. This control schemes can be modelled as follows:

$$\mathbf{v_{ref}} - \frac{\mathbf{v_{band}}}{2} \leq \mathbf{v_{far,t}} \leq \mathbf{v_{ref}} + \frac{\mathbf{v_{band}}}{2}, \tag{5.32}$$

  where, $\mathbf{v_{far,t}}$ is the voltage of the farthest location from the transformer at time step (t).

- **OLTC-3:** OLTC attempts to keep the voltage of all buses in operation range. To implement this scheme, the following constraint should be added to the model.

$$\underline{\mathbf{v}} \leq \mathbf{v_{i,t}} \leq \overline{\mathbf{v}}, \quad i \in \mathcal{N}, \tag{5.33}$$

  where, $\underline{\mathbf{v}}$ and $\overline{\mathbf{v}}$ are the vector of lower and upper voltage limits, respectively.

Inverter Modelling with Different Operation Mode

An important factor that can affect the PVHC of a system is the control strategy that is used in PV systems. Equation (5.34) represents the area that the active and reactive power of PV systems on bus (i) could vary.

$$\left(\mathbf{p_{i,t}^{net}}\right)^2 + \left(\mathbf{q_{i,t}^{g}}\right)^2 \leq \left(\mathbf{Cap_i^g}\right)^2, \tag{5.34}$$

where, $\left(\mathbf{q_{i,t}^{g}}\right)^{\mathbf{2}} = \left[\left(q_{i,t}^{g,a}\right)^{\mathbf{2}}, \left(q_{i,t}^{g,b}\right)^{\mathbf{2}}, \left(q_{i,t}^{g,c}\right)^{\mathbf{2}}\right]^{\mathrm{T}}$ denotes the element-wise square of the vector of generation reactive power at the bus (i), $\left(\mathbf{Cap_i^g}\right)^{\mathbf{2}} = \left[\left(Cap_i^{g,a}\right)^2, \left(Cap_i^{g,b}\right)^2, \left(Cap_i^{g,c}\right)^2\right]^{\mathrm{T}}$ denotes the element-wise square of the vector of inverter capacity at the bus (i), $\left(\mathbf{p_{i,t}^{net}}\right)^{\mathbf{2}} =$

$$\left[\left(p_{i,t}^{\text{net},a}\right)^{\mathbf{2}}, \left(p_{i,t}^{\text{net},b}\right)^{\mathbf{2}}, \left(p_{i,t}^{\text{net},c}\right)^{\mathbf{2}}\right]^{\text{T}} \text{ and}$$

$$\mathbf{p_{i,t}^{net}} = \mathbf{p_{i,t}^{g}} - \mathbf{APC_{i,t}}. \tag{5.35}$$

Equation (5.34) is a quadratic constraint. To linearize it, we rotate the tangent (5.36) around the original circular constraint (5.34) using the counter clockwise rotation matrix (5.37).

$$\mathbf{p_{i,t}^{net}} + \mathbf{q_{i,t}^{g}} \leq \sqrt{2}\, \mathbf{Cap_{i}^{g}}, \tag{5.36}$$

$$A = \begin{bmatrix} \cos(\theta) & -\sin(\theta) \\ \sin(\theta) & \cos(\theta) \end{bmatrix}, \tag{5.37}$$

where, θ is the rotation angle. Applying (5.37) to (5.36) results in:

$$[\cos(\theta) + \sin(\theta)]\mathbf{p_{i,t}^{net}} + [\cos(\theta) - \sin(\theta)]\mathbf{q_{i,t}^{g}} \leq \sqrt{2}\, \mathbf{Cap_{i}^{g}}. \tag{5.38}$$

The circular area presented by equation (5.34) constrains the active and reactive powers of a PV system based on the inverter capacity. Note that grid codes for PV systems usually add some other constraints, followings are some examples:

1. **Constant Power Factor Mode (CPFM):** In this mode, the reactive power consumption of a PV system is proportional to its active power as follows:

$$\mathbf{q_{i,t}^{g}} = tan\left(acos(\mathbf{PF_i})\right) \mathbf{p_{i,t}^{net}}, \tag{5.39}$$

   where, $\mathbf{PF_i}$ is the vector of power factors at bus (i).

2. **Limitation of Active Power Feed-in Mode (LAPFM):** Sometimes, a fixed limit on the feed-in active power of PV systems is mandatory. For instance, in Germany, the feed-in active power of PV systems that have a capacity of less than 30 kW and does not have the capability of being controlled remotely should always be below 70 % of their installed capacity [45]. This constraint can be modelled as follows:

$$\mathbf{p_{i,t}^{net}} \leq \rho_{\mathbf{apc}} \odot \mathbf{Cap_{i}^{g}}, \tag{5.40}$$

   where, $\rho_{\mathbf{apc}}$ is the maximum limitation on the feed-in active power.

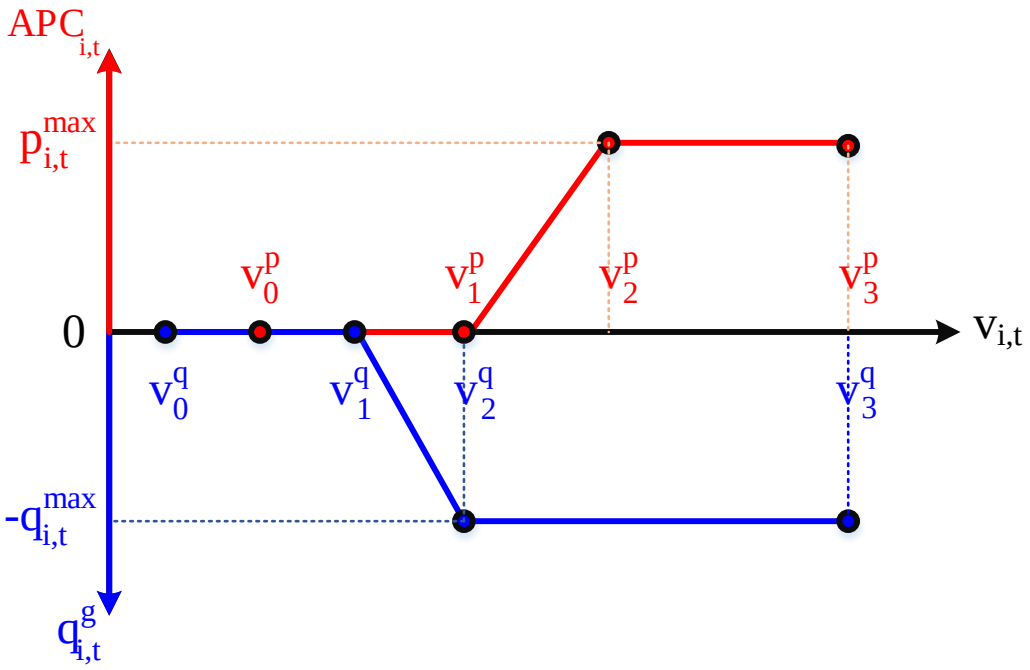

Fig. 5.5 The VWOM and VVOM local control schemes.

3. **Volt-Var Operation Mode (VVOM):** This mode is designed to actively limit the voltage rise at the PV connection point by controlling its reactive power based on the local voltage measurement. As it can be seen in Fig. 5.5, exceeding a certain voltage threshold activates the consumption of reactive power. Further, when the voltage is higher than the maximum acceptable voltage, the PV system absorbs the maximum reactive power that it can. The reactive power consumption is presented using a piecewise linear function as follows:

$$\mathbf{q}^{\mathbf{g}}_{\mathbf{i,t}} = \mathbf{f}\left(\mathbf{v}_{\mathbf{i,t}}\right) = \begin{cases} 0 & \mathbf{v}^{\mathbf{q}}_{\mathbf{0}} \leq \mathbf{v}_{\mathbf{i,t}} \leq \mathbf{v}^{\mathbf{q}}_{\mathbf{1}}, \\ \alpha_{\mathbf{i,t}} \odot \left[\left(\mathbf{v}_{\mathbf{i,t}} - \mathbf{v}^{\mathbf{q}}_{\mathbf{1}}\right) \oslash \mathbf{v}_{\mathrm{nom}}\right] \odot \mathbf{q}^{\mathbf{max}}_{\mathbf{i,t}} & \mathbf{v}^{\mathbf{q}}_{\mathbf{1}} \leq \mathbf{v}_{\mathbf{i,t}} \leq \mathbf{v}^{\mathbf{q}}_{\mathbf{2}}, \\ -\mathbf{q}^{\mathbf{max}}_{\mathbf{i,t}} & \mathbf{v}^{\mathbf{q}}_{\mathbf{2}} \leq \mathbf{v}_{\mathbf{i,t}} \leq \mathbf{v}^{\mathbf{q}}_{\mathbf{3}}, \end{cases} \tag{5.41}$$

where, $\mathbf{q}^{\mathbf{max}}_{\mathbf{i,t}}$ is the maximum available reactive power capacity at time (t); and

$$\alpha_{\mathbf{i,t}} = \mathbf{v}_{\mathrm{nom}} \oslash \left(\mathbf{v}^{\mathbf{q}}_{\mathbf{1}} - \mathbf{v}^{\mathbf{q}}_{\mathbf{2}}\right). \tag{5.42}$$

Note that the above piecewise linear functions are nonlinear over the defined range, as shown in Fig. 5.5. It is possible to represent $\mathbf{q}^{\mathbf{g}}_{\mathbf{i,t}}$ as a set of linear constraints by

defining a set of new variables as follows:

$$\mathbf{q}^{\mathbf{g}}_{\mathbf{i,t}} = \sum_{l=0}^{N_{BC}} \lambda_{\mathbf{i,t,l}} \odot \mathbf{f}\left(\mathbf{v}^{\mathrm{q}}_{l}\right), \tag{5.43a}$$

$$\mathbf{0} \leq \lambda_{\mathbf{i,t,0}} \leq \mathbf{w}_{\mathbf{i,t,0}}, \tag{5.43b}$$

$$\mathbf{0} \leq \lambda_{\mathbf{i,t,l}} \leq \mathbf{w}_{\mathbf{i,t,l-1}} + \mathbf{w}_{\mathbf{i,t,l}}, \;\; l = 1, \cdots, N_{BC} - 1, \tag{5.43c}$$

$$\mathbf{0} \leq \lambda_{\mathbf{i,t,N_{BC}}} \leq \mathbf{w}_{\mathbf{i,t,N_{BC}-1}}, \tag{5.43d}$$

$$\sum_{l=0}^{N_{BC}-1} \mathbf{w}_{\mathbf{i,t,l}} = \mathbf{1}, \tag{5.43e}$$

$$\sum_{l=0}^{N_{BC}} \lambda_{\mathbf{i,t,l}} = \mathbf{1}, \tag{5.43f}$$

$$\mathbf{v}_{\mathbf{i,t}} = \sum_{l=0}^{N_{BC}} \lambda_{\mathbf{i,t,l}} \odot \mathbf{v}^{\mathrm{q}}_{l}, \tag{5.43g}$$

$$\lambda_{\mathbf{i,t,l}} \geq \mathbf{0}, \quad l = 1, \cdots, N_{BC}, \tag{5.43h}$$

$$\mathbf{w}_{\mathbf{i,t,l}} \in \{0, 1\}, \quad l = 0, \cdots, N_{BC} - 1, \tag{5.43i}$$

where, N_{BC} is the number of pieces in the piecewise linear function; $\mathbf{w}_{\mathbf{i,t,l}}$ and $\lambda_{\mathbf{i,t,l}}$ are the vector of binary and continuous variables, respectively. Thus, linear constraints (5.43a)-(5.43i) can replace nonlinear constraint (5.41).

4. **Volt-Watt Operation Mode (VWOM):** This mode is designed to actively limit the voltage rise at the PV connection point by curtailing the PV active power based on the local voltage measurement. As shown in Fig. 5.5, exceeding a certain voltage threshold activate the active power curtailment. Further, when the voltage is higher than the maximum acceptable voltage, the active power of PV system becomes zero. Similar to the VVOM, active power curtailment can be modelled as follows:

$$\mathbf{APC}_{\mathbf{i,t}} = \begin{cases} 0 & \mathbf{v}^{\mathrm{p}}_{\mathbf{0}} \leq \mathbf{v}_{\mathbf{i,t}} \leq \mathbf{v}^{\mathrm{p}}_{\mathbf{1}}, \\ \beta_{\mathbf{i,t}} \odot \left[\left(\mathbf{v}_{\mathbf{i,t}} - \mathbf{v}^{\mathrm{p}}_{\mathbf{1}}\right) \ominus \mathbf{v}_{\mathrm{nom}}\right] \odot \mathbf{p}^{\mathbf{max}}_{\mathbf{i,t}} & \mathbf{v}^{\mathrm{p}}_{\mathbf{1}} \leq \mathbf{v}_{\mathbf{i,t}} \leq \mathbf{v}^{\mathrm{p}}_{\mathbf{2}}, \\ \mathbf{p}^{\mathbf{max}}_{\mathbf{i,t}} & \mathbf{v}^{\mathrm{p}}_{\mathbf{2}} \leq \mathbf{v}_{\mathbf{i,t}} \leq \mathbf{v}^{\mathrm{p}}_{\mathbf{3}}, \end{cases} \tag{5.44}$$

$$\mathbf{APC}_{\mathbf{i,t}} \leq \mathbf{p}^{\mathbf{g}}_{\mathbf{i,t}}, \tag{5.45}$$

where, $\mathbf{p}_{\mathbf{i},\mathbf{t}}^{\mathbf{max}}$ is the maximum active power that can be curtailed at time (t) and

$$\beta_{\mathbf{i},\mathbf{t}} = \mathbf{v}_{\text{nom}} \ominus \left(\mathbf{v}_{\mathbf{2}}^{\text{p}} - \mathbf{v}_{\mathbf{1}}^{\text{p}}\right). \tag{5.46}$$

Further, the linearization technique for (5.41) can be used to linearize the piecewise constraint (5.44) as well.

5. **Volt-Var-Watt Operation Mode (VVWOM):** This mode is the combination of VVOM and VWOM, as shown in Fig. 5.5.

5.3.3 Other Technical Constraints

Over-voltage is the most important technical constraint, which is presented as follows:

$$\mathbf{v}_{\mathbf{i},\mathbf{t}} \leq \overline{\mathbf{v}}. \tag{5.47}$$

Altogether, considering the ANM schemes, the PVHC at time (t) can be modelled as a Mixed Integer Linear Program (MILP) as follows:

$$\begin{aligned} &\text{minimize} \quad \sum_{i \in \mathscr{P}\mathscr{V}} \sum_{k \in \Phi} -p_{i,t}^{\text{g},k} + APC_{i,t}^{k}, \\ &s.t. \\ &(17)-(19), (47), \text{OLTC constraints}, \\ &\text{Inverter constraints}. \end{aligned} \tag{5.48}$$

The CPLEX solver has been used to solve the optimization model.

5.4 Evaluation and Assessment

In this section, simulations are carried out to assess the performance of the proposed methodology. Initially, the performance of the developed method is examined on IEEE 123-bus system. Then, the efficacy of the proposed framework in evaluation of 128 LV UK feeders is shown. Finally, the sensitivity of the results to the PV size is assessed using the proposed framework.

5.4.1 Test Systems

The developed method is applied to IEEE 123-bus system [99] as well as 128 LV UK feeders [47]. Some important characteristics of UK feeders are presented in Fig. 5.7. The topology of 7 UK feeders is presented in Fig. 5.8. The rated power of the service transformers in UK feeders is 800 kVA, and the voltages in primary and secondary circuits are 11 kV and 0.415 kV, respectively. The load profiles are created using the tool presented in [128]. The normalized PV profiles are derived from the tool presented in [101]. As for the size of PV systems, a base capacity of 100 kW is considered for PV systems in IEEE 123-bus system. Further, 37 % of the installed PV systems in the UK is 4 kW, which is the most common PV size in the UK [47]. Thus, a base capacity of 4 kW is considered for PV systems in UK feeders. The maximum acceptable voltage is 1.05p.u.

5.4.2 Performance Assessment in IEEE 123-Bus System

The performance of the proposed method is examined using IEEE 123-bus system. The results of the proposed method is compared with those of power flow-based Monte Carlo approach presented in [70]. The main idea of the approach presented in [70] is increasing the penetration level of PV systems and performing the power flow calculation in MATPOWER [129]. Further, a worst-case assumption is made, which is simulating the low load with high generation condition. In order to increase the accuracy of the presented approach in [70], the procedure is repeated 200 times. Fig. 5.6 demonstrates the MPVHC in IEEE 123-bus system for the proposed and Monte Carlo approaches. As can be seen, both methods show a similar trend in effectiveness of PV-based control strategies. For instance, both methods showed that VVOM is more effective than LAPFM and CPFM in increasing MPVHC. However, there is some differences in performance of the proposed method and the Monte Carlo approach. Observe that the estimated MPVHC for the test network without any PV-based control strategy by the proposed method is 13.187%, which is 3.297% higher than that of the Monte Carlo approach. Further, the estimated MPVHC by the proposed method for VVOM is 10.989% higher than that of the Monte Carlo approach. This is mainly because of the worst-case assumption that has been made in the considered Monte Carlo approach. Thus, the worst-case assumption can cause underestimation of control strategies' effectiveness in increasing the MPVHC. Further, as it was shown, the proposed method provides a more accurate result than the Monte Carlo approach.

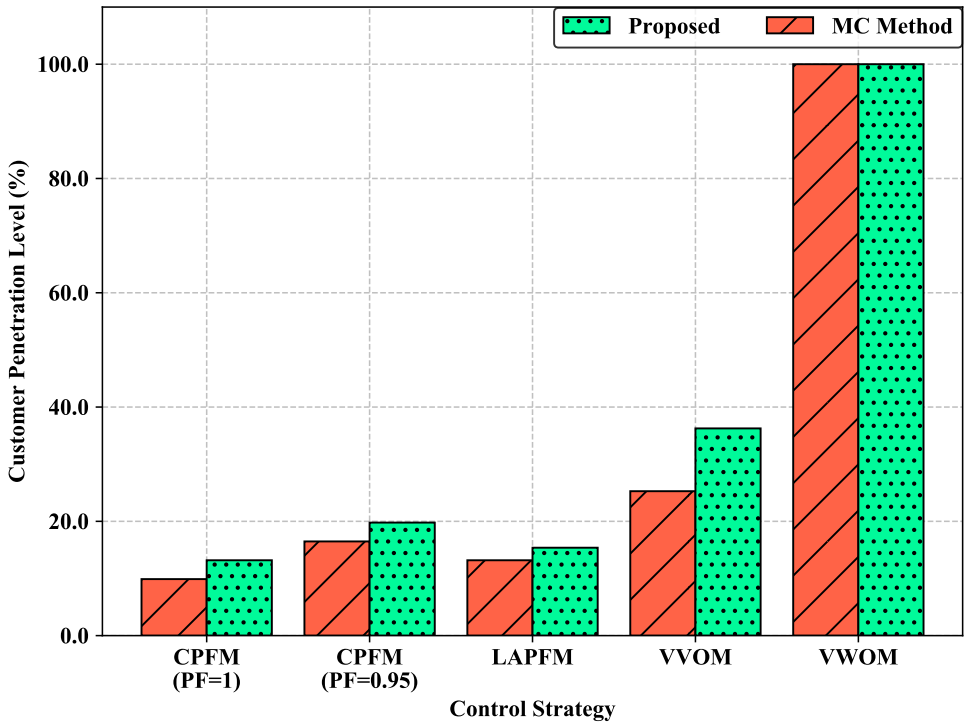

Fig. 5.6 MPVHC in IEEE 123-bus system using the proposed and Monte Carlo methods for different PV-based control schemes.

5.4.3 Performance Assessment in 128 UK Feeders

To clarify the sensitivity of the MPVHC, it is necessary to identify the MPVHC of the systems without exploiting the ANM schemes. The simulation results showed that 72 feeders do not have PVHC issue, i.e., if every customer in these feeders installs a 4 kW PV system, there will be no voltage violation in the system. However, 56 feeders are limited by voltage constraint and have a PVHC of less than 55 %. Thus, 43.75 % of all the studied feeders have an average MPVHC of 20.88 %. This indicates that almost half of the studied feeders will experience voltage violation issues with a high penetration of PV systems.

Fig. 5.9 shows the box plot of the MPVHC for different PV-based ANM schemes. On each box, the red and purple central marks are the mean and median, the horizontal edges are the 25th and 75th percentiles, the whiskers extend to the most extreme values not considered outliers, and outliers, i.e. yellow dots, are plotted individually. Observe that operation of the PV systems at a constant power factor of 0.95 lag only increased the MPVHC with an average of 3.96 %. Further, limiting the output power of the PV systems to 70 % of their installed capacity increased the MPVHC on average by 5.013 %. Whereas, VVOM increased the MPVHC on average by 18.74 %, which is much higher than the MPVHC change due to operation of PVs in CPFM and LAPFM operation modes. It can also be seen in Fig. 5.9 that the most effective PV-based operation mode is VWOM. Observe that using VWOM

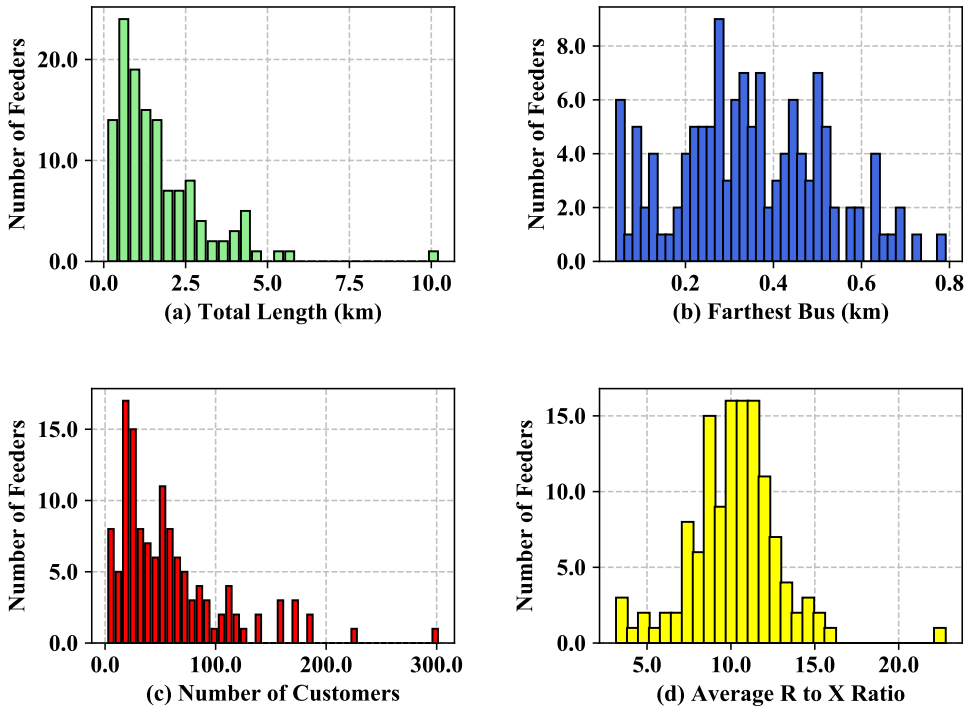

Fig. 5.7 Some of the key characteristics of 128 LV UK feeders including: (a) the distribution of total length of the feeders; (b) the distribution of farthest node from the service transformer; (c) the distribution of number of customers; (d) the distribution of average R to X ratio.

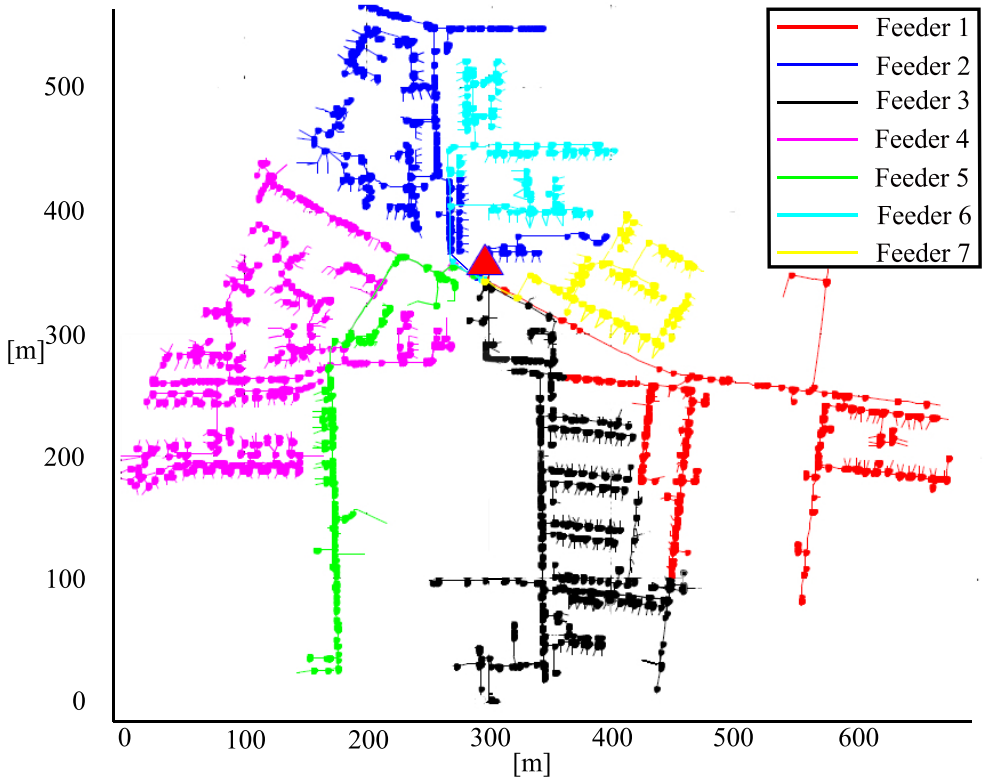

Fig. 5.8 Topology of 7 LV UK feeders.

increased the MPVHC to 100 % in all the studied feeders. VWOM, however, is not an interesting operation strategy from the customers' point of view. If DSOs do not pay the price of the curtailed energy, it is the customers who have to cover the costs of increasing the MPVHC. Thus, if the customers have to be involved in improving the network, VVOM could be a more attractive option from the customers' standpoint. VVOM, however, can increase the costs of DSOs by increasing the power losses in the system.

Fig. 5.10 depicts the average increase in the total annual energy losses including the PV systems' curtailed energy and the feeders' energy loss due to 1 % increase in the MPVHC using PV-based ANM schemes. Observe that CPFM and VVOM, which are reactive power-based ANM schemes, increased the total annual energy losses on average by 2.73 % and 5.05 % per 1 % increase in the MPVHC, respectively. The average change in total annual energy losses per 1 % increase in the MPVHC for these two control strategies is higher than that of other schemes. Hence, although reactive power-based control schemes seem more attractive, they cost more than other schemes to increase the MPVHC. Further, LAPFM caused an average increase of 0.75 %, which is the lowest among all the control strategies. VWOM with an average increase of 1.86 % is the second lowest among all the control schemes. Considering that the LAPFM scheme has much less capability than VWOM to increase the MPVHC, it can be concluded that VWOM is a better scheme for increasing the MPVHC.

Another set of ANM schemes are based on OLTC. Generally, it is believed that OLTC can increase the MPVHC of a system. However, it is the control strategy that determines the effectiveness of OLTC. Fig. 5.11 depicts the box plot of MPVHC for **OLTC-1**, **OLTC-2** and **OLTC-3** with reference to CPFM with unity power factor. It can be seen that when the OLTC controlled the voltage of transformer secondary winding (**OLTC-1**), it only increased the MPVHC on average by 0.49 %. However, when the OLTC controller operated based on the feedback from all buses of the system (**OLTC-3**), it increased the MPVHC on average by 51.08 %. Although **OLTC-3** would increase MPVHC effectively, it requires an extensive communications infrastructure. Interestingly, when the OLTC controlled the voltage of the farthest bus from the transformer (**OLTC-2**), it decreased the MPVHC on average by 7.30 %.

An important parameter that can impact the effectiveness of voltage control schemes is R/X ratio. In this study, the R/X ratio of a feeder is defined as the weighted arithmetic mean of R/X ratio of its lines. As it can be seen in Fig. 5.7 (d), the R/X ratio of the investigated systems has a Gaussian distribution with an average of 10.34 and standard deviation of 2.02. To be able to generalize the results to the systems with a R/X ratio out of the considered range, a sensitivity analysis is done to evaluate the impact of this factor on the effectiveness of the

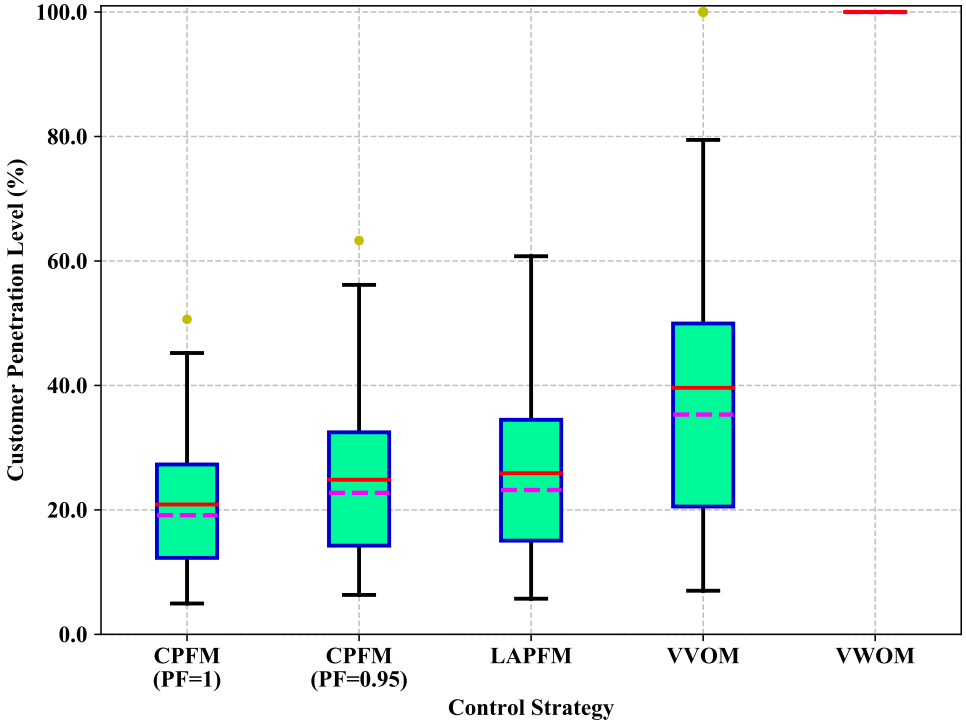

Fig. 5.9 The effect of PV-based ANM including CPFM, LAPFM, VVOM and VWOM on the MPVHC of studied feeders. The red and purple lines are the mean and median, respectively.

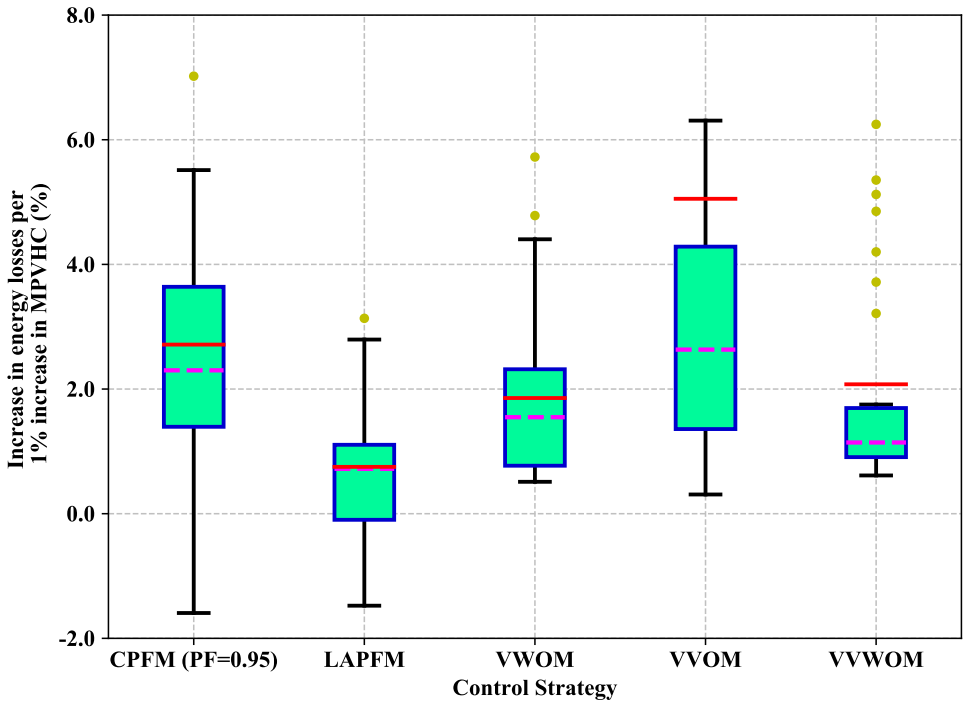

Fig. 5.10 The averaged increase in the total annual energy losses including the PV systems' curtailed energy and the feeders' energy loss due to 1 % increase in the MPVHC using PV-based ANM schemes. The red and purple lines are the mean and median, respectively.

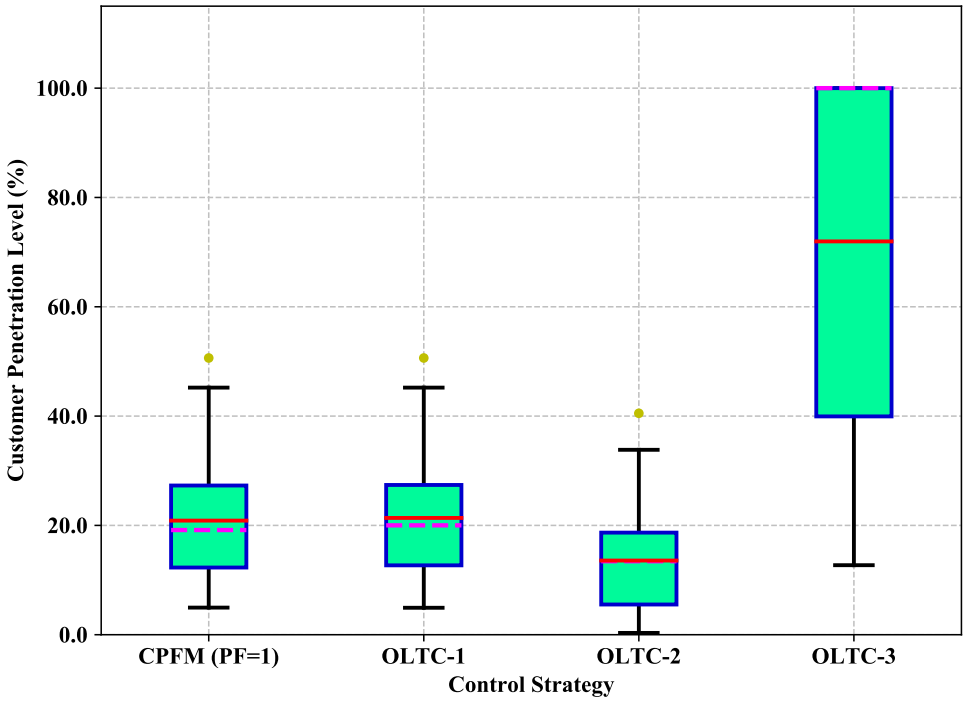

Fig. 5.11 The effect of OLTC-based ANM on the MPVHC of studied feeders. The red and purple lines are the mean and median, respectively.

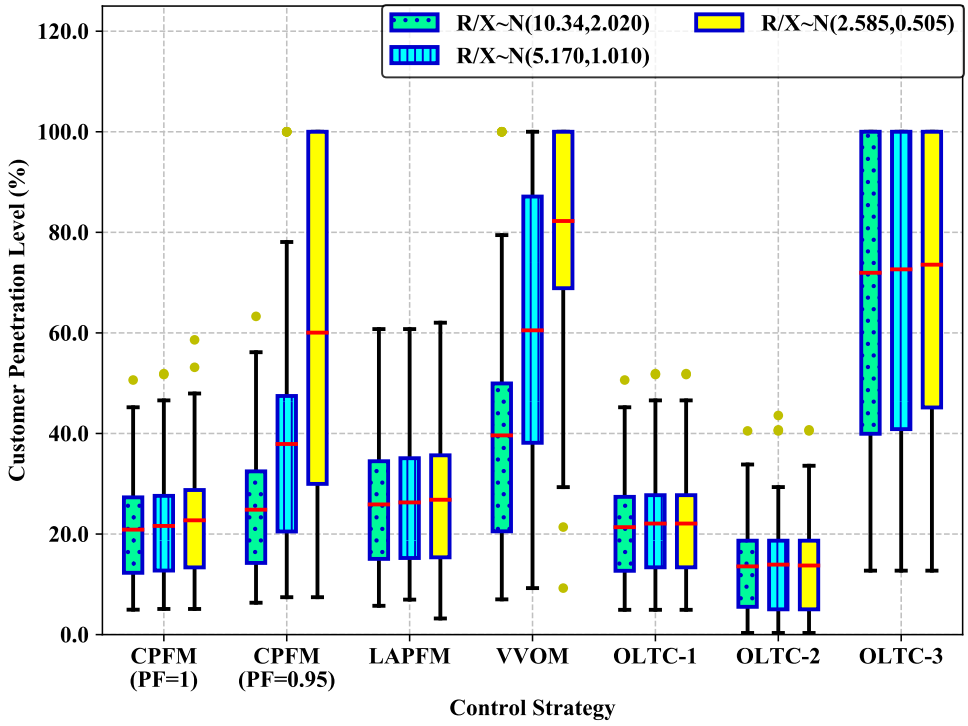

Fig. 5.12 The impact of R/X ratio on the effectiveness of autonomous voltage control strategies in increasing the MPVHC.

autonomous voltage control strategies in increasing the MPVHC. To do so, the R/X ratio of all the investigated systems are changed to half and a quarter of the original values and the PHVC framework is run again. Fig. 5.12 shows the impact of R/X ratio on the effectiveness of voltage control strategies. As it can be seen, the effectiveness of Volt-Var operation mode in increasing the MPVHC increases by decreasing the R/X ratio, which implies that in systems with low R/X ratio, the reactive power-based schemes are really effective for increasing the MPVHC. Nevertheless, as it was shown in Fig. 5.10, these schemes are more costly than others. Further, it was observed that increasing X/R ratio did not have a tangible effect on the performance of OLTC- and APC-based schemes. The simulation results are consistent with the general believe that reactive power control strategies are more effective when R/X ratio is low. Moreover, it is generally believed that APC can be more effective than reactive power control in the networks with a high R/X ratio. However, this does not mean that any APC-based scheme could be more effective than reactive power-based schemes. As shown in Fig. 5.12, VVOM, which is based on exchanging reactive power is more effective than LAPFM, which is based on APC. Therefore, R/X ratio can not be the only index to judge the effectiveness of different control schemes.

In this chapter, the effectiveness of a range of voltage control schemes in increasing MPVHC has been discussed. However, it is also important to discuss the findings of this study from a practical perspective. As it was shown in Fig. 5.11, OLTC could effectively increase MPVHC. Nevertheless, OLTC is usually used in MV systems. Although utilizing OLTCs for voltage management in LV systems has been recently studied, they have not been used very often is real LV systems. Thus, considering the additional cost for installing a transformer with OLTC in LV systems, it is necessary to perform a cost-benefit assessment. Moreover, the costs of network reinforcement measures such as changing transformer and installing additional cables would make the PV-based control schemes a more attractive option to increase MPVHC. It should also be mentioned that the findings of this chapter is generally applicable to feeders with a similar characteristics to the UK feeders. Therefore, if the characteristics of a feeder is totally different from those of UK feeders, the proposed method should be used to estimate the MPVHC.

5.4.4 Sensitivity to the PV Size

In Section 5.4.3, it is assumed that the base capacity of PV systems is 4 kW. However, in this section, it is assumed that the size of PV systems follows an empirical distribution. According to the historical statistics of UK, the probability of installing a PV system with a size of 1, 1.5, 2, 2.5, 3, 3.5, and 4 kW is 1%, 8%, 13%, 14%, 14%, 12% and 37%, respectively [47]. The proposed method is applied to 128 LV UK feeders. Fig. 5.13 demonstrates the MPVHC

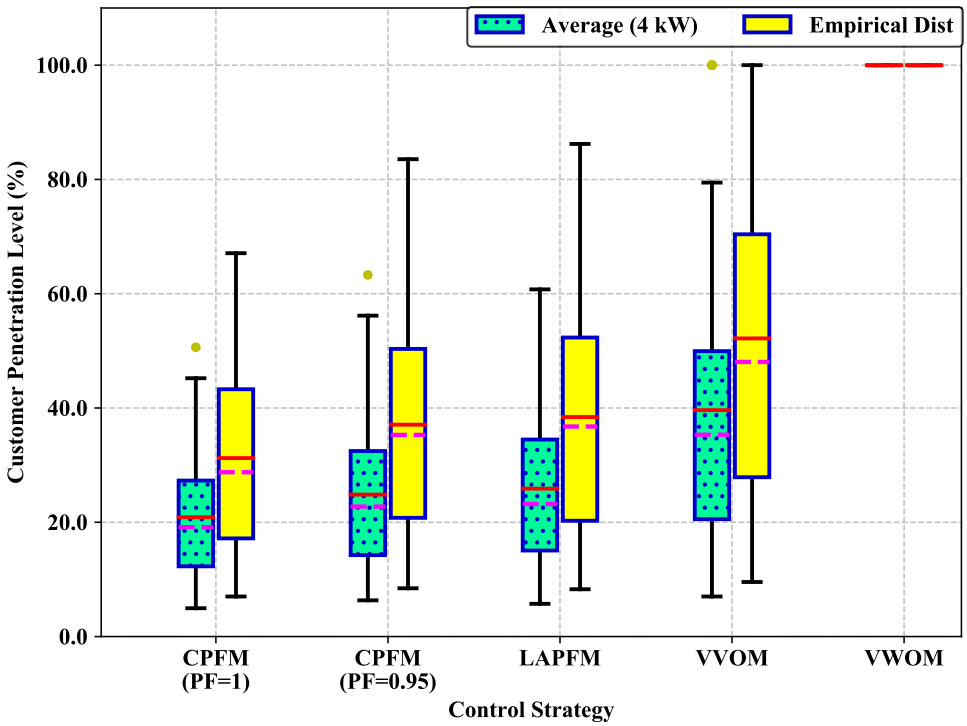

Fig. 5.13 The impact of size of PV systems on the effectiveness of different control schemes. The red and purple lines are the mean and median, respectively.

for different PV-based ANM schemes. It can be observed that the MPVHC is higher when the size of PV systems is selected based on the empirical distribution in comparison to when the base PV size is set at 4 kW. However, in terms of the effectiveness of control schemes to increase the MPVHC, the trend is the same as when the PV size is set at 4 kW. Observe that when the size of PV systems is selected based on the empirical distribution, controlling the PV systems at a constant power factor of 0.95 lag only increased the MPVHC with an average of 5.85%. Further, limiting the output power of the PV systems to 70% of their installed capacity increased the MPVHC on average by 7.19%. Moreover, VVOM increased the MPVHC on average by 20.94%, which is much higher than the MPVHC change due to operation of PVs in CPFM and LAPFM operation modes. Note that sampling from empirical distribution of PV systems mainly increased the MPVHC. However, it would not majorly impact the effectiveness of control schemes in increasing the MPVHC.

5.5 Summary

In this chapter, the impact of different autonomous voltage control strategies for increasing the PVHC in radial distribution systems were studied. The investigated schemes included PV-based local control actions, as well as controlling the OLTC of the transformer. In order

to integrate these voltage control schemes into the PVHC studies, a modular optimization-based framework was proposed. The proposed method is examined on 128 LV UK feeders. Following are the conclusions derived from the simulation results:

- Active power curtailment mode, i.e. VWOM, is the most effective control scheme to increase MPHVC. This control scheme increases MPVHC to 100 % in any distribution feeder. Further, simulation result showed that Volt-Var operation mode of PV systems, i.e. VVOM, is the second most effective PV-based control scheme with an average increase of 18.74 % in MPVHC.
- Active power based control strategies, i.e. LAPFM and VWOM, resulted in the lowest total energy losses per 1 % increase in MPVHC among all PV-based control schemes. This means that in the feeders with R/X ratio higher than 5, the active power based control schemes are more cost effective than reactive power based control schemes to increase MPVHC.
- The impact of OLTC on MPVHC highly depends on its control strategy. It was shown that if the aim of OLTC controller is controlling the voltage at the end of a feeder, it decreases the MPVHC. Nevertheless, if the aim is to maintain the voltage of all the locations in the feeder within permissible bounds, it can increase the MPVHC on average by 51.08 %.

Chapter 6

Probabilistic Impact Assessment of Residential BESSs on the HC of LV Distribution Systems

6.1 Introduction

As mentioned in Chapter 1, the penetration level of residential battery energy storage systems (BESSs) has been increasing in distribution systems. Although different methods for estimating the hosting capacity (HC) have been proposed [47, 96, 48, 9, 130, 39, 37, 46, 18, 42], none of them have considered BESS in photovoltaic hosting capacity (PVHC) assessment. BESSs have different characteristics and provides more operational flexibility compared to photovoltaic (PV) systems alone. Hence, the findings of [47, 96, 48, 9, 130, 39, 37, 46, 18, 42], will be invalidated by the increased up take of BESSs. Therefore, it is necessary to develop a method to integrate BESSs in HC identification.

In Chapter 5, we assessed the impact of controlling the output power of PVs on the PVHC. In this chapter, we take further steps to identify the PVHC considering residential BESSs, which affect the exchange energy between prosumers and the network. To do so, we develop a mathematical formulation, based on the linear HC model presented in Chapter 2, to integrate residential BESSs in PVHC problem. To the best of our knowledge, all the existing mathematical formulations would converge to a value in region (B) of PVHC. However, DSOs are interested in the minimum PVHC (MPVHC) as it is independent of PVs location. The importance of the proposed method in this chapter is that it converges to the MPVHC. Moreover, most of the studies related to the impacts of PV-BESSs on low voltage (LV) distribution systems have only analyzed a few test systems. This means that those studies did

not capture the effects of diversity of LV distribution feeders. In this chapter, we applied the proposed method to 25 real LV networks in the UK including 128 LV feeders. The outcome of this chapter is presented as a journal paper, which is currently under reviewed[1].

The remainder of this chapter is organized as follows: Section 6.2 represents an overview of the developed method. Section 6.3 describes how to prepare the input data. Scheduling models of BESSs are presented in Section 6.4. Section 6.5 describes the proposed model for identifying the MPVHC. Section 6.6 presents the numerical results and discussion. Finally, the major conclusions are presented in Section 6.7.

6.2 Probabilistic Framework Overview

To understand the impacts of BESSs on the MPVHC of LV distribution networks considering the locational and behavioral uncertainties associated with BESSs, PVs and loads, a probabilistic framework is developed, as shown in Fig. 6.1. This framework includes three steps. In the first step, the loads and PVs profiles as well as the input parameters including network tariff; BESS penetration level; and PVs and BESSs sizes, are defined (Section 6.3). Then, the scheduling of BESSs are identified by using a ruled-based scheme or a mixed integer linear program (MILP) optimization model (Section 6.4). Finally, the mathematical HC model is developed to identify the MPVHC based on the BESSs' scheduling, PVs and load profiles (Section 6.5).

6.3 Input Data Preparation

This module is designed to address the uncertainties and to initialize parameters. To model the load and PV uncertainties, the adoption of time-series profiles is required. Residential loads are assumed to have an inductive power factor of 0.98. Further, all PVs are assumed to operate at unity power factor.

Residential Load Profiles

The tool presented in [128] is used to create individual residential loads. To mimic the stochasticity of the load consumption per customer, summer pool with 2000 daily load profiles is created. Different combination of these load profiles can be allocated to the loads in a system. However, running the simulation for a high number of load combinations would

[1] "Probabilistic Impact Assessment of Residential BESSs on the HC of LV Distribution Systems," IEEE Transactions on Smart Grid, 2019 [131].

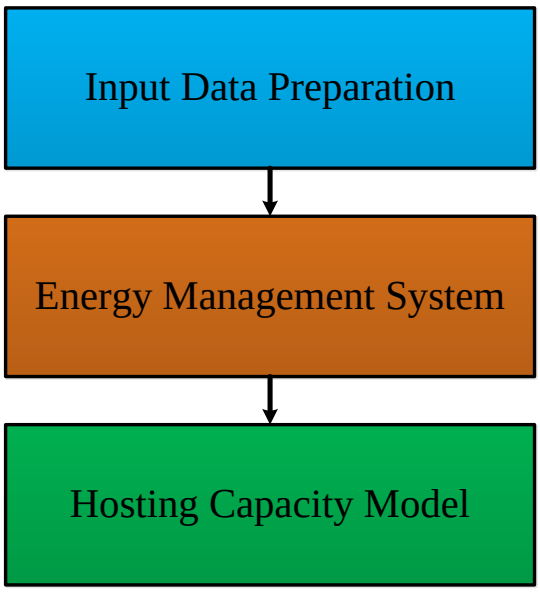

Fig. 6.1 Flowchart of the proposed framework for PVHC estimation in presence of BESSs.

be time consuming. Thus, in order to carry out the simulation in a shorter time, the number of load profile allocated to the loads should be bounded. To do so, the focus should be on the time period that a system might experience over voltage. It is clear that PV systems usually have their maximum generation between hours 11:00 and 13:00. The lower the load during this period, the higher the chance of over voltage problem. Therefore, a high number of different load allocation scenarios should be generated. Then, the total load profile of each scenario needs to be calculated. The scenario that has the minimum total load value at hour 11:00 is the first load combination that will be used in the simulation. The same process is performed for hours 12:00 and 13:00. Thus, simulations will be carried out for 3 days.

PV Profiles

The tool presented in [128] is used to create daily PV profiles. To mimic the stochasticity of PVs' outputs, summer pool with 2000 PV profiles is created. Different combination of these PV profiles can be allocated to the PVs in a system. However, running the simulation for a high number of PV profile combinations would be time consuming. Thus, in order to carry out the simulation in a shorter time, the number of PV profile allocated to the PV systems should be bounded. Since the load profiles are limited to three days, three PV profiles should be selected from the pool. Similar to load profile allocation, maximum PV generation for hours 11:00 -13:00 are selected for simulations.

Size of PV Systems

One of the uncertainties that should be addressed in any HC assessment is the size of PV systems. Historical data of the installed PVs can describe the PV distribution. However, as the focus of this chapter is not assessing the impact of PV size on the MPVHC, the average size of the historical data would be chosen as the size of PV systems. Nevertheless, the proposed framework is general and there is no difficulty to apply the research results to any other size of PV systems.

6.4 Scheduling the BESS

The benefits of BESSs highly depend on the energy management strategy that is used to charge/discharge them. Several strategies have been proposed to find the charging/discharging patterns of BESSs. Generally, energy management strategies can be divided to rule-based heuristic and optimization-based approaches. Although optimization-based methods have attracted attentions, most batteries are operated using heuristic strategies in practice. In this work, a rule-based heuristic strategy and an optimization-based approach are considered as follow:

- Rule-based approach
  - Self consumption maximization (SCM) [70].
- Optimization-base approach
  - Mixed integer linear programming (MILP) [132].

6.4.1 Self Consumption Maximization

Fig. 6.2 represents how this rule-based strategy works. As it can be seen, the battery is charged when the PV generation is higher than the load consumption and discharged when the load is higher than the PV output. This energy management strategy is the default strategy utilized by battery suppliers and retailers [71].

6.4.2 Mixed Integer Linear Programming

This approach employs a MILP optimization to find the charging/discharging patterns of the battery by minimizing electricity costs. This approach requires the load and PV forecasts over a decision horizon, the feed-in-tariff (FIT) and the network tariff. The electrical energy

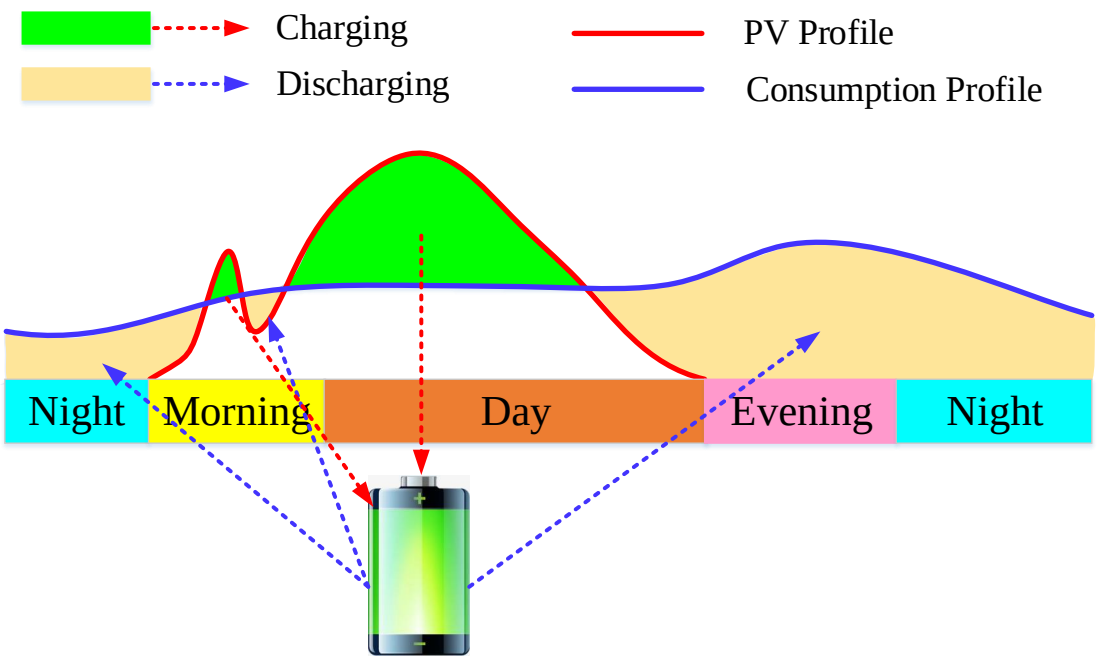

Fig. 6.2 Charging/discharging patterns for SCM mode.

flows in a smart home is shown in Fig .6.3 .The full MILP optimization problem for this energy management strategy is as follows:

$$\underset{\substack{p_t^{\mathrm{n}+},p_t^{\mathrm{n}-},p_t^{\mathrm{bat}+},p_t^{\mathrm{bat}-},\\ d_t^{\mathrm{n}},s_t^{\mathrm{bat}},SoC_t^{\mathrm{bat}}}}{\text{minimize}} \sum_{t\in\mathscr{H}} T_t^{\mathrm{grid}} p_t^{\mathrm{n}+} - T^{\mathrm{FIT}} p_t^{\mathrm{n}-}, \tag{6.1a}$$

s.t.

$$p_t^{\mathrm{n}+} - p_t^{\mathrm{n}-} = \eta_{\mathrm{i}} \left(\eta^{\mathrm{bat}+} p_t^{\mathrm{bat}+} - \left(1/\eta^{\mathrm{bat}-} \right) p_t^{\mathrm{bat}-} \right) - \eta_{\mathrm{i}} p_t^{\mathrm{g}} + p_t^{\mathrm{d}}, \tag{6.1b}$$

$$SoC_t^{\mathrm{bat}} = SoC_{t-1}^{\mathrm{bat}} + \Delta t \left(\eta^{\mathrm{bat}+} p_{t-1}^{\mathrm{bat}+} \right) - \Delta t \left(\left(1/\eta^{\mathrm{bat}-} \right) p_{t-1}^{\mathrm{bat}-} \right), \tag{6.1c}$$

$$p_t^{\mathrm{n}+} \leq \overline{p}^{\mathrm{n}} d_t^{\mathrm{n}}, \tag{6.1d}$$

$$p_t^{\mathrm{n}-} \leq \overline{p}^{\mathrm{n}} \left(1 - d_t^{\mathrm{n}} \right), \tag{6.1e}$$

$$p_t^{\mathrm{bat}+} \leq \overline{p}^{\mathrm{bat}+} \times s_t^{\mathrm{bat}}, \tag{6.1f}$$

$$p_t^{\mathrm{bat}-} \leq \overline{p}^{\mathrm{bat}-} \times \left(1 - s_t^{\mathrm{bat}} \right), \tag{6.1g}$$

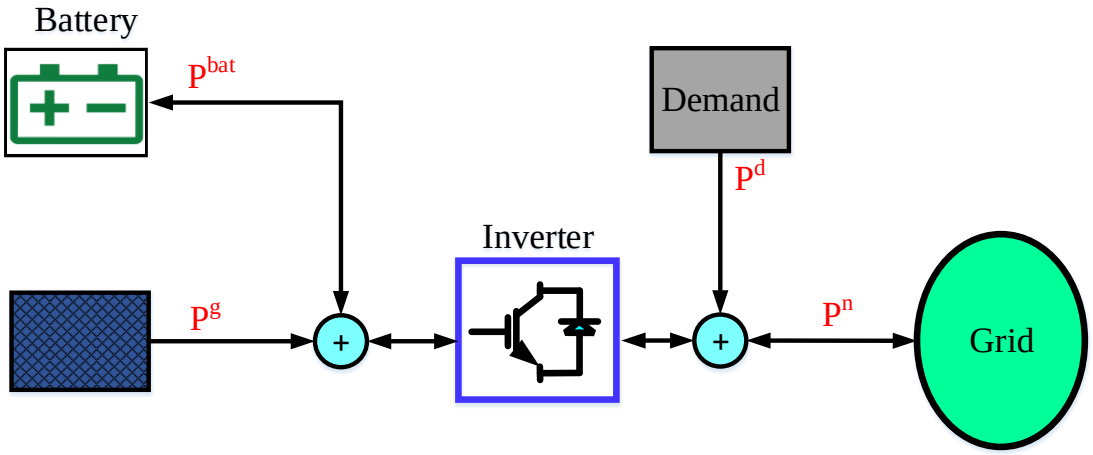

Fig. 6.3 Illustration of electrical energy flows in a smart home.

$$0 \leq p_t^{\mathrm{n}+} \leq \overline{p}^{\mathrm{n}}, \tag{6.1h}$$

$$0 \leq p_t^{\mathrm{n}-} \leq \overline{p}^{\mathrm{n}}, \tag{6.1i}$$

$$0 \leq p_t^{\mathrm{bat}+} \leq \overline{p}^{\mathrm{bat}+}, \tag{6.1j}$$

$$0 \leq p_t^{\mathrm{bat}-} \leq \overline{p}^{\mathrm{bat}-}, \tag{6.1k}$$

$$\underline{SoC}^{\mathrm{bat}} \leq SoC_t^{\mathrm{bat}} \leq \overline{SoC}^{\mathrm{bat}}, \tag{6.1l}$$

$$d_t^{\mathrm{n}}, s_t^{\mathrm{bat}} \in \{0,1\}, \tag{6.1m}$$

where, $\mathscr{H}$ are the set of time steps; T_t^{grid} and T^{FIT} are the network tariff and FIT, respectively; $p^{\mathrm{n}+/-}$ represents the power flows from/to network; $p^{\mathrm{bat}+/-}$ is the charge/discharge power of battery; SoC_t^{bat} represents the state of charge of the battery; η_{i} and $\eta^{\mathrm{bat}+/-}$ are the inverter and charging/discharging efficiencies, respectively; $\underline{SoC}^{\mathrm{bat}}$, $\overline{SoC}^{\mathrm{bat}}$ and $\overline{p}^{\mathrm{bat}+/-}$ are the minimum state of charge (SoC), the maximum SoC and the maximum charging/discharging rate of battery; Δt is the hourly time step; p^{d} and p^{g} are the customer total load and output power of DER, respectively; s^{bat} is the operation status of battery; and $\overline{p}^{\mathrm{n}}$ is the maximum power that can be exchanged with network. The battery power at time step (t) is as follows:

$$P_t^{\mathrm{ESS}} = p_t^{\mathrm{bat}+} - p_t^{\mathrm{bat}-}. \tag{6.2}$$

6.5 MPVHC Identification

The MPVHC is modelled as a MILP optimization problem. To do so, the focus is the definition of MPVHC. Considering the definition of MPVHC, it is possible to interpret the MPVHC as the minimum PV penetration below which any penetration level would not cause a constraint violation in the system.

Objective Function

Consider a distribution system in which every customer has a PV system. If the MPVHC of the system is below 100%, installing a PV system by all customers would yield in a technical problem. In such a system, it is possible to remove some of the PVs in a way that remaining PVs would still yield in a constraint violation. If one continues to remove PV systems, there would be a point that removing any one of the remaining PV system would resolve the technical issues. The total capacity of the remained PV systems is the margin of MPVHC. Any PV penetration below MPVHC margin would not cause a constraint violation. However, any PV penetration above MPVHC can cause a technical problem. Therefore, the objective of the developed model is maximizing the total capacity of PVs that can be removed from the system while making sure that the maximum voltage in the system is higher than the maximum acceptable voltage. The solution of the optimization model is a set of PVs that would cause a voltage higher than the maximum acceptable voltage. If the optimization problem does not converge to a solution, it means that installing a PV at every bus of the system would not cause an over-voltage problem. The objective function can be represented as follows:

$$\underset{B^{\mathrm{g}}_{i,k},B^{\mathrm{ESS}}_{i,k}}{\text{maximize}} \left(\sum_{i\in\mathscr{N}} \sum_{k\in\Phi} (1-B^{\mathrm{g}}_{i,k}) Cap^{\mathrm{g},k}_{i} \right), \tag{6.3}$$

where, B^{g} and B^{ESS} are the status of DER and BESS systems (1: active, 0: inactive); $\mathscr{N}$ and Φ are the set of all buses and phases, respectively.

Distribution System Model

In a radial distribution system with $n+1$ buses, the linear power flow equation for branch (i,j) is formulated as follows:

$$\mathbf{v_{j,t}} = \mathbf{v_{i,t}} - \left(\widetilde{\mathbf{r}}_{\mathbf{ij}}\mathbf{P_{ij,t}} + \widetilde{\mathbf{x}}_{\mathbf{ij}}\mathbf{Q_{ij,t}}\right) \ominus \mathbf{v}_{\mathrm{nom}} + \mathrm{Wlin}^{\mathrm{v}}_{ij}\left(\mathbf{P_{ij,t}}, \mathbf{Q_{ij,t}}\right) \ominus (2\mathbf{v}_{\mathrm{nom}}), \tag{6.4}$$

where, $\mathbf{v_{i,t}} = |\mathbf{V_{i,t}}| = \left[|V_{i,t}^a|, |V_{i,t}^b|, |V_{i,t}^c|\right]^{\mathrm{T}}$; $\mathbf{v}_{\mathrm{nom}}$ is the vector of nominal voltage in the system; $\mathrm{Wlin}_{ij}^{\mathrm{v}}$ is a linear function of $\left(\mathbf{P_{ij,t}}, \mathbf{Q_{ij,t}}\right)$; and

$$\widetilde{\mathbf{r}}_{\mathbf{ij}} = Re\left\{\mathbf{a}_i\mathbf{a}_i^H\right\} \odot Re\left\{\mathbf{Z_{ij}}\right\} + Im\left\{\mathbf{a}_i\mathbf{a}_i^H\right\} \odot Im\left\{\mathbf{Z_{ij}}\right\}, \tag{6.5}$$

$$\widetilde{\mathbf{x}}_{\mathbf{ij}} = Re\left\{\mathbf{a}_i\mathbf{a}_i^H\right\} \odot Im\left\{\mathbf{Z_{ij}}\right\} - Im\left\{\mathbf{a}_i\mathbf{a}_i^H\right\} \odot Re\left\{\mathbf{Z_{ij}}\right\}, \tag{6.6}$$

$$\mathbf{a}_i = \begin{bmatrix} 1 & e^{-j2\pi/3} & e^{j2\pi/3} \end{bmatrix}^{\mathrm{T}} \tag{6.7}$$

where, $\odot$ and $\ominus$ denote the element-wise multiplication and division, respectively; $\mathbf{Z_{ij}} \in \mathbb{C}^{3\times3}$ is the impedance complex matrix and $\mathbf{V_{i,t}} = [V_{i,t}^a, V_{i,t}^b, V_{i,t}^c]^{\mathrm{T}}$ represents the vector of phase voltages at time (t); $\mathbf{S_{ij,t}} = \mathbf{P_{ij,t}} + i\mathbf{Q_{ij,t}}$ denotes the vector of complex power from bus (i) to bus (j) at time (t). For every branch $(i, j) \in \mathscr{B}$, the active and reactive power balance equations are formulated as follows:

$$\mathbf{P_{ij,t}} = \sum_{k:j\longrightarrow k} \mathbf{P_{jk,t}} + \mathbf{p_{j,t}^d} - \mathbf{p_{j,t}^g} + \mathbf{p_{j,t}^{bat}} + \mathrm{Wlin}_{ij}^{\mathrm{p}}\left(\mathbf{P_{ij,t}}, \mathbf{Q_{ij,t}}\right), \tag{6.8}$$

$$\mathbf{Q_{ij,t}} = \sum_{k:j\longrightarrow k} \mathbf{Q_{jk,t}} + \mathbf{q_{j,t}^d} - \mathbf{q_{j,t}^g} + \mathrm{Wlin}_{ij}^{\mathrm{q}}\left(\mathbf{P_{ij,t}}, \mathbf{Q_{ij,t}}\right), \tag{6.9}$$

$$\mathbf{p_{j,t}^g} = \eta_{\mathbf{j,t}}^{\mathbf{g}} \odot \mathbf{Cap_j^g} \odot \mathbf{B_j^g}, \tag{6.10}$$

$$\mathbf{p_{j,t}^{bat}} = \mathbf{p_{j,t}^{ESS}} \odot \mathbf{B_j^{ESS}}, \tag{6.11}$$

$$\mathbf{B_j^g} = [B_{j,a}^{\mathrm{g}}, B_{j,b}^{\mathrm{g}}, B_{j,c}^{\mathrm{g}}]^{\mathrm{T}} \in \{0,1\}^3 \tag{6.12}$$

$$\mathbf{B_j^{ESS}} = [B_{j,a}^{\mathrm{ESS}}, B_{j,b}^{\mathrm{ESS}}, B_{j,c}^{\mathrm{ESS}}]^{\mathrm{T}} \in \{0,1\}^3 \tag{6.13}$$

where, $\mathrm{Wlin}_{ij}^{\mathrm{p}}$, and $\mathrm{Wlin}_{ij}^{\mathrm{q}}$ are linear functions of $\left(\mathbf{P_{ij,t}}, \mathbf{Q_{ij,t}}\right)$; $\mathscr{B}$ represents the set of all branches; $\eta_{\mathbf{j,t}}^{\mathbf{g}}$ denotes DERs capacity factor vector at bus (j) and time (t); $\mathbf{s_{j,t}^d} = \mathbf{p_{j,t}^d} + i\mathbf{q_{j,t}^d}$ and $\mathbf{s_{j,t}^g} = \mathbf{p_{j,t}^g} + i\mathbf{q_{j,t}^g}$ are the complex vector of load and DER generation at bus (j) and time (t); $\mathbf{Cap_j^g} = [Cap_j^{\mathrm{g},a}, Cap_j^{\mathrm{g},b}, Cap_{j,c}^{\mathrm{g},c}]^{\mathrm{T}}$ is the vector of DER capacity; $\mathbf{B_j^g} = [B_{j,a}^{\mathrm{g}}, B_{j,b}^{\mathrm{g}}, B_{j,c}^{\mathrm{g}}]^{\mathrm{T}}$ and $\mathbf{B_j^{ESS}} = [B_{j,a}^{\mathrm{ESS}}, B_{j,b}^{\mathrm{ESS}}, B_{j,c}^{\mathrm{ESS}}]^{\mathrm{T}}$ are the status vector for DERs and BESSs; and $\mathbf{p_{j,t}^{ESS}}$ is the vector of the charging/discharging rate of BESSs at bus (j) and time (t) obtained from energy management systems.

Technical Constraints

The constraint for making sure that the maximum voltage in the system is higher than the maximum acceptable voltage is as follows:

$$\max_{\substack{i\in\mathscr{N},\\ t\in\mathscr{H}}} \left\{\mathbf{v_{i,t}}\right\} \geq \overline{\mathbf{v}}, \tag{6.14}$$

This constraint can be linearized as follows:

$$\mathbf{LL_i} \leq \mathbf{v_{i,t}} \leq \mathbf{UL_i}, \qquad \forall i \in \mathscr{N}, \forall t \in \mathscr{H}, \tag{6.15}$$

$$\mathbf{v}_{\max} \geq \mathbf{v_{i,t}}, \qquad \forall i \in \mathscr{N}, \forall t \in \mathscr{H}, \tag{6.16}$$

$$\mathbf{v}_{\max} \leq \mathbf{v_{i,t}} + (\mathbf{UL}_{\max} - \mathbf{LL_i})\left(\mathbf{1} - \mathbf{D_{i,t}}\right), \ \forall i \in \mathscr{N}, \forall t \in \mathscr{H}, \tag{6.17}$$

$$\sum_{t\in\mathscr{H}} \sum_{i\in\mathscr{N}} D^{\mathrm{a}}_{i,t} + D^{\mathrm{b}}_{i,t} + D^{\mathrm{c}}_{i,t} = 1 \tag{6.18}$$

$$\mathbf{D_{i,t}} = \left[D^{\mathrm{a}}_{i,t}, D^{\mathrm{b}}_{i,t}, D^{\mathrm{c}}_{i,t}\right]^{\mathrm{T}} \in \{0,1\}^3, \tag{6.19}$$

where, $v_{\max} = \max\limits_{\substack{i\in\mathscr{N},\\ t\in\mathscr{H},\phi\in\Phi}} \left\{|V^{\phi}_{i,t}|\right\}$, $\mathbf{v}_{\max} = [v_{\max}, v_{\max}, v_{\max}]^{\mathrm{T}}$, $\mathbf{D_{i,t}} = \left[D^{\mathrm{a}}_{i,t}, D^{\mathrm{b}}_{i,t}, D^{\mathrm{c}}_{i,t}\right]^{\mathrm{T}}$, $UL_{\max} = \max(\mathbf{UL_i})$ and $\mathbf{UL}_{\max} = [UL_{\max}, UL_{\max}, UL_{\max}]^{\mathrm{T}}$. It should be mentioned that $\mathbf{UL_i} = \left[UL^a_i, UL^b_i, UL^c_i\right]^{\mathrm{T}}$. Finally, following constraint is required to set the penetration level of BESSs in the system.

$$\left| \sum_{i\in\mathscr{N}} \sum_{k\in\Phi} B^{\mathrm{ESS}}_{i,k} - \sum_{i\in\mathscr{N}} \sum_{k\in\Phi} B^{\mathrm{g}}_{i,k} \times BESS_{\mathrm{Pen}} \right| \leq \alpha_{\mathrm{Pen}}, \tag{6.20}$$

$$B^{\mathrm{g}}_{i,k} \geq B^{\mathrm{ESS}}_{i,k} \qquad \forall k \in \Phi, \ \forall i \in \mathscr{N} \tag{6.21}$$

Altogether, the hosting capacity model is formulated as follows:

$$\begin{aligned} &\underset{B^{\mathrm{g}}_{i,k}, B^{\mathrm{ESS}}_{i,k}}{\text{maximize}} \left(\sum_{i\in\mathscr{N}} \sum_{k\in\Phi} (1 - B^{\mathrm{g}}_{i,k}) Cap^{\mathrm{g},k}_i \right), \\ &s.t. \\ &(4)-(12), (14)-(20). \end{aligned} \tag{6.22}$$

Table 6.1 Key parameters of the 128 LV UK feeders.

Parameter	Mean	Standard Deviation	90% range
Total length (km)	1.6717	1.4223	0.204 - 4.359
Distance from transformer to the farthest circuit node (km)	0.3466	0.1693	0.0684 - 0.642
Number of customers	59	51	7 - 170
Average R/X ratio	10.2144	2.6613	5.386 - 14.339

6.6 Evaluation and Assessment

In this section, simulations are carried out to examine the performance of the proposed framework. Initially, the effectiveness of the proposed HC model to identifying the PVHC is demonstrated in subsection 6.6.2. Then, the impact of control scheme of BESSs, minimum SoC of BESSs, penetration level of BESSs and network tariffs on the MPVHC is discussed in subsection 6.6.3.

6.6.1 Test Systems

The test systems are 128 LV UK feeders [47]. Table 6.1 presents the main characteristics of these feeders. All service transformers in the feeders are 800 kVA, with the primary and the secondary voltages of 11 kV and 0.415 kV, respectively. The maximum acceptable voltage is 1.05 p.u. Regarding the size of PVs, the average size of small-scale PVs based on the historical data is 3.08 kW in the UK [133]. Therefore, the base PV capacity for a household is assumed to be 3 kW. As for the size of BESSs, it is supposed that the base battery size, initial SoC, maximum charging/discharging rate and charging/discharging efficiency are 3 kWh, 50 %, 0.43 kW and 95 %, respectively. The network tariffs are presented in Table 6.2 [134]. The FIT in the UK for PV systems smaller than 10 kW is 3.79 pence per kWh in 2018/19 [135].

Table 6.2 Network tariff Data.

Tariff type	**fixed charge p/day**	**Single rate p/kWh**	**Day p/kWh**	**Night (22-8) p/kWh**
Flat	31.740	16.700	16.700	16.700
Time-of-Use (ToU)	33.450	-	18.810	7.790

6.6.2 Performance Assessment of the Proposed Framework

The performance of the proposed method is examined using two LV UK feeder. The important features of the networks are presented in Table 6.3. We assume that the power factor of the PV systems is unity. The results of the proposed method is compared with those of the Monte Carlo approach presented in [46]. The main aim of the Monte Carlo approach is to identify a PV expansion scenario with the lowest penetration level that would cause a violation in the technical constraints. To increase the accuracy, the Monte Carlo simulation is run for multiple times. As it was shown in [46], the HC results for multiple Monte Carlo simulations follows a Gaussian distribution. The Monte Carlo method is implemented for the two LV UK feeders. The number of generated scenarios for each penetration level is 100 and the number of repetition of Monte Carlo simulations is 200. The power flow calculation is run in OpenDSS. Fig. 6.4 shows the PVHC distribution of the two test systems obtained from the Monte Carlo approach. As can be seen, the MPVHC estimated using the Monte Carlo approach for the test systems is 20.51 % and 22.43 %, respectively. However, there is no guarantee that these values are the actual MPVHC of the test system. In fact, to be able to guarantee the solution of the Monte Carlo method, 2^{N_C} different PV expansion scenarios should be assessed, where N_C is the total number of householders in a feeder. Assessing such a number of PV expansions is computationally cumbersome.

The MPVHC of the test systems calculated using the proposed method is 16.67 % and 18.69 %, respectively. As the proposed method is based on a mathematical model of the HC, it would directly converge to the PV expansion scenario with the lowest penetration level that would cause a constraint violation in the system. Therefore, the proposed method does not need to assess a high number of scenarios to identify the MPVHC. Fig. 6.5 presents the MPVHC for both test systems for different BESS penetration level using the proposed and Monte Carlo-based methods. The self consumption maximization (SCM) method is implemented to charge/discharge BESSs. As can be seen, the results of the proposed method are always lower than those of the Monte Carlo approach. The lowest difference between the result of the two methods is 1.86 %. Note that a zero difference means that the Monte Carlo

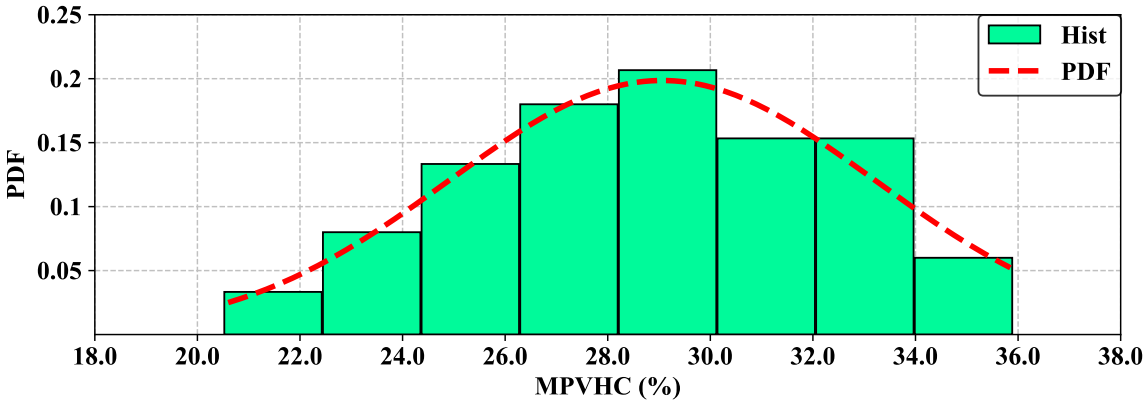

(a) Feeder 1

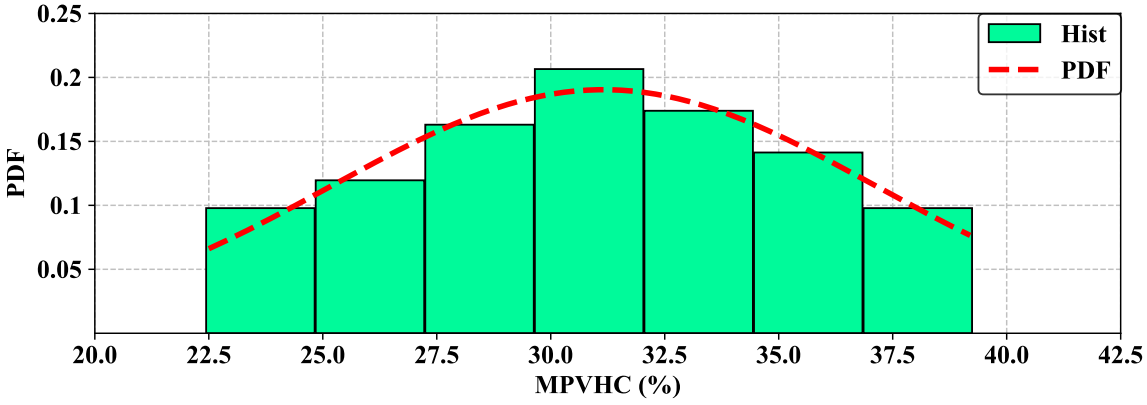

(b) Feeder 2

Fig. 6.4 PVHC distribution obtained from the Monte Carlo approach.

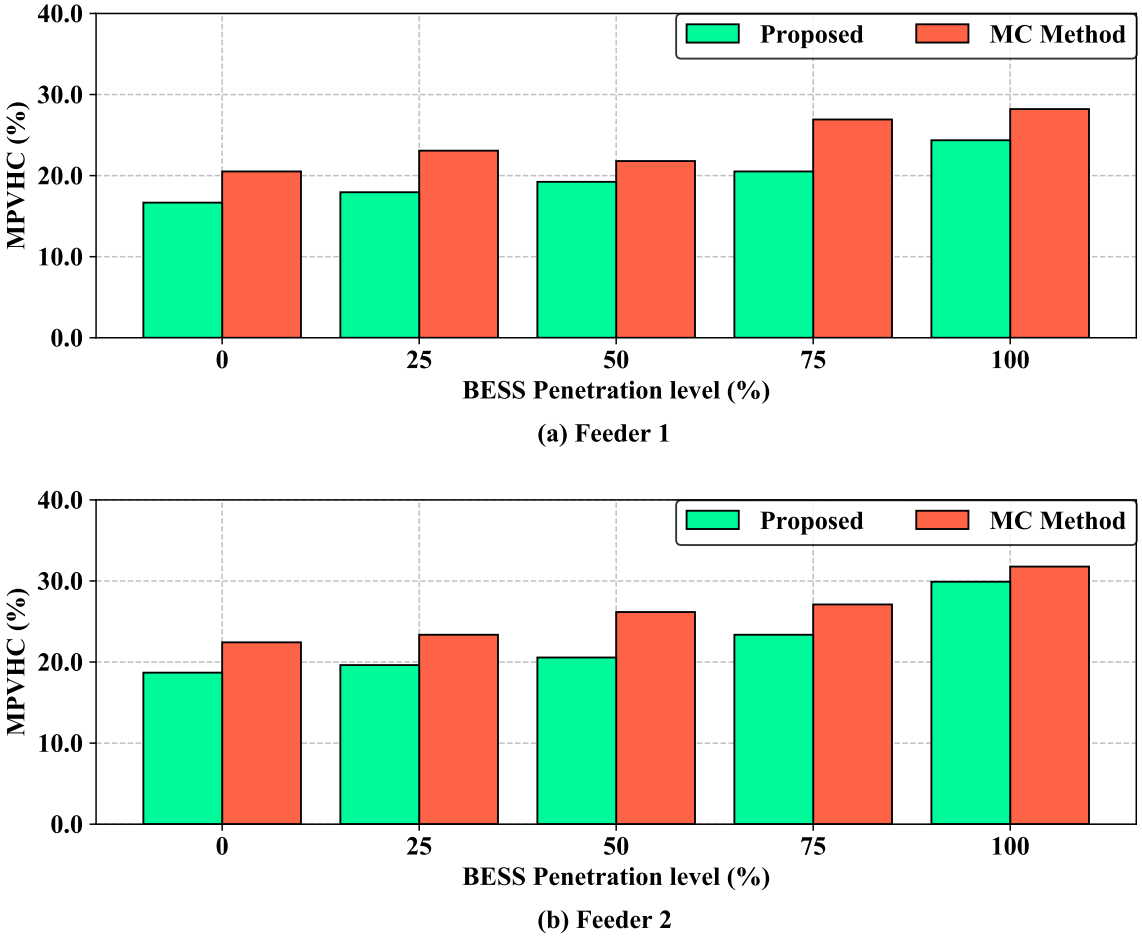

Fig. 6.5 MPVHC in the two test feeders using the proposed and Monte Carlo methods for different BESS penetration level.

approach accurately estimated the MPVHC. The highest differences between the results is 6.41 %, which indicates that the MPVHC estimated using the Monte Carlo approach has 6.41 % error from the actual MPVHC of the test systems.

6.6.3 Technical Assessment

The proposed method is used to assess the impacts of the residential BESS on the MPVHC. The simulation results showed that 72 feeders had the MPVHC of 100 % before considering any residential BESS. Therefore, the remaining 56 feeders was used as the test systems to perform the BESS impact assessment study. Fig. 6.6 represents the MPVHC of the 56 LV UK feeders for different penetration levels of BESS. As can be seen, increasing the BESS penetration level could increase the MPVHC on average by 8.67 % when the BESSs are controlled to minimize the costs. However, if the BESSs are controlled based on

Table 6.3 Important features of the two example UK feeders.

Feeder	Total Length (km)	Number of Households	Transformer to The Farthest Point (km)	Distribution of Loads (%)		
				Phase A	Phase B	Phase C
1	1.838	78	0.601	33.33	38.46	28.21
2	2.867	107	0.352	41.12	28.97	29.91

SCM strategy, increasing the BESS penetration to 100 % only can increase the MPVHC, on average by 3.2 %. The reason that optimization-based control strategy would cause a higher MPVHC can be explained by focusing on the charging/discharging pattern of the considered strategies. Fig. 6.7 demonstrates the load, PV and BESS profiles of a random customer. The PV has its maximum output between hours 12:00 and 13:00. As most of the householder in a feeder would receive almost the same level of irradiance, it could be concluded that all the customers would have the maximum PV output during this time period. Thus, the MPVHC would happen in this time period. As can be seen in Fig. 6.7, the BESS is charging with its maximum rate from hour 12:00 to 13:00 when the control strategy is minimizing the costs. However, the charging rate of the BESS is 0.2 p.u at hour 13:00 when the control strategy is SCM. Therefore, the injected power to the network at hour 13:00 for the SCM strategy is higher than that of MILP method. The main reason that BESS charging rate at hour 13:00 is 0.2 p.u is the limitation of the BESS capacity. Observe that the SoC of the battery reaches the maximum limit at hour 13:00 for the SCM strategy. Although this behavior has been observed in most of the test feeders, it is not proper to draw a general conclusion regarding the impact of BESS control schemes on increasing the MPVHC. In fact, to draw a more general conclusion, the impact of the size and initial SoC of BESS on the results should be assessed.

Fig. 6.8 illustrates the impact of the size of BESS on the MPVHC. As can be seen, increasing the size from 3 kWh to 4 kWh would change the impact of BESS penetration on the MPVHC. In fact, 100 % penetration of BESS with the capacity of 3 kWh and cost minimization objective would increase the MPVHC, on average, by 8.67 %. However, the increase in the MPVHC due to 100 % penetration of BESS with the capacity of 4 kWh was, on average, 3.78 % less than that of BESS with the capacity of 3 kWh. This is because changing the BESS size changes the BESS charging/discharging profile. Fig. 6.9 represents the BESS power and SoC of a random customer for two different sizes of BESS. As can be seen, the general trend of both sizes are almost the same. However, when the BESS capacity is 4 kWh, the BESS charging rate at hour 12:00 is zero. The time period from hour 12:00 to

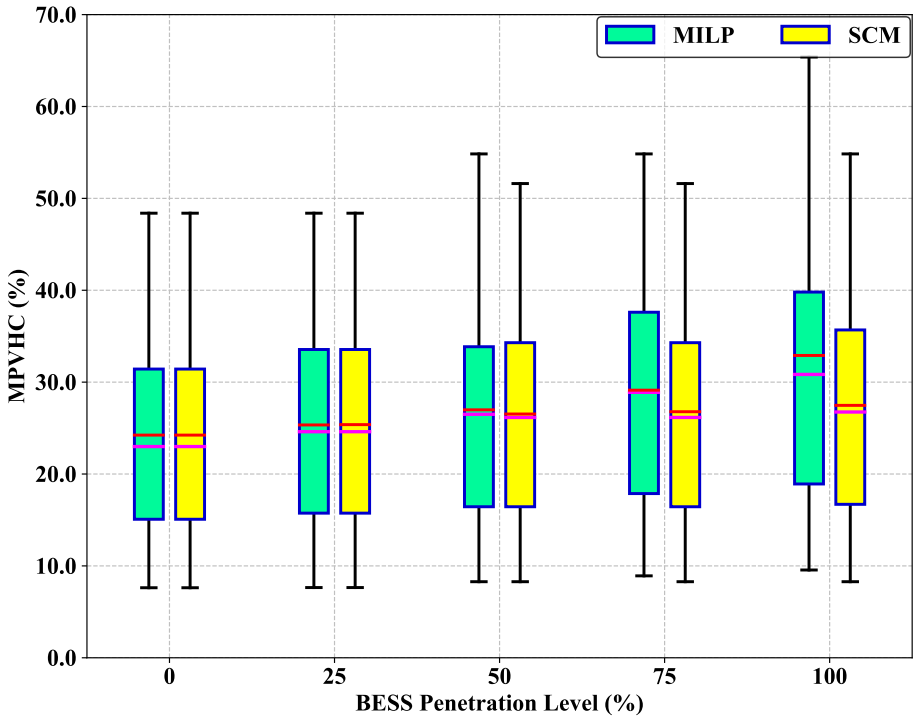

Fig. 6.6 MPVHC for different BESS penetration levels using MILP and SCM charging/discharging approaches for BESSs. The red and purple lines are the mean and median, respectively.

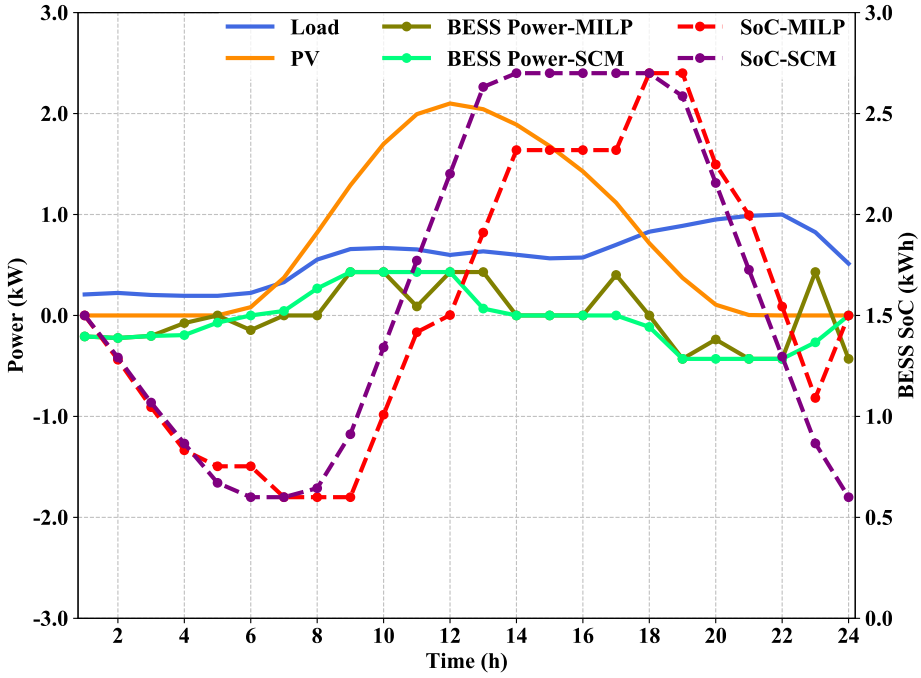

Fig. 6.7 Load, PV, BESS's power and SoC profiles for a random customer using MILP and SCM charging/discharging approaches.

13:00 is a critical period for the MPVHC. As the BESS power at hour 12:00 is zero, it has no impact on the PV injected power to the system. Thus, such a BESS could not increase the MPVHC. Further, as shown in Fig. 6.8 (a), the impact of BESS size on the BESS profile could be more tangible when the control scheme is SCM. Note that a BESS with a higher size has a higher capacity to store the excess PV energy. Therefore, the BESS can stay in charging mode during the time period from hour 12:00 to 13:00. Thus, generally, it can be concluded that when the control scheme is SCM, increasing the size of BESS has a positive impact on the MPVHC. However, increasing the capacity of the BESSs would not improve the MPVHC if the BESSs are charging with the rating power between hours 12:00 and 13:00. In such a condition, increasing the rating power of BESSs could improve the MPVHC.

Another factor that affects the BESS impact on the MPVHC is the initial SoC. Fig. 6.10 shows the MPVHC for different BESS penetration level and initial SoC. As can be seen in Fig. 6.10 (b), increasing the initial SoC from 20 % to 50 % for the BESS penetration level of 100 % and for the control scheme of cost minimization, increases the MPVHC, on average, by 6.9 %. Further, it is observed that increasing the initial SoC of the BESS from 20 % to 50 % when the control scheme is SCM, has insignificant impact on the MPVHC. This is because lower initial SoC means that there is higher storage capacity to be used to store the excess PV generation. Therefore, increasing the initial SoC decreases the available BESS capacity to store the excess energy from hour 12:00 to 13:00. Thus, as can be seen in Fig. 6.10 (a), a higher initial SoC for the SCM scheme could have a negative impact on the MPVHC.

Last, but not the least factor that should be discussed is the network tariff. Since SCM scheme is only based on the difference between load and PV generation, the network tariff has insignificant impact on the MPVHC when BESS follows SCM scheme. Fig. 6.11 shows the impact of network tariff on the MPVHC for two BESS penetration level. As can be seen, both ToU and flat tariffs yield in the same MPVHC for different BESS penetration level. This is because the BESSs are in the charging mode from hour 12:00 to 13:00 for both SCM and MILP schemes.

6.7 Summary

In this chapter, an optimization-based framework was developed to assess the impact of BESSs and network tariffs on the MPVHC of LV distribution systems. The framework was based on a new mathematical model for the HC. Unlike the existing Monte Carlo-based HC methods, which exploited a scenario generator to address the uncertainty associated with the location of PVs and to estimate the MPVHC, the proposed HC model considered the

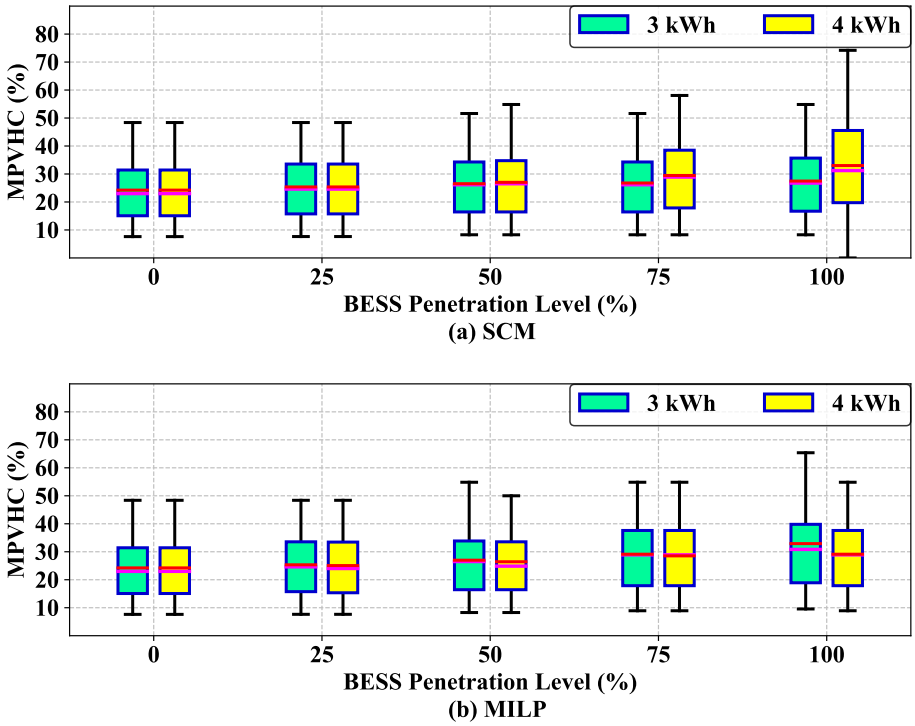

Fig. 6.8 Impact of BESS capacity on MPVHC for different BESS penetration levels using SCM and MILP charging/discharging approaches for BESSs. The red and purple lines are the mean and median, respectively.

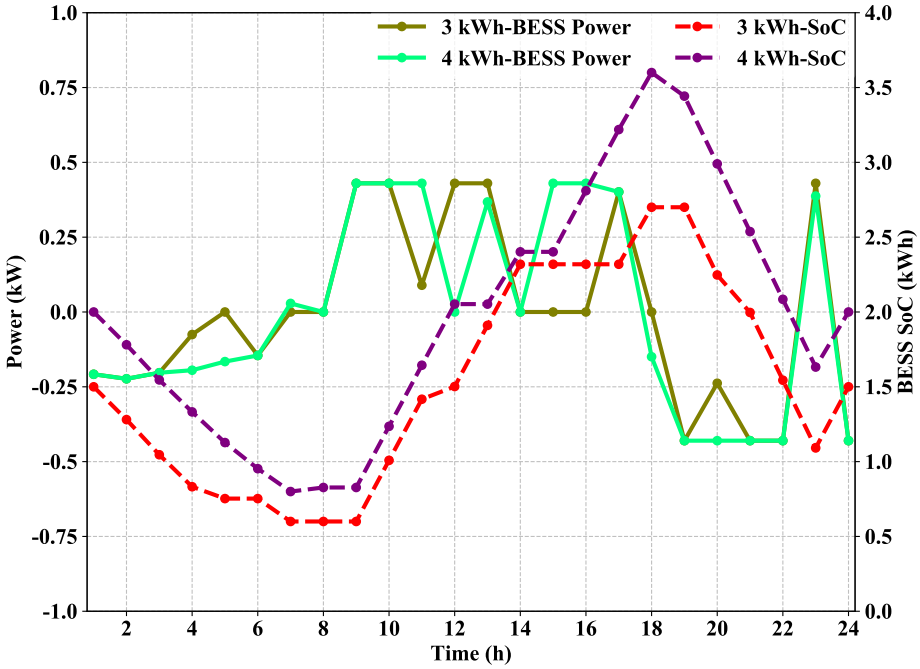

Fig. 6.9 Impact of BESS capacity on the BESS's power and SoC profiles of a random customer using MILP charging/discharging approach.

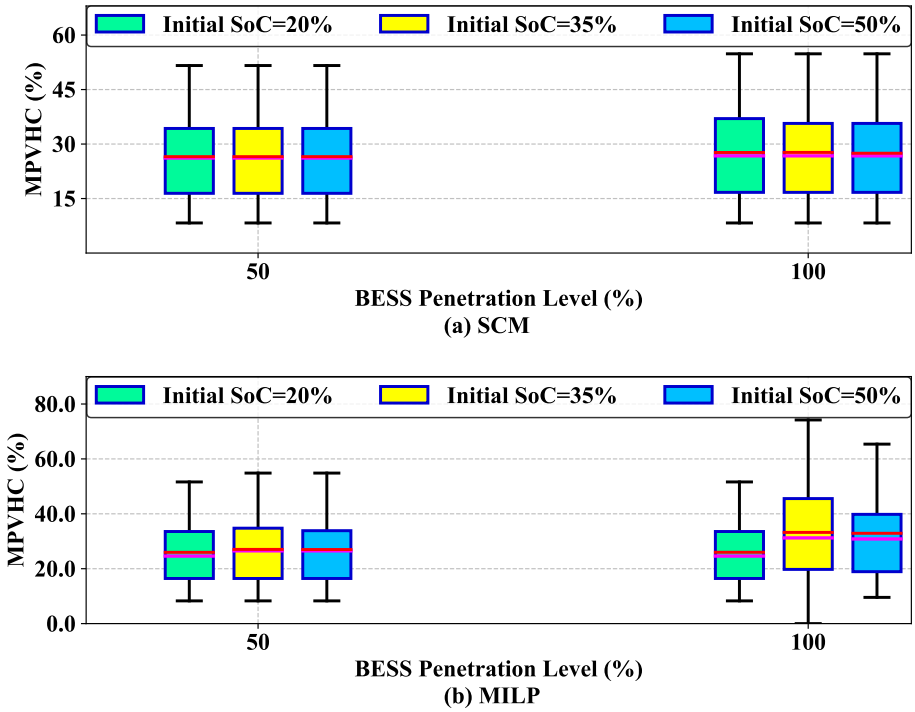

Fig. 6.10 Impact of initial SoC on MPVHC for different BESS penetration levels using SCM and MILP charging/discharging approaches for BESSs. The red and purple lines are the mean and median, respectively.

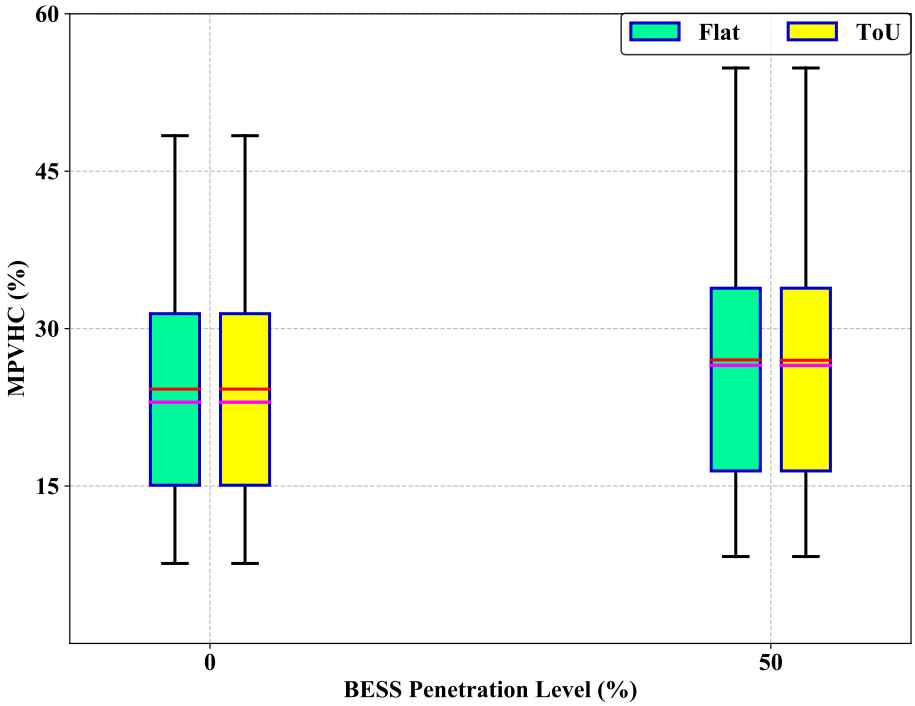

Fig. 6.11 Impact of network tariff on MPVHC for different BESS penetration levels using MILP charging/discharging approach for BESSs. The red and purple lines are the mean and median, respectively.

location of PVs as a binary variable in the optimization problem. Therefore, unlike the Monte Carlo-based methods, which could only estimate an upper bound for MPVHC, the proposed model converged to the MPVHC. Then, proposed methodology was applied to 128 real LV feeders in the U.K. Followings are the conclusion driven from the simulation results:

- The effectiveness of BESSs in increasing the MPVHC depends on the size, initial SoC and the scheduling scheme of BESSs.
- BESSs with both SCM and MILP control schemes improves the MPVHC as long as the BESSs stay in the charging mode during the critical period, i.e. between hours 12:00 and 13:00. For instance, in the test feeders, 100 % BESS penetration with MILP control scheme would increase the MPVHC, on average, by 8.67 %. However, 100 % BESS penetration with SCM control scheme increased the MPVHC, on average, by 3.2 %.
- If the control scheme of BESSs is SCM, increasing the size of BESSs has a positive impact on the MPVHC. However, increasing the capacity of the BESSs would not improve the MPVHC if the BESSs are charging with the maximum rate between hours 12:00 and 13:00.
- The BESS impact on the MPVHC is not dependent on the network tariff. This is because BESSs are charging during the critical period irrespective of the network tariff.

Chapter 7

A Scenario-based Approach for storage capacity determination to improve the hosting capacity of distribution systems

7.1 Introduction

As explained in Chapter 1, distribution system operators (DSOs) could count on different options including distributed energy resources' (DERs') control schemes and residential and community battery energy storage systems (BESSs) to increase the hosting capacity (HC) in their systems. In Chapters 5 and 6, we assessed the effectiveness of DERs' control schemes and residential BESSs on increasing PVHC. In this chapter, a comprehensive method has been proposed to identify the minimum required BESSs for increasing the HC of a system considering the uncertainties associated with the DERs and loads. Then, an economic model has been developed to assess the minimum required BESS from an economic perspective. Finally, the performance of the developed method is assessed on an agricultural feeder in Australia. The outcome of this chapter is published as a conference paper[1] and a book chapter[2].

The remainder of this chapter is organized as follows: the storage sizing framework is presented in Section 7.2. Section 7.3 represents the economic assessment of community BESSs. Numerical results and discussions are presented in Section 7.4. Finally, Section 7.5 summarizes the chapter.

[1] "Impacts of community and distributed energy storage systems on unbalanced low voltage networks," in 2017 Australasian Universities Power Engineering Conference (AUPEC), Nov 2017, pp. 1–6 [93].

[2] Hosting Capacity for Modern Power Grids. Springer, 2019, ch. A Scenario-based approach for storage capacity determination to improve the hosting capacity of distribution systems [136].

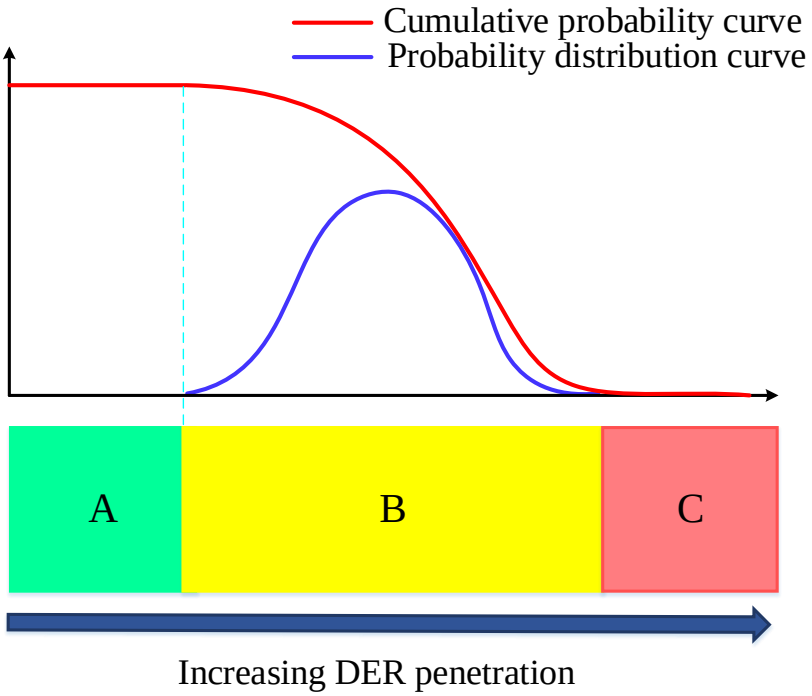

Fig. 7.1 Possible regions as well as the distribution curve of HC.

7.2 Storage Sizing Framework

As shown in Fig. 7.1, the HC of a distribution system could be divided into three regions. Region (A) shows the DER penetration levels that do not cause any violation in technical constraints, regardless of DER locations. Region (B) represents the DER penetration levels that do not cause any technical violation when DERs are located at certain locations. It was demonstrated in [96] that the probability distribution curve of the HC in the region (B) could be approximated by a Gaussian-shape distribution. The start point of the probability distribution curve is the border between regions (A) and (B). This start point is defined as the minimum HC of the system. Region (C) represents all DER penetration levels that would cause a violation of the technical constraints, regardless of the location of DERs. The border between regions (B) and (C) is defined as the maximum HC. Any HC in the region (B) would cause a technical constraint violation for some DER location scenarios. However, it is possible to resolve the constraint violations by curtailing DERs. The optimization model for calculating the minimum active power curtailment required to avoid technical constraints violation is as follows:

$$\underset{APC_{i,t}}{\text{maximize}} \sum_{i \in \mathscr{D}\mathscr{G}} p^{\text{g}}_{i,t} - APC_{i,t}, \tag{7.1}$$

Subjected to

$$P_{ij,t} = \sum_{k:j\longrightarrow k} P_{jk,t} + p^{\mathrm{d}}_{j,t} - p^{\mathrm{g}}_{j,t} + APC_{j,t} \quad \forall j \in \mathscr{DG}, \tag{7.2}$$

$$P_{ij,t} = \sum_{k:j\longrightarrow k} P_{jk,t} + p^{\mathrm{d}}_{j,t} \quad \forall j \in \{\mathscr{N} \setminus \mathscr{DG}\}, \tag{7.3}$$

$$Q_{ij,t} = \sum_{k:j\longrightarrow k} Q_{jk,t} + q^{\mathrm{d}}_{j,t} - q^{\mathrm{g}}_{j,t} \quad \forall j \in \mathscr{DG}, \tag{7.4}$$

$$Q_{ij,t} = \sum_{k:j\longrightarrow k} Q_{jk,t} + q^{\mathrm{d}}_{j,t} \quad \forall j \in \{\mathscr{N} \setminus \mathscr{DG}\}, \tag{7.5}$$

$$\upsilon_{j,t} = \upsilon_{i,t} - 2(r_{ij}P_{ij,t} + x_{ij}Q_{ij,t}) \quad \forall (i,j) \in \mathscr{B}, \tag{7.6}$$

$$\upsilon_{i,t} \leq \bar{\upsilon} \quad \forall i \in \mathscr{N}, \tag{7.7}$$

$$APC_{j,t} \leq p^{\mathrm{g}}_{j,t} \quad \forall j \in \mathscr{DG}, \tag{7.8}$$

$$p^{\mathrm{g}}_{j,t} = \eta^{\mathrm{g}}_{j,t} \times Cap^{\mathrm{g}}_{j} \quad \forall j \in \mathscr{DG}, \tag{7.9}$$

$$q^{\mathrm{g}}_{j,t} = (p^{\mathrm{g}}_{j,t} - APC_{j,t}) \times \tan(\phi_{j,t}) \quad \forall j \in \mathscr{DG}, \tag{7.10}$$

Solving the optimization model (7.1)-(7.10), results in the active power curtailment required at each time step. To identify the minimum required BESS for a scenario, the model (7.1)-(7.10) should be solved over the studied period. The maximum curtailed power during an hour over the studied period is the minimum rating power required for the BESS for that scenario. Similarly, the maximum curtailed energy during a day over the studied period is the minimum energy rating of the required BESS. As the size and location of DERs are uncertain variables, identifying the minimum required BESS for one scenario could not guarantee the normal operation of the system for other DER expansion scenarios. Therefore, the rating power and energy capacity of the required BESS should be identified for different scenarios that would result in the same HC. However, assessing all possible DER expansion scenarios is not a feasible option from a computation point of view. Therefore, we need to make a compromise between the computation burden and accuracy of the solution. Fig. 7.2 represents the framework for identifying the minimum BESS required to increase the minimum HC to a certain level (HC_{ref}) in the region (B). The main idea of the framework is generating expansion scenarios that would result in the total DER capacity of HC_{ref}. Then, the required rating power and energy capacity of BESS should be identified. Finally, the required BESS is estimated based on the designed BESS for the generated scenarios. In the following, the steps of the framework are explained in detail.

- **Step I:** The focus of this step is addressing the uncertainty associated with the size of DERs. Depend on the DER technology, there is a distribution curve for the size

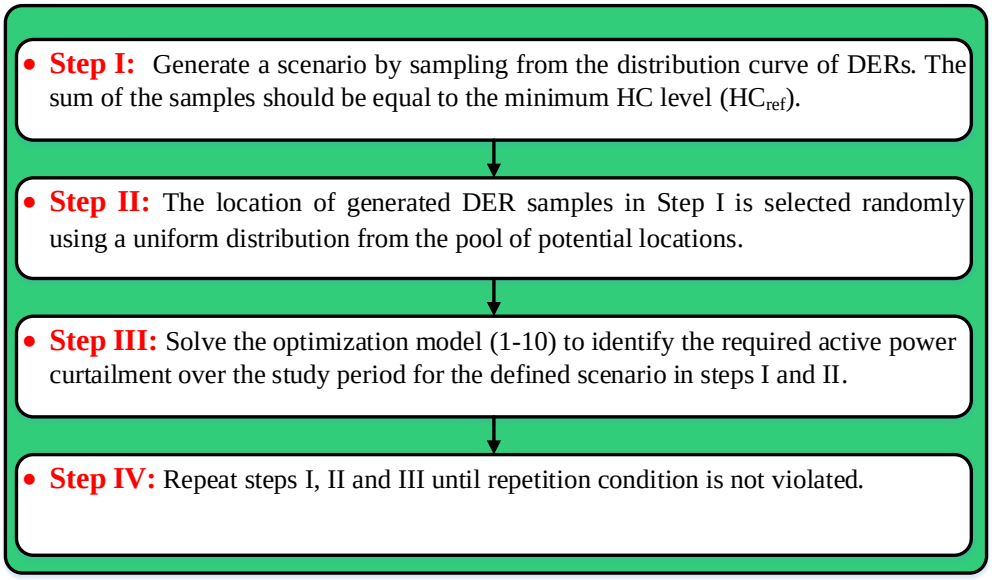

Fig. 7.2 The proposed framework for minimum BESS estimation.

of the units based on the historical statistics. For instance, Fig. 7.3 represents the distribution curve of PV systems in California. Generate a scenario by sampling from the distribution curve of DERs. The sum of the samples should be equal to the target minimum HC level (HC_{ref}).

- **Step II:** This step is designed to address the uncertainty associated with the location of DERs. To do so, the location of generated DER samples in *Step I* is selected randomly, using a uniform distribution from the pool of potential locations.

- **Step III:** After carrying out the *Steps I* and *II*, the optimization model (7.1)-(7.10) should be used to identify the required active power curtailment over the study period. Then, based on the obtained curtailed power, determine the required BESS for the scenario. If the curtailed power over the studied period is zero, the scenario is not a valid scenario as it does not cause any technical constraint violation over the study period. Thus, the following indicator for scenario (j) is defined to identify the validity of each scenario.

$$\Theta_{\text{BESS}}(j) = \begin{cases} 1 & Total\ APC > 0 \\ 0 & Otherwise \end{cases} \tag{7.11}$$

- **Step IV:** Repeat *Steps I, II* and *III* until repetition condition is not violated. As it was mentioned, the HC in the region (B) has a distribution function. Therefore, it is possible to calculate the probability of constraint violations for the new minimum

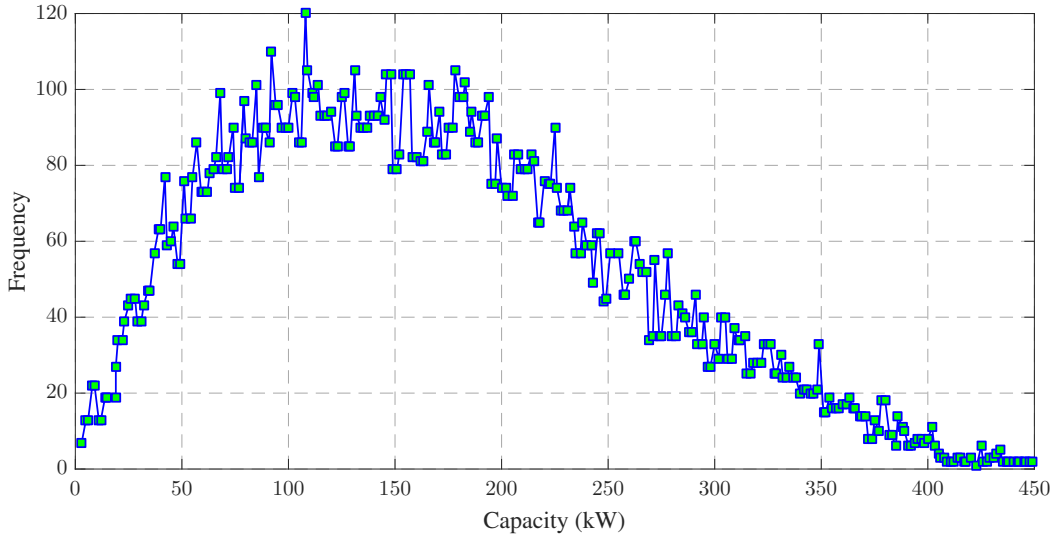

Fig. 7.3 The distribution curve of PV systems based on California solar statistics [1].

HC (HC_{ref}) as follows:

$$Prob_{\text{CV}} = \int_{0}^{HC_{\text{ref}}} f_{\text{HC}}, \tag{7.12}$$

where f_{HC} is the probability distribution function of the HC. It was also mentioned that the active power curtailment over the study period is zero for some of the generated scenarios in *Steps I* and *II*. The probability of valid generated scenarios is as follows:

$$Pr_{\text{APC}} = \frac{\sum_{j=1}^{N_{\text{BESS}}} \Theta_{\text{BESS}}(j)}{N_{\text{BESS}}}, \tag{7.13}$$

where, N_{BESS} is the total generated scenarios. Repeat *Steps I, II* and *III* while the following condition is held:

$$N_{\text{BESS}} \geq 100 \;\; \&\&, \tag{7.14}$$

$$0 < Pr_{\text{APC}} \leq Prob_{\text{CV}}, \tag{7.15}$$

7.3 Economic Assessment

This section explains the proposed method for performing the economic assessment of the designed BESSs. It should be mentioned that the economic assessment in this section is based on the annual costs and benefits of the BESSs.

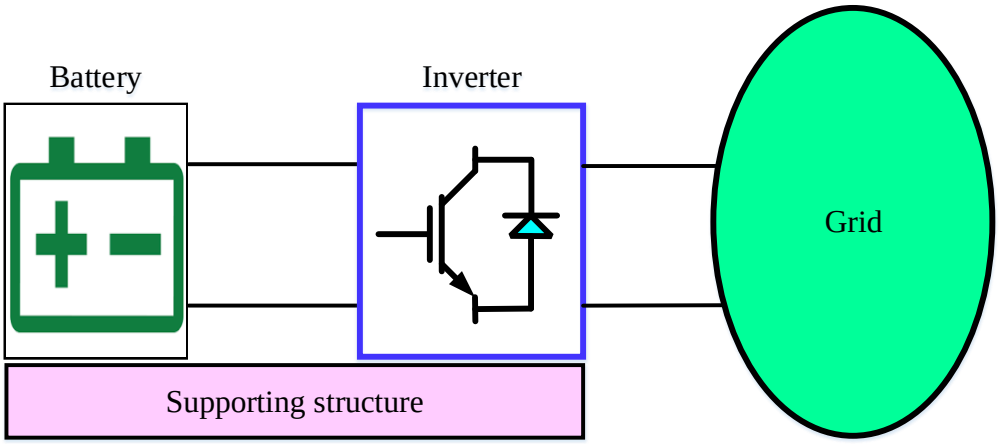

Fig. 7.4 The structure of a BESS.

7.3.1 The Annual Costs of the Estimated BESSs

The annual cost of BESS comprises of three main terms as follows:

- **Total annual capital cost:** the total capital cost of an energy storage system includes the capital costs required for different parts of a BESS. Fig. 7.4 shows the structure of a BESS. Three terms should be considered as the capital costs of the BESS: 1) energy cost for BESS, which is the cost of the devices that store the energy; 2) cost of power, which is the cost of power electronic devices (inverter) in the BESS; and 3) the total cost for the balance of plant, which is defined as the cost of all the auxiliary systems of a BESS including the transformer and supporting structures that are required to exchange the energy.
- **Operation and maintenance cost:** this term is defined to identify the annual cost of maintenance and operation of the BESSs.
- **Replacement cost:** this term is designed to cover the cost of battery replacement at the end of the life cycle of the battery. If the planning horizon is longer than the life cycle of batteries, then this term should be considered.

The calculation of the total annual capital cost is as follows [137]:

$$BEC = UCSC \times \frac{E_{\text{Total}}^{\text{CES}}}{\eta^{\text{CES}}}, \tag{7.16}$$

where, BEC and $UCSC$ represent the total cost ($) and the unit cost ($/kWh) of storage device, respectively; $E_{\text{Total}}^{\text{CES}}$ is the designed energy capacity of the storage device (kWh); and

η^{CES} represents the community BESS efficiency.

$$PEC = UCPE \times S_{\text{Total}}^{\text{CES}}, \tag{7.17}$$

where, PEC and $UCPE$ represent the total cost ($) and the unit cost ($/kW) of power electronic device, respectively; and $S_{\text{Total}}^{\text{CES}}$ is the rated power of the BESS (kW).

$$BOP = UBOP \times \frac{E_{\text{Total}}^{\text{CES}}}{\eta^{\text{CES}}}, \tag{7.18}$$

where, BOP and $UBOP$ represent the total cost ($) and the unit cost ($/kWh) of the balance of plant, respectively. Thus, the total capital cost can be calculated as follows:

$$TCC = BEC + PEC + BOP, \tag{7.19}$$

where TCC denotes the total capital cost. Then, the total annual capital cost is as follows:

$$ACC = TCC \times CAF, \tag{7.20}$$

where,

$$CAF = \frac{IR(1+IR)^{hzn}}{(1+IR)^{hzn}-1}, \tag{7.21}$$

where IR is the annual interest rate, and hzn is the planning horizon. Further, the operation and maintenance cost can be calculated as follows:

$$AOMC = FOM \times S_{\text{Total}}^{\text{CES}}, \tag{7.22}$$

where, $AOMC$ and FOM denote the total annual cost ($/year) and the fixed unit cost ($/(kW.year)) of the maintenance and operation of BESS, respectively. Finally, the replacement cost can be calculated as follows:

$$ARC = A_{\text{Factor}} \times \frac{E_{\text{Total}}^{\text{CES}}}{\eta^{\text{CES}}}, \tag{7.23}$$

where,

$$A_{\text{Factor}} = F_{\text{Factor}} \times [(1+IR)^{-r} + (1+IR)^{-2r} + \ldots] \times CAF, \tag{7.24}$$

$$r = \frac{Cycle_{\text{Total}}}{Cycle_{\text{Day}} \times N_{\text{year}}}, \tag{7.25}$$

where, F_{Factor} represents the future value of the battery replacement cost (\$/kWh); $Cycle_{\text{Total}}$ and $Cycle_{\text{Day}}$ denote the number of charge/discharge cycles of the storage during its life cycle and during a day, respectively; and N_{year} is the number of operating days in a year for the storage system. Therefore, the total annual cost (TAC) can be calculated as follows:

$$TAC = ACC + AOMC + ARC. \tag{7.26}$$

7.3.2 The Annual Costs of Active Power Curtailment

Compensation of the curtailed energy highly depends on the contract between the off-taker and the generator owner. Usually, the compensation of active power curtailment of renewable generators is based on the type of curtailment, the technology of renewable generation, and the amount of curtailed energy. Most commonly, generators are compensated based on the market value for the curtailed energy. However, usually, this compensation does not include revenue lost from support mechanisms such as green energy credits. Some countries such as Ireland and Romania have such a compensation policy. In some countries, the curtailment compensation only covers a fraction of the curtailed energy. This fraction could vary from 15% to 50% or more. For instance, Greece only compensates 30% of the curtailed energy of the wind facilities. However, there is no curtailment compensation for other technologies in Greece. Moreover, the classification and reason behind the curtailment are important in the compensation policies. For example, the congestion curtailments are usually compensated while the curtailments related to the security of the system are not. This policy has been used in Belgium and Germany. Other countries might use a different dichotomy. For instance, real-time curtailments are compensated while the scheduled ones are not [138]. If it is supposed that there is no compensation for the curtailed energy, then the curtailed energy is an opportunity cost for the DER owner. In such a case, the annual cost of the active power curtailment for all DER owners can be calculated as follows:

$$Cost_{\text{APC}} = \sum_{i \in \mathscr{D}\mathscr{G}} \sum_{t=1}^{8760} T_t^{\text{grid}} \times APC_{i,t}, \tag{7.27}$$

where, T_t^{grid} is the network electricity price at time (t).

7.3.3 The Annual Benefit of BESSs for the Utility

The focus of this section is identifying the benefits of the integration of BESSs in the system for the utility. Two obvious options could benefit the utility, which are the reduction in the network losses as well as the energy arbitrage between peak and off-peak periods. Both of

these objectives can be achieved by minimizing the costs of supplying energy from a utility perspective. Therefore, the objective function can be defined as follows:

$$\textit{minimize costs} = \sum_{(i,j)\in\mathscr{B}} \sum_{t=1}^{8760} T_t^{\text{grid}} \times r_{ij} \times \ell_{ij,t} - \sum_{i} \sum_{t=1}^{8760} p_{i,t}^{\text{CES}} \times T_t^{\text{grid}}. \tag{7.28}$$

The decision variables are the optimal size and location of BESSs. The constraints of the optimization problem include the BESSs installation and operation constraints, network constraints and DERs constraints, which are given as follows:

BESSs Installation Constraints:

$$\sum_{i} B_i^{\text{CES}} \leq B_{\text{Total}}^{\text{CES}}, \tag{7.29}$$

$$B_i^{\text{CES}} \times S_i^{\text{CES},min} \leq S_i^{\text{CES}} \leq B_i^{\text{CES}} \times S_i^{\text{CES},max}, \tag{7.30}$$

$$B_i^{\text{CES}} \times E_i^{\text{CES},min} \leq E_i^{\text{CES}} \leq B_i^{\text{CES}} \times E_i^{\text{CES},max}, \tag{7.31}$$

$$\sum_{i} S_i^{\text{CES}} \leq S_{\text{Total}}^{\text{CES}}, \tag{7.32}$$

$$\sum_{i} E_i^{\text{CES}} \leq E_{\text{Total}}^{\text{CES}}, \tag{7.33}$$

$$B_i^{\text{CES}} \in \{0,1\}, \tag{7.34}$$

where, $B_{\text{Total}}^{\text{CES}}$ is the total number of locations in which BESSs could be installed; B_i^{CES} represents the binary variable to allocate BESS at bus (i); S_i^{CES} and E_i^{CES} denote the power rating and energy capacity of a given BESS at bus (i), respectively; $S_i^{\text{CES},max}$ and $E_i^{\text{CES},max}$ represent the maximum power rating and energy capacity of a given BESS at bus (i); and $S_i^{\text{CES},min}$ and $E_i^{\text{CES},min}$ denote the minimum power rating and energy capacity of a given BESS at bus (i). Constraints (7.32) and (7.33) limit the total power rating and energy capacity of the BESS to the minimum required BESS, which was identified in section 7.2.

BESSs Operation Constraints [82]:

$$\sum_{\acute{t}=0}^{t} (p_{i,\acute{t}}^{\text{CES}} \times \Delta t + Loss_{i,\acute{t}}^{\text{CES}}) \leq E_{i,\acute{t}=0}^{\text{CES}} \;\; \forall t \in \mathscr{H}, \tag{7.35}$$

$$\sum_{\acute{t}=0}^{t} (-p_{i,\acute{t}}^{\text{CES}} \times \Delta t - Loss_{i,\acute{t}}^{\text{CES}}) \leq E_i^{\text{CES}} - E_{i,\acute{t}=0}^{\text{CES}} \;\; \forall t \in \mathscr{H}, \tag{7.36}$$

$$E_{i,t}^{\text{CES}} = E_{i,t-1}^{\text{CES}} - p_{i,t}^{\text{CES}} \times \Delta t - Loss_{i,t}^{\text{CES}} \times \Delta t, \;\; \forall t \in \mathscr{H}, \tag{7.37}$$

$$-S_i^{\text{CES}} \leq p_{i,t}^{\text{CES}} \leq S_i^{\text{CES}} \ \ \forall t \in \mathscr{H}, \tag{7.38}$$

$$\varepsilon_i^{min} \times E_i^{\text{CES}} \leq E_{i,t}^{\text{CES}} \leq \varepsilon_i^{max} \times E_i^{\text{CES}} \ \ \forall t \in \mathscr{H}, \tag{7.39}$$

$$Loss_{i,t}^{\text{CES}} = (1-\eta_i^{\text{CES}}) \times |p_{i,t}^{\text{CES}}| \ \ \forall t \in \mathscr{H}, \tag{7.40}$$

$$p_{i,t}^{\text{CES}} \leq p_{i,t-1}^{\text{CES}} + p_i^{RURD} \ \ \forall t \in \mathscr{H}, \tag{7.41}$$

$$p_{i,t}^{\text{CES}} \geq p_{i,t-1}^{\text{CES}} - p_i^{RURD} \ \ \forall t \in \mathscr{H}, \tag{7.42}$$

where, $\mathscr{H}$ and Δt are the set of time steps and the length of each time step, respectively; $E_{i,t=0}^{\text{CES}}$ represents the initial stored energy in BESS at bus (i); ε_i^{min}, ε_i^{max} and η_i^{CES} denote the minimum and maximum allowable stored energy level as well as the efficiency of the BESS at bus (i), respectively; p_i^{RURD} is the charging/discharging rate of BESS at bus (i). Constraint (7.35) is defined to make sure that the sum of all stored and taken energy over all the steps of the study period is less than the initial stored energy. Similarly, constraint (7.36) is defined to keep the sum of all stored and taken energy over all the steps of the study period below the initial available capacity of BESS. Constraint (7.37) models the relationship between the state of charge and the output power of BESS at bus (i) and time (t). Constraint (7.38) keeps BESSs power below their rating power; constraint (7.39) is defined to set the minimum and maximum state of charge of BESS at bus (i); constraint (7.40) is defined to model the energy losses in each BESS at each time step; constraints (7.41) and (7.42) define the maximum charging and discharging rate of BESSs. Finally, constraint (7.40) can be written in a linear form by defining new variables as follows:

$$p_{i,t}^{\text{CES}} = XX_{i,t} - YY_{i,t}, \tag{7.43}$$

$$0 \leq XX_{i,t} \leq S_i^{\text{CES},max}, \tag{7.44}$$

$$0 \leq YY_{i,t} \leq S_i^{\text{CES},max}, \tag{7.45}$$

$$0 \leq Loss_{i,t}^{\text{CES}} - (1-\eta_i^{\text{CES}})(XX_{i,t} - YY_{i,t}) \leq 2 \times S_i^{\text{CES},max} \times DD_{2,i,t}, \tag{7.46}$$

$$0 \leq Loss_{i,t}^{\text{CES}} - (1-\eta_i^{\text{CES}})(YY_{i,t} - XX_{i,t}) \leq 2 \times S_i^{\text{CES},max} \times DD_{1,i,t}, \tag{7.47}$$

$$DD_{1,i,t} + DD_{2,i,t} = 1, \tag{7.48}$$

$$DD_{1,i,t}, DD_{2,i,t} \in \{0,1\}, \tag{7.49}$$

where, $DD_{1,i,t}$ and $DD_{2,i,t}$ are binary variables that identify the charging/discharging status of the BESS. $DD_{1,i,t} = 1$ when the BESS is discharging and $DD_{2,i,t} = 1$ when the BESS is charging.

Network Constraints:

These constraints include the power flow as well as over-voltage constraints. Any other technical constraints such as thermal capacity could be also defined as a network constraint. The network constraints considered in this study are modelled as follows:

$$P_{ij,t} = \sum_{k:j\longrightarrow k} P_{jk,t} + p^{\mathrm{d}}_{j,t} - p^{\mathrm{g}}_{j,t} - p^{\mathrm{CES}}_{j,t} + r_{ij}\ell_{ij,t} \;\; \forall j \in \mathscr{DG}, \tag{7.50}$$

$$P_{ij,t} = \sum_{k:j\longrightarrow k} P_{jk,t} + p^{\mathrm{d}}_{j,t} - p^{\mathrm{CES}}_{j,t} + r_{ij}\ell_{ij,t} \;\; \forall j \in \{\mathscr{N} \setminus \mathscr{DG}\}, \tag{7.51}$$

$$Q_{ij,t} = \sum_{k:j\longrightarrow k} Q_{jk,t} + q^{\mathrm{d}}_{j,t} - q^{\mathrm{g}}_{j,t} + x_{ij}\ell_{ij,t} \;\; \forall j \in \mathscr{DG}, \tag{7.52}$$

$$Q_{ij,t} = \sum_{k:j\longrightarrow k} Q_{jk,t} + q^{\mathrm{d}}_{j,t} + x_{ij}\ell_{ij,t} \;\; \forall j \in \{\mathscr{N} \setminus \mathscr{DG}\}, \tag{7.53}$$

$$\upsilon_{j,t} = \upsilon_{i,t} - 2(r_{ij}P_{ij,t} + x_{ij}Q_{ij,t}) + (r^2_{ij} + x^2_{ij})\ell_{ij,t} \;\; \forall (i,j) \in \mathscr{B}, \tag{7.54}$$

$$\ell_{ij,t} = \frac{P^2_{ij,t} + Q^2_{ij,t}}{\upsilon_{i,t}} \;\; \forall (i,j) \in \mathscr{B}, \tag{7.55}$$

$$\underline{\upsilon} \leq \upsilon_{i,t} \leq \overline{\upsilon} \;\; \forall i \in \mathscr{N}, \tag{7.56}$$

Considering the objective function and the constraints, the defined optimization is an optimal power flow (OPF) problem. The relaxed OPF problem, which is formed by eliminating voltage and current angles from power flow equations, is still non-convex due to the quadratic constraint (7.55). This quadratic term can be approximated using a piecewise linear function. Generally, a nonlinear function $f(t)$ can be approximated over an interval $[a,b]$ by a piecewise linear function $\hat{f}(t)$ by using the break points $a = t_0 < t_1 < t_2 < \cdots < t_k = b$ as follows:

$$t = \sum_{v=0}^{k} \lambda_v t_v, \quad \sum_{v=0}^{k} \lambda_v = 1, \;\; \lambda_v \geq 0 \;\; \forall v \in \{0,1,2,\ldots,k\}, \tag{7.57}$$

$$\hat{f}(t) = \sum_{v=0}^{k} \lambda_v \hat{f}(t_v), \tag{7.58}$$

where $t_0 < t_1 < t_2 < \cdots < t_k$ represent the ending points of the pieces. Further, only two adjacent λ_v are non-zero. This restriction can be removed by using binary variables as follows:

$$0 \leq \lambda_0 \leq w_0, \tag{7.59}$$

$$0 \leq \lambda_v \leq w_{v-1} + w_v, \; \forall v \in \{1,2,\ldots,k-1\}, \tag{7.60}$$

$$0 \leq \lambda_k \leq w_{k-1}, \tag{7.61}$$

$$\sum_{v=0}^{k-1} w_v = 1, \tag{7.62}$$

$$w_v \in \{0,1\}. \tag{7.63}$$

Please refer to Chapter 2 for more information regarding approximating the nonlinear term (7.55) with a piecewise linear function.

DERs Constraints:

$$p_{i,t}^{\mathrm{g}} = \eta_{i,t}^{\mathrm{g}} \times Cap_i^{\mathrm{g}} \;\; \forall i \in \mathscr{DG}, \tag{7.64}$$

$$q_{i,t}^{\mathrm{g}} = p_{i,t}^{\mathrm{g}} \times tan(\phi_{i,t}) \;\; \forall i \in \mathscr{DG}, \tag{7.65}$$

where, $\eta_{i,t}^{\mathrm{g}}$ is the capacity factor of the DER at bus (i) and time (t); Cap_i^{g} and $\phi_{i,t}$ are the capacity and power factor angle of DER at bus (i). Thus, the BESS allocation problem is modelled as a mixed-integer linear programming (MILP).

7.3.4 Cost/Benefit Assessment

The total benefits for DER owner as well as the utility are compared to the annual cost of installing the required BESS. If the annual benefit is higher than the annual costs, using BESSs to improve the HC is justifiable. It should also be mentioned that there are different electrical energy storage, including Lead-acid (LA), sodium sulfur (NaS), vanadium redox (VRB) and zinc/bromine (ZnBr). Further, there is a considerable difference between the capital cost of these BESSs technologies, which can affect the feasibility of the required BESS capacity from an economic perspective. Therefore, the economic feasibility assessment should be performed for a variety of BESS technology. Moreover, economic feasibility could change over the course of time. For instance, it is expected to have up to 66% decrease in capital costs by 2030. Similarly, it is expected to experience an increase in the efficiency of battery storage [139]. This means that although a BESS technology might not be economically feasible now, it may become feasible in the future.

7.4 Numerical Results

In this section, simulations are carried out to assess the performance of the proposed methodology. Initially, the effectiveness of the proposed method for identifying the minimum BESS

Table 7.1 Parameters for BESS economical assessment.

Parameter	LA	VRLA	NaS	ZnBr	VRB
Efficiency	0.75	0.75	0.77	0.7	0.7
Unit cost for power electronic inverter (US $/kW)	175	175	1000	175	included in the unit cost for battery storage
Unit cost for battery storage (US $/kWh)	305	360	500	225	740
Unit cost for balance of plant (US $/kWh)	50	50	0	0	30
Fixed operation and maintenance cost (US $/kW)	15	5	20	20	20
Future replacement cost (US $/kWh)	305	360	500	225	222
Number of charge/discharge life cycle	3200	1000	2500	10000	10000

Table 7.2 Electricity price data.

Electricity price scheme	Anytime Energy (c/kWh)	Off-peak Energy (c/kWh)	Shoulder Energy (c/kWh)	Peak Energy (c/kWh)
Flat	29.8	–	–	–
Time of Use (ToU)	–	19.6	36.8	45

capacity is evaluated. Then, the economic feasibility of the minimum required BESS for different technologies is discussed.

7.4.1 Input Data

The proposed methodology is examined on a balanced distribution system. The system is a 33kV feeder in Australia, as shown in Fig. 3.3. The detail of this network is presented in 3.4.1. The load profile is derived from the data made available by the Australian Energy Market Operator (AEMO) [140]. The normalized PV and wind profiles are derived from [101] and [102], respectively. The distribution of PV and wind sizes are derived from [96]. Table 7.1 represents all the parameters required for calculating the annual installation cost of BESS for different technologies [137]. Table 7.2 shows the electricity price rate for two different schemes from Origin Energy [141]. Peak period mentioned in Table 7.2 is from 1pm to 8pm; shoulder period is from 7am to 1pm and from 8pm to 10pm; and off-peak period is from 10pm to 7am.

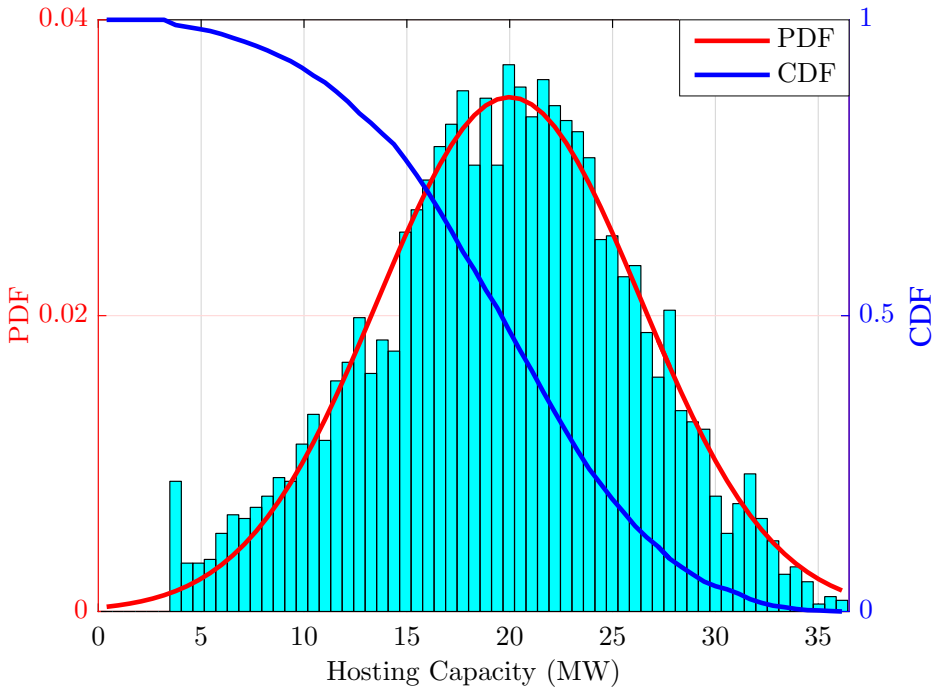

Fig. 7.5 PVHC probability curve for the agricultural feeder.

7.4.2 Hosting Capacity Discussion

PV and wind HC of the test system are estimated based on the HC calculation method presented in Chapter 3. Fig. 7.5 presents PVHC curve for the test system, which can be approximated using the Gaussian-shape distribution as (7.66) with $\alpha = 0.56$, $\mu = 19.97$MW and $\sigma = 6.42$MW. The minimum PVHC for the test system is 3.198MW.

$$HC \sim \alpha \times N(\mu, \sigma^2) = \frac{\alpha}{\sqrt{2\pi\sigma^2}} e^{-\frac{(x-\mu)^2}{2\sigma^2}} \tag{7.66}$$

Fig. 7.6 presents the wind HC curve for the test system, which can be approximated using the Gaussian-shape distribution as (7.66) with $\alpha = 0.956$, $\mu = 37.21$MW and $\sigma = 0.7092$MW. The minimum wind HC for the test system is 2.92MW. As it can be seen, the HC distribution for wind is significantly different from PVHC. This is mainly due to the difference between the wind and PV generation profiles as well as the distribution of wind and PV sizes.

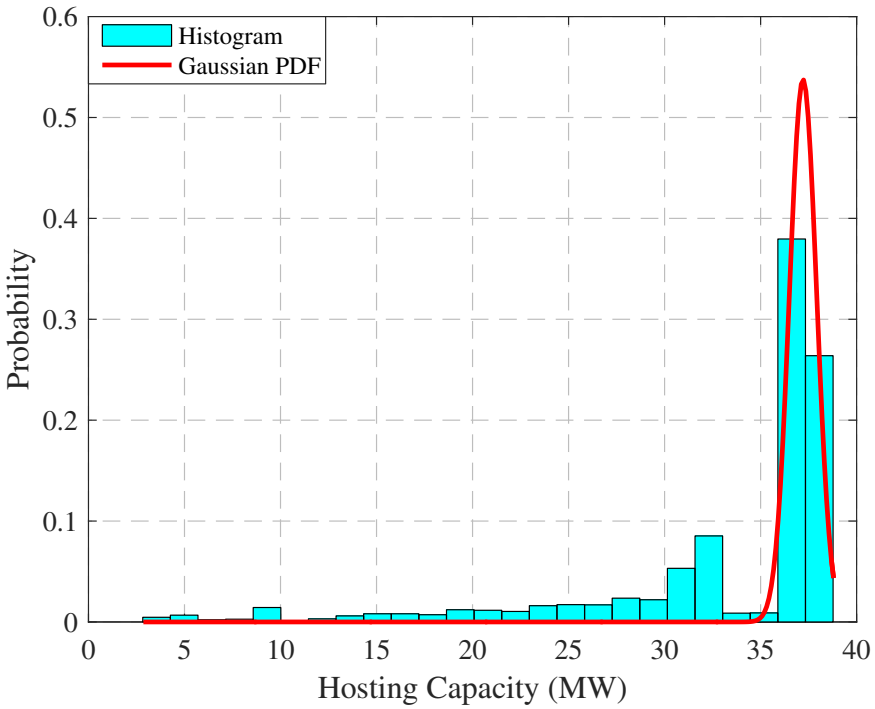

Fig. 7.6 Wind HC probability curve for the agricultural feeder.

Minimum Required BESS

Table 7.3 presents the estimated required BESS to increase the minimum HC to 4MW. To assess the robustness of the identified solution, we generated 100 expansion scenarios with a total DER capacity of 4MW. The curtailed energy for generated scenarios were calculated over the study period. We observed that the identified BESS by the proposed method could store the daily curtailed energy over the study period for both PV and wind technology. This does not guarantee that the estimated BESS by the proposed method would be enough to store the required active power curtailment. However, it supports that the estimated BESS by the proposed method could store the curtailed energy with a probability of $1 - Prob_{\mathrm{CV}} + Pr_{\mathrm{APC}}$. Another observation from Table 7.3 is that the minimum required BESS energy capacity for increasing the wind HC to 4MW is 87.28% higher than that of PVHC. Further, the minimum power rating of the required BESS for wind technology is 22.17% lower than of that for PV technology. This shows that the minimum required BESS capacity in a system highly depends on the type of distributed energy resources that would be accommodated in that system.

Table 7.3 Minimum required BESS to increase the HC to 4MW for PV and wind technologies using the proposed method.

DER Technology	Energy capacity (MWh)	Rating power (MW)
PV	5.275	0.6697
Wind	9.879	0.5212

Table 7.4 Total annual costs of the required BESS for different technologies in US $ (2014).

DER Technology	BESS Technology				
	LA	**VRLA**	**NaS**	**ZnBr**	**VRB**
PV	902323	2124994	1696292	370760	1056548
Wind	1656803	3953947	3036043	657629	1964038

7.4.3 Economic Feasibility Assessment of the Required BESS

This section discusses the economic feasibility of the estimated BESS that is required for different technologies. To do so, the total annual cost of the required BESS for different technologies are compared with the annual benefits of the corresponding BESS. Table 7.4 shows the total annual cost for the required BESS estimated using the proposed method for PV and wind technologies, respectively. As can be seen, using ZnBr battery would result in the lowest total annual costs for both PV and wind technologies, while VRLA battery has the highest total annual costs.

Table 7.5 presents the optimal allocation of the required BESS in the system for both PV and wind technologies under flat and ToU network tariffs. As can be seen, the required BESS capacity is not distributed equally. Further, the optimal BESS location for PV technology is different from that of wind technology. Another important factor that has a considerable impact on the allocation of the required BESS for both PV and wind technologies is the electricity price. Considering Table 7.5, it can be noted that the optimal location of BESSs for both flat and ToU electricity prices are the same. However, the energy capacity as well as the rating power of the optimal BESSs are different.

Fig. 7.7 demonstrates the annual benefit that utility would gain from installing the BESSs for both PV and wind technologies. As can be seen, the annual profit of the utility with ToU tariff is higher than that of the flat tariff. Further, the BESS benefit for PV generation is much higher than that of wind generation in the test system. Moreover, the total annual profit of the utility is below the total annual costs of the minimum required BESS for different storage technologies, which might convey that BESS is not an economically feasible solution for increasing the HC. Nevertheless, the utility benefit is only a part of the BESS benefit. DERs owners also gain some benefit from avoiding active power curtailment. Fig. 7.8 shows the

Table 7.5 Optimal allocation of the required BESS in the test system for PV and wind generation under flat and ToU network tariffs.

			BESS1	BESS2
PV	Flat	Location	149	159
		Energy Capacity (MWh)	3.6	1.675
		Rating Power (MW)	0.3	0.3697
	ToU	Location	149	159
		Energy Capacity (MWh)	1.675	3.6
		Rating Power (MW)	0.297	0.3727
Wind	Flat	Location	151	162
		Energy Capacity (MWh)	5.4	4.479
		Rating Power (MW)	0.2643	0.2569
	ToU	Location	151	162
		Energy Capacity (MWh)	5.4	4.479
		Rating Power (MW)	0.2468	0.2749

total annual profit of both utility and DERs owners compared with the total annual costs of different BESS technologies. As it can be seen, the total annual profit of the BESS with both flat and ToU electricity price rates is still lower than the total annual costs of all BESS technologies, which means that although BESSs can increase the HC of the system, they are not a feasible option from an economic perspective. However, it is also noted that the total annual profit of BESS for PV technology, when the electricity price followed ToU rate, is 325 353$, which is considerably close to the total annual cost of ZnBr battery technology, i.e. 370 760$. This means that although community BESS is not an economically feasible option, it can become a feasible option with a small change in one of the considered parameters such as network tariff and efficiency and price of BESSs. Another considerable point in Fig. 7.8 is that the total annual profit of BESS for wind generation is considerably lower than the total annual cost of all BESS technologies. This implies that there are a few days that the spilled wind energy is very high, but the spilled wind energy for the rest of the days is at a low level.

Finally, it should be mentioned that although some of BESS technologies are economically infeasible now, it does not mean that they will continue to be infeasible in the future. As it was mentioned in section 7.3.4, it is predicted that the price of BESSs would decrease and their efficiency would increase. Fig. 7.9 presents the total annual profit of both utility

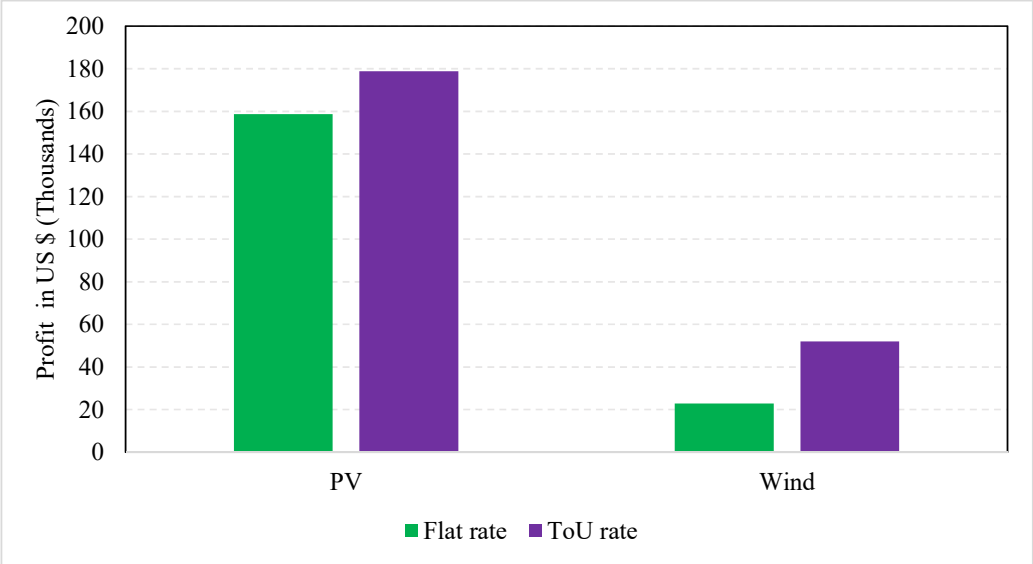

Fig. 7.7 Utility annual profit from installing the required BESS for PV and wind generation for both flat and ToU electricity price rates.

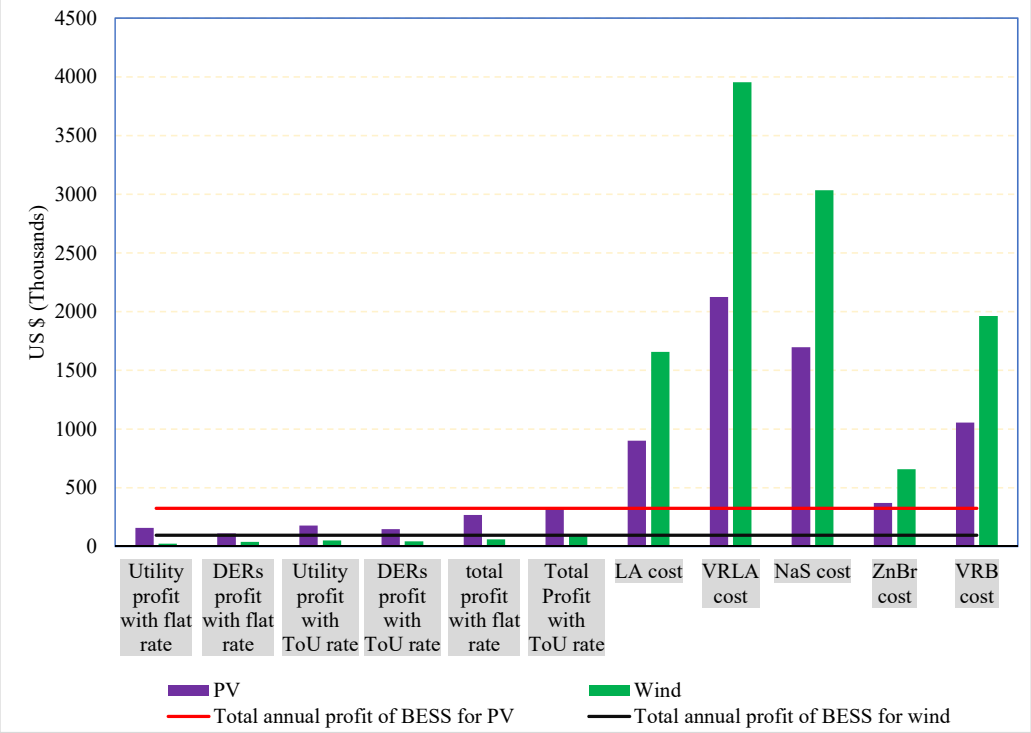

Fig. 7.8 Total annual profit compared with the total annual cost for different BESS technologies.

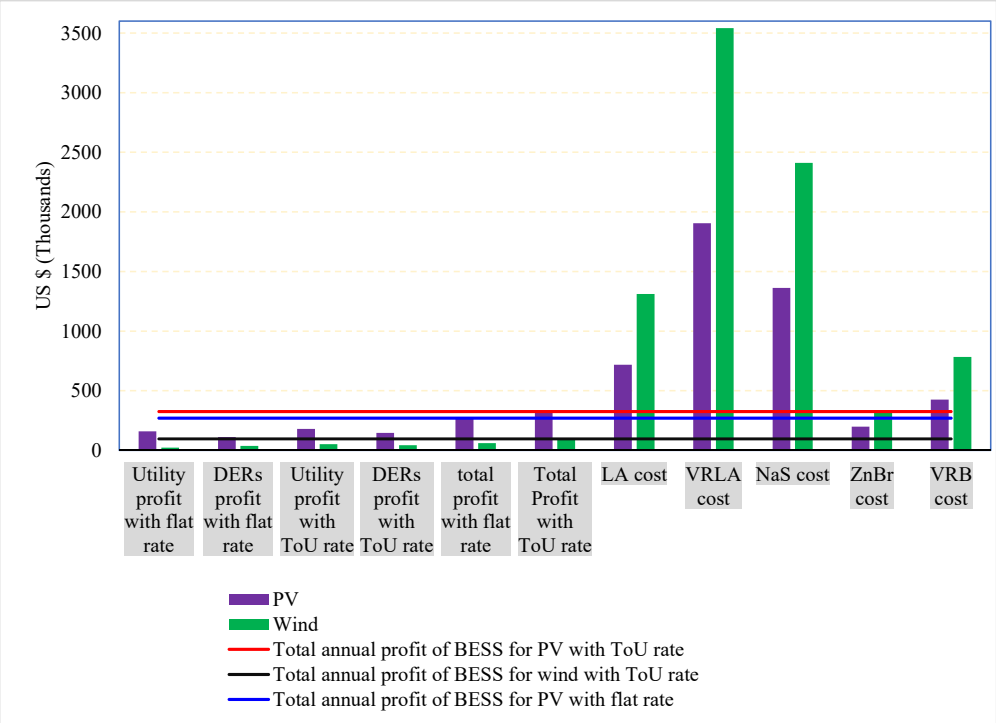

Fig. 7.9 Expected total annual profit in 2030 compared with the total annual cost for different BESS technologies.

and DERs owners compared with the expected annual costs of different BESS technologies in 2030. As can be seen, ZnBr battery technology is expected to be economically feasible in 2030 with both flat and ToU electricity rates for PV technology. However, even the future decrease in the price of energy storages would not make BESSs a feasible option for increasing the HC for wind technology.

7.5 Summary

Technical issues such as over-voltage and overloading of lines and transformers limits DERs capacity in distribution systems. Therefore, it is of great importance to know how distribution systems can accommodate a higher level of DERs. This chapter proposed a method to identify the minimum required battery energy storage to increase the HC of a system to a certain level. The method aims to maximize the injected power in the system while minimizing the curtailed energy. The outcomes of this methodology are the minimum required power and energy capacity rating of BESSs to increase the HC of the system. The second step of the methodology is the economic assessment of the determined BESSs capacity. The performance of the developed method is examined on an agricultural distribution system

in Australia. Then, the cost/benefit analysis is carried out to assess the feasibility of the obtained BESSs. It was shown that the BESS technology highly affects the feasibility of BESSs for HC improvement. Further, it was demonstrated that none of the considered BESS technologies is economically feasible for increasing the HC of the test system. Next, the impact of DER technology (i.e. PV and wind) on the size as well as the economic feasibility of the required BESS was assessed in the test system. It was shown that the required BESSs for increasing the HC of the test system for PV technology is 46.6% less than what is required for wind technology. Moreover, it was demonstrated that the use of BESS for increasing the HC of the system for PV technology would be economically feasible in 2030. However, the use of BESSs for increasing the HC would not be a feasible option for wind technology in the test system in 2030. Another factor that has been assessed in the test system was the effect of electricity price on the allocation of the required BESS. It was shown that the ToU electricity price rate would yield in a higher profit level for the utility than the flat electricity price rate, i.e. 12.78% for PV and 126.8% for wind technology.

Chapter 8

Conclusion and Future Work

As discussed in Chapter 1, the capacity of distribution systems to host distributed energy resources (DERs) is bounded. With the increasing penetration of DERs in distribution systems and new technologies such as electric vehicles (EVs) and battery energy storage systems (BESSs), it is of great importance for distribution system operators (DSOs) to identify the hosting capacity (HC) of their systems. Thus, in this thesis, we proposed a comprehensive framework to estimate the HC of any radial distribution system. In addition, we proposed proper HC models to assess and quantify the impacts of new technologies such as EVs on the HC. Furthermore, we quantified the contribution of different voltage control schemes and residential BESSs on the HC. Then, to increase the HC in a system, we optimally allocated and controlled comunity BESSs. The steps we took to address different aspects of HC problem as well as the finding of this thesis are summarized as follows:

First, in Chapter 2, we developed a deterministic HC model for radial distribution systems. We proved that the conic relaxation of the HC model is not exact, which means that we cannot solve a convex conic program instead of the original non-convex HC model. Then, we identified the conditions under which the linearized HC model is valid. We demonstrated that linearizing the HC model is valid if the linear approximation of the branch losses is less than the actual quadratic term. Furthermore, we linearized the HC problem based on the identified criteria.

Second, in Chapter 3, we proposed a probabilistic framework based on an accurate HC model considering the over-voltage and voltage deviation constraints, to deal with the uncertainties associated with loads and DERs. We developed a two-step technique to linearize the HC model. Further, the impacts of voltage deviation constraint, load growth, network structure, and the DER type on HC have been assessed using the proposed methodology. Following are the conclusions derived from the simulation results:

- Voltage deviation constraint does not have a tangible effect on the HC probability curve. Further, the voltage deviation constraint often limits the locational HC and distributing DERs in the network would reduce the importance of this constraint.
- The annual load growth would increase the HC. So, the HC estimated now would be an underestimation of the HC in the future.
- The HC probability curve highly depends on DER technology.

Third, in Chapter 4, we took a further step and studied the impact of EVs and their charging station on the HC. To do so, we proposed a distributionally robust optimization (DRO) to model the HC. The DRO HC model is proposed to replace the time series impact analysis module of the framework presented in Chapter 3. In the proposed method, the uncertain variables are modelled as stochastic variables following ambiguous distributions defined based on the historical data. The DRO model guarantees that the probability of the constraint violation does not exceed a given risk level, which can control the robustness of the solution. To solve the DRO model of the HC, we reformulated it as a joint chance constrained (JCC) problem, which was solved using the sample average approximation (SAA) technique. The simulation result demonstrated that shortage of historical data can exponentially increase the conservativeness of the estimated HC. Further, our assessment showed that although aggregated demand of residential EVs increases the peak load in the system, it does not improve the HC significantly. This is because the system reaches its maximum HC value during the time periods that the aggregated demand of EVs is very low. We also observed that the impact of charging stations' demand on the HC depends on the DER technology.

Forth, in Chapter 5, we focused on increasing the HC by exploiting different control schemes. The investigated operation strategies are based on the active and reactive power control capabilities of photovoltaic (PV) systems as well as the on-load tap changer (OLTC) of transformers. We proposed an optimization-based framework to determine the photovoltaic HC (PVHC) considering the voltage control capabilities. We did this by utilizing the linear mathematical model of the PVHC, in which the voltage control strategies were modelled as equality and inequality constraints. The proposed methodology was examined on 128 LV UK feeders. We showed besides the active power curtailment mode, i.e. VWOM, Volt-Var operation mode of PV systems, i.e. VVOM, is more effective than other considered operation modes of PV systems. Further, we showed that the control strategy of OLTC significantly impacts the minimum PVHC (MPVHC). We demonstrated that if the aim of OLTC controller is controlling the voltage of the farthest location from the substation transformer, it would decrease the MPVHC. Nevertheless, if the aim is to keep the voltage in the feeder within permissible range, it can increase the MPVHC on average by 51.08 %.

Then, as it is a general assumption that residential BESSs would increase the HC, we performed a comprehensive study to assess their impacts in a systematic way. To do so, we presented an optimization-based framework in Chapter 6. The framework is based on a new mathematical model for the HC. Unlike the Monte Carlo-based HC methods, which can only provide an estimation of MPVHC, the proposed model can converge to the actual MPVHC. We demonstrated the advantage of the proposed method over the Monte Carlo approach. Then, the proposed methodology is examined on 128 real LV feeders in the U.K. The simulation results showed the effectiveness of residential BESSs in increasing the MPVHC depends on the penetration of BESSs in the system and the scheduling scheme of BESSs. Further, we demonstrated that the MPVHC increases more in the cost minimization scheme compared to the self-consumption minimization. In addition, we showed that both flat and Time-of-Use tariffs have similar effect on the MPHVC.

Finally, in Chapter 7, we proposed a method for determining the minimum required community BESS to increase the HC of a system to a certain level. The proposed method is based on an optimization problem aiming to maximize the injected power in the system while minimizing the active power curtailment (APC). The optimization model is the core part of a probabilistic framework, which is designed to address the uncertainties associated with the loads as well as the location and output power of DERs. Then, we carried out an economic analysis to assess the feasibility of the required community BESS. We showed that the BESS technology highly affects the economic feasibility of BESSs for HC improvement. Further, we demonstrated that none of the considered BESS technologies is currently economically feasible for increasing the HC of the test system. However, with the decreasing trend in the BESS price, using community storage to increase the HC becomes an economically feasible solution.

The aim of this thesis is to assess and enhance the HC of distribution systems. To do this in a systematic way, we modelled the HC as an optimization problem. Then, we proposed a framework based on the HC optimization model to identify the HC, probabilistically. Furthermore, we assessed the impacts of new technologies such as EVs, residential BESSs on the HC. In addition, we identified the effectiveness of different options such as ANM schemes as well as installing community BESS in increasing the HC. Considering these, the work of thesis can be extended into the following directions:

- DSOs require a simple but accurate methodology to estimate the HC of their networks. Considering this, we developed a probabilistic optimization-based method based on the most important HC technical constraints, which is a pragmatic approach to estimate the HC. However, this approach is computationally expensive. An idea to avoid extensive computation of the HC estimation is using some machine learning techniques. Thus,

we can define some representative feeders. Then, we can identify the HC of the representative feeders. Finally, the estimated HC and other characteristics of the representative feeders is used in a machine learning process, which could be used to predict the HC of a new feeder based on its characteristics.

- Wind and solar farms may be connected to the medium voltage (MV) distribution systems. As it has been discussed in the AEMO report [142, 143], these renewable generations decrease the system strength. System strength is usually measured by available fault level (AFL) or short circuit ratio (SCR). Low system strength can lead to an increased voltage volatility during system normal and disturbance conditions. Further, it can also compromise the correct operation of protection systems, and result in converter connected generations disconnecting during disturbances. In this thesis, we considered the short circuit level (SCL) as a constraint in the HC optimization model. However, AFL is generally less than SCL in the systems with considerable penetration of converter connected generations. Increasing the penetration of converter connected generations would decrease AFL, hence decrease system strength. Therefore, to guarantee a minimum system strength, the system strength can be added as another constraint in the HC optimization model.

- In this thesis, we assessed the impacts of APC and reactive power control (RPC) based on local controllers. However, the progress in the smart grid technologies is paving the way for implementation of distributed control of DERs in distribution systems. In distributed control approach, DERs can communicate with each other. Therefore, unlike the local control approach, a group of DERs would work together to resolve the technical issue. Thus, the next question is how effective are the distributed control strategies in increasing the HC.

References

[1] A. Dubey, S. Santoso, and A. Maitra, "Understanding photovoltaic hosting capacity of distribution circuits," in *2015 IEEE Power Energy Society General Meeting*, July 2015, pp. 1–5.

[2] M. A. Akbari and et al, "New metrics for evaluating technical benefits and risks of DGs increasing penetration," *IEEE Transactions on Smart Grid*, vol. 8, no. 6, pp. 2890–2902, Nov 2017.

[3] R. Passey, T. Spooner, I. MacGill, M. Watt, and K. Syngellakis, "The potential impacts of grid-connected distributed generation and how to address them: A review of technical and non-technical factors," *Energy Policy*, vol. 39, no. 10, pp. 6280 – 6290, 2011.

[4] N. K. Roy and H. R. Pota, "Current status and issues of concern for the integration of distributed generation into electricity networks," *IEEE Systems Journal*, vol. 9, no. 3, pp. 933–944, Sept 2015.

[5] R. Tonkoski, L. A. C. Lopes, and T. H. M. El-Fouly, "Coordinated active power curtailment of grid connected PV inverters for overvoltage prevention," *IEEE Transactions on Sustainable Energy*, vol. 2, no. 2, pp. 139–147, April 2011.

[6] G. Mokhtari, G. Nourbakhsh, and A. Ghosh, "Smart coordination of energy storage units (ESUs) for voltage and loading management in distribution networks," *IEEE Transactions on Power Systems*, vol. 28, no. 4, pp. 4812–4820, Nov 2013.

[7] T. Stetz, K. Diwold, M. Kraiczy, D. Geibel, S. Schmidt, and M. Braun, "Techno-economic assessment of voltage control strategies in low voltage grids," *IEEE Transactions on Smart Grid*, vol. 5, no. 4, pp. 2125–2132, Jul 2014.

[8] W. Huang, D. Gan, X. Xia, N. Kobayashi, and X. Xu, "Distributed generation on distribution system voltage regulation: An optimization-based approach," in *IEEE PES General Meeting*, Jul 2010, pp. 1–7.

[9] F. Ding and B. Mather, "On distributed PV hosting capacity estimation, sensitivity study and improvement," *IEEE Transactions on Sustainable Energy*, vol. PP, no. 99, pp. 1–1, 2016.

[10] *Small Generator Interconnection Procedures, Section 2.2.1.2*, FERC, 2014.

[11] J. Smith and et al, "Stochastic analysis to determine feeder hosting capacity for distributed solar PV," Electric Power Research Institute, Palo Alto, CA, Tech. Rep., 2012.

[12] N. Baldenko and S. Behzadirafi, "Determination of photovoltaic hosting capacity on radial electric distribution feeders," in *2016 IEEE International Conference on Power System Technology (POWERCON)*, Sept 2016, pp. 1–4.

[13] *Connection of a Power Generator System*, Endeavour Energy, 2014.

[14] S. Heslop, I. MacGill, and J. Fletcher, "Maximum PV generation estimation method for residential low voltage feeders," *Sustainable Energy, Grids and Networks*, vol. 7, pp. 58 – 69, 2016.

[15] *Western Australian Distribution Connections Manual*, Horizon Power and Western Power, 2015, fifth Edition.

[16] *NS194A, Inverter energy systems up to 200kVA connected to the Ausgrid low voltage distribution system*, Ausgrid, 2014.

[17] *Connection Standard for Micro Embedded Generating Units Less Than 30 kVA*, Ergon Energy, August,2016.

[18] X. Chen, W. Wu, and B. Zhang, "Robust capacity assessment of distributed generation in unbalanced distribution networks incorporating ANM techniques," *IEEE Transactions on Sustainable Energy*, 2017.

[19] "Capacity of distribution feeders for hosting DER," CIGRE, Tech. Rep., 2014.

[20] "IEEE standard for interconnecting distributed resources with electric power systems," *IEEE Std 1547-2003*, pp. 1–28, July 2003.

[21] A. B. C. for Sustainable Energy, *Technical Guide for Connection of Renewable Generators to the Local Electricity Network*. Australian Business Council for Sustainable Energy, 2004.

[22] J. Morren and S. W. H. de Haan, "Maximum penetration level of distributed generation without violating voltage limits," in *Electricity Distribution - Part 1, 2009. CIRED 2009. 20th International Conference and Exhibition on*, Jun 2009, pp. 1–4.

[23] E. Zio, M. Delfanti, L. Giorgi, V. Olivieri, and G. Sansavini, "Monte carlo simulation-based probabilistic assessment of DG penetration in medium voltage distribution networks," *International Journal of Electrical Power & Energy Systems*, vol. 64, pp. 852 – 860, 2015.

[24] R. A. Shayani and M. A. G. de Oliveira, "Photovoltaic generation penetration limits in radial distribution systems," *IEEE Transactions on Power Systems*, vol. 26, no. 3, pp. 1625–1631, Aug 2011.

[25] M. S. S. Abad, G. Verbic, A. Chapman, and J. Ma, "A linear method for determining the hosting capacity of radial distribution systems," in *2017 Australasian Universities Power Engineering Conference (AUPEC)*, Nov 2017, pp. 1–6.

[26] F. Spertino, P. D. Leo, and V. Cocina, "Which are the constraints to the photovoltaic grid-parity in the main european markets?" *Solar Energy*, vol. 105, pp. 390 – 400, 2014.

[27] P. N. Vovos, G. P. Harrison, A. R. Wallace, and J. W. Bialek, "Optimal power flow as a tool for fault level-constrained network capacity analysis," *IEEE Transactions on Power Systems*, vol. 20, no. 2, pp. 734–741, May 2005.

[28] C. J. Dent, L. F. Ochoa, and G. P. Harrison, "Network distributed generation capacity analysis using OPF with voltage step constraints," *IEEE Transactions on Power Systems*, vol. 25, no. 1, pp. 296–304, Feb 2010.

[29] M. A. Mahmud, M. J. Hossain, and H. R. Pota, "Voltage variation on distribution networks with distributed generation: Worst case scenario," *IEEE Systems Journal*, vol. 8, no. 4, pp. 1096–1103, Dec 2014.

[30] G. Koutroumpezis and A. Safigianni, "Optimum allocation of the maximum possible distributed generation penetration in a distribution network," *Electric Power Systems Research*, vol. 80, no. 12, pp. 1421 – 1427, 2010.

[31] L. F. Ochoa, A. Padilha-Feltrin, and G. P. Harrison, "Time-series-based maximization of distributed wind power generation integration," *IEEE Transactions on Energy Conversion*, vol. 23, no. 3, pp. 968–974, Sept 2008.

[32] M. Alturki, A. Khodaei, A. Paaso, and S. Bahramirad, "Optimization-based distribution grid hosting capacity calculations," *Applied Energy*, vol. 219, pp. 350 – 360, 2018.

[33] T. E. C. d. Oliveira, P. M. S. Carvalho, P. F. Ribeiro, and B. D. Bonatto, "PV hosting capacity dependence on harmonic voltage distortion in low-voltage grids: Model validation with experimental data," *Energies*, vol. 11, no. 2, 2018.

[34] A. Hoke, R. Butler, J. Hambrick, and B. Kroposki, "Steady-state analysis of maximum photovoltaic penetration levels on typical distribution feeders," *IEEE Transactions on Sustainable Energy*, vol. 4, no. 2, pp. 350–357, April 2013.

[35] M. Akbari, J. Aghaei, and M. Barani, "Convex probabilistic allocation of wind generation in smart distribution networks," *IET Renewable Power Generation*, vol. 11, no. 9, pp. 1211–1218, 2017.

[36] M. A. Akbari, J. Aghaei, M. Barani, T. Niknam, S. Ghavidel, H. Farahmand, M. Korpas, and L. Li, "Convex models for optimal utility-based distributed generation allocation in radial distribution systems," *IEEE Systems Journal*, vol. 12, no. 4, pp. 3497–3508, Dec 2018.

[37] S. Wang, S. Chen, L. Ge, and L. Wu, "Distributed generation hosting capacity evaluation for distribution systems considering the robust optimal operation of OLTC and SVC," *IEEE Transactions on Sustainable Energy*, vol. 7, no. 3, pp. 1111–1123, July 2016.

[38] S. F. Santos, D. Z. Fitiwi, M. Shafie-khah, A. W. Bizuayehu, C. M. P. Cabrita, and J. P. S. Catalao, "New multistage and stochastic mathematical model for maximizing res hosting capacity-part I: Problem formulation," *IEEE Transactions on Sustainable Energy*, vol. 8, no. 1, pp. 304–319, Jan 2017.

[39] H. Al-Saadi, R. Zivanovic, and S. F. Al-Sarawi, "Probabilistic hosting capacity for active distribution networks," *IEEE Transactions on Industrial Informatics*, vol. 13, no. 5, pp. 2519–2532, Oct 2017.

[40] A. Rabiee and S. M. Mohseni-Bonab, "Maximizing hosting capacity of renewable energy sources in distribution networks: A multi-objective and scenario-based approach," *Energy*, vol. 120, no. Supplement C, pp. 417 – 430, 2017.

[41] S. F. Santos, D. Z. Fitiwi, M. Shafie-khah, A. W. Bizuayehu, C. M. P. Cabrita, and J. P. S. Catalao, "New multi-stage and stochastic mathematical model for maximizing RES hosting capacity-part II: Numerical results," *IEEE Transactions on Sustainable Energy*, vol. 8, no. 1, pp. 320–330, Jan 2017.

[42] X. Chen, W. Wu, B. Zhang, and C. Lin, "Data-driven DG capacity assessment method for active distribution networks," *IEEE Transactions on Power Systems*, vol. 32, no. 5, pp. 3946–3957, Sept 2017.

[43] P. Xiong, P. Jirutitijaroen, and C. Singh, "A distributionally robust optimization model for unit commitment considering uncertain wind power generation," *IEEE Transactions on Power Systems*, vol. 32, no. 1, pp. 39–49, Jan 2017.

[44] Z. Wang, Q. Bian, H. Xin, and D. Gan, "A distributionally robust co-ordinated reserve scheduling model considering CVaR-based wind power reserve requirements," *IEEE Transactions on Sustainable Energy*, vol. 7, no. 2, pp. 625–636, April 2016.

[45] T. Stetz, F. Marten, and M. Braun, "Improved low voltage grid-integration of photovoltaic systems in Germany," *IEEE Transactions on Sustainable Energy*, vol. 4, no. 2, pp. 534–542, Apr 2013.

[46] A. Dubey and S. Santoso, "On estimation and sensitivity analysis of distribution circuit's photovoltaic hosting capacity," *IEEE Transactions on Power Systems*, vol. PP, no. 99, pp. 1–1, 2016.

[47] A. Navarro-Espinosa and L. F. Ochoa, "Probabilistic impact assessment of low carbon technologies in LV distribution systems," *IEEE Transactions on Power Systems*, vol. 31, no. 3, pp. 2192–2203, May 2016.

[48] R. Torquato, D. Salles, C. Oriente Pereira, P. C. M. Meira, and W. Freitas, "A comprehensive assessment of PV hosting capacity on low-voltage distribution systems," *IEEE Transactions on Power Delivery*, vol. 33, no. 2, pp. 1002–1012, April 2018.

[49] A. Arshad, M. Lindner, and M. Lehtonen, "An analysis of photo-voltaic hosting capacity in Finnish low voltage distribution networks," *Energies*, 2017.

[50] E. Demirok, P. C. Gonzalez, K. H. B. Frederiksen, D. Sera, P. Rodriguez, and R. Teodorescu, "Local reactive power control methods for overvoltage prevention of distributed solar inverters in low-voltage grids," *IEEE Journal of Photovoltaics*, vol. 1, no. 2, pp. 174–182, Oct 2011.

[51] A. Safayet, P. Fajri, and I. Husain, "Reactive power management for overvoltage prevention at high PV penetration in a low-voltage distribution system," *IEEE Transactions on Industry Applications*, vol. 53, no. 6, pp. 5786–5794, Nov 2017.

[52] D. V. Bozalakov, T. L. Vandoorn, B. Meersman, G. K. Papagiannis, A. I. Chrysochos, and L. Vandevelde, "Damping-based droop control strategy allowing an increased penetration of renewable energy resources in low-voltage grids," *IEEE Transactions on Power Delivery*, vol. 31, no. 4, pp. 1447–1455, Aug 2016.

[53] A. Molina-Garcia, R. A. Mastromauro, T. Garcia-Sanchez, S. Pugliese, M. Liserre, and S. Stasi, "Reactive power flow control for PV inverters voltage support in LV distribution networks," *IEEE Transactions on Smart Grid*, vol. 8, no. 1, pp. 447–456, Jan 2017.

[54] V. Calderaro, V. Galdi, F. Lamberti, and A. Piccolo, "A smart strategy for voltage control ancillary service in distribution networks," *IEEE Transactions on Power Systems*, vol. 30, no. 1, pp. 494–502, Jan 2015.

[55] "IEEE standard for interconnection and interoperability of distributed energy resources with associated electric power systems interfaces," *IEEE Std 1547-2018 (Revision of IEEE Std 1547-2003)*, pp. 1–138, April 2018.

[56] M. Zeraati, M. E. Hamedani Golshan, and J. M. Guerrero, "Distributed control of battery energy storage systems for voltage regulation in distribution networks with high PV penetration," *IEEE Transactions on Smart Grid*, vol. 9, no. 4, pp. 3582–3593, July 2018.

[57] X. Liu, A. Aichhorn, L. Liu, and H. Li, "Coordinated control of distributed energy storage system with tap changer transformers for voltage rise mitigation under high photovoltaic penetration," *IEEE Transactions on Smart Grid*, vol. 3, no. 2, pp. 897–906, June 2012.

[58] Y. Wang, K. T. Tan, X. Y. Peng, and P. L. So, "Coordinated control of distributed energy-storage systems for voltage regulation in distribution networks," *IEEE Transactions on Power Delivery*, vol. 31, no. 3, pp. 1132–1141, June 2016.

[59] B. Bletterie, S. Kadam, R. Bolgaryn, and A. Zegers, "Voltage control with PV inverters in low voltage networks: In depth analysis of different concepts and parameterization criteria," *IEEE Transactions on Power Systems*, vol. 32, no. 1, pp. 177–185, Jan 2017.

[60] C. Long and L. F. Ochoa, "Voltage control of PV-rich LV networks: OLTC-fitted transformer and capacitor banks," *IEEE Transactions on Power Systems*, vol. 31, no. 5, pp. 4016–4025, Sep. 2016.

[61] T. Aziz and N. Ketjoy, "Enhancing PV penetration in LV networks using reactive power control and on load tap changer with existing transformers," *IEEE Access*, vol. 6, pp. 2683–2691, 2018.

[62] S. N. Salih and P. Chen, "On coordinated control of OLTC and reactive power compensation for voltage regulation in distribution systems with wind power," *IEEE Transactions on Power Systems*, vol. 31, no. 5, pp. 4026–4035, Sep. 2016.

[63] M. N. Kabir, Y. Mishra, G. Ledwich, Z. Y. Dong, and K. P. Wong, "Coordinated control of grid-connected photovoltaic reactive power and battery energy storage systems to improve the voltage profile of a residential distribution feeder," *IEEE Transactions on Industrial Informatics*, vol. 10, no. 2, pp. 967–977, May 2014.

[64] X. Liu, A. Aichhorn, L. Liu, and H. Li, "Coordinated control of distributed energy storage system with tap changer transformers for voltage rise mitigation under high photovoltaic penetration," *IEEE Transactions on Smart Grid*, vol. 3, no. 2, pp. 897–906, June 2012.

[65] M. Bahramipanah, D. Torregrossa, R. Cherkaoui, and M. Paolone, "A decentralized adaptive model-based real-time control for active distribution networks using battery energy storage systems," *IEEE Transactions on Smart Grid*, vol. 9, no. 4, pp. 3406–3418, July 2018.

[66] S. Hashemi, J. Ostergaard, and G. Yang, "A scenario-based approach for energy storage capacity determination in LV grids with high PV penetration," *IEEE Transactions on Smart Grid*, vol. 5, no. 3, pp. 1514–1522, May 2014.

[67] C. Keerthisinghe, G. Verbic, and A. C. Chapman, "A fast technique for smart home management: ADP with temporal difference learning," *IEEE Transactions on Smart Grid*, vol. 9, no. 4, pp. 3291–3303, July 2018.

[68] Y.-S. Cheng, H. Hesse, N. Truong, A. Jossen, and Y.-H. Liu, "Charging strategy for a residential battery storage system using fuzzy logic controller," in *NEIS Conference 2016*, D. Schulz, Ed. Wiesbaden: Springer Fachmedien Wiesbaden, 2017, pp. 182–189.

[69] Y. Zhang, A. Lundblad, P. E. Campana, F. Benavente, and J. Yan, "Battery sizing and rule-based operation of grid-connected photovoltaic-battery system: A case study in Sweden," *Energy Conversion and Management*, vol. 133, pp. 249 – 263, 2017.

[70] J. von Appen, T. Stetz, M. Braun, and A. Schmiegel, "Local voltage control strategies for pv storage systems in distribution grids," *IEEE Transactions on Smart Grid*, vol. 5, no. 2, pp. 1002–1009, March 2014.

[71] D. Azuatalam, M. Forst, K. Paridari, Y. Ma, A. C. Chapman, and G. Verbic, "Techno-economic analysis of residential PV-battery self-consumption," in *ASIA-PACIFIC SOLAR RESEARCH CONFERENCE*, 2018.

[72] C. Keerthisinghe, G. Verbic, and A. C. Chapman, "Evaluation of a multi-stage stochastic optimisation framework for energy management of residential PV-storage systems," in *2014 Australasian Universities Power Engineering Conference (AUPEC)*, Sep. 2014, pp. 1–6.

[73] J. Linssen, P. Stenzel, and J. Fleer, "Techno-economic analysis of photovoltaic battery systems and the influence of different consumer load profiles," *Applied Energy*, vol. 185, pp. 2019 – 2025, 2017, clean, Efficient and Affordable Energy for a Sustainable Future.

[74] A. Arshad, V. Puvi, and M. Lehtonen, "Monte carlo-based comprehensive assessment of PV hosting capacity and energy storage impact in realistic finnish low-voltage networks," *Energies*, vol. 11, no. 6, 2018. [Online]. Available: https://www.mdpi.com/1996-1073/11/6/1467

[75] V. C. Cunha, R. Torquato, T. R. Ricciardi, W. Freitas, and B. Venkatesh, "Assessing energy storage potential to facilitate the increased penetration of photovoltaic generators and electric vehicles in distribution networks," in *2017 IEEE Power Energy Society General Meeting*, July 2017, pp. 1–5.

[76] S. Hashemi and J. Ostergaard, "Efficient control of energy storage for increasing the PV hosting capacity of LV grids," *IEEE Transactions on Smart Grid*, vol. 9, no. 3, pp. 2295–2303, May 2018.

[77] R. Zafar, J. Ravishankar, J. E. Fletcher, and H. R. Pota, "Multi-timescale model predictive control of battery energy storage system using conic relaxation in smart distribution grids," *IEEE Transactions on Power Systems*, vol. 33, no. 6, pp. 7152–7161, Nov 2018.

[78] Y. M. Atwa and E. F. El-Saadany, "Optimal allocation of ESS in distribution systems with a high penetration of wind energy," *IEEE Transactions on Power Systems*, vol. 25, no. 4, pp. 1815–1822, Nov 2010.

[79] P. Hasanpor Divshali and L. Soder, "Improving hosting capacity of rooftop PVs by quadratic control of an LV-central BSS," *IEEE Transactions on Smart Grid*, vol. 10, no. 1, pp. 919–927, Jan 2019.

[80] B. Bocker, S. Kippelt, C. Weber, and C. Rehtanz, "Storage valuation in congested grids," *IEEE Transactions on Smart Grid*, vol. 9, no. 6, pp. 6742–6751, Nov 2018.

[81] M. C. Di Piazza, M. Luna, G. La Tona, and A. Di Piazza, "Improving grid integration of hybrid pv-storage systems through a suitable energy management strategy," *IEEE Transactions on Industry Applications*, vol. 55, no. 1, pp. 60–68, Jan 2019.

[82] M. Nick, R. Cherkaoui, and M. Paolone, "Optimal allocation of dispersed energy storage systems in active distribution networks for energy balance and grid support," *IEEE Transactions on Power Systems*, vol. 29, no. 5, pp. 2300–2310, Sep. 2014.

[83] A. Jalali and M. Aldeen, "Risk-based stochastic allocation of ESS to ensure voltage stability margin for distribution systems," *IEEE Transactions on Power Systems*, vol. 34, no. 2, pp. 1264–1277, March 2019.

[84] Q. Li, R. Ayyanar, and V. Vittal, "Convex optimization for DES planning and operation in radial distribution systems with high penetration of photovoltaic resources," *IEEE Transactions on Sustainable Energy*, vol. 7, no. 3, pp. 985–995, July 2016.

[85] A. Giannitrapani, S. Paoletti, A. Vicino, and D. Zarrilli, "Optimal allocation of energy storage systems for voltage control in LV distribution networks," *IEEE Transactions on Smart Grid*, vol. 8, no. 6, pp. 2859–2870, Nov 2017.

[86] M. S. S. Abad, J. Ma, and X. Han, *Smart Power Distribution Systems, Control, Communication, and Optimization*. Academic Press, 2018, ch. Distribution systems hosting capacity assessment: Relaxation and linearization.

[87] M. Farivar and S. H. Low, "Branch flow model: Relaxations and convexification-part I," *IEEE Transactions on Power Systems*, vol. 28, no. 3, pp. 2554–2564, Aug 2013.

[88] M. E. Baran and F. F. Wu, "Optimal capacitor placement on radial distribution systems," *IEEE Transactions on Power Delivery*, vol. 4, no. 1, pp. 725–734, Jan 1989.

[89] M. Baran and F. F. Wu, "Optimal sizing of capacitors placed on a radial distribution system," *IEEE Transactions on Power Delivery*, vol. 4, no. 1, pp. 735–743, Jan 1989.

[90] S. M. Stefanov, *Separable Programming Theory and Methods*. Springer, 2001.

[91] M. R. K. Gharigh, M. Seydali Seyf Abad, J. Nokhbehzaeem, and A. Safdarian, "Optimal sizing of distributed energy storage in distribution systems," in *2015 Smart Grid Conference (SGC)*, Dec 2015, pp. 60–65.

[92] R. Fourer, D. M. Gay, and B. W. Kernighan, *AMPL: A Modeling Language for Mathematical Programming*. Duxbury Press, 2002.

[93] Y. Ma, M. Seydali Seyf Abad, D. Azuatalam, G. Verbic, and A. Chapman, "Impacts of community and distributed energy storage systems on unbalanced low voltage networks," in *2017 Australasian Universities Power Engineering Conference (AUPEC)*, Nov 2017, pp. 1–6.

[94] B. A. Robbins and A. D. Dominguez-Garcia, "Optimal reactive power dispatch for voltage regulation in unbalanced distribution systems," *IEEE Transactions on Power Systems*, vol. 31, no. 4, pp. 2903–2913, July 2016.

[95] M. S. S. Abad, J. Ma, D. Zhang, A. S. Ahmadyar, and H. Marzooghi, "Sensitivity of hosting capacity to data resolution and uncertainty modeling," in *2018 Australasian Universities Power Engineering Conference (AUPEC)*, Nov 2018, pp. 1–6.

[96] M. S. S. Abad, J. Ma, D. Zhang, A. S. Ahmadyar, and H. Marzooghi, "Probabilistic assessment of hosting capacity in radial distribution systems," *IEEE Transactions on Sustainable Energy*, vol. 9, no. 4, pp. 1935–1947, Oct 2018.

[97] P. Sulc, S. Backhaus, and M. Chertkov, "Optimal distributed control of reactive power via the alternating direction method of multipliers," *IEEE Transactions on Energy Conversion*, vol. 29, no. 4, pp. 968–977, Dec 2014.

[98] A. Berry, T. Moore, J. Ward, S. Lindsay, and K. Proctor, "National feeder taxonomy : Describing a representative feeder set for Australian networks," CSIRO, Newcastle, N.S.W, Tech. Rep., 2013.

[99] W. H. Kersting, "Radial distribution test feeders," *IEEE Transactions on Power Systems*, vol. 6, no. 3, pp. 975–985, Aug 1991.

[100] AEMO, "National Transmission Network Development Plan 2015," Tech. Rep. Nov, 2015.

[101] S. Pfenninger and I. Staffell, "Long-term patterns of european PV output using 30 years of validated hourly reanalysis and satellite data," *Energy*, vol. 114, pp. 1251 – 1265, 2016.

[102] I. Staffell and S. Pfenninger, "Using bias-corrected reanalysis to simulate current and future wind power output," *Energy*, vol. 114, pp. 1224 – 1239, 2016. [Online]. Available: http://www.sciencedirect.com/science/article/pii/S0360544216311811

[103] "Small and medium wind UK market report," RenewableUK, Tech. Rep., 2015.

[104] C. L. Masters, "Voltage rise: the big issue when connecting embedded generation to long 11 kV overhead lines," *Power Engineering Journal*, vol. 16, no. 1, pp. 5–12, Feb 2002.

[105] F. Shahnia, P. J. Wolfs, and A. Ghosh, "Voltage unbalance reduction in low voltage feeders by dynamic switching of residential customers among three phases," *IEEE Transactions on Smart Grid*, vol. 5, no. 3, pp. 1318–1327, May 2014.

[106] M. Seydali Seyf Abad, J. Ma, A. S. Ahmadyar, and H. Marzooghi, "Distributionally robust distributed generation hosting capacity assessment in distribution systems," *Energies*, vol. 11, no. 11, 2018. [Online]. Available: https://www.mdpi.com/1996-1073/11/11/2981

[107] T. N. Boutsika and S. A. Papathanassiou, "Short-circuit calculations in networks with distributed generation," *Electric Power Systems Research*, vol. 78, no. 7, pp. 1181 – 1191, 2008.

[108] A. Keane and M. O'Malley, "Optimal allocation of embedded generation on distribution networks," *IEEE Transactions on Power Systems*, vol. 20, no. 3, pp. 1640–1646, Aug 2005.

[109] M. E. Baran, H. Hooshyar, Z. Shen, and A. Huang, "Accommodating high PV penetration on distribution feeders," *IEEE Transactions on Smart Grid*, vol. 3, no. 2, pp. 1039–1046, June 2012.

[110] Y. Xu, Z. Y. Dong, R. Zhang, and D. J. Hill, "Multi-timescale coordinated voltage/var control of high renewable-penetrated distribution systems," *IEEE Transactions on Power Systems*, vol. 32, no. 6, pp. 4398–4408, Nov 2017.

[111] A. Fabbri, T. G. S. Roman, J. R. Abbad, and V. H. M. Quezada, "Assessment of the cost associated with wind generation prediction errors in a liberalized electricity market," *IEEE Transactions on Power Systems*, vol. 20, no. 3, pp. 1440–1446, Aug 2005.

[112] Y. M. Atwa, E. F. El-Saadany, M. M. A. Salama, and R. Seethapathy, "Optimal renewable resources mix for distribution system energy loss minimization," *IEEE Transactions on Power Systems*, vol. 25, no. 1, pp. 360–370, Feb 2010.

[113] Z. Wang, J. Wang, B. Chen, M. M. Begovic, and Y. He, "MPC-based voltage/var optimization for distribution circuits with distributed generators and exponential load models," *IEEE Transactions on Smart Grid*, vol. 5, no. 5, pp. 2412–2420, Sept 2014.

[114] G. Li and X. P. Zhang, "Modeling of plug-in hybrid electric vehicle charging demand in probabilistic power flow calculations," *IEEE Transactions on Smart Grid*, vol. 3, no. 1, pp. 492–499, March 2012.

[115] N. H. Tehrani and P. Wang, "Probabilistic estimation of plug-in electric vehicles charging load profile," *Electric Power Systems Research*, vol. 124, pp. 133 – 143, 2015.

[116] W. Alharbi and K. Bhattacharya, "Electric vehicle charging facility as a smart energy microhub," *IEEE Transactions on Sustainable Energy*, vol. 8, no. 2, pp. 616–628, April 2017.

[117] R. Jiang and Y. Guan, "Data-driven chance constrained stochastic program," *Mathematical Programming*, vol. 158, no. 1, pp. 291–327, Jul 2016.

[118] J. Luedtke and S. Ahmed, "A sample approximation approach for optimization with probabilistic constraints," *SIAM Journal on Optimization*, vol. 19, no. 2, pp. 674–699, 2008.

[119] B. K. Pagnoncelli, S. Ahmed, and A. Shapiro, "Sample average approximation method for chance constrained programming: Theory and applications," *Journal of Optimization Theory and Applications*, vol. 142, no. 2, pp. 399–416, Aug 2009.

[120] J. Tan and L. Wang, "Integration of plug-in hybrid electric vehicles into residential distribution grid based on two-layer intelligent optimization," *IEEE Transactions on Smart Grid*, vol. 5, no. 4, pp. 1774–1784, July 2014.

[121] Z. Darabi and M. Ferdowsi, "Aggregated impact of plug-in hybrid electric vehicles on electricity demand profile," *IEEE Transactions on Sustainable Energy*, vol. 2, no. 4, pp. 501–508, Oct 2011.

[122] C. Draxl, A. Clifton, B.-M. Hodge, and J. McCaa, "The wind integration national dataset (WIND) toolkit," *Applied Energy*, vol. 151, pp. 355 – 366, 2015.

[123] H. Sun, Q. Guo, J. Qi, V. Ajjarapu, R. Bravo, J. Chow, Z. Li, R. Moghe, E. Nasr-Azadani, U. Tamrakar, G. N. Taranto, R. Tonkoski, G. Valverde, Q. Wu, and G. Yang, "Review of challenges and research opportunities for voltage control in smart grids," *IEEE Transactions on Power Systems*, pp. 1–1, 2019.

[124] A. Singhal, V. Ajjarapu, J. C. Fuller, and J. Hansen, "Real-time local volt/var control under external disturbances with high PV penetration," *IEEE Transactions on Smart Grid*, pp. 1–1, 2018.

[125] M. Seydali Seyf Abad and J. Ma, "Photovoltaic hosting capacity sensitivity to active distribution network management," *Under review in IEEE Transaction on Power Systems*, vol. Under Review, 2019.

[126] H. Zhu and H. J. Liu, "Fast local voltage control under limited reactive power: Optimality and stability analysis," *IEEE Transactions on Power Systems*, vol. 31, no. 5, pp. 3794–3803, Sept 2016.

[127] W. Wu, Z. Tian, and B. Zhang, "An exact linearization method for OLTC of transformer in branch flow model," *IEEE Transactions on Power Systems*, vol. 32, no. 3, pp. 2475–2476, May 2017.

[128] I. Richardson, M. Thomson, D. Infield, and C. Clifford, "Domestic electricity use: A high-resolution energy demand model," *Energy and Buildings*, vol. 42, no. 10, pp. 1878 – 1887, 2010.

[129] R. D. Zimmerman, C. E. Murillo-Sánchez, and R. J. Thomas, "MATPOWER: Steady-state operations, planning, and analysis tools for power systems research and education," *IEEE Transactions on Power Systems*, vol. 26, no. 1, pp. 12–19, Feb 2011.

[130] M. Rylander, J. Smith, and W. Sunderman, "Streamlined method for determining distribution system hosting capacity," *IEEE Transactions on Industry Applications*, vol. 52, no. 1, pp. 105–111, Jan 2016.

[131] M. Seydali Seyf Abad and J. Ma, "Probabilistic impact assessment of residential BESSs on the HC of LV distribution systems," *Under review in IEEE Transaction on Smart Grid*, vol. Under Review, 2019.

[132] D. Azuatalam, G. Verbic, and A. Chapman, "Impacts of network tariffs on distribution network power flows," in *2017 Australasian Universities Power Engineering Conference (AUPEC)*, Nov 2017, pp. 1–6.

[133] "Weekly solar PV installation and capacity based on registration date," *UK Department of Energy and Climate Change (DECC)*, 2012.

[134] "British Gas: Energy tariffs A-Z." [Online]. Available: https://www.britishgas.co.uk/energy/gas-and-electricity/tariffs-a-z.html

[135] "Ofgem: Feed-In Tariff (FIT) rates." [Online]. Available: https://www.ofgem.gov.uk/environmental-programmes/fit/fit-tariff-rates

[136] M. Seydali Seyf Abad, J. Ma, and J. Qiu, *Hosting Capacity for Modern Power Grids*. Springer, 2020, ch. A Scenario-based approach for storage capacity determination to improve the hosting capacity of distribution systems.

[137] P. Poonpun and W. T. Jewell, "Analysis of the cost per kilowatt hour to store electricity," *IEEE Transactions on Energy Conversion*, vol. 23, no. 2, pp. 529–534, June 2008.

[138] L. Bird, J. Cochran, and X. Wang, "Wind and solar energy curtailment: Experience and practices in the United States," National Renewable Energy Lab (NREL), Tech. Rep., 2014.

[139] P. Ralon, M. Taylor, A. Ilas, H. Diaz-Bone, and K. Kairies, "Electricity storage and renewables: costs and markets to 2030," *International Renewable Energy Agency*, 2017.

[140] "National transmission network development plan," *Australian Energy Market Operator*, 2011.

[141] Origin Energy, "Nsw residential energy price fact sheet," 2018.

[142] AEMO, "System strength impact assessment guidelines," Australian Energy Market Operator, Tech. Rep., 2018.

[143] ——, "Fact sheet: System strength," Australian Energy Market Operator, Tech. Rep., 2019.